THOMAS FUNCK

STRUCTURE OF THE VOLCANIC APRON NORTH OF GRAN CANARIA DEDUCED FROM REFLECTION SEISMIC, BATHYMETRIC AND BOREHOLE DATA

GEOMAR
Forschungszentrum
für marine Geowissenschaften
der Christian-Albrechts-Universität
zu Kiel

Kiel 1996

GEOMAR REPORT 51

GEOMAR
Research Center
for Marine Geosciences
Christian Albrechts University
in Kiel

Dissertation
zur Erlangung des Doktorgrades
der mathematisch-naturwissenschaftlichen Fakultät
der Christian-Albrechts-Universität zu Kiel
Zum Druck genehmigt am 7.2.1996

Redaktion der Serie: Gerhard Haass
Umschlag: Kerstin Kreis, Harald Gross,
GEOMAR Technologie GmbH

Managing Editor: Gerhard Haass
Cover: Kerstin Kreis, Harald Gross,
GEOMAR Technologie GmbH

GEOMAR REPORT
ISSN 0936 - 5788

GEOMAR REPORT
ISSN 0936 - 5788

GEOMAR
Forschungszentrum
für marine Geowissenschaften
D-24148 Kiel
Wischhofstr. 1-3
Telefon (0431) 600-2555, 600-2505

GEOMAR
Research Center
for Marine Geosciences
D-24148 Kiel / Germany
Wischhofstr. 1-3
Telephone (49) 431 / 600-2555, 600-2505

Contents

List of Figures

List of Tables

Summary

High resolution reflection seismic profiles through the volcanic apron north of Gran Canaria collected during the METEOR cruise 24 (1993) were interpreted in the light of results of ODP Leg 157 (Sites 953 and 954) drilled in 1994. The 1158 m deep Site 953 is linked with the seismic data by a synthetic seismogram and therefore represents the key site for calibration of seismic stratigraphy in the apron. The high resolution bathymetric map compiled from swath bathymetry of METEOR cruises 16 (1991) and 24 provides essential information for the seismic interpretation.

The shape of the island flanks of Gran Canaria and the two adjacent islands of Fuerteventura to the east and Tenerife to the west were reconstructed by seismic penetration of the sediments covering the deeper portions of the volcanic pedestals. These mainly basaltic flanks are clear features on the seismic lines because of their generally high reflection amplitudes and systematic onlap patterns. The flanks dip up to 32°. Seismic mapping reveals the geometry of the volcanic flanks and demonstrates that the ca. 4750 m deep flank of Fuerteventura is the oldest one, influencing the subsequent shield-building of Gran Canaria to the east, whose ca. 16–15 my old shield (Schmincke, Weaver, Firth et al., 1995) is ponded against Fuerteventura, forming a topographic barrier between the islands. The associated reduction of the current cross-section has caused strong bottom currents, indicated by erosional features and contourites. To the north, the flank of Gran Canaria extends some 60 km seaward to a depth of ca. 4500 m. The shield of the Anaga massif (northeast Tenerife) onlaps the flank of Gran Canaria to the east. Seismic correlation of the feather edge of the Anaga shield to the bio- and magnetostratigraphy at Site 953 results in an age of ca. 6 Ma. To the northeast, the shield of Tenerife extends some 50 km with a maximum depth of 4000 m.

The surrounding sedimentary basin is characterized by chaotic and discontinuous reflection patterns of the slope facies, turning into the well-stratified basin facies some 30–40 km off the coast. A synthetic seismogram for Site 953 was computed from logging data and discrete core measurements for calibration of the seismic data, resulting in the identification of 55 reflectors. Most reflectors represent thin (< 1m) volcaniclastic interbeds in the hemipelagic background sedimentation, reflecting the volcanic activity and erosion on the adjacent islands.

The westward decrease of reflectivity in the northern apron is interpreted to be caused by the Galdar Ridge, a submarine ridge at the western limit of the north coast of Gran Canaria, through which mass flows from Gran Canaria entering the sea in the north were diverted to the northeastern part of the apron. The lapillistones of the Pliocene Roque Nublo phase of volcanism on Gran Canaria can be correlated in the entire northern apron where they form the most prominent reflector band. The minimum volume of the lapillistones has been computed to be 7 km^3, based on the drilled thickness (2 m) and the lateral extension in the survey area (3500 km^2). The thickness is possibly up to 8 m at Site 953, obscured by the low core recovery which was most likely due to the coarse-

grained nature of these deposits. Hence, the total volume may exceed 50 km^3. The lowest sedimentation rates correlate with the volcanic hiatus on Gran Canaria with 3–4 cm/ky, the highest (up to 12 cm/ky) were found subsequent to the shield building.

The ca. 14 my old reflector M represents an unconformity, dipping at 0.3° towards Gran Canaria, in contrast to the overlying horizontal strata. This feature is interpreted to reflect the flexure of the lithosphere due to the volcanic load of Gran Canaria.

The lowermost lithologic unit at Site 954 is composed of ca. 14 my old basaltic breccia. However, seismic correlation to Site 953 suggests an age of ca. 12 Ma for the deposition of this unit. The unit may represent deposits associated with a slope failure at the northern flank of Gran Canaria at 12 Ma. The seismic mapping reveals more than 60 km^3 of debris advanced at least 70 km into the apron – exceeding the limit of the survey area. The mapped volume fits well with the dimensions of an amphitheatre at the northern flank of Gran Canaria between the Galdar Ridge in the west and the La Isleta peninsula in the east, the suspected source region for the mass wasting event.

The Quaternary volcanism on La Isleta extends further seawards, where the bathymetric map shows a submarine volcano with three radial ridges, interpreted from the seismic data as young lava flows. Between Gran Canaria and Fuerteventura the seismic and bathymetric data show a volcanic complex consisting of two cones, flanked by erosional channels to the east and the west, suggesting a re-orientation and strengthening of bottom currents between the islands after the build-up of the complex, which is probably older than 5 Ma.

Onland canyons and their submarine extensions are well seen in the merged topographic and bathymetric data set. One of the most prominent canyons is the Barranco de Guiniguada, which can be traced some 60 km from northeast Gran Canaria into the apron, where it is some 3.5 km wide and 150 m deep.

Zusammenfassung

Hochauflösende reflexionsseismische Profile der METEOR 24 Fahrt (1993) im vulkanischen Schuttfächer nördlich von Gran Canaria wurden unter Zuhilfenahme der ODP–Bohrungen 953 und 954 (ODP Leg 157) aus dem Jahre 1994 interpretiert. Die 1158 m tiefe Bohrung 953 wurde mit Hilfe eines synthetischen Seismogrammes mit den seismischen Daten verknüpft und stellt den Schlüssel für die Kalibrierung der seismischen Stratigraphie im Becken nördlich der Insel dar. Die Fächerecholot–Daten der METEOR-Fahrten 16 (1991) und 24 wurden zu einer detaillierten bathymetrischen Karte verarbeitet, die eine wesentliche Hilfe bei der seismischen Interpretation war.

Die Form der Inselflanken von Gran Canaria und den beiden Nachbarinseln Fuerteventura im Osten, bzw. Tenerife im Westen, konnte auch dort kartiert werden, wo Sedimente die tieferen Teile des vulkanischen Sockels bedecken. Auf den seismischen Profilen ist der überwiegend basaltische Sockel durch seine meist hohen Amplituden und die systematischen onlap-Schichtterminierungen deutlich erkennbar. Die Flanken fallen bis zu 32° ein. Die seismische Kartierung der Sockel zeigt, daß die 4750 m tiefe Flanke Fuerteventuras am ältesten ist und die spätere Schildbildung Gran Canarias in östliche Richtung beeinflußt hat, wo der etwa 16 bis 15 Millionen Jahre alte Sockel Gran Canarias (Schmincke, Weaver, Firth et al., 1995) gegen Fuerteventura gestaut wurde. Dabei entstand eine topographische Schwelle zwischen den beiden Inseln. Durch die damit verbundene Verringerung des Stömungsquerschnittes kam es zu einer Verstärkung der Bodenströmungen, die sich in Erosionsstrukturen und Konturiten bemerkbar macht. In nördliche Richtung erstreckt sich die Flanke Gran Canarias etwa 60 km seewärts, wo sie eine Tiefe von ca. 4500 m erreicht. Die Flanke Tenerifes erstreckt sich ca. 50 km in Richtung Nordosten mit einer maximalen Tiefe von 4000 m. Im Osten terminiert sie onlap auf der Flanke Gran Canarias. Die seismische Korrelation der äußersten Begrenzung des Anaga-Massivs auf Nordost-Tenerife zur Bio-und Magnetostratigraphie der Bohrung 953 ergibt ein Alter von etwa 6 Millionen Jahren.

Das den Sockel umgebende Sedimentbecken ist durch die chaotischen und diskontinuierlichen Reflexionsmuster der Hangfazies gekennzeichnet, die in 30 bis 40 km Entfernung zur Küste in die gut geschichtete Beckenfazies übergeht. Zur Kalibrierung der seismischen Daten wurde an der Bohrung 953 mithilfe der Logging-Daten und diskreter Kernmessungen ein synthetisches Seismogramm berechnet, durch das 55 Reflektoren identifiziert werden konnten. Die meisten Reflektoren stellen dünne vulkaniklastische Zwischenlagen (< 1 m) in der hemipelagischen Hintergrundsedimentation dar, die die vulkanische Aktivität und Erosion der umgebenden Inseln widerspiegeln.

Im nördlichen Schuttfächer ist eine Abnahme der Reflektivität nach Westen hin zu beobachten, deren Ursache im Galdar Rücken zu sehen ist. Dies ist ein untermeerischer Rücken an der westlichen Begrenzung der Nordküste von Gran Canaria, durch den Schuttströme, die an der Nordflanke Gran Canarias ins Meer gelangten, nach Nordosten abgeleitet wurden. Die Lapillisteine der pliozänen vulkanischen Phase auf Gran

Canaria (Roque Nublo) sind im gesamten nördlichen Schuttfächer zu finden und stellen das kräftigste Reflexionsband dar. Basierend auf der erbohrten Mächtigkeit von 2 m und der Verbreitung im Meßgebiet (3500 km^2) wurde für die Lapillisteine ein Minimalvolumen von 7 km^3 ermittelt. An der Bohrung 953 ist die Mächtigkeit möglicherweise jedoch bis zu 8 m – verdeckt durch den geringen Kerngewinn, der wahrscheinlich durch die Grobkörnigkeit der Lapillisteine bedingt war. Daher könnte das tatsächliche Volumen 50 km^3 übersteigen. Die niedrigsten Sedimentationsraten (3–4 cm/ky) korrelieren mit dem vulkanischen Hiatus auf Gran Canaria, die schnellste Sedimentation mit bis zu 12 cm/ky folgte im Anschluß an die Schildphase der Insel.

Der ca. 14 Millionen Jahre alte Reflektor M stellt eine Diskontinuität dar und fällt im Gegensatz zu den darüberliegenden horizontalen Reflektoren mit etwa 0.3° in Richtung Gran Canaria ein. Dieses Phänomen wird als Lithosphärenflexur durch die vulkanische Auflast Gran Canarias gedeutet.

Die unterste litholgische Einheit der Bohrung 954 besteht aus ca. 14 Millionen Jahre alten basaltischen Brekzien. Die seismische Korrelation zur Bohrung 953 führt jedoch zu einem Ablagerungsalter von etwa 12 Millionen Jahren. Die Einheit könnte daher Teil einer Ablagerung sein, die durch eine Hangrutschung an der Nordflanke Gran Canarias vor 12 Millionen Jahren entstanden ist, bei der mehr als 60 km^3 Schutt über 70 km weit in den Schuttfächer vordrangen – und damit die Grenzen des Meßgebietes überschreiten. Dieses aus der Kartierung ermittelte Volumen stimmt gut mit der Größe eines Kars an der Nordflanke Gran Canarias überein. Dieses erstreckt sich vom Galdar Rücken im Westen bis zur La Isleta Halbinsel im Osten und wird als Ausgangsregion für die beschriebene Bodenverlagerung (*mass wasting*) angenommen.

Der quartäre Vulkanismus auf La Isleta setzt sich submarin nach Nordosten fort, wo die bathymetrische Karte einen Vulkan mit drei radialen Rücken zeigt, die auf Grund der seismischen Daten als junge Lavaströme interpretiert werden. Im Bereich zwischen Gran Canaria und Fuerteventura zeigen sowohl die Seismik als auch die Bathymetrie einen aus zwei Vulkankegeln bestehenden submarinen vulkanischen Komplex, der im Osten und Westen von Erosionsrinnen flankiert ist. Dies läßt eine Neuorientierung und Verstärkung der Bodenströmungen im Anschluß an die Bildung des Vulkankomplexes vermuten, der wahrscheinlich älter als 5 Millionen Jahre ist.

Das Canyonsystem auf Gran Canaria und dessen submarine Fortsetzung ist sehr gut in der kombinierten topographischen und bathymetrischen Karte zu erkennen. Einer der augenfälligsten Canyons ist der Barranco de Guiniguada im Nordosten der Insel, der über 60 km weit bis in den Schuttfächer hinein verfolgt werden kann, wo er etwa 3.5 km breit und 150 m tief ist.

1 Introduction

Menard (1956) found that volcanic islands and seamounts are surrounded by large volcaniclastic aprons, consisting of material derived through volcanic activity, slides and erosion on the island/seamount, intercalating with the background sedimentation. The apron harbors a great wealth of material from which the temporal, bathymetric and compositional evolution of the island can be reconstructed (Schmincke et al., 1994).

The first systematic deep drilling into a volcaniclastic apron was carried out during ODP Leg 157 in August/September 1994 (Schmincke, Weaver, Firth et al., 1995). Four holes were drilled at different distances around Gran Canaria, Canary Islands. Gran Canaria was chosen because it is one of the best studied oceanic volcanic islands.

Prior to drilling, a number of presite surveys were carried out in order to locate suitable drill sites, chiefly METEOR cruises M16/4 (Wefer et al., 1992) and M24 (Schmincke and Rihm, 1994). During the main presite survey (cruise M24), 2117 km of high resolution multichannel seismic reflection profiles were obtained covering an area of some 20,000 km^2 around Gran Canaria. The M24 seismic reflection lines in the apron north of Gran Canaria are studied here in detail and will be compared to drillsites 953 and 954 of ODP Leg 157. Site 953 is the deepest hole (1158 mbsf=meters below seafloor) and, since the volcanic pedestal was penetrated (Schmincke, Weaver, Firth et al.,1995), contains a major part of the volcanic evolution of Gran Canaria.

The apron north of Gran Canaria contains volcanic deposits derived not only from this island but also from two neighbouring islands, Fuerteventura in the east and Tenerife in the west. With increasing distance from the islands, sedimentation changes from a chaotic to a more stratified pattern, with numerous high amplitude reflectors due to the large impedance contrast between the volcaniclastic deposits and the pelagic/hemipelagic sediments.

Close to the islands, the interpretation of the unmigrated sections was hampered by numerous diffraction hyperbolas. In order to recognize the structure of the apron and to distinguish different source areas, the seismic lines were time-migrated. Correlation with the drillsites was obtained by computing synthetic seismograms. A number of reflections could be identified as volcaniclastic material intercalated with the hemipelagic background sediments. Some reflectors were dated by means of bio–and magnetostratigraphy at Site 953. By applying the depth-velocity relation found at Site 953, the isopach maps were converted to depth. This is important in order to calculate sedimentation rates and to map the submarine geometry of the island flanks allowing more detailed computations of the submarine island volumes.

A bathymetric map was compiled from the swath-bathymetry collected during METEOR cruises M16/4 and M24. The three-dimensional bathymetry illustrates the complex structure of the volcanic apron around Gran Canaria, featuring the steep island flanks, slides and erosional features which are discussed here with special emphasis on mass wasting.

Until recently, relatively few extensive seismic reflection experiments have been carried out around volcanic islands. Apart from the Canary Islands, only the Hawaiian Islands are seismically well known (Watts et al., 1985; ten Brink and Watts, 1985; ten Brink and Brocher, 1987; Rees et al., 1993). Recently, some seismic work was also done around the Marquesas Islands (Filmer et al., 1994; Wolfe et al., 1994). These papers have in common their presentation of a description of the apron structure based on the distinction of seismic units. A detailed temporal correlation with the volcanic evolution is not given. This paper presents, in contrast, a seismic analysis of a volcaniclastic apron based on drilling results.

2 Geology

2.1 Introduction

The Canarian Archipelago is built on the African continental slope and rise and consists of seven major volcanic islands: Lanzarote and Fuerteventura to the east, Gran Canaria, Tenerife, Gomera in the center, and Hierro and La Palma to the west (Fig. 1). The archipelago extends some 450 km from east to west, and 200 km in north–south direction. The closest proximity to the African continent is 115 km, across from the Spanish Sahara. The total surface area is 7273 km^2 (Tenerife 2057 km^2, Fuerteventura 1731 km^2, and Gran Canaria 1532 km^2). The three highest islands are Tenerife (Pico de Teide, 3718 m), La Palma (2429 m), and Gran Canaria (1949 m). Detailed recent reviews on the general evolution of the Canary Islands are given by Schmincke (1976; 1982; 1994).

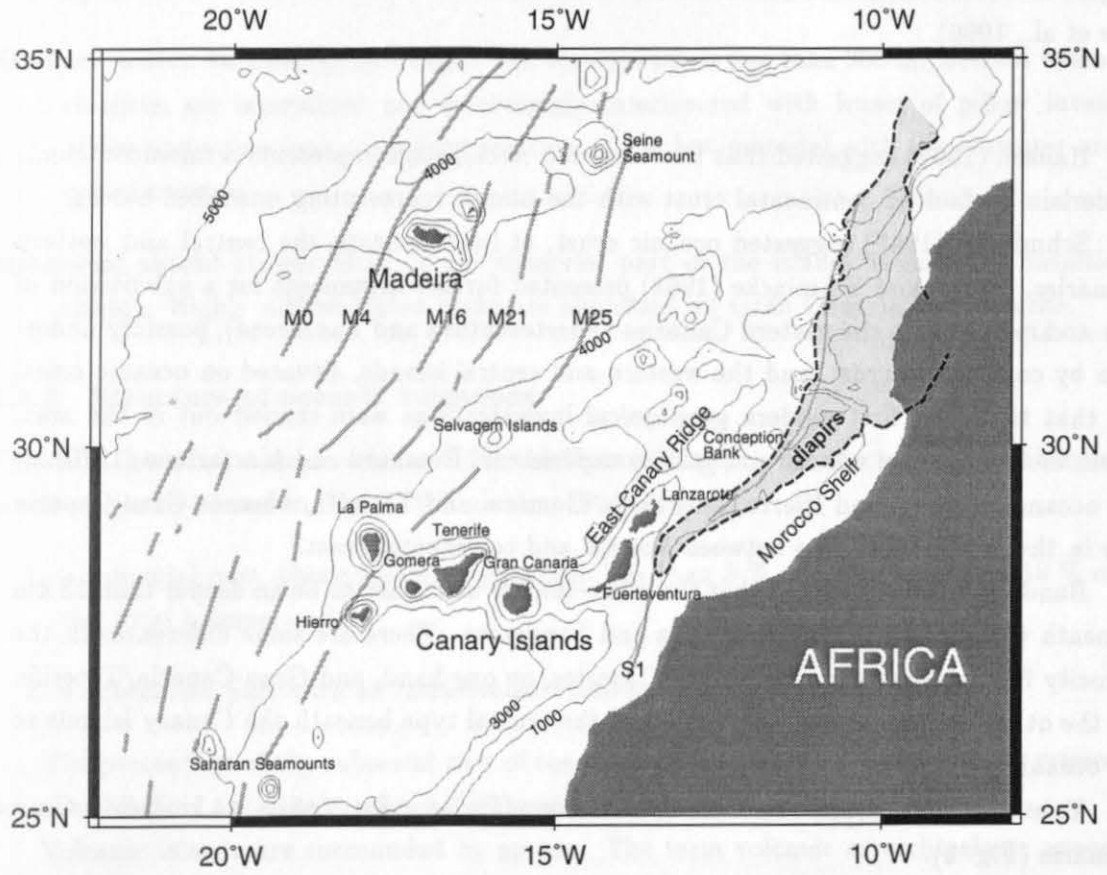

Figure 1: Magnetic anomalies in the vicinity of the Canary Islands (from Verhoef et al., 1991), plotted together with the bathymetry and the salt diapir zone between the Eastern Canaries and Africa (from Hinz et al., 1982).

2.2 The crust beneath the Canary Islands

Whether the crust beneath the Canary Islands is of continental or oceanic type is one of the oldest and most controversial discussions.

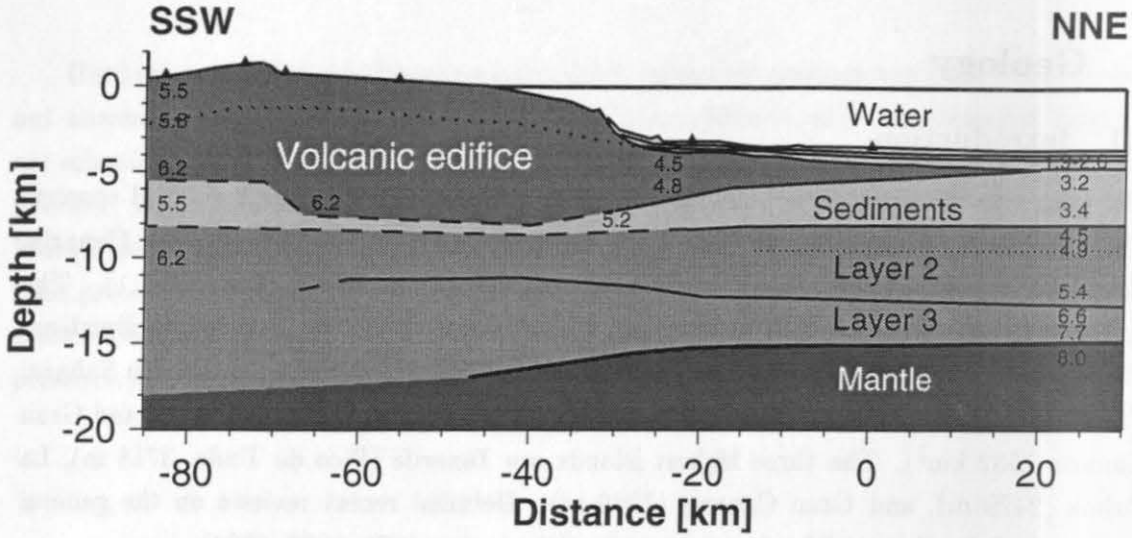

Figure 2: Crustal structure beneath Gran Canaria, deduced from refraction seismic studies (Ye et al., 1996).

Hausen (1962) suggested that the Canarian Archipelago represents a microcontinent, underlain by faulted continental crust with the islands representing unsunken blocks.

Schmincke (1967) suggested oceanic crust, at least beneath the central and western Canaries. Rothe and Schmincke (1968) presented further arguments for a subdivision of the archipelago into the eastern Canaries (Fuerteventura and Lanzarote), possibly underlain by continental crust, and the western and central islands, situated on oceanic crust. At that time, the first modern geophysical investigations were carried out in the area. From their refraction seismic and gravity experiment, Bosshard and Macfarlane (1970) infer oceanic crust around Hierro, La Palma, Gomera, and Tenerife, whereas Gran Canaria lies in the transitional zone between oceanic and continental crust.

Banda et al. (1981) found that the crust–mantle boundary to be no deeper than 15 km beneath Gran Canaria, Fuerteventura and Lanzarote. There are some differences in the velocity function between the eastern Canaries, on one hand, and Gran Canaria/Tenerife, on the other. In conclusion, they interpret the crustal type beneath the Canary Islands to be oceanic.

Ye et al. (1996) found the crust–mantle boundary at a depth of ca. 14 km below Gran Canaria (Fig. 2).

Further evidence for the oceanic crust type beneath the Canaries comes from the plate kinematic reconstruction of Klitgord and Schouten (1986), who localized the Canary Islands on sea floor with an age ranging from 175 to 150 Ma. These ages are confirmed by Verhoef et al. (1991). They traced the 156 Ma old magnetic anomaly M25 between the two westernmost islands La Palma and Hierro (Fig. 1). The anomaly east of Fuerteventura and Lanzarote was called S1 by Roeser (1982). This location agrees with the seaward extent of a series of salt diapirs, marking the approximate landward edge of oceanic crust (Hinz et al., 1982). Roest et al. (1992) interpret the anomaly S1 as true oceanic and Klitgord and Schouten (1986) dated the anomaly at 175 Ma.

To summarize, the present concensus is that all Canary Islands are located on oceanic crust.

2.3 Oceanic volcanoes

2.3.1 Growth stages of oceanic volcanoes

The evolution of volcanic islands can be subdivided into three stages, each of which is characterized by typical deposits in the apron (Schmincke, 1994):

Deep water stage: The submarine part is composed of pillow lavas, densely packed and non-vesicular at depth, becoming increasingly vesicular and interlayered with pillow breccias and pillow fragment breccias and primary and resedimented hyaloclastites upwards.

Shallow water to emergent stage: The water depth is less than 300 m. Bedded hyaloclastites are intermixed and increasingly interlayered with lenses of pillow lavas. Slides and explosions caused by reaction of the hot material with the seawater are quite common.

Subaerial shield stage: Most of the subaerial part of the islands is made of basaltic shields. Highly differentiated rocks are abundant on Gran Canaria and Tenerife.

2.3.2 Structure of oceanic volcanoes

The evolution of an oceanic volcano – like the Canary Islands – as reflected by its structure is schematically shown in Fig. 3. Schmincke (1994) divides

1. a subaerial part whose volume is generally less than 5 % and rarely exceeds 10 % of the total volume, and
2. a submarine part with an intrusive core and submarine extrusive rocks.

The percentage of the subaerial part of the total volume for the Canary Islands ranges between 1.1 % (Lanzarote) and 8.4 % (Tenerife) (Schmincke, 1982).

Volcanic islands are surrounded by aprons. The term volcanic or archipelagic apron was originally introduced by Menard (1956) who defined the apron bathymetrically for a number of Pacific volcanoes. He noticed the smooth relief in the vicinity of these volcanoes, whereas the seafloor distant from the islands is hilly. His definition includes all deposits surrounding the islands, volcanic and non-volcanic. Later, geophysicists used the term *volcanic apron* in a more restricted sense synonymously with what Schmincke (1994) defines as flank facies (see below). Since this paper concentrates on the sediments north of Gran Canaria, the expression *apron* here includes also the sedimentary basins adjacent to the volcanic edifice. Following the definition of Schmincke (1994, see also Fig. 3), a volcanic apron peripheral to an oceanic island consists of three main facies:

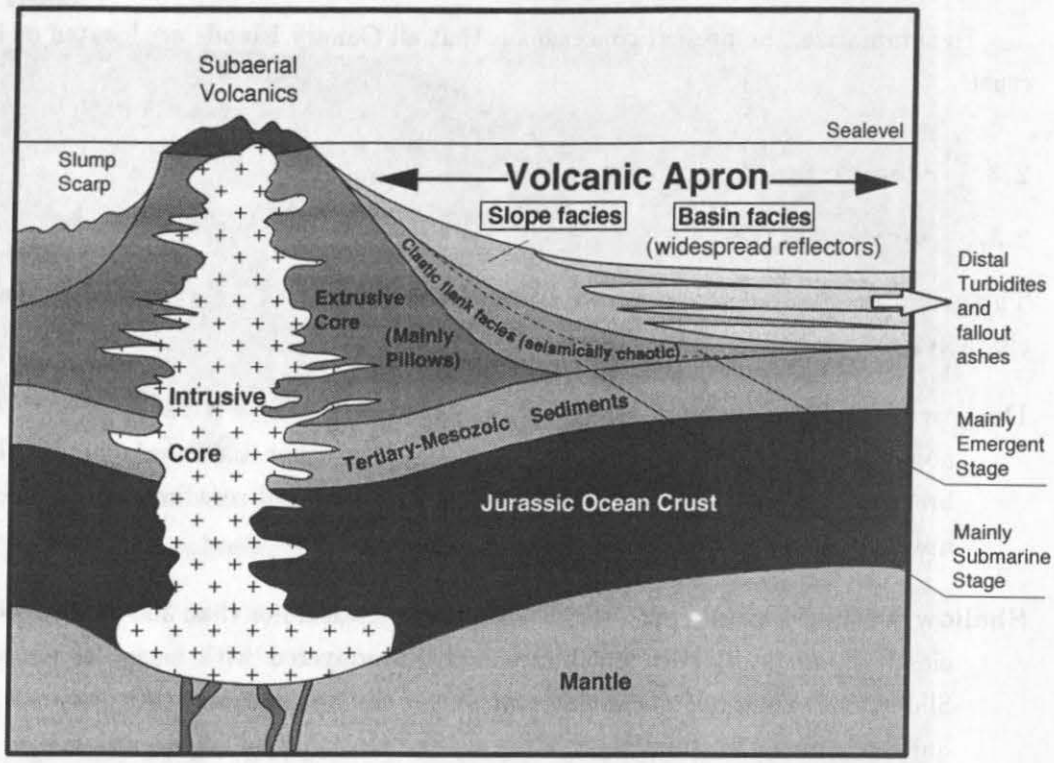

Figure 3: Structure of an oceanic volcano (from Schmincke, 1994).

1. The **flank or core facies** is characterized by rough topography and discontinuous reflectors (chaotic seismic facies or volcanic apron in geophysics, e.g. Wissmann, 1979; Holik and Rabinowitz, 1991). The flanks representing the seamount stage of a volcanic island are thought to largely consist of submarine lavas and coarse breccias (Staudigel and Schmincke, 1984).

2. The proximal or **slope facies** is characterized by slumps, discontinuous bedded units, debris flows, erosional channels, etc.

3. The slope facies grades laterally into the **basin facies** which is characterized by well developed reflectors and groups of reflectors and consists of diverse types of volcaniclastic deposits of medium to small grain size including fallout ash layers, debris flows, distal ignimbrites and lahars, and other volcaniclastic rocks generated by eruptions and by erosion of volcanic rocks. It may also contain slump sheets recording larger volcanic or slope failures relocating sediments initially deposited higher on the slope. The volcaniclastic deposits are interbedded with biogenic and/or siliciclastic terrigeneous sediments forming the background sedimentation to the volcaniclastic influx from the islands.

The basin sediments are further subdivided stratigraphically into different zones reflecting the islands growth stages:

- Volcaniclastic rocks formed under submarine conditions (pillow fragment breccias and nonvesicular hyaloclastites) form the **lower apron facies**.

- Vesicular hyaloclastites formed at very shallow water and voluminous hyaloclastic/pyroclastic/epiclastic deposits formed during the shield-building stage represent the **middle apron facies.**

- Volcaniclastic rocks transported into water by primary flow (lava flows, ash flows), reworked epiclastic debris and fallout from explosive eruptions make up the **upper apron facies.**

2.3.3 Volcanic aprons

Although the general structure of volcanic aprons is already presented above, some points are worthy of discussion in more detail. This includes why aprons of different islands show different structural patterns, and the discussion of some sedimentary processes in the apron. As a starting point for the discussion, a summary of the apron structures of the Canaries, Marquesas and Hawaii is helpful.

The extent of the Hawaiian apron is limited to the flexural moat between the islands and the Hawaiian Arch, some 250 km away from the islands (Rees et al., 1993). The moat and arch were both generated by the response of the lithosphere to loading of the island (Watts et al., 1985). The fill of the moat is divided by Rees et al. (1993) into four main units (Fig. 4):

1. a basal unit of relatively constant thickness, pelagic sediment predating the formation of the flexural moat,
2. a thick wedge onlapping the flexural arch, highly chaotic internal reflectivity, interpreted as buried landslide deposits,
3. a sequence of highly reflective, continuous horizons that offlap the flexural arch and are tilted toward the islands,
4. a ponded unit confined to the deepest part of the moat representing the youngest sediments.

At the Marquesas Islands the moat and arch architecture is not as prominent as that of Hawaii, and no flexural depression is evident in the bathymetry (Wolfe et al., 1994). The apron is characterized by a smooth surface and low slope, and internally by the presence of two sediment units not observed on undisturbed seafloor in the area (Filmer et al., 1994). Filmer et al. (1994) as well as Wolfe et al. (1994) conclude that only a small portion of the apron sediments is pelagic in origin. Most of the apron material must be volcaniclastic turbidites and debris derived from mass wasting of the volcanoes. Filmer et al. (1994) noticed the first evidence of acoustically reflective apron turbidites at about 300 km distance from the islands.

From flexure studies based on refraction seismic and gravity, Watts (1994) deduced a flexure of the crust beneath the Canaries of as much as 4 km with a lateral extent of the moat between 150–200 km away from the islands, fitting the Selvagem Islands in

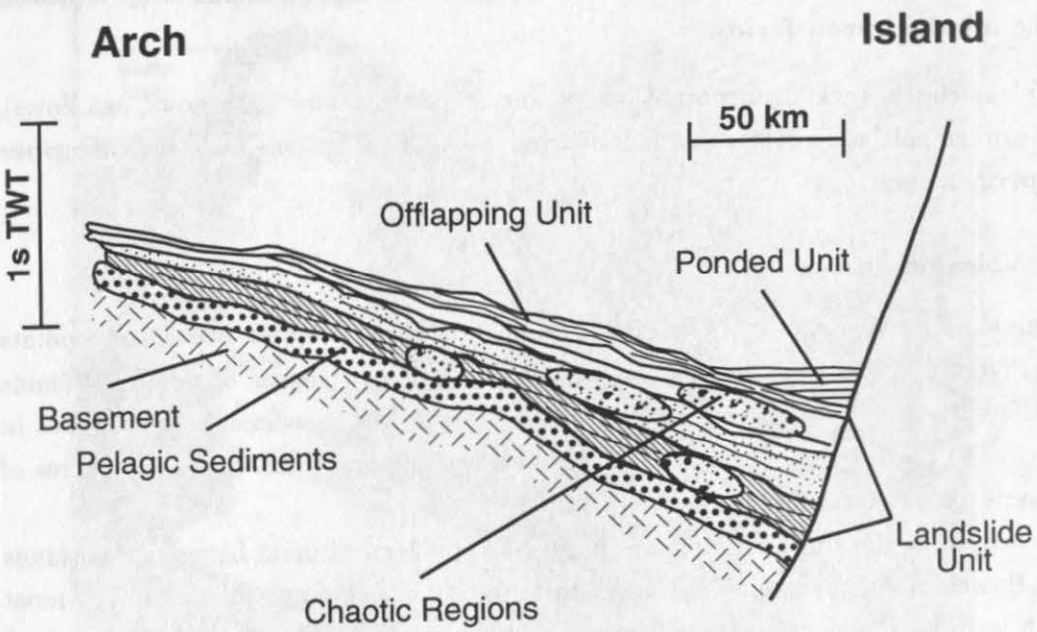

Figure 4: Moat stratigraphy at Hawaii (from Rees et al., 1993).

the north and the Saharan Seamounts in the south as a location of the arch. Funck et al. (1996) found a small islandward dip (0.5°) of a reflector dated slightly younger than the shield stage of Gran Canaria indicating flexure in response to the load of the island. They also found the transition from slope to basin facies at a distance of some 40 km from Gran Canaria. Drilling into the apron (Schmincke, Weaver, Firth et al., 1995) showed that the non-volcanic sediment-influx at this distance is much larger than the island-derived volcaniclastic deposits. The frequent change of these two sediment types ensures a sequence of high seismic impedance contrasts, resulting in a number of high amplitude, continuous reflectors. The aprons south of the Canary Islands contain slumped intervals derived from the African continental margin contrasting with the northern basin (von Rad, Ryan et al., 1979; Schmincke, Weaver, Firth et al., 1995). This is interpreted as a result of the East Canary Rise (Fuerteventura, Lanzarote) forming a morphological barrier towards the northern basin.

Two main factors influence the structure of the apron:

1. the geometry of the lithospheric/crustal flexure with its moat-arch architecture, and
2. the type and volume of sediments available for the apron-fill.

The geometry of the flexure, is controlled by several factors, such as (Watts, 1994):

- the elastic thickness of the underlying lithosphere,

- the amount and distribution of the lithospheric/volcanic load,
- the migration of the load, i.e. rate of plate motion, and
- the superposition with other flexures.

The elastic thickness is influenced by the age of the lithosphere and the amount of thermal rejuvenation caused by a hypothetical underlying *mantle plume*. The amount and distribution of load gives the mechanical boundary conditions. The migration of the load (due to the plate motion) is important in so far as the lithosphere does not respond as an ideal elastic body, but instead with a delay of up to 1 Ma (Bodine et al., 1981). The superposition with other flexures (e.g. those of continental margins) can strongly influence the flexure geometry (Weddeling, 1996) as well as the elastic thickness of the lithosphere (Watts, 1994). It is obvious that there are interdependences.

Type and amount of available sediments strongly determines the internal structure of the apron. If chiefly volcaniclastic deposits are deposited, the impedance contrast is not as high as in the case of intercalated beds of non-volcanic sediments which result in reduced reflectivity. The total amount of sediments controls whether the moat can be filled or not. In the case of small sediment supply, the arch offlapping units and ponded sediments are predominant and a bathymetric moat remains visible.

The main point responsible for the large flexure at the Hawaiian Islands compared to the Marquesas may be seen in the larger load of the Hawaiian volcanoes (Wolfe et al., 1994). The elastic thickness seems to be of minor importance as it is 25–30 km for Hawaii (Watts, 1978; McNutt, 1984; Wessel, 1993) and 17 km for the Marquesas (Filmer et al., 1993). Because the moat volume in the Marquesas is smaller, less sediment is necessary to fill the moat. Hence, the Marquesas moat is overfilled and lacks a bathymetric moat, whereas the Hawaiian flexural moat is underfilled (Filmer et al., 1993), explaining the major stratigraphic patterns at Hawaii (Rees et al., 1993).

The aprons of the Marquesas and Hawaiian Islands largely consists of volcaniclastic sediments whereas in the Canaries non-volcanic interbeds are common and voluminous. The higher non-volcanic sediment-influx can be explained by the higher productivity and deposition of calcareous nannoplankton above the carbonate compensation depth (Schmincke, 1994) and by the proximity of the Canaries to the African continent.

Mass wasting are of two general types: slumps and debris avalanches. Moore et al. (1989) use the following distinction: slumps are slow moving, wide, and thick with transverse blocky ridges and steep toes, while debris avalanches are fast moving, long (compared to width), and thinner. They commonly have a well-defined amphitheater at their head and hummocky terrain in the lower part. The slope failures that produce the slides begin early in the history of individual volcanoes, culminate near the end of subaerial shield building, and apparently continue long after dormancy (Moore et al., 1989).

Slump motion consists of a long-term creeping (e.g. 6 cm/year at southern Hawaii, Segall et al., 1992) and short-term displacements triggered e.g. by earthquakes, whereas avalanches move rapidly in a single event. Parts of slumps may collapse and produce a

debris avalanche, forming a compound landslide (Moore and Normark, 1994).

Slope failures occur both at volcanic slopes and continental margins, but slump deposits in the volcanic environment are seismically difficult to document due to the acoustically opaque behaviour of volcanic deposits (Moore et al., 1989).

The identification of mass failures on the submarine slopes of oceanic volcanoes must thus be based primarily on surface features. Moore et al. (1989) recognized as many as 17 large submarine slides in the vicinity of the Hawaiian Islands using the side-beam sonar system GLORIA. Until now, 68 landslides more than 20 km long are known along the Hawaiian Ridge (Moore and Normark, 1994). Some of them are up to 5000 km^3 in volume and, therefore, of the same scale as the largest known slide at continental margins, the Storegga slide off Norway (Bugge et al., 1988). Recently, Moore et al. (1995) found large slide blocks of up to 10 km length and 500 m height embedded in the toe of the South Kona landslide at Hawaii, forming a field of blocky sea-floor hills 60 to 80 km off the island.

In the Canary Islands, two major slides have been documented so far, the well studied Canary slide east of Hierro (Holcomb and Searle, 1991; Masson et al., 1992) and at the north flank of Tenerife (Watts and Masson, 1995). The volume of the latter was estimated to be at least 1000 km^3.

A reason for the comparatively small number of documented slides at the Canaries might be seen in the high sedimentation rates, masking earlier slides.

Debris flows are associated with many submarine slope failures, transporting large particles, up to boulder size, downslope in a sediment–water slurry (Kearey, 1993). Debris flows and slides may turn into turbidity currents under appropriate hydrodynamic conditions. Voluminous debris flows are reported in the vicinity of the Canary Islands, both of volcanic and continental margin origin. Thick volcanic debris flows were found north and south of Gran Canaria (von Rad, Ryan et al., 1979; Schmincke, Weaver, Firth et al., 1995) and Embley (1976) has mapped a debris flow immediately south of the Canaries, covering 30,000 km^2 of seafloor and extending 700 km from its source scar at the Northwest African continental margin.

2.4 Volcanism on the Canary Islands

2.4.1 Origin of the volcanism

The origin of the Canary Islands is still under dispute, with models proposing e.g. a hot spot origin, a connection with tectonic features on Africa, or fracture zones in the oceanic lithosphere.

The hot spot origin was suggested for the first time by Wilson (1963), noting an age progression in the Canary Islands, interpreted as migration of volcanism over a hot spot (see Fig. 5). Some features at the Canary Islands contrast the classical hot spot model developed for Hawaii:

- The long volcanic history of the entire Canary Archipelago with multiple cycles of

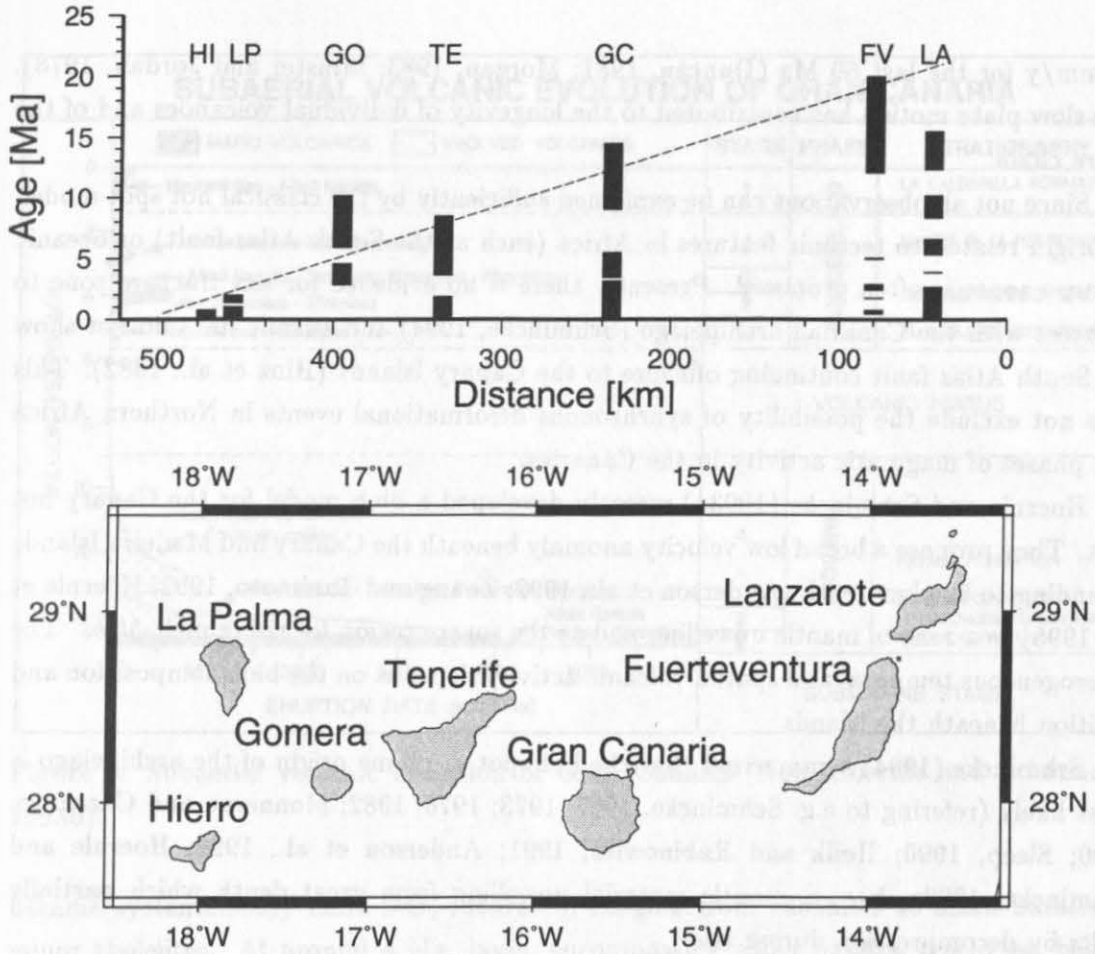

Figure 5: Age progression of the subaerial volcanism on the Canary Islands. Data sources: Lanzarote and Fuerteventura: Coello et al. (1992); Gran Canaria: McDougall and Schmincke (1976), Schmincke (1994); Tenerife: Ancochea et al. (1990); Gomera: Cantagrel et al. (1984); La Palma: Staudigel et al. (1986), Ancochea et al. (1994); Hierro: Fúster et al. (1993).

volcanism on the (older) islands.

- On all Canary islands, except Gomera, volcanic activity is reported for the last 5000 years.
- There is no broad topographic swell and gravity/geoid high typical for other hot spots, e.g. Cape Verde and Hawaii (Watts, 1994; Filmer and McNutt, 1989).
- A low melt productivity for individual islands and the whole chain (Hoernle and Schmincke, 1993a).
- Large temporal and spatial variations in geochemistry (Hoernle and Schmincke, 1993a).

Some of these peculiarities can be explained by the extreme tectonic setting of the Canaries (Hoernle and Schmincke, 1993a): The rate of plate motion has been very low, around

10 mm/y for the last 60 Ma (Duncan, 1981; Morgan, 1983; Minster and Jordan, 1978). The slow plate motion has contributed to the longevity of individual volcanoes and of the entire chain.

Since not all observations can be explained sufficiently by the classical hot spot model, an origin related to tectonic features in Africa (such as the South Atlas fault) or oceanic fracture zones is often proposed. Presently there is no evidence for any fracture zone to intersect with the Canarian archipelago (Schmincke, 1994) and seismic data do not show the South Atlas fault continuing offshore to the Canary Islands (Hinz et al., 1982). This does not exclude the possibility of synchronous deformational events in Northern Africa and phases of magmatic activity in the Canaries.

Hoernle and Schmincke (1993a) recently developed a blob model for the Canary hot spot. They propose a broad low velocity anomaly beneath the Canary and Madeira Islands extending to 500 km depth (Anderson et al., 1992; Zhang and Tanimoto, 1992; Hoernle et al., 1995) as a zone of mantle upwelling and as the source region for rising melt-*blobs*. The heterogeneous temporal and spatial volcanic activity depends on the blob composition and position beneath the islands.

Schmincke (1994) summarized that the hot spot or plume origin of the archipelago is most likely (refering to e.g. Schmincke, 1967; 1973; 1976; 1982; Monnerau and Cazenave, 1990; Sleep, 1990; Holik and Rabinowitz, 1991; Anderson et al., 1992; Hoernle and Schmincke, 1993a, b), i.e. mantle material upwelling from great depth which partially melts by decompression during rise.

2.4.2 Volcanism on Gran Canaria

Three major magmatic/volcanic cycles have been distinguished on Gran Canaria, which have been further subdivided into several stages (Schmincke, 1976; 1982; 1994; Hoernle and Schmincke, 1993a, b). All subaerially exposed volcanic and intrusive rocks were formed during the last 15 Ma (McDougall and Schmincke, 1976).

The subaerial **Miocene Cycle** started with the rapid formation (0.5 Ma) of the exposed tholeiitic to mildly alkalic shield basalts (Guigui and Hogarzales Formation, Fig. 6). At 14 Ma the basaltic shield phase was followed by 0.6 Ma long magmatism of trachytic to rhyolitic composition (Mogan Formation). A large caldera (*Tejeda Volcano*, ca. 20 km diameter, Fig. 7) was formed during the beginning of the phase, synchronously with the deposition of composite ignimbrite P1 on top of the Miocene basaltic shield (Freundt and Schmincke, 1995a, b). P1 was dated 14.1 Ma (van den Boogard et al., 1988) and presents the first of 15 ignimbrites erupted during the Mogan formation. The following Fataga Formation (ca. 13 to ca. 9.5 Ma), with silica–undersaturated trachyphonolites, was accompanied and followed by intrusive syenites and a large cone sheet swarm in the central caldera complex lasting until ca. 8 Ma, except for a few very late dikes. The Miocene phase was followed by a major volcanic hiatus lasting approximately 3–4 Ma.

The **Pliocene Cycle** began with the local emplacement of small volumes of nephelinites and basanites at ca. 5 Ma. The eruption rate increased at ca. 4 Ma and the lavas

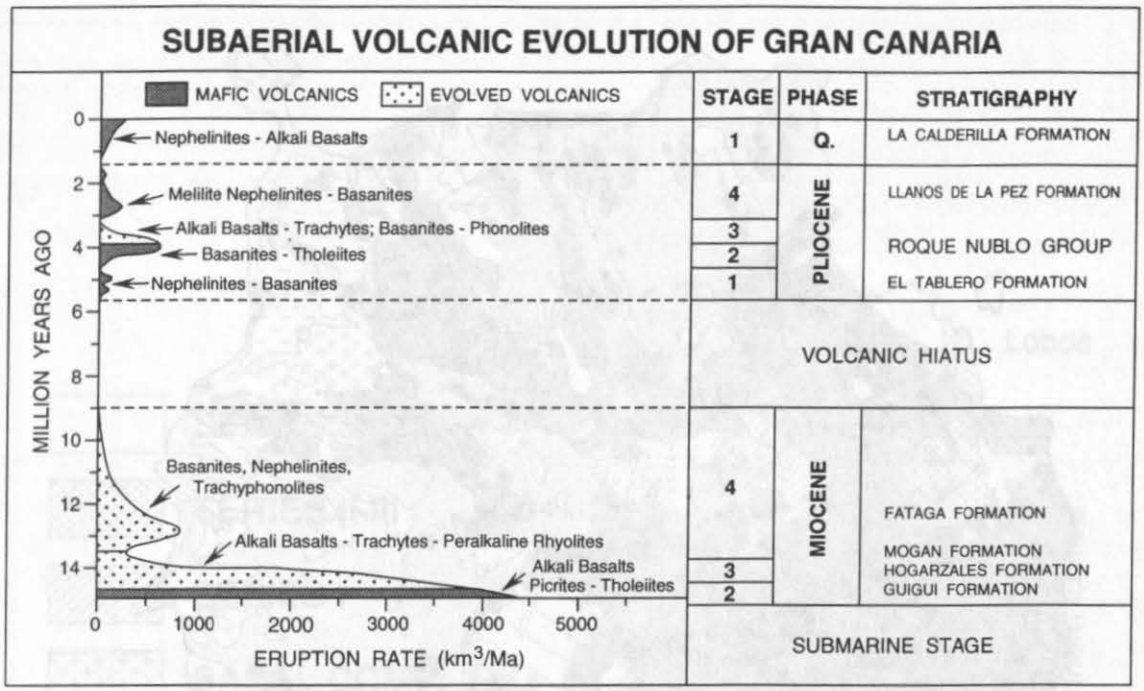

Figure 6: Subaerial volcanic evolution of Gran Canaria (from Hoernle and Schmincke, 1993b).

became systematically more SiO_2-saturated, ranging from basanites to alkali basalts to minor tholeiites. At around 4 Ma, lavas, encompassing alkali basalts, trachytes, basanites, tephrites and phonolites, were intercalated with massive hauyne-phonolite breccia flows, fallout ashes and lithic-rich pumice flows, which were intruded by trachytic and hauyne phonolite domes (**Roque Nublo Group**). The bulk of Roque Nublo volcanics was deposited in the northern half of the island (Fig. 7), where the island had been eroded much more severely. Following a brief hiatus there was a resurgence in volcanism, during which only highly undersaturated mafic volcanics, chiefly nephelinites and basanites, were erupted (3.2–1.8 Ma, Llanos de la Pez Formation).

Quaternary volcanism occurred exclusively in the northern half of the island. The more recent Quaternary volcanics are predominantly basanites. Very young scoria cones (probably prehistoric to subrecent) and lava flows form the La Calderilla Formation.

During the evolution of Gran Canaria, twice the volcanic edifices may have topped as much as 3000 m (Schmincke, 1994; Anguita et al., 1991). The current top of Gran Canaria Pozo de las Nieves is just 1949 m above sea level.

2.4.3 Volcanism on Fuerteventura

Fuerteventura and Lanzarote are part of the East Canary Ridge, roughly parallel to the African coast. The depth of the narrow strait between the two islands is only 40 m. The most recent K-Ar age determinations for the volcanic activity on Fuerteventura have been published by Coello et al. (1992). Therefore, the description below closely follows their paper.

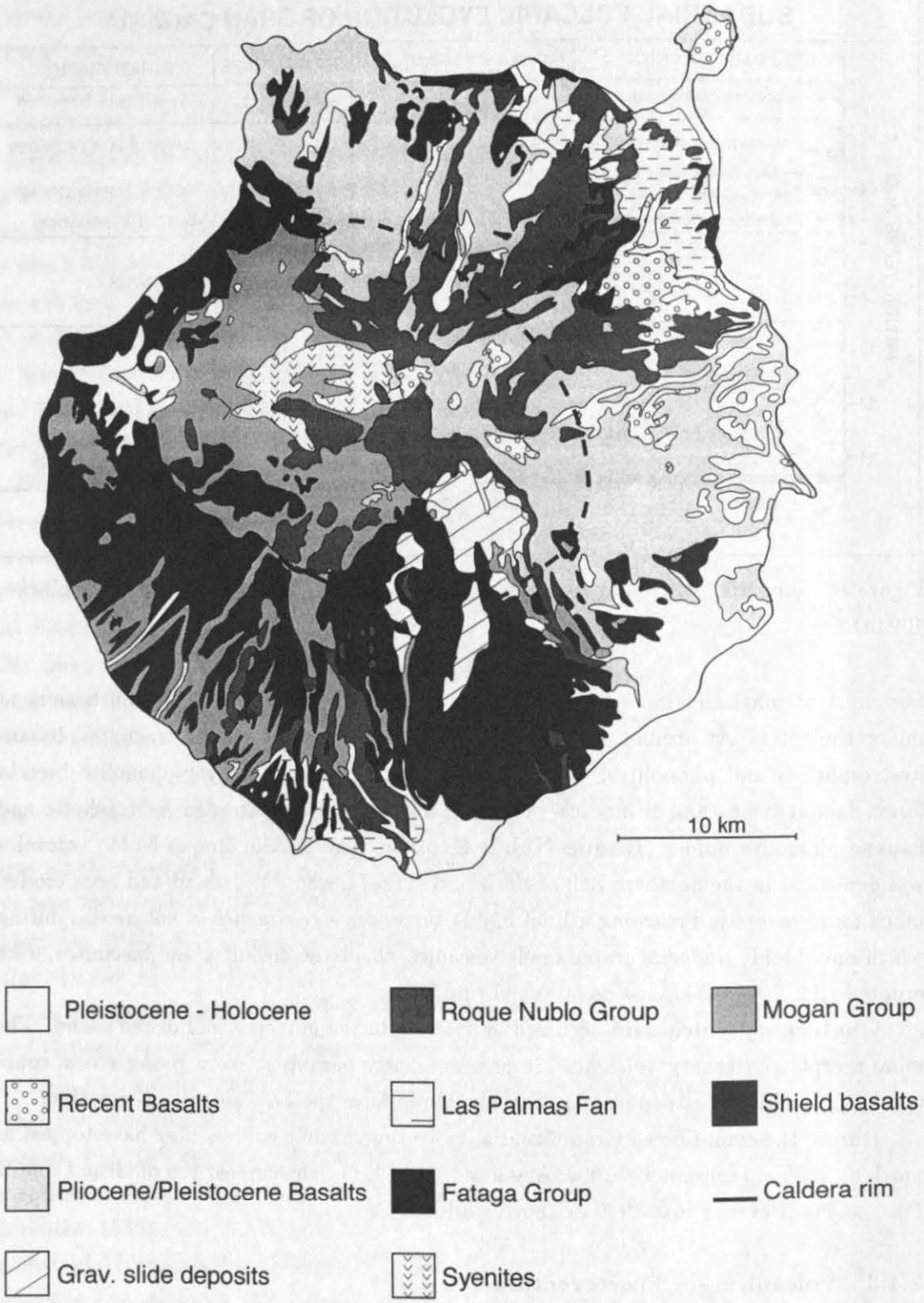

Figure 7: Geological map of Gran Canaria (modified from Instituto Tecnológico Geo Minero de España, 1990).

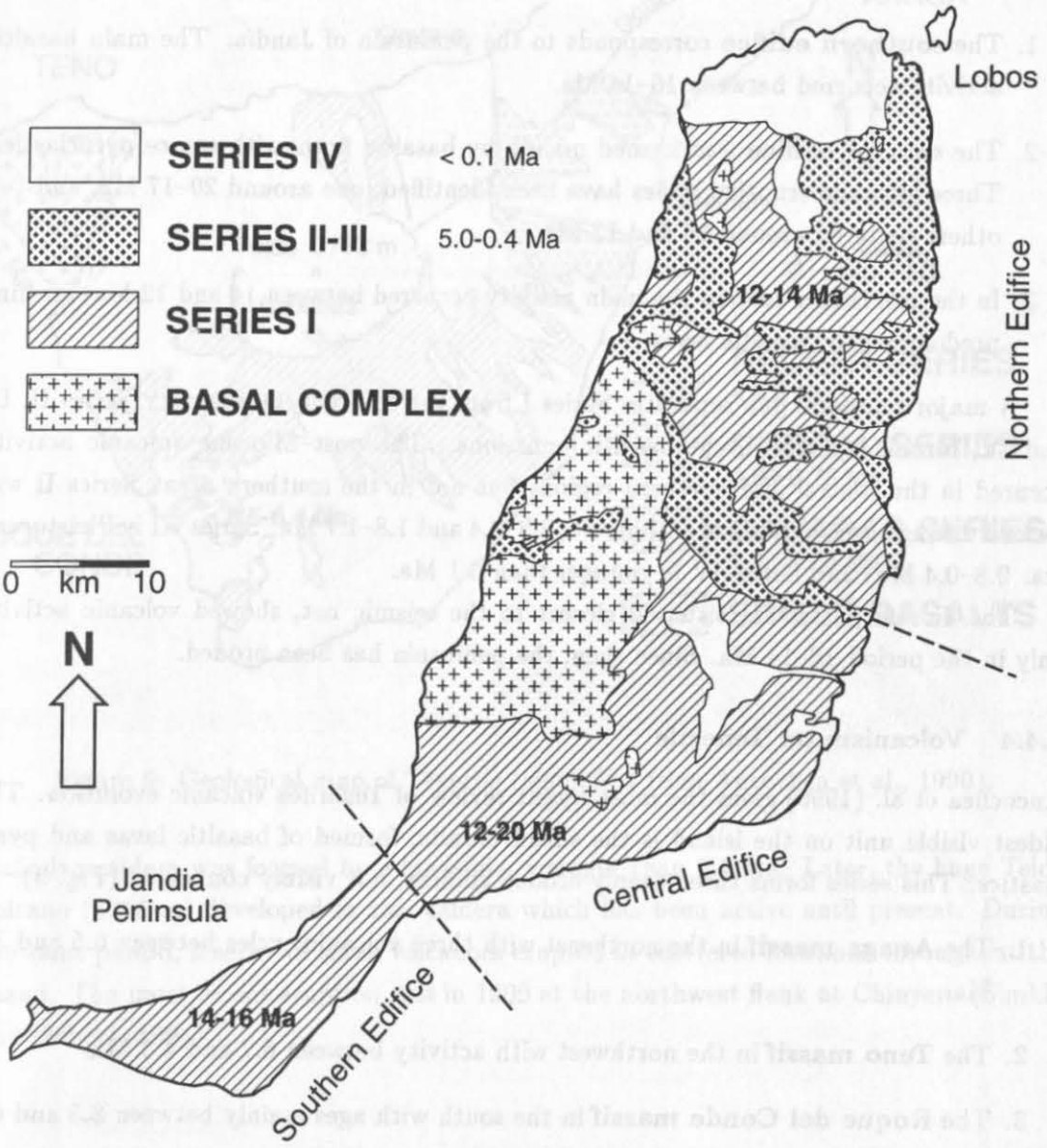

Figure 8: Geological map of Fuerteventura (simplified from Coello et al., 1992).

Two major formations can be distinguished in Fuerteventura: an emerged basal complex and a younger subaerial volcanic series. The basal complex is exposed in the western central part of Fuerteventura (Fig. 8) and consists of Cretaceous turbidites overlain by interbedded Albian-Oligocene sediments and submarine volcanics which are intruded by a very dense dyke network and alkaline plutonics. One dyke was dated as old as 48 Ma (Le Bas et al., 1986). The subaerial Series I was formed by three independant edifices:

1. The **southern edifice** corresponds to the peninsula of Jandía. The main basaltic activity occurred between 16–14 Ma.

2. The **central edifice** was formed mainly by basaltic flows with scarce pyroclastics. Three Miocene eruptive cycles have been identified, one around 20–17 Ma, and two others centered around 15 and 13 Ma.

3. In the **northern edifice** the main activity occurred between 14 and 12 Ma, forming predominantly basaltic lavas.

A major temporal gap separates Series I from the Pliocene/Quaternary Series II, III and IV, formed by multi–vent basaltic emissions. The post–Miocene volcanic activity occured in the central and northern regions but not in the southern area. Series II was formed during three periods of activity: 5, 2.9–2.4 and 1.8–1.7 Ma. Series III is Pleistocene (ca. 0.8–0.4 Ma) and Series IV is younger than 0.1 Ma.

The Jandía peninsula, situated closest to the seismic net, showed volcanic activity only in the period 16–14 Ma. Since then, the peninsula has been eroded.

2.4.4 Volcanism on Tenerife

Ancochea et al. (1990) gives the most recent review of Tenerifes volcanic evolution. The oldest visible unit on the island is the shield basalts, formed of basaltic lavas and pyroclastics. This series forms three deeply eroded edifices, not visibly connected (Fig. 9):

1. The **Anaga massif** in the northeast with three volcanic cycles between 6.5 and 3.6 Ma.

2. The **Teno massif** in the northwest with activity between 6.7 and 4.5 Ma.

3. The **Roque del Conde massif** in the south with ages mainly between 8.5 and 6.4 Ma.

According to Ancochea et al. (1990), the large Cañadas volcano, made up of basalts, trachytes and phonolites, was built essentially between 1.9 and 0.2 Ma. Recently, Martí et al. (1994) and ODP drilling (Schmincke, Weaver, Firth et al., 1995) found several cycles of volcanic activity at the Cañadas edifice as old as 3 Ma. To the northeast this central volcano is linked with Anaga by a chain of basaltic emission centers, the Cordillera Dorsal, with a peak activity around 0.8 Ma. The two large valleys of Guimar and La Orotava were formed by large landslides less than 0.8 Ma ago, possibly before 0.6 Ma. The present

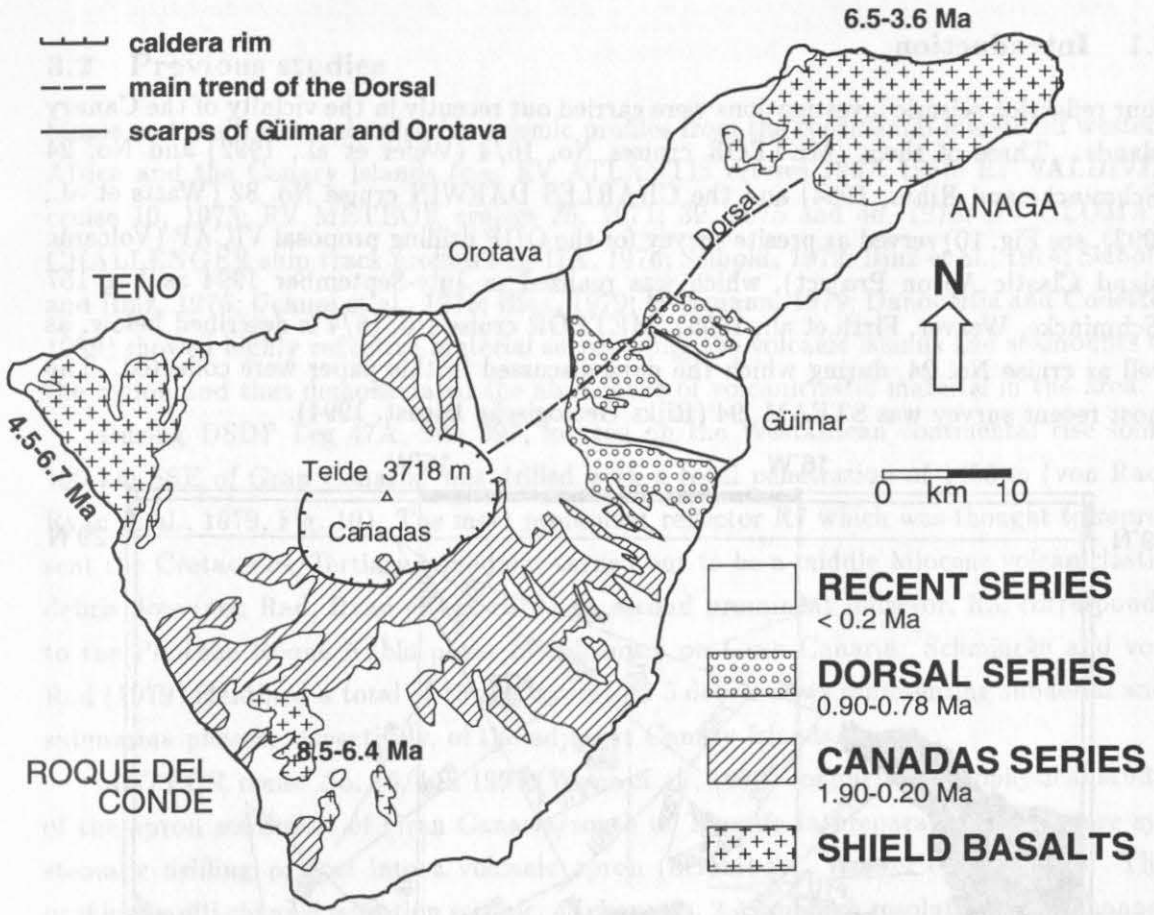

Figure 9: Geological map of Tenerife (simplified from Ancochea et al., 1990).

Cañadas caldera was formed by a landslide, younger than 0.6 Ma. Later, the huge Teide volcano (3718 m) developed in this caldera which has been active until present. During the same period, a series of small volcanoes erupted at scattered locations throughout the island. The most recent eruption was in 1909 at the northwest flank at Chinyero (Simkin and Siebert, 1994).

3 Data collection

3.1 Introduction

Four reflection seismic investigations were carried out recently in the vicinity of the Canary Islands. Three of them (METEOR cruises No. 16/4 (Wefer et al., 1992) and No. 24 (Schmincke and Rihm, 1994) and the CHARLES DARWIN cruise No. 82 (Watts et al., 1993), see Fig. 10) served as presite survey for the ODP drilling proposal VICAP (Volcanic Island Clastic Apron Project), which was realized in July-September 1994 as Leg 157 (Schmincke, Weaver, Firth et al., 1995). METEOR cruise No. 16/4 is described below, as well as cruise No. 24, during which the data discussed in this paper were collected. The most recent survey was STEAM '94 (Rijks Geologische Dienst, 1994).

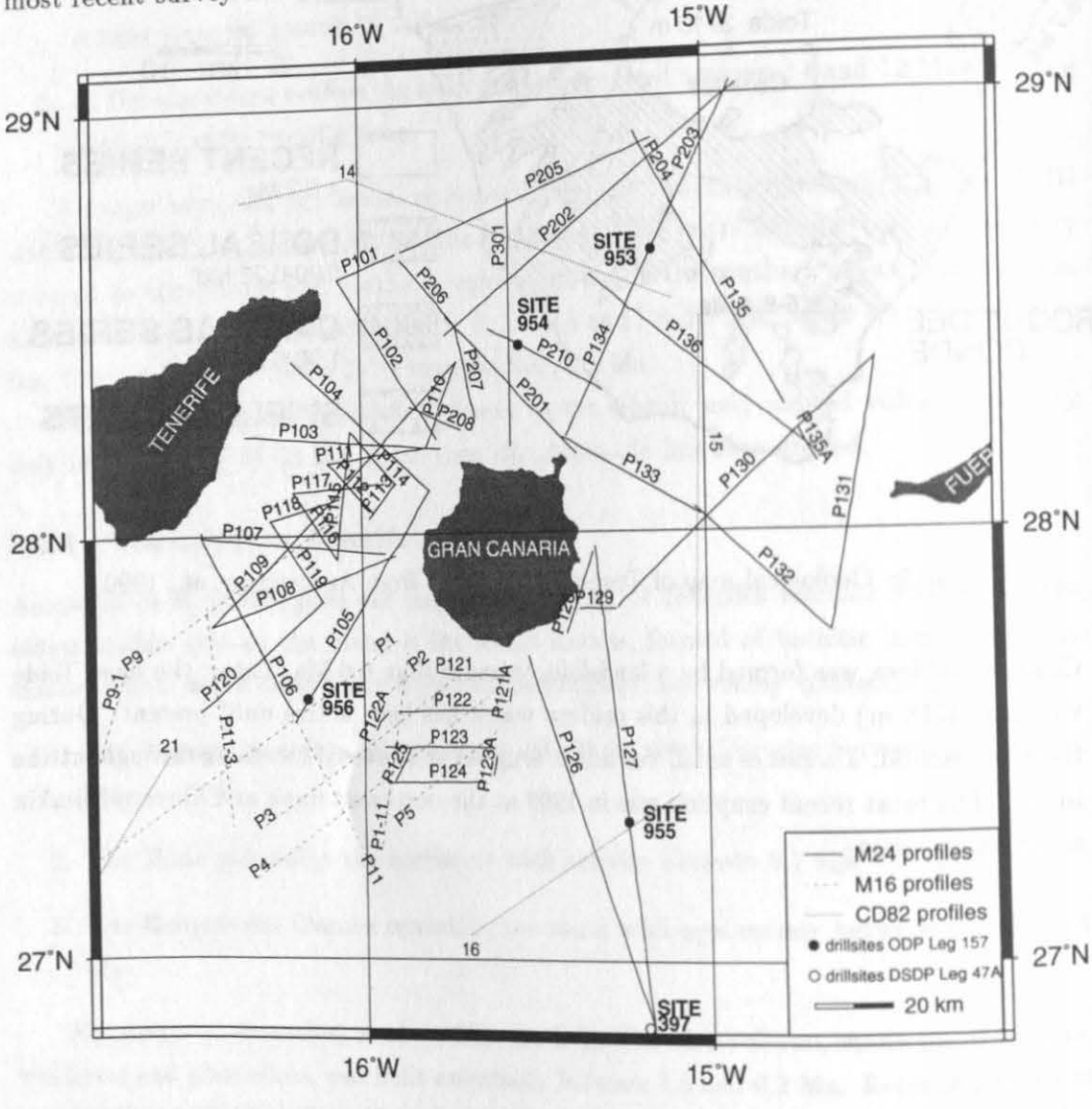

Figure 10: Seismic lines around Gran Canaria collected on the presite–surveys of ODP Leg 157.

The good coverage of high resolution seismic lines around Gran Canaria contributed to the success of ODP Leg 157 during which 4 holes were drilled in the volcanic apron,

and the seismic interpretation has benefitted to a high degree from the drilling results.

3.2 Previous studies

Single and multi channel reflection seismic profiles from the continental margin off western Africa and the Canary Islands (e.g. RV ATLANTIS cruises 1967, 1975; RV VALDIVIA cruise 10, 1975; RV METEOR cruises 25, 1971; 39, 1975 and 46, 1978; DV GLOMAR CHALLENGER ship track profiles Leg 47A, 1976; Seibold, 1972; Hinz et al., 1974; Seibold and Hinz, 1976; Uchupi et al., 1976; Hinz, 1979; Wissmann, 1979; Dañobeitia and Collette, 1989) showed highly reflective material surrounding the volcanic islands and seamounts of the region and thus demonstrated the abundance of volcaniclastic material in the area.

During DSDP Leg 47A, Site 397, located on the Westafrican continental rise some 100 km SSE of Gran Canaria, was drilled with a total penetration of 1453 m (von Rad, Ryan et al., 1979, Fig. 10). The most prominent reflector R7 which was thought to represent the Cretaceous/Tertiary boundary, turned out to be a middle Miocene volcaniclastic debris flow (von Rad, Ryan et al., 1979). A second prominent reflector, R3, corresponds to the Pliocene Roque Nublo phase of volcanism on Gran Canaria. Schmincke and von Rad (1979) identified a total of 15 ash layers and 5 debris flows representing subaerial and submarine phases, respectively, of the adjacent Canary Islands.

METEOR cruise No. 16/4 in 1991 (Wefer et al., 1992) conducted a geophysical study of the apron southwest of Gran Canaria/south of Tenerife in preparation for a more systematic drilling project into a volcanic apron (Schmincke, Weaver et al., 1992). The profiles (multi channel reflection seismic, 48 channels, 2.4 km; high resolution multi channel reflection seismic, 6 channels, 80 m; gravity; magnetic; sedimentechography (Parasound) and swath bathymetry (Hydrosweep)) are shown in Fig. 10. The profile orientation and spacing with a total length of 950 km was chosen in order to allow identification of the outer limit of the island flanks. Results of this cruise are presented in Hirschleber et al. (1992), Geisslinger (1993), and Thywissen and Wong (1993).

3.3 METEOR cruise No. 24

METEOR cruise No. 24 in April and May 1993 was the main presite-survey for ODP Leg 157. The goal was to complete the METEOR 16/4 dataset with emphasis on the channel between Gran Canaria and Tenerife, and the apron north and northeast of Gran Canaria. A connection to DSDP Site 397 was established (Fig. 10). A detailed description of the reflection seismic experiment is given below.

3.3.1 High resolution reflection seismic acqusition

High resolution reflection seismic data were recorded along 50 profiles with a total length of 2117 km (Fig. 10), using the equipment of the Department of Earth Sciences, University of Århus, Denmark. Source and recording parameters are summarized in Table 1.

A sleevegun cluster consisting of 4 guns with a total volume of 2.3 litres was used

Acquisition control unit:		EG&G Geometrics ES2420
	No. of channels:	24
	Sample interval:	1 ms
	Bandpass–filter:	20–360 Hz
	Data format:	SEG-D demuliplexed
Acoustic source:		4 x HGS sleeveguns
	Configuration:	cluster 0.5 x 0.5 m
	Volume:	4 x 40 inch^3 (0.65 l)
	Pressure:	100 bar
	Firing rate:	5, 7.5, 10 s
	Ship speed:	4.9 knots
	Firing delay:	12 ms
	Firing syncronization:	+/- 1 ms
	Tow wire length:	30 m
	Towing depth:	2 m
Streamer:		Teledyne
	Channels:	24
	Hydrophones per group:	7
	Group length:	3.125 m
	Group spacing:	6.25 m
	Total length:	143.75 m
	Tow cable length:	90 m
	Nominal towing depth:	4 m

Table 1: Seismic equipment and field parameters.

as an acoustic source. Bubble-oscillations were effectively suppressed by the narrow gun clustering, increasing the signal to noise ratio. The 24 channel streamer had a group spacing of 6.25 m resulting in a total length of 143.75 m. Before storage in SEG-D demultiplexed format (Northwood, 1967), the data were bandpass-filtered (20–360 Hz). The sampling rate was 1 ms. The firing rate was chosen depending on the water depth in order to get a high data coverage; the recording windows were adapted accordingly (Table 2). The firing rates of 5, 7.5 and 10 s correspond to a nominal shotpoint distance of 12.5, 18.75, and 25 m, respectively, with a ship speed of 4.9 knots (2.5 m/s). Results of the reflection seismic investigations in the channel between Gran Canaria and Tenerife are given in Krastel (1995).

3.3.2 Other measurements

Magnetic and gravity data were also collected (see also Dañobeitia et al., 1994). The sedimentechographic system Parasound transmits a parametric pulse with a differential

Water depth [m]	Start delay [ms]	Record length [ms]	Firing rate [s]
< 1125	0	3000	5
1125–3000	1500	4000	7.5
> 3000	3500	4000	10

Table 2: Relationship between water depth, record window and firing rate.

frequency between 3.5 and 5.5 kHz, and is therefore comparable to the classical 3.5 kHz echosounder. Due to the parametric pulse, the horizontal resolution is enlarged (Spieß, 1992). The swath bathymetry system Hydrosweep recorded continuously during the entire cruise. A swath of 59 beams provides bathymetric information from twice the width of the actual water depth.

A deep seismic study was carried out during the cruise using ocean bottom seismographs in combination with land based seismometers, concentrating on the northern apron of Gran Canaria (Ye et al., 1996).

At some stations, sediments were sampled, accompanied by heat flow measurements. These results are presented in Schmincke and Rihm (1994).

3.4 ODP Leg 157

ODP Leg 157 drilled 7 Sites (Sites 950 through 956) in August and September 1994. Three are located in the Madeira Abyssal Plain (Sites 950–952) and four (Sites 953–956) in the volcaniclastic apron of Gran Canaria. The first results are published in the *Initial Reports of the Ocean Drilling Program* (Schmincke, Weaver, Firth et al., 1995).

Sites 953 and 954 were drilled in the basin north of Gran Canaria, Sites 955 and 956 to the southeast and southwest of the island, respectively (Fig. 10). The main drilling parameters are summarized in Table 3.

Site	Position	distance from Gran Canaria	water depth [m]	penetration [m]	recovered core [m]	recovery [%]
953	28.6503°N, 15.1446°W	58 km	3578	1158.70	761.68	65.7
954	28.4366°N, 15.5321°W	30 km	3485	446.90	249.36	55.9
955	27.3258°N, 15.2308°W	56 km	2854	599.40	534.08	89.1
956	27.6151°N, 16.1633°W	44 km	3442	703.50	457.88	65.1

Table 3: ODP–Leg 157 drillsites around Gran Canaria.

When the cores were on board, a number of procedures were carried out, described in detail in the *Explanatory Notes* in Schmincke, Weaver, Firth et al. (1995). This includes e.g. core description and sampling in order to determine the litho-, bio-, and magnetostratigraphy, the petrography, mineralogy, geochemistry, and physical properties

of the sediments.

The logging program used the following tools: a seismic stratigraphic tool string, a lithoporosity tool string, a geochemical tool string, and the formation microscanner (FMS). Downhole measurements were affected by bad hole conditions at two sites in the northern basin: at Site 953 logging was limited to the interval between 372 and 975 mbsf (=meters below seafloor), and at Site 954 logging was cancelled after technical problems.

The two main parameters relevant for reflection seismic purposes are density and velocity since they determine the reflectivity. Measurements concerning these properties are thus briefly described below. The P-wave velocity was determined using four different methods:

1. The **P-wave logger** (PWL) of the multi-sensor-track (MST) had sampling intervals between 1.5 and 3 cm. Measurements were made along sections of up to 1.5 m length with the sediments inside the plastic core barrel liner. At the ends of the sections, values are erroneous as well as when voids occurred in the liner.

2. The **Digital Sound Velocimeter** (DSV) was used in soft sediments. Two piezoelectric transducers were inserted into the split sediment cores, measuring the travel time of an acoustic pulse between them.

3. The **Hamilton frame** was used when the material became more consolidated. One transducer is placed on the cut surface of the core while the other is directly beneath it, in contact with the core barrel liner. The sample interval using DSV and Hamilton frame was typically between 1 to 5 per 1.5 m-section.

4. The **digital sonic tool** (SDT) for downhole measurements recorded the traveltime along the borehole wall between a source–receiver array. The vertical resolution of the tool is approximately 2 feet (61cm).

Method 4 is an in-situ measurement, whereas the first three methods were carried out shipboard, on sediment cores which had experienced rebound.
The density was calculated according to three procedures:

1. The **gamma-ray attenuation porosity evaluator** (GRAPE) of the multi-sensor-track had a sampling interval of 0.5 to 2.5 cm along whole sections. The method is based on comparing the attenuation of gamma rays through the cores with the attenuation through an aluminium standard (Boyce, 1976).

2. Bulk density was determined within the framework of the **Index Properties** measurements. The mass of a discrete sample was measured using an electronic balance and subsequently the volume was measured with a helium pycnometer.

3. The **High-temperature Lithodensity Tool** (HLDT) uses a ^{137}Ce source of gamma rays. Attenuation of gamma rays is caused primarily by Compton scattering, which is a function of electron density. This is converted to bulk density

assuming that the ratio of atomic weight and the atomic number for most common rock-forming elements is about 2:1.

4 Data processing

4.1 Reflection seismic

The seismic data were processed in two steps:

1. Prestack processing at the Department of Earth Sciences, University of Århus, Denmark.
2. Poststack processing at GEOMAR, Kiel.

The final goal of the processing was to obtain optimized time-migrated sections. Each processing step was carefully checked to prevent a reduction of the bandwidth of the signal, i.e. to preserve the high resolution of the data. Since the profiles were needed urgently at the ODP–databank in order to evaluate the drilling proposal, the processing attempted to minimize CPU-time whenever possible. This was most important with regard to the time consuming migration, especially in view of the data density (trace-distance 3.125 m, sampling rate 1 ms).

The individual processing sequences for each line are shown in the Appendix. The description of the processing follows below and is mainly a summary of the more exhaustive description in Schmincke and Rihm (1994) and Krastel (1995).

4.1.1 Prestack processing

For the prestack processing in Århus the software package NORSEIS, developed by GECO, Norway, was used. The following processing sequence was applied:

Editing: The demultiplexed data were dumped and near-trace plots were displayed in order to identify missing shots and noisy/bad channels which then were excluded from further processing. In addition, the front mute was determined.

Delay: The airgun delay and start delay of the record window were compensated.

Reverse polarity: The polarity of the data was set according to the standard of the Society of Exploration Geophysicists (normal polarity).

CMP sorting: The data were sorted to common mid point (CMP) coordinates, using the field geometry setup. In addition the static corrections for the depth of the source and receiver were applied.

NMO correction: The short streamer length (143.75 m) and the large water depths (as deep as 3650 m) in the survey area did not allow a detailed velocity analysis. Even in shallow water, a velocity analysis was mostly meaningless, because here the seafloor was generally formed by the volcanic basement and, hence, only the seafloor reflection was visible. Therefore, a regional stack velocity was used: 1500 m/s in the water, 1600 m/s in the upper 400 ms of sediment, and 3000 m/s below and in the basalts. The uncertainty of stack velocities is not expected to affect the stack quality because data will stack under a broad fan of velocities.

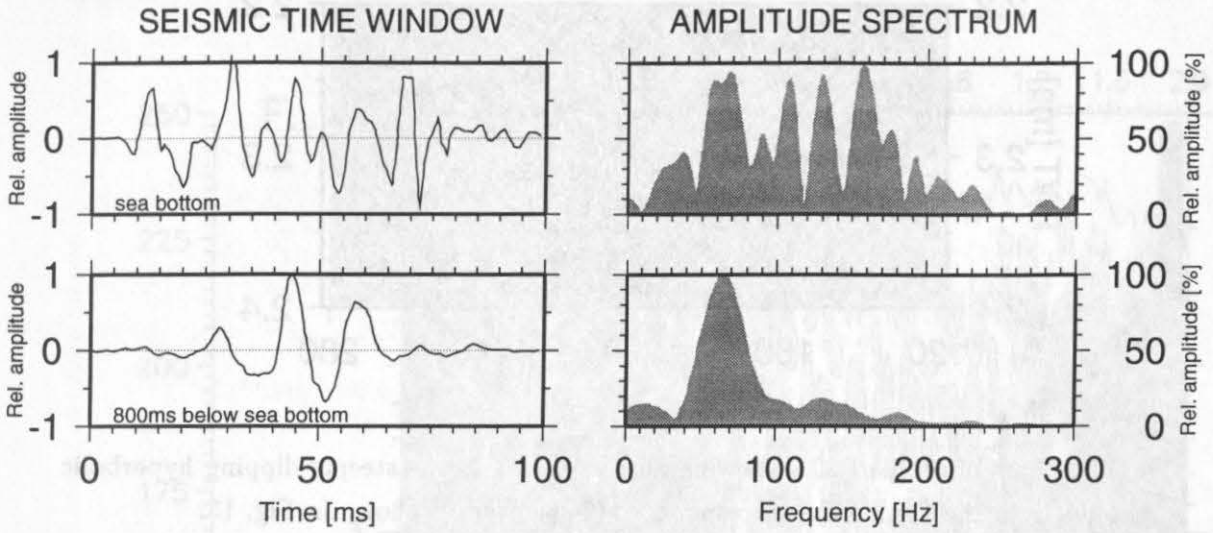

Figure 11: Frequency spectra of CMP 1080 of line P203: a) at sea bottom, and b) of a reflector 800 ms below sea bottom.

Offset-dependant scaling: In order to obtain the statistically optimal stack, offset dependant scaling was done. This is a time invariant scaling, aiming at a constant amplitude level for the 24 traces in the offset direction.

Stacking: Data were stacked 3, 4, and 6 fold depending on the firing rate given in Table 2. The stacked traces were normalized with 1/(number of folds) and written on tape in SEG-Y format.

4.1.2 Poststack processing

The peculiarities of the survey area are reflected in the stacked lines. These are mainly the steep island flanks and the rough topography close to the islands, resulting in numerous diffractions. Therefore, a migration of the profiles was absolutely necessary in order to move dipping reflectors into their true subsurface position and to collapse diffractions, in order to improve the spatial resolution and facilitate interpretation. For the poststack processing, the software package GEOSYS (GECO–Prakla) was used and each process was considered carefully, because the success of the final migration is not only dependent on the proper choice of parameters but also on the effectiveness of the previous processing steps.

Eighteen lines in the apron north of Gran Canaria and in the channel between Gran Canaria and Fuerteventura were migrated (listed in Appendix).

Resampling: The analysis of the amplitude spectra (Fig. 11) shows that the seismic energy lies between 20 Hz and 240 Hz. Resampling from 1ms to 2 ms was therefore possible without aliasing effects, since the Nyquist frequency is 250 Hz. The resampling saved time for all subsequent processes, particularly for the migration.

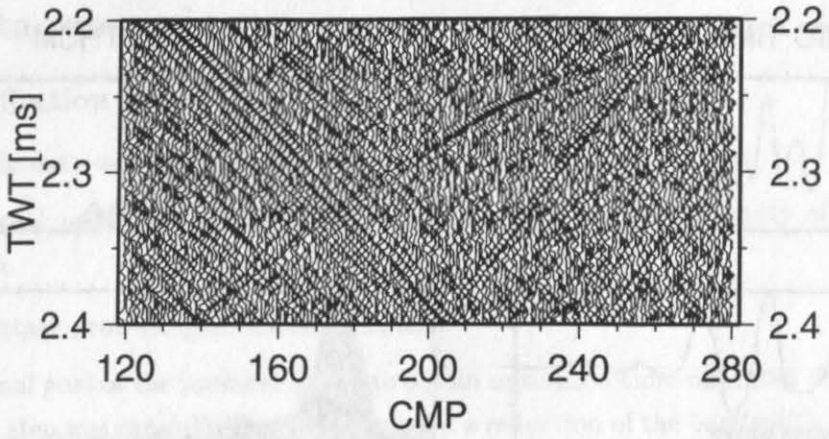

Figure 12: Part of profile P201, showing aliased energy at the steeply dipping hyperbolic reflections from the flank. The corresponding fk-spectrum is shown in Fig. 13.

Band-pass filter: In order to improve the signal/noise ratio, time variant band-pass filters were applied. The filter parameters were determined by means of amplitude spectra and band-pass filtered panels. In general, the low cut frequency lies between 20 and 40 Hz, the high cut frequency between 235 and 160 Hz (decreasing with depth/time).

Coherency filter: In one case (line 204) a coherency filter was applied to improve the correlation of reflectors. The use of the filter has to be weighed very carefully since CPU–time consumption is considerable.

fk-filter: Although the CMP trace spacing is very dense (3.125 m), some spatial aliasing occurred at very steep diffraction hyperbolas (Fig. 12). Without counteracting, dispersive noise would have been introduced during migration. Therefore, two methods were applied: sometimes a high-cut filter was sufficient to eliminate the energy, in other cases a dip filter (fk-filter) removed the aliased energy (Fig. 12, 13). Dip filtering below 3 ms/trace was suitable in most cases.

Deconvolution: In general primary reflections were not disturbed by water–bottom multiples as the penetration of seismic energy (1–2.5 s in the basins) was mostly less than the water depth (4.7 s in the basins). Strong water–bottom multiples only occurred at the volcanic flanks with no or only minor sediment coverage. Some of these multiples could be removed by the use of a predictive deconvolution. The area in consideration lies mostly at the steep island flanks where the CMP stacked data can not assume approximately vertical incidence and zero-offset recording. Nevertheless, the amplitude of the multiples could be reasonably reduced. The Automatic Gain Control (AGC) applied to the final display increased the amplitude again where no other reflections were inside the scaling window.

Stacked data composition: On the more or less horizontally layered parts of the sections, no spatial aliasing is expected. This could influence the success of the migra-

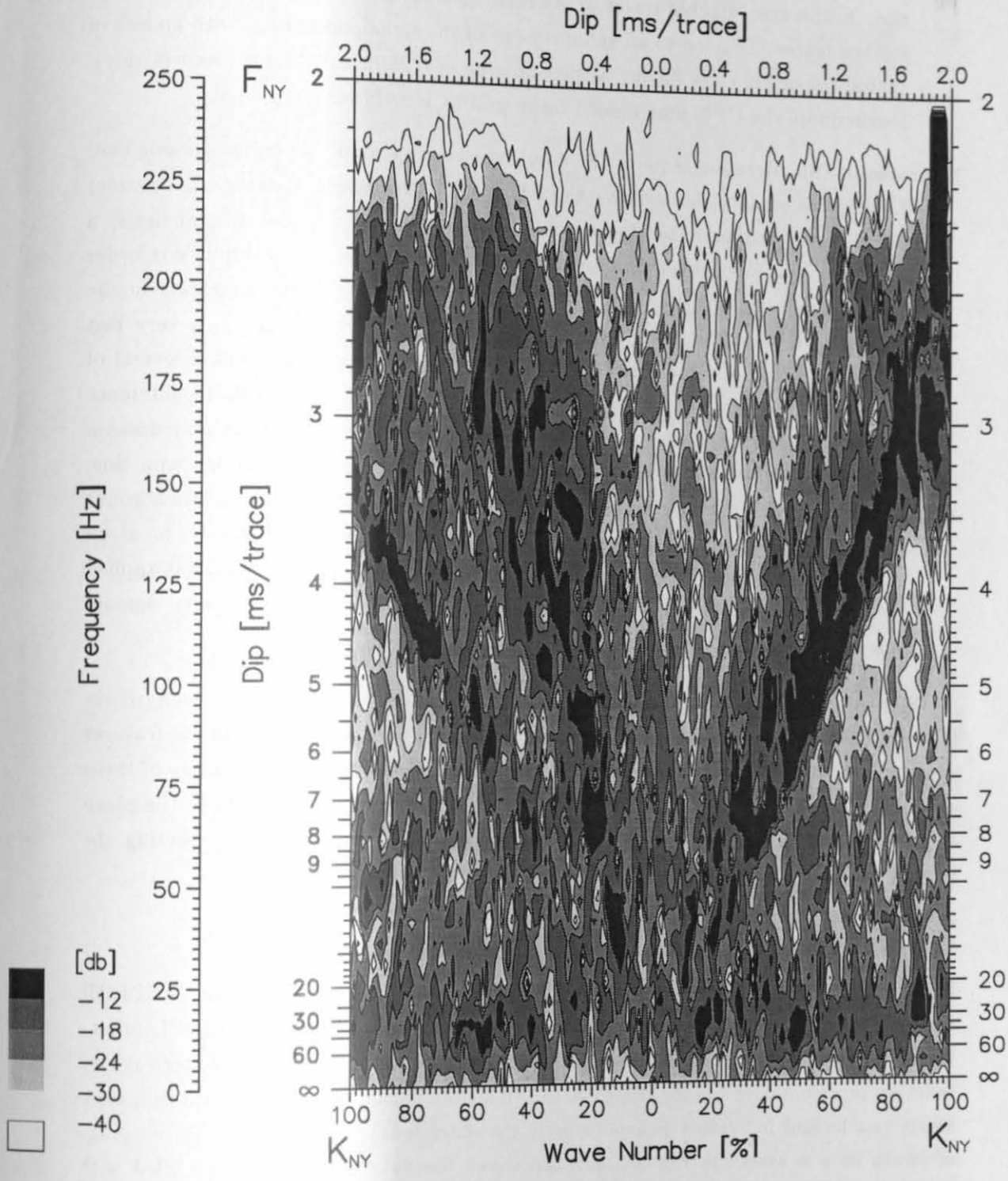

Figure 13: fk–spectrum of data shown in Fig. 12, showing aliased energy. In order to avoid introduction of dispersive noise by migration, a dip filter has to be applied.

tion. In this area, stacked traces were usually generated from every two or four CMP stacked traces. This led to an enhancement of the signal/noise ratio with no loss of spatial resolution (now having a trace spacing of 6.25 m and 12.5 m, respectively). Furthermore the CPU-time needed for migration is reduced accordingly.

Migration: The migration requires the input of a velocity model along the seismic line. Usually this model is derived from the velocity analysis prior to stacking. As streamer length compared to water depth was not sufficient to carry out this analysis, a number of test migrations with variable migration velocities were computed in order to find a suitable velocity distribution. For this purpose, a time migration in the frequency–wavenumber (fk)–domain was used (Stolt, 1978). This is a very fast algorithm which assumes a homogeneous subsurface. Along each profile several of these tests were carried out to define a macro model for the final finite–difference (fd) migration in the time–space (tx)–domain or in the frequency–space (fx)–domain using a 63 degree or 45 degree operator, respectively. The fd migration as a time migration is very robust and tolerates large velocity errors while taking into account vertical and lateral variations of velocity. The fx–algorithm is very effective for steep dipping events without introducing much dispersive noise and, therefore, was applied to the steep island flanks, whereas the slightly faster fd migration in the tx–domain was applied further basinwards.

Since the island flanks are characterized by a rough morphology, some energy is reflected and diffracted from structures beside the profile. Such three-dimensional features can not be treated properly with the applied 2D–migration and hence remnants of these side echoes are still visible. In particular, diffraction hyperbolas from outside the plane could not be collapsed completely. This has to be kept in mind when interpreting the lines.

4.2 Bathymetry

Processing of the Hydrosweep swath bathymetry data collected during the METEOR cruises No. 16/4 and 24 was carried out using the software *mbsystem* developed at Lamont–Doherty Earth Observatory. After computing new depth values based on a water velocity function representative for the survey area (mblevitus databank of the mbsystem), erroneous swaths and individual beams (mostly the outer four) were deleted. The coverage of swath lines is shown in Fig. 14 and also shows the data gaps which were filled with GEODAS data (National Geophysical Data Center, 1993) and, at a few locations, with GEBCO data (British Oceanographic Data Center, 1994).

The bathymetric data were merged with a topographic data set in order to identify relations between submarine features and structures onshore. For this reason the 1:100,000 scale Spanish military maps (Servicio Geográfico del Ejército, 1981–1992) of Gran Canaria (100,000 points), Tenerife (50,000 points), and partly Fuerteventura (20,000 points) were digitized.

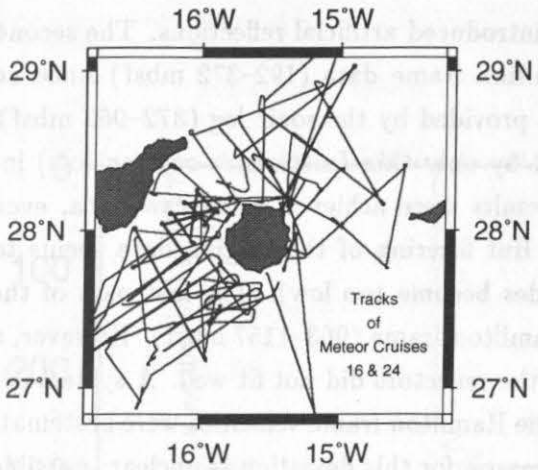

Figure 14: Coverage with Hydrosweep swath-bathymetry lines around Gran Canaria, collected during METEOR cruises No. 16/4 and 24.

The final gridding was made with the mbsystem, applying a spline interpolation for data gaps. The grid cell size was chosen between 0.2 and 0.5 minutes, according to the size of the actual map. The layout of the maps (Fig. 19, 20, 23, 24) was generated using the GMT–software (Wessel and Smith, 1991) with options of 3D-view and artificial illumination (shading).

4.3 Synthetic seismograms

The computation of synthetic seismograms is an important tool for correlating seismic data with the lithostratigraphy of drillholes. The standard method to obtain synthetic seismograms is to use impedance logs from downhole measurements. Impedance is the product of P-wave velocity and bulk density. However, since the two ODP drillsites in the apron north of Gran Canaria were not logged intensely (at Site 953 only 53 % of the hole was logged, and at Site 954 no logging was carried out at all), the logging dataset was not sufficient to compute complete synthetic seismograms. For integration of the drilling results, the intervals missing in the logging data were filled with laboratory measurements carried out on the recovered sediments. This was quite successful in the case of Site 953 and, with limitations, for a larger part of Site 954 (as discussed below).

At Site 953, a huge amount of different velocity and density measurements was available, which were, to a large extent, overlapping each other. Velocity data were provided by the P-wave logger of the multi-sensor-track (MST, depth interval 0–192 mbsf), DSV (0–76 mbsf), Hamilton frame (187–1157 mbsf), and sonic log (372–963 mbsf). Density data were available from the GRAPE sensor of the MST (0–1157 mbsf), the Index Properties (0–1157 mbsf), and the density log (372–987 mbsf). These data had to be processed and merged in a trial and error process to find the best correlation between the seismic line P134 (on which Site 953 is located) and the computed synthetic seismogram.

In the end, the MST data (0–192 mbsf) were used for the upper part of the final velocity function (Fig. 15), because the data density of the overlapping DSV–data was only about 1 per 5 m. The erroneous values at the ends of each measured core-section (1.5 m length) were deleted. Furthermore, a median filter (filter length 0.25 m) had to be

applied because the broad scatter in the data introduced artificial reflections. The second part of the velocity function consists of Hamilton frame data (192–372 mbsf) since no other data were available. The third part was provided by the sonic log (372–963 mbsf). Since the main part of reflections is produced by only thin (meter-size or even less) interbeds of volcaniclastic material, the best results were achieved using raw data, even though some spikes are probably erroneous. But filtering of the logging data seems to flatten the characteristics too much (amplitudes become too low). The last part of the velocity function was again made using the Hamilton frame (963–1157 mbsf). However, a velocity correction had to be applied because the reflectors did not fit well. A systematic offset was detected below ca. 720 mbsf where the Hamilton frame velocities were systematically higher than the logging velocities. The reason for this deviation is unclear; possible explanations include:

- systematic error in the Hamilton frame measuring instrument (improbable),
- selective coring, i.e. softer sediments with a lower velocity tend to be washed out of the core,
- selective measuring, that is the measured points are not representative for the cored sediments,
- anisotropy, because the velocity measured using the Hamilton frame was made perpendicular to the core axis, i.e. in the bedding plane, not along the core axis.

Nevertheless, the average velocity for the interval 720–963 mbsf was 306 m/s higher for the Hamilton frame than for the sonic log. Therefore, 306 m/s was applied as the velocity correction.

The final density function contains only Index Properties measurements. The GRAPE density was eliminated because the necessary filtering of the values for the upper interval (0–192 mbsf), in combination with the smooth-filtered MST velocities, did not produce the necessary impedance variations to fit the observed reflections. In the lower interval down to 1157 mbsf, the GRAPE densities are erroneous, since the applied rotary drilling technique resulted in core disturbances and variable core diameters. The decision as to whether to use Index Properties or the density log was made on the basis of a comparison of the correlation with the seismic data. The Index Properties proved to be slightly better.

At Site 954, the situation is more complicated. On the one hand, the seismic reference line P210 for comparison with the synthetic seismogram is located 200 m downslope of the drillsite where different reflectors of different dip result in a more difficult correlation. On the other hand, only core measurements are available, i.e. no quality check is possible with in-situ downhole measurements. Moreover, the core recovery was only 55 %. In other words, no data are available for 45 % of the hole. Therefore, the velocity function was composed of the DSV (0–50 mbsf), and Hamilton frame data below 50 mbsf. The MST data were excluded, since the loose sand intervals did not transmit sound effectively. For the density function, Index Properties values were used again.

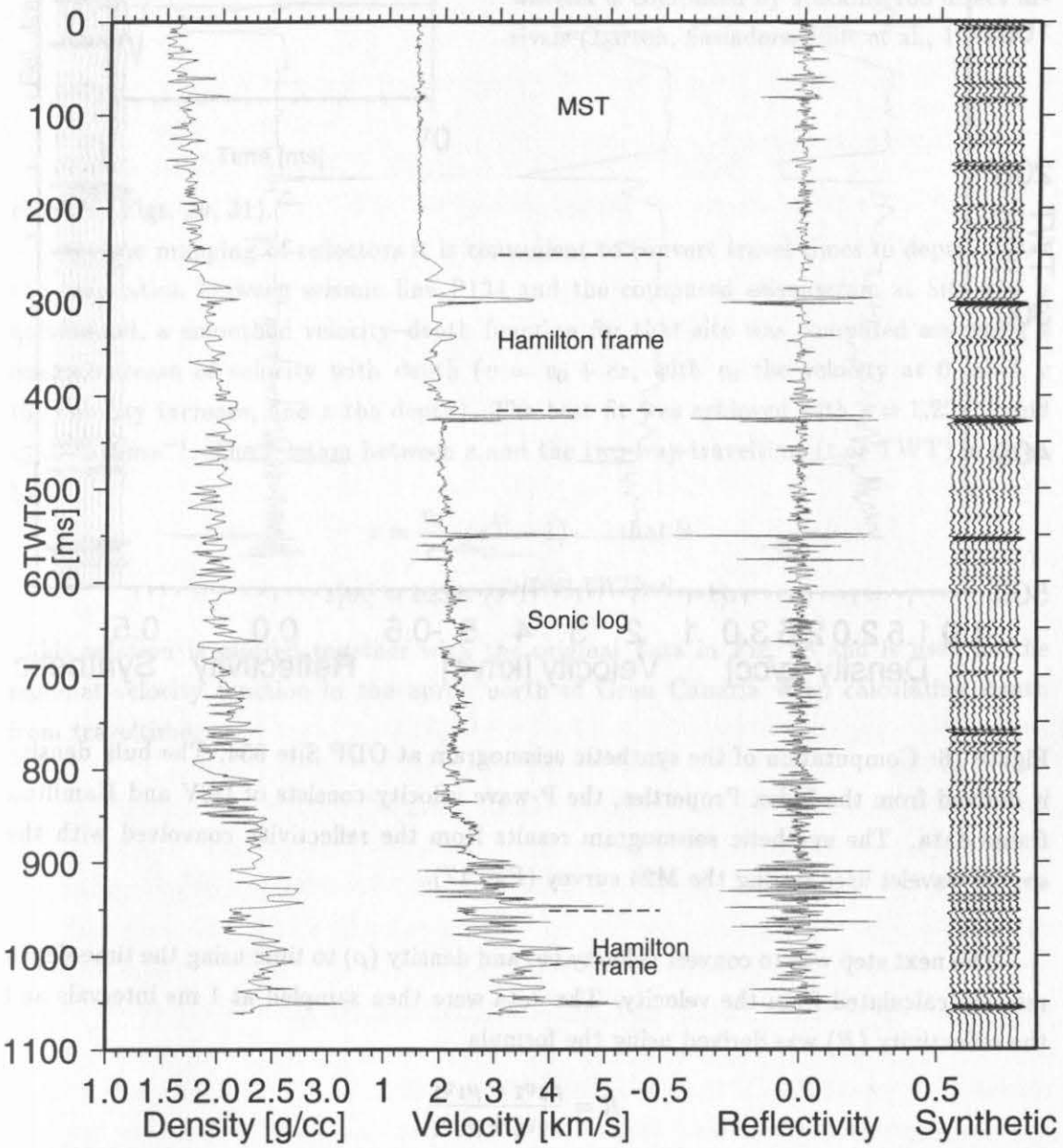

Figure 15: Computation of the synthetic seismogram at ODP Site 953. The bulk density is derived from the Index Properties, the P-wave velocity is composed of MST, Hamilton frame, and sonic log data. The synthetic seismogram results from the reflectivity convolved with the source wavelet used during the M24 survey (Fig. 17).

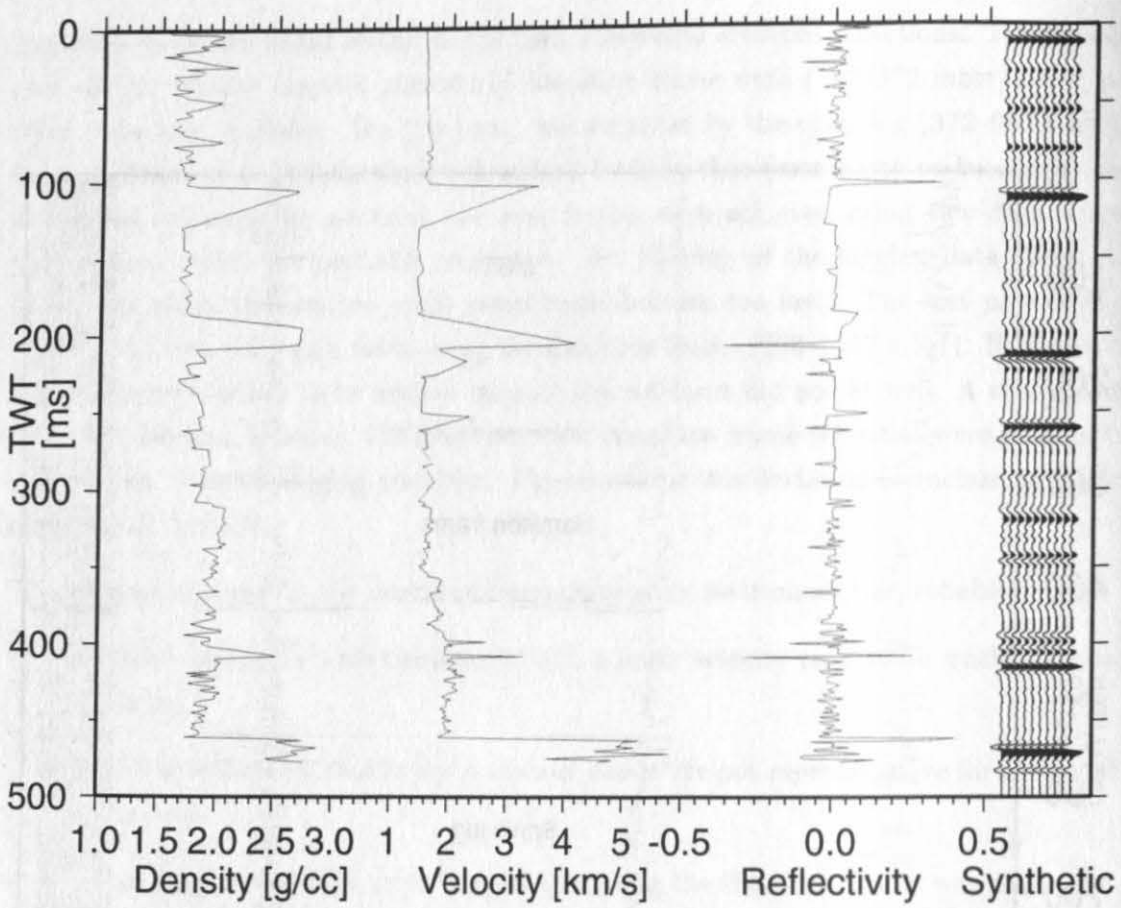

Figure 16: Computation of the synthetic seismogram at ODP Site 954. The bulk density is derived from the Index Properties, the P-wave velocity consists of DSV and Hamilton frame data. The synthetic seismogram results from the reflectivity convolved with the source wavelet used during the M24 survey (Fig. 17).

The next step was to convert velocity (v) and density (ρ) to time using the time-depth relation calculated from the velocity. The data were then sampled at 1 ms intervals and the reflectivity (R) was derived using the formula

$$R = \frac{\rho_2 v_2 - \rho_1 v_1}{\rho_2 v_2 + \rho_1 v_1}$$

with the indices 1 and 2 distinguishing two successive samples. The reflectivity was then convolved with the source wavelet used during the reflection seismic survey (Fig. 17). The wavelet was computed from stacking 100 direct arrivals using the same sleevegun cluster as during METEOR cruise No. 24 (Larsen, Saunders, Clift et al., 1994). The computed synthetic seismograms do not consider internal multiples. However, comparsion with the seismic data justifies this simplification.

To closely match the original seismic lines, the synthetic seismograms were resampled at 2 ms, random noise was added, the data were band-pass-filtered correspondingly (time variant) and an AGC normalization was applied. The synthetic seismograms are shown in Figs. 15 and 16; the correlation with the original seismic lines is discussed in the next

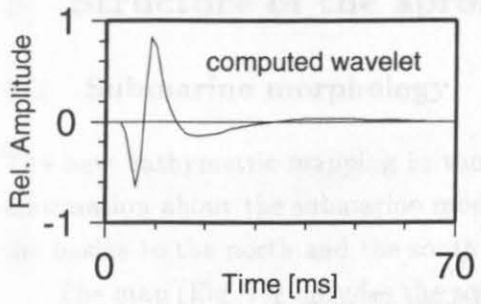

Figure 17: Source wavelet of the sleevegun cluster used during METEOR cruise No. 24. The wavelet is computed by stacking 100 direct arrivals (Larsen, Saunders, Clift et al., 1994).

chapter (Figs. 29, 31).

For the mapping of reflectors it is convenient to convert travel times to depth. Since the correlation between seismic line P134 and the computed seismogram at Site 953 is quite good, a smoothed velocity–depth function for that site was computed assuming a linear increase of velocity with depth ($v = v_0 + cz$, with v_0 the velocity at 0 mbsf, c the velocity increase, and z the depth). The best fit was achieved with $c = 1.22s^{-1}$ and $v_0 = 1532ms^{-1}$. The relation between z and the two-way-traveltime (t or TWT) is given by

$$z = \frac{v_0}{c} \cdot (e^{\frac{tc}{2}} - 1) \quad \text{, that is}$$

$$z[m] = 1256 \cdot (e^{0.00061 \cdot TWT[ms]} - 1).$$

This relation is plotted together with the original data in Fig. 18 and is used as the regional velocity function in the apron north of Gran Canaria when calculating depth from traveltime.

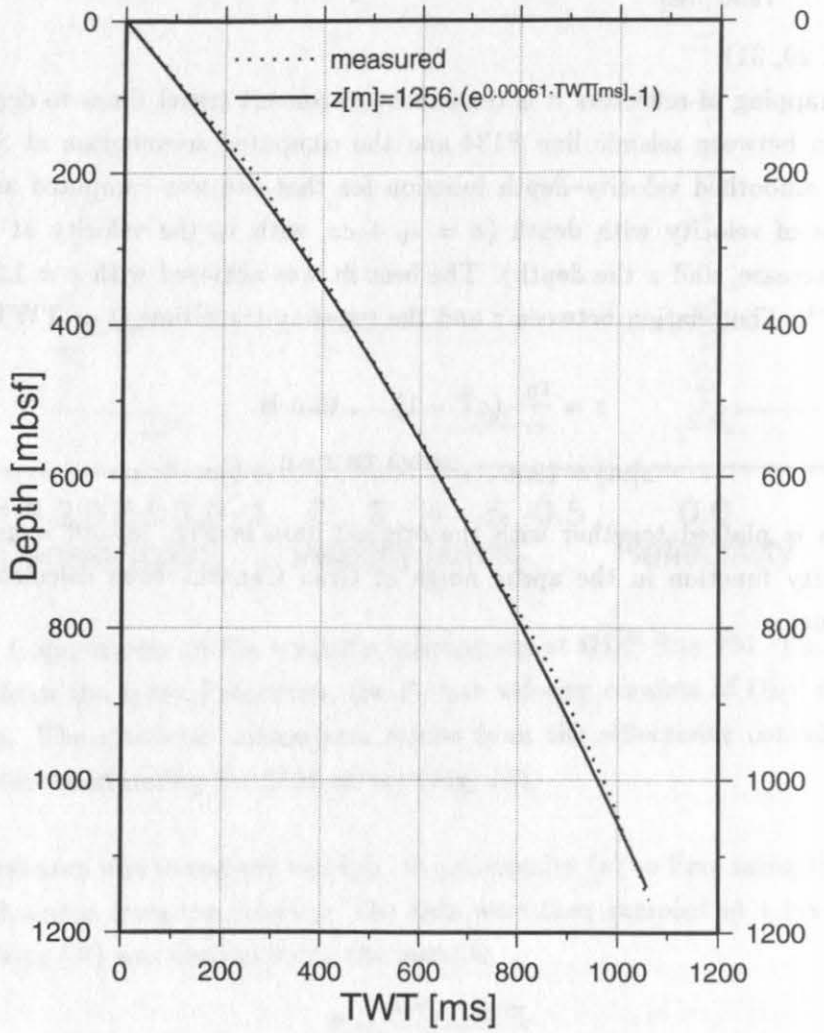

Figure 18: Relation between two-way-traveltime and depth below sea floor at ODP Site 953. The dotted line shows the original data used for computation of the synthetic seismograms, the solid line gives the best fit to the data assuming a linear increase of velocity with depth ($v = v_0 + cz$).

5 Structure of the apron

5.1 Submarine morphology

The new bathymetric mapping in the area between Fuerteventura and Tenerife provides information about the submarine morphology of Gran Canaria, the adjacent islands, and the basins to the north and the south.

The map (Fig. 19) includes the southwestern tip of Fuerteventura, Gran Canaria, and the larger part of Tenerife. The submarine shelf of Fuerteventura extends some 30 km to the WSW, reflecting 14 million years of erosion at the abrasion platform on the tip of the Jandia peninsula. Some 25 km to the northwest (28°13'N, 14°46'W), there is a ca. 60 m deep round to elliptic plateau with a diameter of 12 km. The channel between the plateau and Fuerteventura is ca. 850 m deep. In navigational charts (e.g. Bundesamt für Seeschiffahrt und Hydrographie, 1991) the plateau is annotated as *Bajo de Amanay* (engl. Amanay Shallow).

As the word shallow is not an appropriate geological term, the structure has to be discussed in more detail. The expression *guyot* fits very well the observed morphology. Hess (1946) originally defined a guyot as a flat-topped peak, circular or oval in plan view, and with relatively steep side slopes suggesting a volcanic cone. All these criteria are fulfilled, apart from the fact that later Smoot (1980) demanded a minimum summit plateau area of 167 km^2 (= 50 nm^2). Even though the plateau area is smaller, in a morpholigical sense it is a guyot. The depth of the flat plateau is 60 m and hence shallower than 200 m, where an arbitrary boundary separates guyots (> 200 m) from oceanic banks (< 200 m) which are morphologically identical (Menard, 1964). Therefore the name Amanay Bank is the correct term for the plateau. The slope of the Amanay Bank is up to 16° (towards the northwest between the 1000 and 2000 m isobath).

Gran Canaria lies 85 km to the west of Fuerteventura, an almost circular island with a diameter of ca. 45 km. Deviations from these circular patterns are visible in the form of concave indentations in the coast-and shelfline. The channel between the two islands forms a topographic swell between the basins north and south of Gran Canaria. The depth of the channel is 1550 m, whereas the channel between Gran Canaria and Tenerife is 60 km wide and 2250 m deep. Tenerife, with its volominous Pleistocene volcanism, has no pronounced shelf; the steep slopes onshore Tenerife seems to continue under water.

The basin north of Gran Canaria is 3650 m deep and is protected from continent-derived sediment influx by the East Canary Ridge (Schmincke, Weaver, Firth et al., 1995), formed by Fuerteventura, Lanzarote and, as northward submarine continuation, the Concepcion Bank (Fig. 1). The north-south elongation of the ridge is 350 km. The southern basin, however, has received a large terrigeneous input from Africa, and has frequently derived slumps from the continental margin (von Rad, Ryan et al., 1979; Schmincke, Weaver, Firth, et al., 1995), resulting in a slight decrease in water depth towards the continental margin (0.5° slope dip south of Gran Canaria). The water depth south of Gran Canaria (3000–3400 m) is less than north of the island (3650 m).

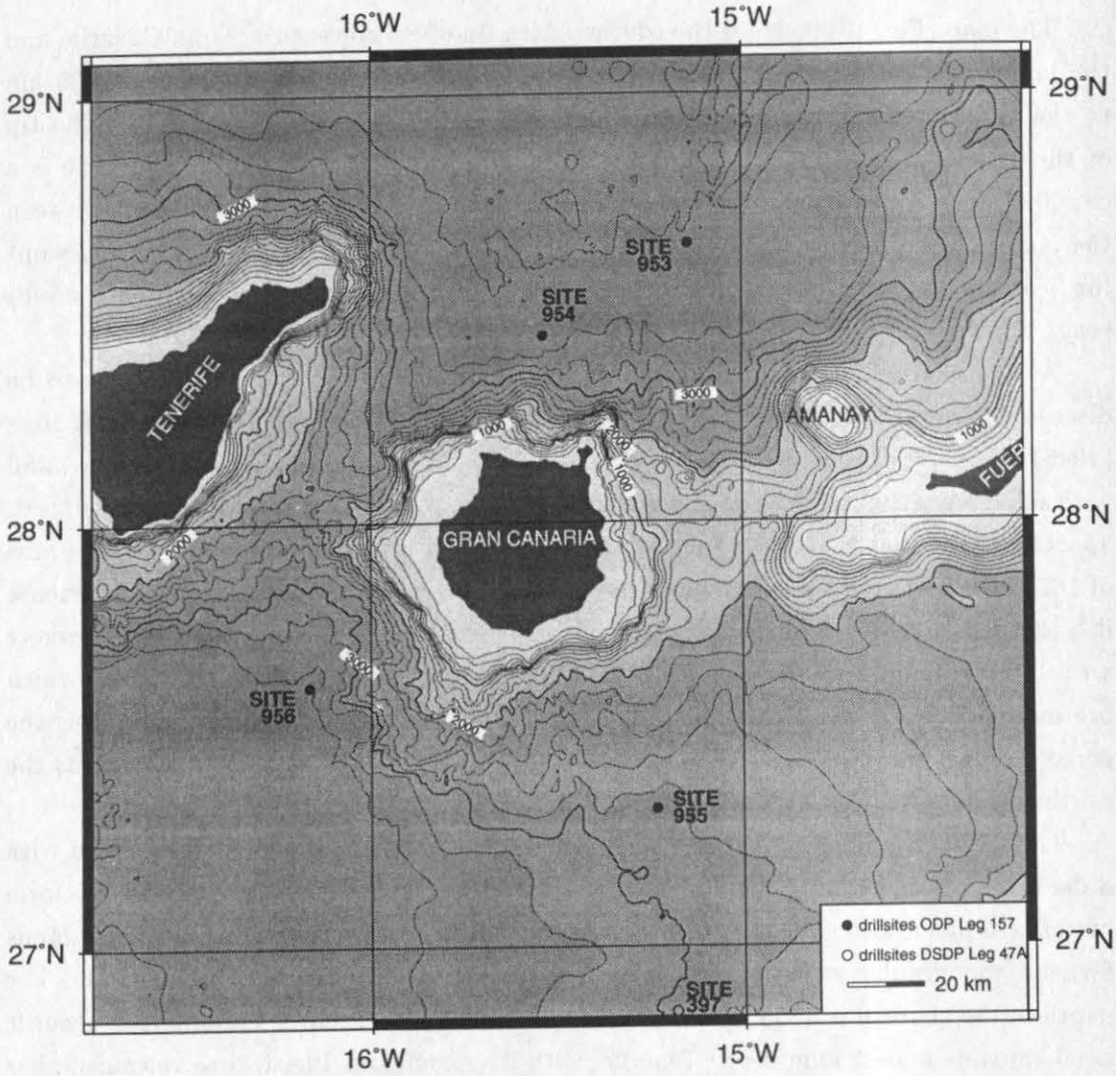

Figure 19: Bathymetric map around Gran Canaria. The data coverage is shown in Fig. 14, gaps are filled with GEODAS and GEBCO data. The contour-interval is 200 m, the grid-interval is 0.5'.

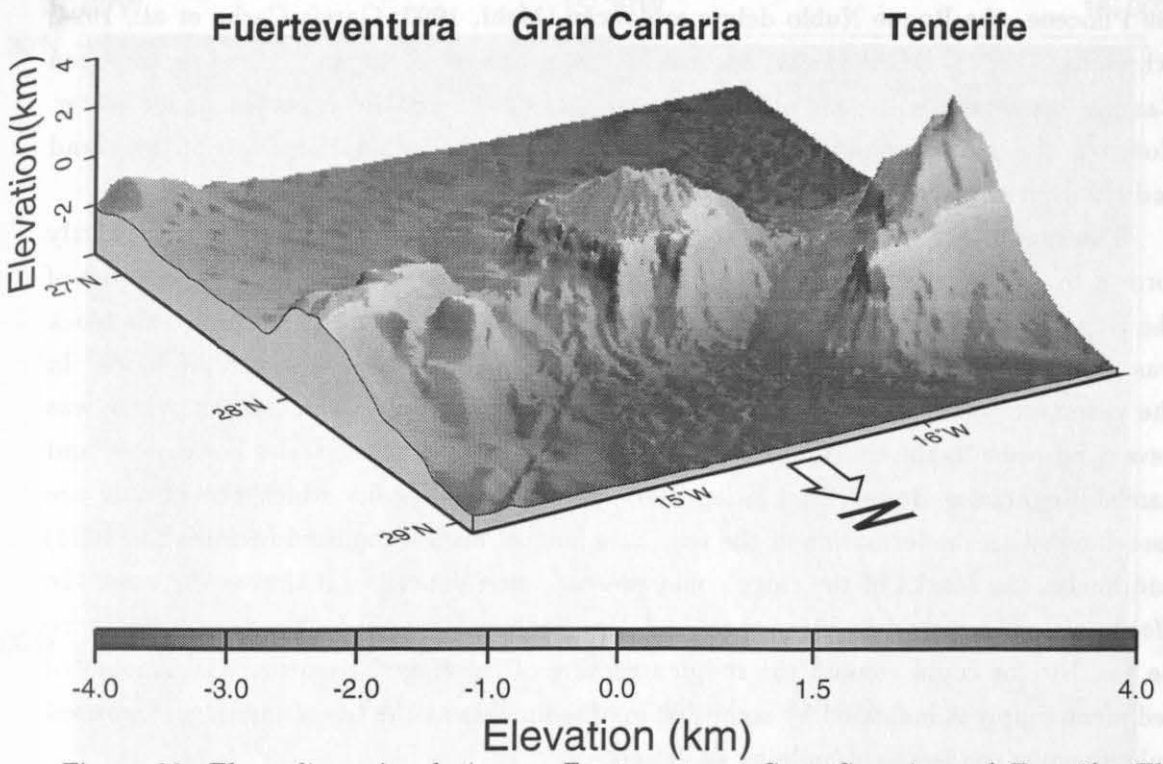

Figure 20: Three dimensional view on Fuerteventura, Gran Canaria, and Tenerife. The view is from the northeast, the artificial illumination from the northwest. The vertical exaggeration is 10, the grid interval is 0.5'.

In the three-dimensional view of the area (Fig. 20), the influence of the continental margin is noticeable, with a slight increase of water depth basinwards in the south due to additional sediment input, whereas the northern basin, better shielded from Africa, has an almost constant water depth. Furthermore, the progressive erosion is well illustrated with a very flat relief and a broad shelf at Fuerteventura, a smaller shelf at Gran Canaria with a volcanic edifice clearly characterized by erosion, even though the island is almost 2000 m high, whereas the youngest island, Tenerife, seems not to have been much influenced by erosion.

The close-up view of Gran Canaria (Fig. 21) displays many details, illustrating the dynamics in growth and erosion of a volcanic island. The subaerial part of the island is surrounded by a shelf before turning into the steep submarine flanks. At their foot region, the slope flattens into the basins. The width of the shelf is variable, as well as the shape and slope of the flank. Larger scalloped zones are visible in the south, west and north.

The extension of the shelf/flank to the SSW (Figs. 21, 22, 23) represents a sediment apron. The canyon system on Gran Canaria provides the path for the transport of erosional products from the island into the sea. The canyons (span. barranco) run radial from the center of the island to the coast and are up to several hundred meters deep, like the Barranco de Arguineguin, one of the most prominent canyons on the island, which runs to the sediment apron. The lateral extension of the apron fits with the seaward continuation of a collapsed sector (Fig. 22) on Gran Canaria and triggered a large debris avalanche in

the Pliocene, the Roque Nublo debris avalanche (Mehl, 1993; García Cacho et al., 1994; Schmincke, 1994). Mehl (1993) has calculated a volume of 14 km^3 of debris on Gran Canaria connected with this avalanche. Further debris can be expected under water. However, the main part of the sediments in the apron are erosional products of the island and have entered the sea through the canyon system for the past 15 million years.

The radial ridge at the west coast of Gran Canaria (Hogarzales) is at least partly formed by slide deposits. Krastel (1995) found a blocky basement structure at the toe of the ridge. One block is 4 km long and some 500 m high. The deposition of this block was prior to the shield-building phase of Tenerife, whose flank onlaps onto the block. In the vicinity of the ridge is a major scar in the shield volcano of Gran Canaria which was developed prior to the emission of the youngest basalt series (Hogarzales Formation) and named Hogarzales Basin (Schmincke, 1968). The slide deposits which presumably are associated with the formation of the scar have not yet been recognized (Schmincke, 1994) and hence, the blocks of the ridge could present these deposits. If that is the case, the *Hogarzales* ridge would be older than 14.1 Ma. Sediment supply by the nearby Barranco de San Nicolas could smooth the rough structure of the ridge basement. The amount of sediment supply is indicated by some 800 m of sediments at the toe of the ridge deposited subsequently to the shield-building of Tenerife.

In the northwest, the coast of Gran Canaria is characterized by a large indentation close to the western rim of the Tejeda caldera (Fig. 7, 22, 24). The landward indentation is still visible in the 100 m contour-line. Further downslope a broad mass was deposited, characterized by a hummocky morphology, particularly in the foot region. This description suggests a slide origin of the mass, probably a debris avalanche, with a well defined amphitheater at its head and the apron-like, hummocky terrain at its end, with several longitudinal ridges/valleys. The indentation represents the wall of the amphitheater. Scars are not visible onshore suggesting that the involved region on the island was eroded subsequent to the mass wasting event by marine abrasion. The average shelf widening for the Canary Islands is given by Menard (1983) to be between 0.6 to 0.7 km per million year. Hence, the shoreline has moved landwards several kilometers since the slide event, possibly triggered by the formation of the caldera, 14.1 my ago. Approximately simultaneous caldera collapse and landslide generation is reported e.g. on Piton de la Fournaise (Lénat et al., 1989).

The shape of the shelf and flank to the north of Gran Canaria suggests that this was the source region of a landslide since the broad scallop between the NNW and La Isleta, with its steep flanks, shows typical features of a failure scarp. The seismic data show an up to 80 m thick debris flow unit north of the scallop, advancing more than 60 km into the basin. The deposition of the unit was at ca. 12 Ma and can be seismically correlated with lithologic unit IV at ODP Site 954, composed of basaltic breccia, representing the basaltic shield of Gran Canaria (Schmincke, Weaver, Firth et al., 1995). Therefore, the debris flow is interpreted to be the result of a collapse at the northern flank of Gran Canaria. The patterns of the slide, a well defined amphitheater at the island flank and the dimensions

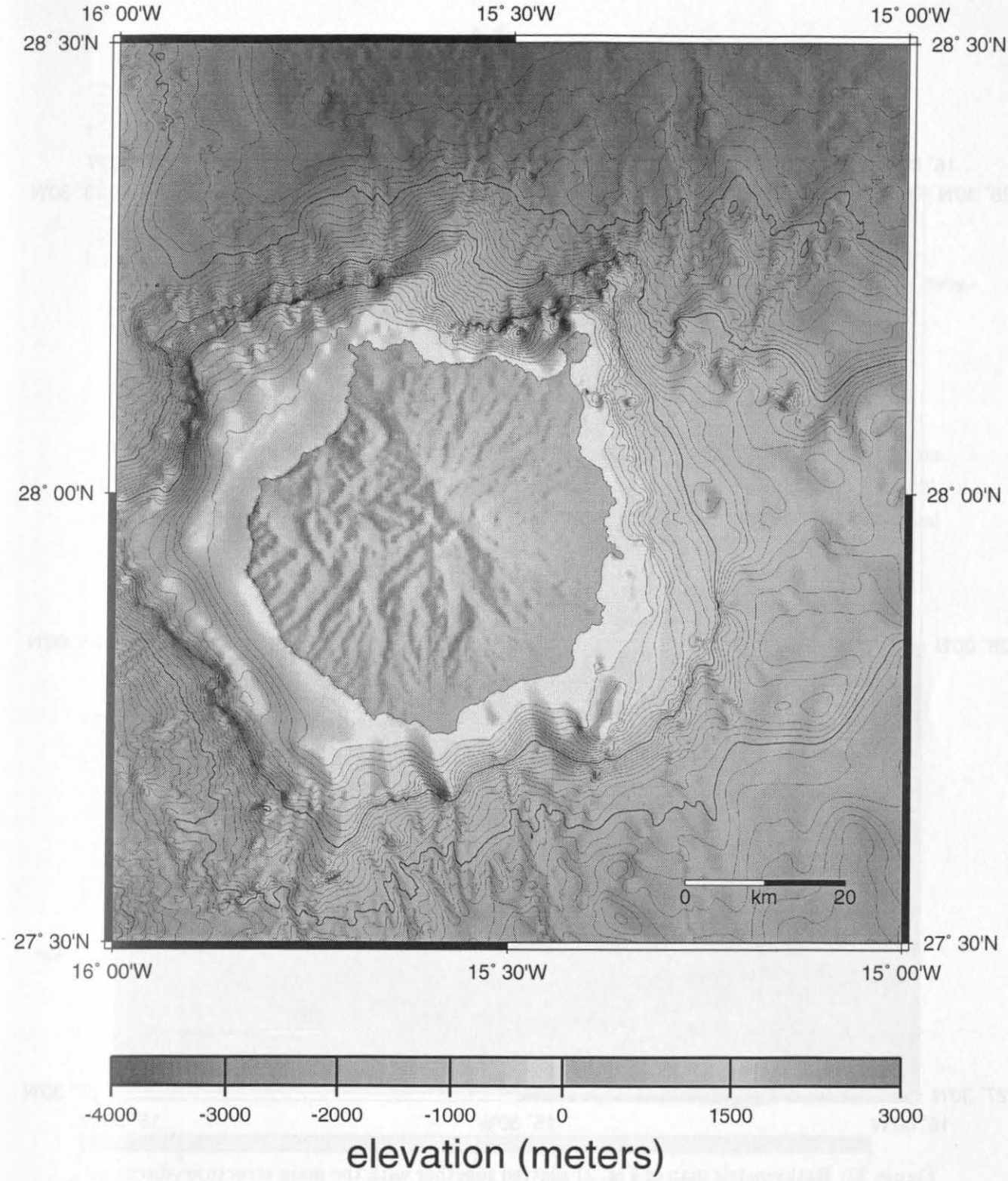

Figure 21: Close-up of the bathymetry around Gran Canaria, plotted together with the topography. The data coverage with swath-bathymetry is shown in Fig. 14. Gaps are filled with GEODAS and GEBCO-data. The contour-interval is 100 m; the 1000 m isobaths are plotted bold. The grid-interval is 0.2'. The plot is shaded by an artificial illumination from the east.

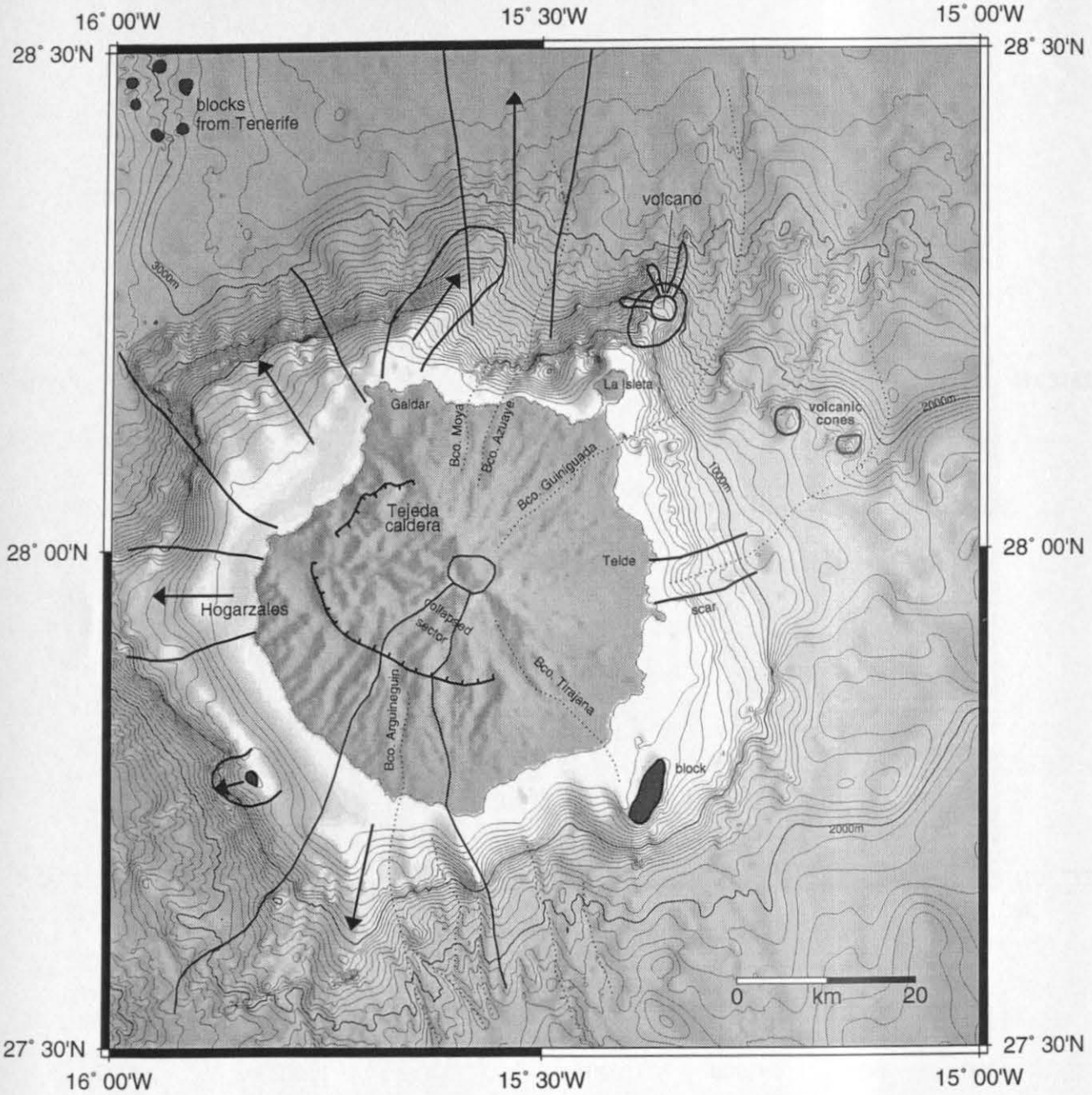

Figure 22: Bathymetric map of Fig. 21 plotted together with the main structures discussed in the text. Canyons are dotted; arrows indicate the direction of mass transport.

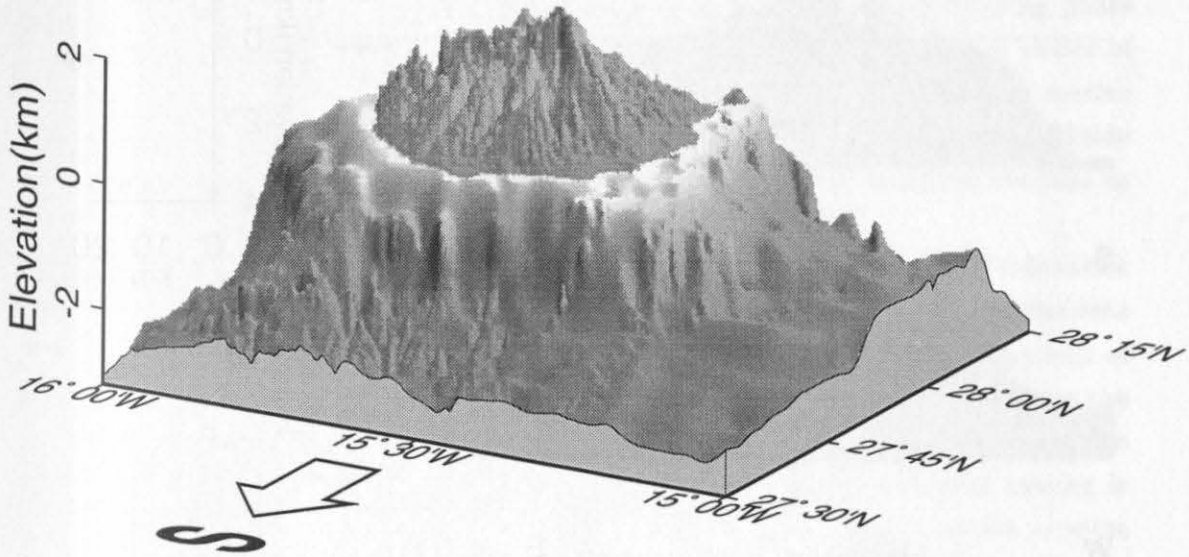

Figure 23: Three dimensional view of the southern part of Gran Canaria. View is from the southeast, shading by artificial illumination from the northeast. Grid interval is 0.2', vertical exaggeration is 10. The apron in the SSW is interpreted as formed by erosional deposits of the island.

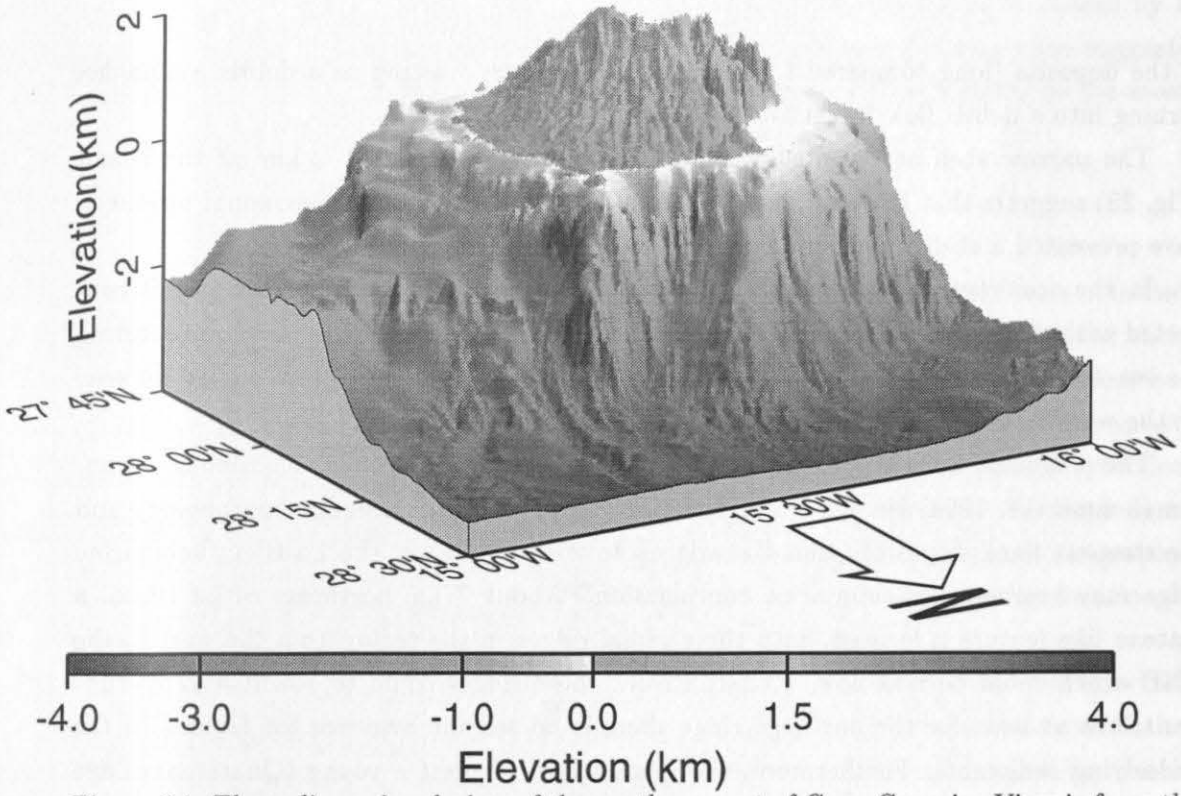

Figure 24: Three dimensional view of the northern part of Gran Canaria. View is from the northeast, shading by artificial illumination from the west. Grid interval is 0.2', vertical exaggeration is 10. The deposits in front of the coastline indentation in the northwest may represent slide deposits.

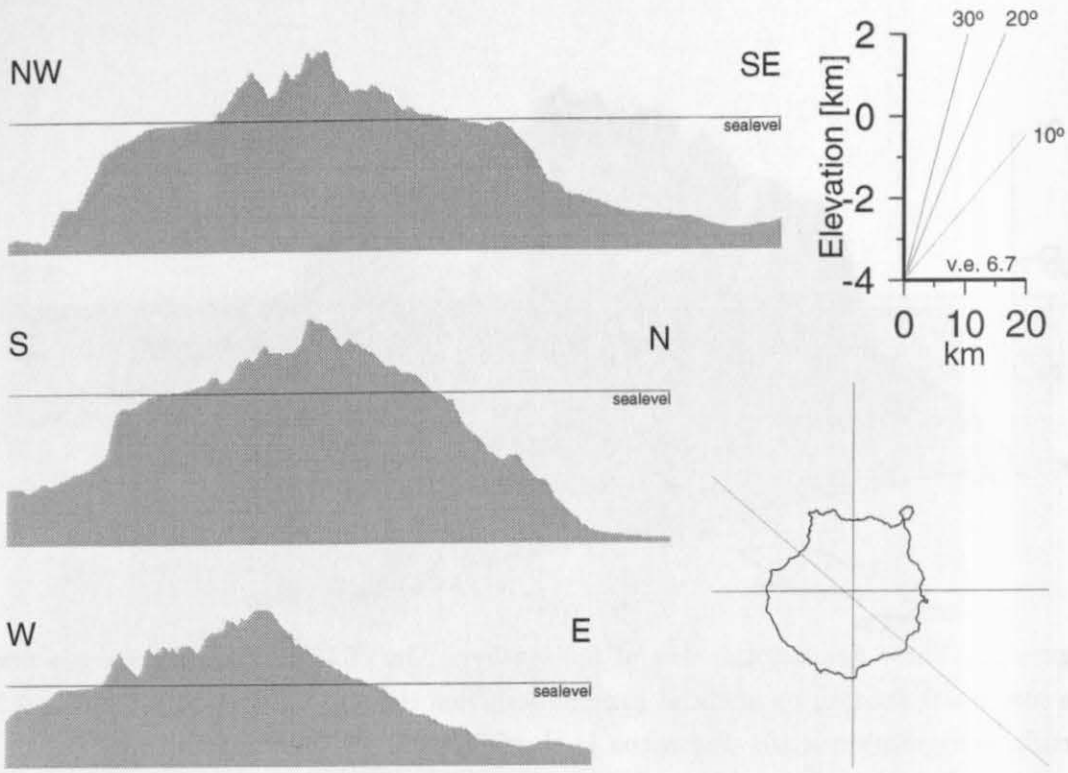

Figure 25: Morphologic profiles crossing Gran Canaria. The locations of the profiles are shown in the small inset. Vertical exaggeration is 10.

of the deposits (long compared to width), indicate mass wasting as a debris avalanche, turning into a debris flow further downslope.

The narrow shelf at the northern flank with the shelf break 1–2 km off the island (Fig. 25) suggests that Pliocene and Quaternary volcanism, as well as erosional products, have prevented a shelf widening.

In the northwest another small ridge (Galdar) extends to the northeast and is connected with the small indentation at the coast. This ridge has deflected mass flows entering the sea at northern Gran Canaria to the northeastern part of the apron, as can be seen by the westward decrease of reflectivity in the apron.

The peninsula La Isleta in the northeast is characterized by young volominous volcanism (Schmincke, 1994; see also geological map Fig. 7) with an irregular morphology and the steepest flank slopes of Gran Canaria up to 25–30°. Hence, the La Isleta submarine ridge may represent its submarine continuation. About 7 km northeast of La Isleta, a plateau like feature is located, with three radial ridges in the sector from the west to the NNE which could be lava flows. Alternatively, these ridges could represent fissure eruptions, but at least for the northern ridge there is no seismic evidence for fissures in the underlying sediments. Furthermore, the seismic data suggest a young (Quaternary) age for the ridges.

No typical shelf developed at most parts off the east coast. The subaerial flanks seem to continue under water without a major change in slope dip or shelf break (Figs. 21, 22, 25) which may be due to several reasons. First, the already flat slope (due to the topographic

swell between Gran Canaria and Fuerteventura) formed during the shield-building phase of Gran Canaria. Second, the severe and prolonged erosion along the eastern slopes of Gran Canaria (Schmincke, 1994), provided enough material to compensate for marine abrasion. At least some of these deposits seem to be supplied by slides, e.g. east of Telde a scar can be traced from the coast line down to the 800 m isobath and may continue as an erosional channel towards the northeast and further to the north.

The combination of bathymetry and topography also allows identification of submarine continuations of the well-developed canyon system on Gran Canaria. Even though the data coverage close the shore line is often sparse, a number of the submarine continuations of the canyons can be recognized. The most prominent offshore continuation is seen at the Barranco de Guiniguada in the northeast, which is connected with a 53 km-long submarine channel, terminating in the deep northern basin (Fig. 21, 22). The channel cutting is up to 3.5 km wide and 200 m deep. The age of the Barranco de Guiniguada is some 4 my (Schmincke, personal communication). In the north, two other barrancos show a submarine continuation (Barranco de Moya, Barranco de Azuaje). In the southern region several submarine channels are recognizable, some like the continuation of the Barranco de Arguineguin are branched downslope and then again intersect with other channels, forming a channel system.

A last point to mention is the hummocky region located some 10 km southeast of the northeastern tip of Tenerife (northwest corner of Fig. 21). The structure is caused by a number of large blocks with a diameter up to 500 or even 1000 m. Their location suggests a larger mass wasting event as the origin, with the Anaga massif on Tenerife as the most probable source area.

5.2 Stratigraphy

The two drillsites in the volcanic apron north of Gran Canaria provide for a detailed analysis of the apron by analysis of the volcanic and non-volcanic sediments, and their lithostratigraphic and biostratigraphic correlation. Correlation of seismic reflectors between the drillsites and across the apron allows a detailed reconstruction of the apron. The synthetic seismograms used to link the drilled lithology with the seismic reflection data enables assigning many individual reflectors to volcaniclastic layers. The large number of reflectors, in conjunction with the combined litho–, magneto–and biostratigraphy, allows a detailed temporal resolution of the basin evolution. Fig. 26 shows the location of the two drillsites and the seismic lines in the northern apron.

The classic seismic sequence stratigraphy introduced by Mitchum et al. (1977), which defines the boundaries of depositional sequences by unconformities and their correlative conformities, is extremely difficult to apply to the apron studied. The reason for this is the type of sedimentation of volcaniclastics in the vicinity of the steep island flanks, which is characterized by discontinuous, irregular and partly chaotic patterns caused by mass wasting events as one of the main depositional processes in this area. Terminations are in general not systematic, irregular, not confined to special horizons and are distributed

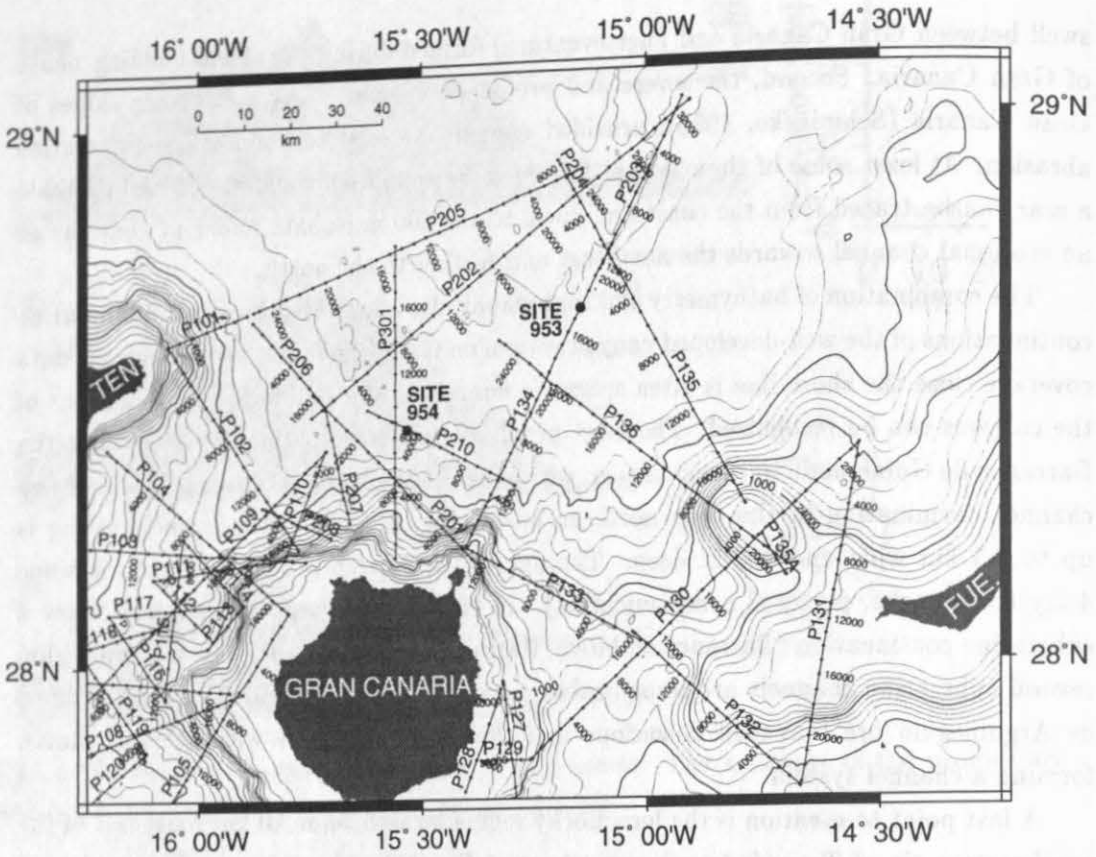

Figure 26: Location map of seismic profiles in the northern apron of Gran Canaria. Every 1000th CMP is dotted, every 4000th CMP is labeled. Contour interval of the bathymetry is 200 m. The two ODP drillsites in the area are marked by filled circles. All lines between profile P102 in the west and profile P130 in the east are discussed in this paper.

over the entire sediment column. Therefore, it is more applicable to combine groups of reflectors with respect to vertical facies changes which can be related to changes in volcanic activity on the islands. Prominent reflectors or reflector bands are suitable markers for such vertical facies changes.

The seismic stratigraphy is also often used to determine sea-level changes. In the case of Gran Canaria, such analysis is not possible because only minor sediments are deposited on the shelf and the island flanks. Nonetheless, sea-level changes are known to be reflected on Gran Canaria (Lietz and Schmincke, 1975) and uplift of submarine basement complexes causing relative sea-level changes seems to be common on the Canary Islands, documented e.g. on La Palma (Staudigel and Schmincke, 1984) and Fuerteventura (Le Bas et al., 1986).

5.2.1 Lithostratigraphy of ODP Sites 953 and 954

The lithostratigraphy of ODP Sites 953 and 954 is described in full by Schmincke, Weaver, Firth et al. (1995). Only a short summary of their description is given here.

Site 953: The sedimentary succession ranges in age from middle Miocene to Recent and is 1158.7 m thick. The sequence is subdivided into seven major lithologic units and three

subunits (Fig. 27):

Unit I from 0–197 meters below seafloor is late Pliocene to Recent in age. The dominant lithology is clayey nannofossil ooze which is formed by pelagic and hemipelagic sedimentation. The remaining interbeds (clay-silt, massive foraminifer sands, stratified foraminifer lithic sands, foraminifer lithic silts and sands, pumice sands and volcanic ash) represent emplacement of mixed volcaniclastic and carbonate sediments by gravity flow processes and eolian transport following explosive volcanic eruptions.

Unit II from 197–264 mbsf is late Pliocene in age. It is distinguished from Unit I by an increase in the amount of coarse, basaltic volcaniclastic sediment and the presence of thick to very thick bedded basaltic lapillistones and coarse sandstones.

Unit III from 264–398 mbsf is early Pliocene to late Miocene in age. The dominant lithology is clayey nannofossil ooze which is interbedded with minor graded nannofossil clay-silt, foraminifer lithic silts and sands, and foraminifer sands. In many cases the sequences show soft sediment deformation structures indicating slumping of unconsolidated sediments (from about 321–388 mbsf).

Unit IV from 398–850 mbsf is late to middle Miocene in age. The major lithologies include nannofossil chalk, nannofossil mixed sedimentary rock, foraminifer sands, lithic-crystal sands and silts, lapillistones, vitric tuffs, nannofossil claystone and claystone. Unit IV has been subdivided into three subunits based on the frequency and lithology of volcaniclastic sediments emplaced by sediment gravity flows.

Subunit IVa from 398–504 mbsf consists of nannofossil mixed sedimentary rock and nannofossil chalk which is interbedded with nannofossil claystones and claystones which typically grade downward into lithic-crystal siltstone or sandstone.

Subunit IVb from 504–754 mbsf consists of nannofossil mixed sedimentary rock which is interbedded with nannofossil claystones and claystones which typically grade downward into lithic, crystal or vitric siltstone and sandstone bases. The unit is distinguished from Subunit IVa by the increasing thickness and grain size of volcaniclastic sandstones and the more common occurence of debris flow and slump deposits.

Subunit IVc from 754–850 mbsf consists of interbedded nannofossil mixed sedimentary rocks, crystal vitric sandstones and siltstones, lapillistones, vitric tuff, graded nannofossil clay-sandstones. Nannofossil chalk is present as a minor lithology. The primary distinction from Subunit IVb is the major increase in the abundance of coarse and fine vitric material in the siltstone and sandstone units.

Unit V from 850–889 mbsf is middle Miocene in age and is comprised of nannofossil mixed sedimentary rock, nannofossil claystone, claystone, lithic crystal siltstones

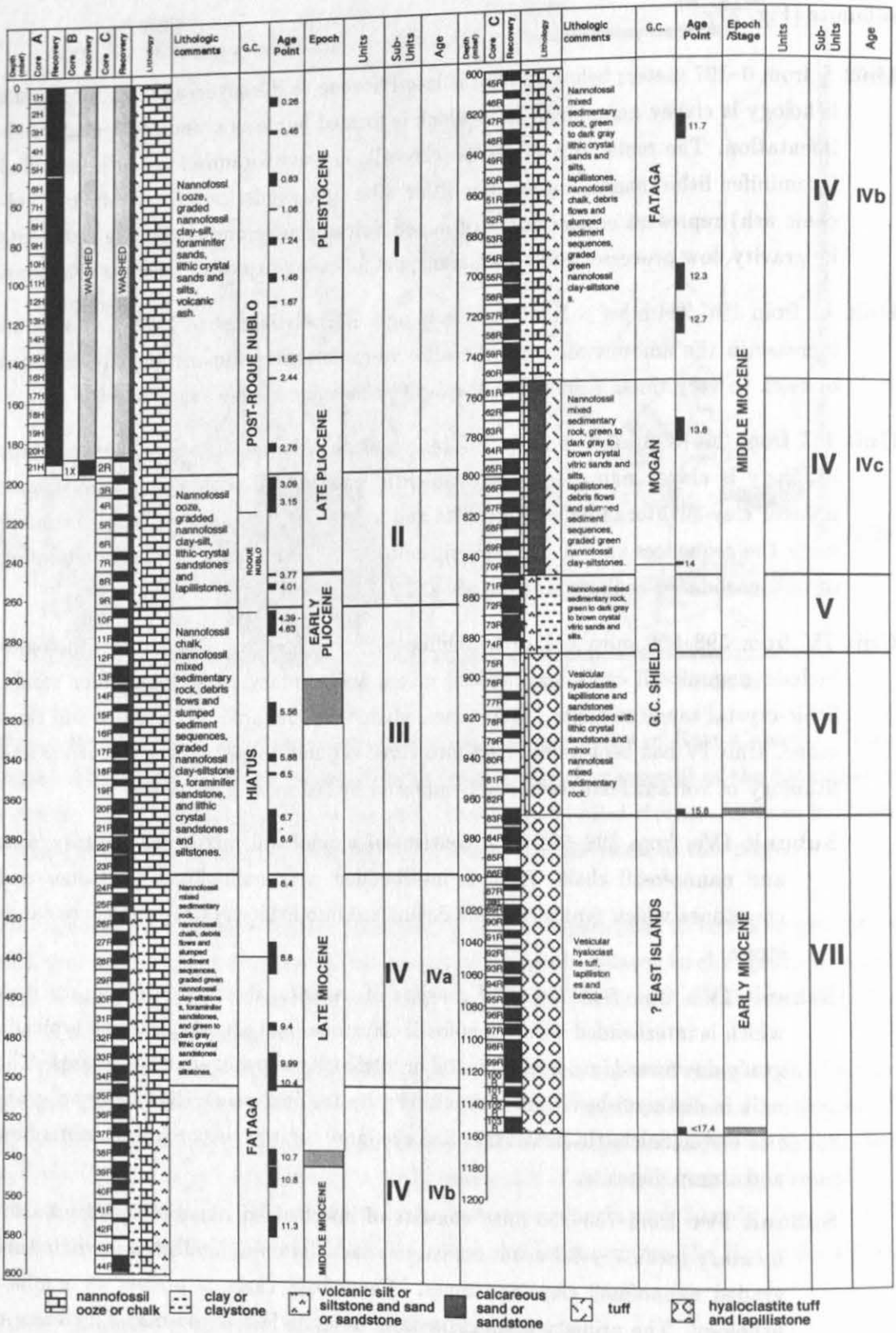

Figure 27: Lithostratigraphy at ODP Site 953 (from Schmincke, Weaver, Firth et al., 1995). Depth values are given in meters below seafloor (mbsf). Black fields in the Core Recovery Column represent the amount of sediment recovered in each core. Age points are given in million years and are accompanied by a correlation with the volcanic activity on Gran Canaria.

and sandstones, and lapillistones. The dominant lithology id graded sequences of nannofossil claystone or claystone which grade downward into basal lithic-crystal siltstone and sandstone.

Unit VI from 889–969 mbsf consists largely of thick to very thick bedded basaltic sandstone, lapillistone and breccia which are occasionally interbedded with thinner units of calcareous claystone and nannofossil mixed sedimentary rock. The age is middle Miocene but the time represented by the unit is difficult to constrain because microfossil-bearing sediments are not common.

Unit VII from 969–1159 mbsf consists entirely of hyaloclastite tuffs, lapillistones and breccias. The age of the unit is early Miocene, but its duration is poorly constrained.

The **depositional history** of the above mentioned volcaniclastic sediments at Site 953 starts with

- Unit VII, mainly emplaced by debris flows; fine-grained, parallel laminated tuffs were more likely deposited from high concentration turbidity currents. The hyaloclastite fragments were probably formed by shallow submarine eruption of basaltic magma.
- Unit VI at Site 953 is believed to present the outermost flank of the shield volcano of Gran Canaria comprising both subaerial and shallow submarine volcanism deposits. The emplacement of material was by debris flows and turbidity currents.
- Sedimentation in Unit V was dominated by numerous turbidite events with a very regular repetition.
- The highly explosive dominantly ignimbritic Mogan phase of volcanism on Gran Canaria (13.4–14 Ma) was probably a major source of volcaniclastics in Subunit IVc in which material was transported to the basin by turbidity currents.
- The Fataga phase of volcanism and erosion of its subaerial products were a major source of volcaniclastics in Subunit IVb, primarily deposited by turbidity currents.
- In Subunit IVa the flux of volcaniclastic material decreased but the number of turbidite events increased.
- The influx of volcaniclastic material further decreased in Unit III, coinciding with the major hiatus in volcanic activity on Gran Canaria. The sedimentation was dominantly pelagic with rare influxes of coarse volcaniclastic or shallow water carbonate.
- The Roque Nublo phase of volcanism is presented in Unit II by a sequence of thick-bedded turbidites.
- In the remaining 3 my to present (Unit I), sedimentation has been dominantly pelagic with an increase in the amount of shallow water carbonate delivered by turbidity currents and an intermittent supply of volcaniclastic material most likely derived by

the reworking of subaerial volcanic deposits. The remarkable coarse beach sands, rich in neritic biogenic material recovered in the upper 100 m, are interpreted as turbidites possibly related to glacially controlled changes in sea level.

Site 954 was drilled more proximal to Gran Canaria (Fig. 26). The sedimentary succession is 446 m thick and is subdivided into 4 lithologic units (Fig. 28):

Unit I from 0–177 mbsf is Pleistocene to late Pliocene in age and consists predominantly of nannofossil ooze with foraminifers and massive bioclastic sand with interbeds of crystal lithic sands, vitric ash and lapillistone.

Unit II from 177–179 mbsf is late Pliocene in age and consists of lapillistone.

Unit III from 179–408 mbsf is early Pliocene to late Miocene in age. The dominant lithology is nannofossil chalk interbedded with minor clayey nannofossil mixed sedimentary rock and crystal-lithic siltstones and sandstones. The unit contains a thick slumped sediment sequence (302–359 mbsf).

Unit IV from 408–446 mbsf is middle Miocene in age (ca. 14 Ma) and is comprised exclusively of basaltic breccia. Between the units III and IV there is a hiatus.

The **depositional history** at Site 954 is as follows:

- The breccias in Unit IV resemble those of Unit VI at Site 953. The breccia is basically a mixture of subaerially-derived and shallow-water volcanics which typically occur during the emergent phase of volcanic islands. The poor sorting, matrix-support of clasts, and structureless character suggests emplacement by one or more debris flows. The hiatus between these ca. 14 my old rocks and the 10.7 my old base of Unit III is interpreted in Schmincke, Weaver, Firth et al. (1995) as due to the removal by slumping of the missing sediments. The analysis of the seismic data suggests an alternate explanation, namely that some of the missing sediments have been overridden by a large debris flow representing Unit IV (reworked, 14 Ma old material). This ca. 12 Ma old debris flow could have originated from a larger debris avalanche further upslope. Site 954 was drilled into the top of a mound and, hence, the debris flow was followed by an interval of nondeposition, lasting from ca. 12 to 10.7 Ma.

- In Unit III the sedimentation was dominated by pelagic deposits punctuated by the influx of volcaniclastic sand, silt and clay in the form of turbidity currents. The slumped sediment sequence is most likely correlative with that of Site 953 and represents a period of instability which affected a large part of the northern flank of Gran Canaria.

- The only 2 m thick lapillistone layer recovered in Unit II was deposited by debris flows during the Roque Nublo phase of volcanism on Gran Canaria.

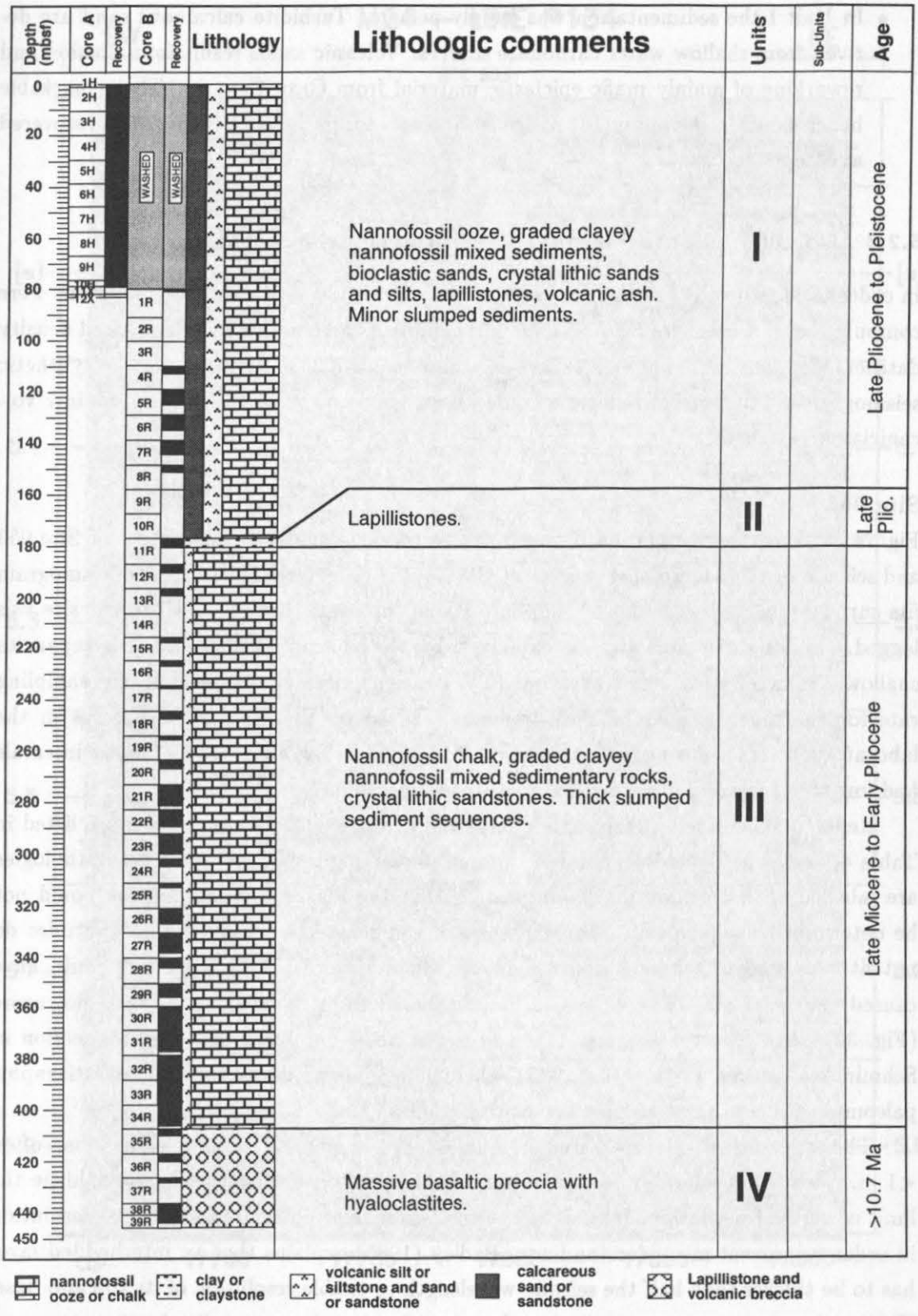

Figure 28: Lithostratigraphy at ODP Site 954 (from Schmincke, Weaver, Firth et al., 1995). Depth values are given in meters below seafloor (mbsf). Black fields in the Recovery column represent the amount of sediment recovered in each core.

- In Unit I the sedimentation was mainly pelagic. Turbidite calcareous sand are derived from shallow water carbonate sources. Volcanic sands result from erosion and reworking of mainly mafic epiclastic material from Gran Canaria. The remarkable beach sands in the upper 100 m are more coarse grained than similar sands recovered at Site 953.

5.2.2 Correlation of the seismic data with the drillsite lithology

In order to identify the drilled lithologies in the seismic data, synthetic seismograms were computed, even though for Sites 953 and 954 complete and continuous velocity and density datasets were not available (see *Processing* chapter, page 33). By means of the synthetic seismograms, a number of reflectors could be assigned to specific lithologies, mainly volcaniclastic interbeds.

Site 953

Figure 29 shows the correlation between the synthetic seismogram computed for Site 953 and seismic line P134, crossing the site at CMP 17780 (Fig. 26). The synthetic seismogram fits surprisingly well with the seismic data if one considers that only half of the site was logged. Minor differences can be explained by the incomplete dataset. Discrepancies shallower than 5.0 s two-way travel time (TWT) are mainly due to an insufficient sampling rate for the Index Properties measurements, caused by the rapid flow of cores in the laboratory. Further downcore (down to ca. 5.15 s and below 5.65 s TWT) many intervals had low core recovery, probably masking some reflectors.

Reflectors identified in the seismic data and in the synthetic seismogram are listed in Table 4, and, where possible, the reflecting lithology is given. Several of these lithologies are labelled with question marks, indicating that the reason of the reflection could not be determined unequivocally. For example, this might be the case where amplitudes do not fit very well or where lithologies in the vicinity were not sampled but could have caused the reflection. The reflectors are numbered from the seafloor (No. 0) downcore (Fig. 30). The reflector ages are taken from the *Sediment accumulation rates* section in Schmincke, Weaver, Firth et al. (1995), where 88 age points derived from biostratigraphy, paleomagnetic and stratigraphic correlation to Gran Canaria are given.

The volcaniclastic layers listed in Table 4 are in general thinner than 2 m, often <1 m. This is considerably less than half of the seismic wavelength which would be the limit of vertical resolution. It therefore seems reasonable to discuss the vertical resolution in order to prevent misunderstandings. Badley (1985) explains that an interbedded layer has to be thicker than half the seismic wavelength to enable resolution of its top and base. Thinner layers appear as one single reflector with a maximum amplitude at one quarter of the wavelength – the tuning thickness. For thicknesses below one quarter wavelength, the reflection remains the same shape but decreases in amplitude. Once the thickness is about one-thirtieth wavelength or less, there is no detectable response. This explains why thin volcaniclastic beds can be detected as single reflectors. Applying this knowledge to

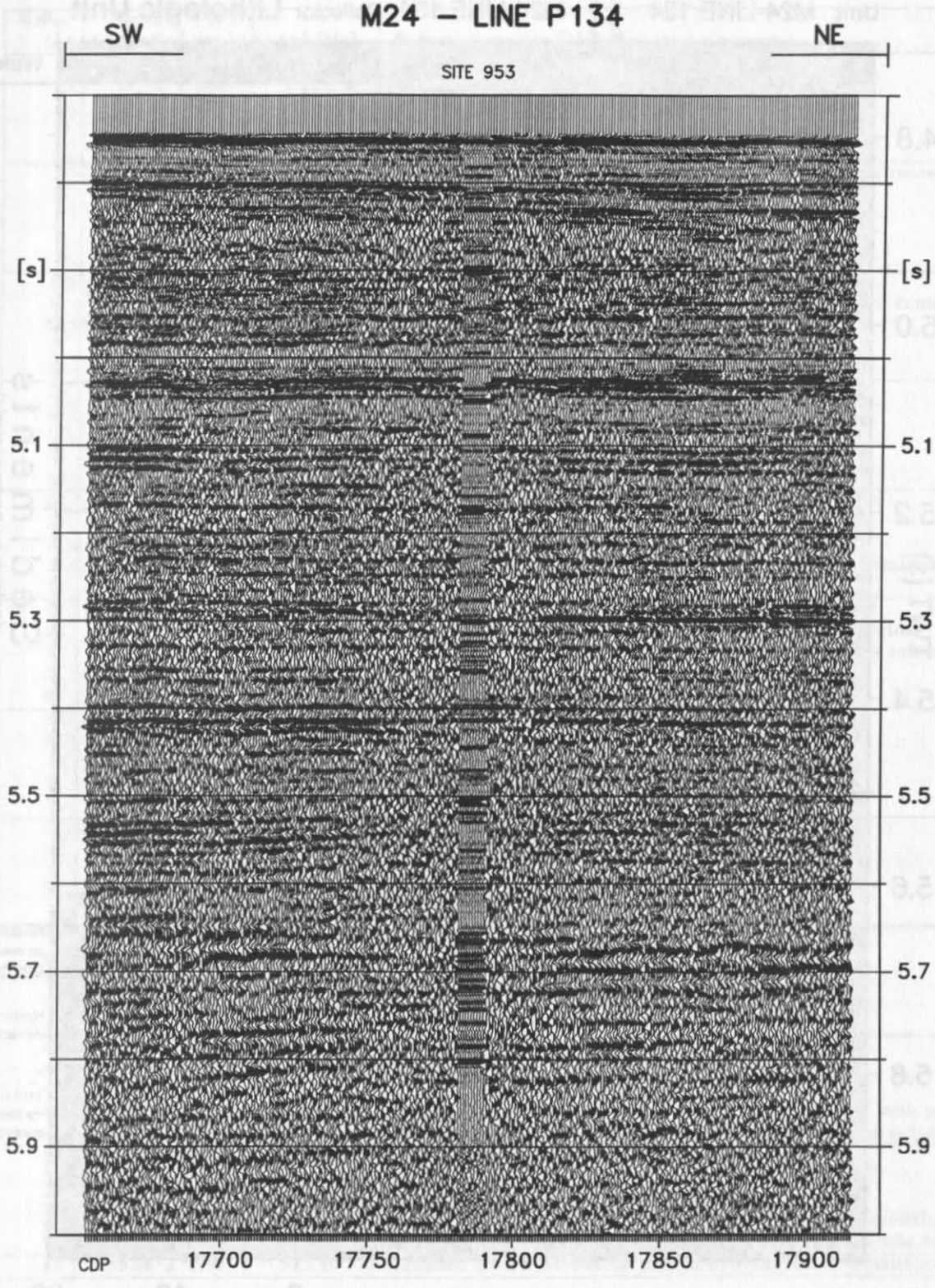

Figure 29: Part of seismic line P134 plotted together with the synthetic seismogram at ODP Site 953. The seismic data are stacked, scaled with an AGC (50-200 ms) and band-pass filtered (30–230/160 Hz). Random noise was added to the 10 synthetic traces.

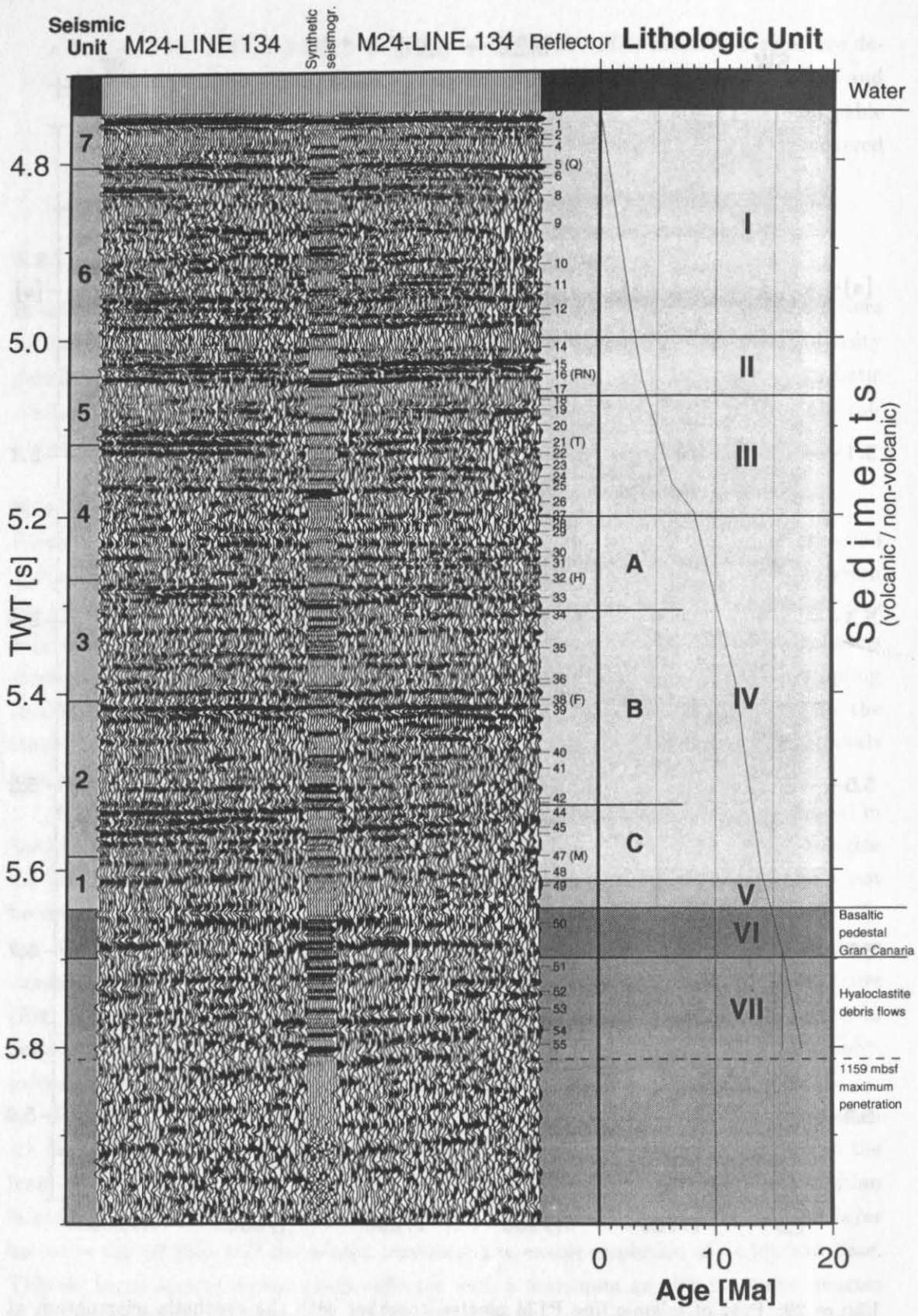

Figure 30: Part of seismic line P134 with synthetic seismogram at ODP Site 953 and the seismic and lithologic units converted to two-way travel time (TWT). The age is taken from the *Sediment accumulation rates* chapter in Schmincke, Weaver, Firth et al. (1995). The two age lines in Unit VII give minimum and maximum ages. The small numbers to the right of the seismic data refer to individual reflectors as listed in Table 4.

Reflector	Depth [mbsf]	TWT [ms]	Age [Ma]	Reflection causing lithologies (and comments)
0	0.00	4745	0.0	seafloor
1	11.45	4760	0.26	clayey medium to coarse-grained silty pumice sand
2	20.60	4772	0.26–0.46	silty fine–medium grained foraminifer pumice sand
3	23.90	4777	0.26–0.46	calcareous sand
4	30.17	4785	0.46–0.78	basaltic sand
5	45.85	4805	0.78–0.83	silty crystal lithic sand (amplitude difference due to low recovery)
6	55.49	4818	0.99–1.06	clayey nannofossil ooze (weak reflector)
7	60.77	4826	0.99–1.06	crystal lithic sand
8	72.61	4840	1.07–1.24	calcareous sand with volcanic lithics
9	96.40	4871	1.24–1.46	foraminifer lithic sand
10	130.73	4916	1.77–1.92	massive lithic to calcareous sand
11	149.74	4940	1.92	massive foraminifer sand with lithics (weak reflector, low continuity)
12	170.53	4967	2.61–2.76	foraminifer silt with lithics and crystals
13	176.00	4974	2.61–2.76	clayey nannofossil ooze?
14	206.23	5010	3.09	foraminifer sandstone
15	225.70	5030	3.22–3.58	foraminifer lithic sandstone
16	237.59	5041	3.79	lapillistone
17	257.54	5058	4.01	lapillistone (weak reflector, low continuity)
18	267.67	5070	4.29	silty, foraminifer nannofossil chalk (weak reflector)
19	278.07	5081	4.39	nannofossil chalk (weak, discontinuous reflector)
20	296.19	5099	4.80	density/velocity increase in a nannofossil chalk sequence
21	313.12	5118	5.23–5.56	lithic crystal sand
22	325.53	5130	5.56–5.87	indurated nannofossil ooze (weak reflector)
23	337.50	5144	5.87–5.88	clay with nannofossils (grading to lithic crystal sand), weak reflect.
24	350.81	5157	5.88–6.50	slump unit consisting of ooze, clay, silt, mixed rock
25	361.35	5167	6.64–6.70	?
26	385.85	5185	7.62–8.03	foraminifer lithic crystal sand (weak, discontinuous reflector)
27	399.73	5200	8.17–8.20	indurated clay with nannofossil (weak and discontinuous reflector)
28	409.80	5210	8.40–8.63	calcareous sandstone ?
29	417.79	5219	8.40–8.63	indurated clay ?
30	442.71	5242	8.80	silty claystone
31	455.00	5254	8.80–9.22	claystone ?
32	470.39	5271	9.22–9.40	nannofossil chalk ?
33	495.30	5293	9.99	lithic crystal sandstone ?
34	516.44	5312	10.40–10.70	nannofossil claystone
35	556.83	5350	10.99–11.30	lithic crystal sandstone
36	594.71	5385	11.30–11.70	lithic crystal sandstone
37	601.86	5390	11.30–11.70	lapillistone
38	621.49	5408	12.10–12.30	lithic crystal sandstone?
39	633.90	5419	12.10–12.30	? (logged and not recovered?)
40	689.14	5467	12.10–12.30	siltstone
41	710.40	5485	12.93–13.08	siltstone ? (weak and discontinuous reflector)
42	749.72	5519	13.25–13.45	nannofossil claystone, graded to crystal siltstone
43	755.34	5524	13.25–13.45	claystone ? (close to not sampled sandstone)
44	768.32	5535	13.45–13.60	vitric tuff
45	787.20	5552	13.60–13.67	calcareous vitric siltstone ? (weak reflector)
46	794.45	5559	13.67–14.00	lithic crystal vitric tuff
47	822.44	5584	13.67–14.00	vitric rich claystone with sandy vitric tuff
48	842.17	5602	13.67–14.00	nannofos. clayst. grading down to lithic crystal sandst. with pumice
49	863.22	5618	14.00–15.80	claystone grading down to lithic crystal sandstone (weak reflector)
50	920.42	5660	14.00–15.80	lapillistone with basaltic breccia
51	988.44	5709	14.00–15.80	pebble-and granule sized fine-grained hyaloclastite tuff
52	1029.97	5737	>15.80	high velocity unit in hyaloclastite lapillistone
53	1066.83	5756	>15.80	transition from hyaloclastite lapillistone breccia to hyaloclastite tuff
54	1110.61	5781	>15.80	transition from basaltic hyaloclastite breccia to hyaloclastite tuff
55	1139.86	5797	>15.80	transition from hyaloclastite breccia to hyaloclastite lapillistone

Table 4: Correlated reflectors ODP Site 953. Reflector numbers are shown in Fig. 30. The reflections are caused by the impedance contrasts between the given lithologies and the (hemipelagic) background sediments. Lithologies and ages are from Schmincke, Weaver, Firth et al. (1995).

the data reported here, the signal contains frequencies of up to 200 Hz and the velocity in the volcaniclastic layers is typically around 2000 m/s. Thus, one-thirtieth of a wavelength corresponds to only 33 cm. If the lithologies above and below the thin layer are slightly different, a resolution thickness of less than 33 cm is conceivable. Weak and discontinuous reflectors seem to represent thin layers with a thickness varying around one-thirtieth of the wavelength.

The vertical seismic facies changes in the vicinity of Site 953 have been used to distinguish seven seismic units in the sediments above the island flank (Fig. 30). The seismic units are not identical with the lithologic units since most of the lithologic boundaries are not characterized by reflections, at least not by reflections which could be correlated far away from the drillsite. Each seismic unit starts with a prominent reflector band at its base. Reflectors at the base or close to the base of these reflector bands showing a good correlation in the apron serve as boundary layers between these units. These boundary reflectors are from the base upwards: reflector 47, 38, 32, 21, 16, and 5 (Fig. 30). These reflectors are called M (deposited during **Mogan** phase of volcanism), F (deposited during **Fataga** phase of volcanism), H (deposited during the transition from the Fataga phase to the large Miocene **hiatus** of volcanism on Gran Canaria), T (deposited subsequent to the shield phase of the Anaga massif at northern **Tenerife**), RN (deposited during the **Roque Nublo** phase), and Q (**Quaternary** deposit).

The seven seismic units (Fig. 30) are therefore:

Unit 1 lies between the top of the submarine island flank and reflector M (47) consists of parallel to subparallel reflectors with low to moderate amplitudes and a variable cycle breadth. The continuity is moderate to high.

Unit 2 lies between reflectors M (47) and F (38) with parallel, continuous, high amplitude reflectors at its base with a narrow uniform cycle breadth. Amplitude and continuity decrease upwards and the frequency becomes more variable.

Unit 3 between the reflectors F (38) and H (32) with parallel to subparallel reflectors. The reflector band at the base has a high amplitude and good continuity, whereas the upper part is characterized by good to fair continuity, medium amplitudes and a varying cycle breadth.

Unit 4 lies between reflectors H (32) and T (21) with a high amplitude band at its base. The reflectors are parallel to subparallel, the amplitude is high to medium, connected with good to fair continuity. The cycle breadth is narrow but varying.

Unit 5 lies between reflectors T (21) and RN (16). The base is characterized by a narrow band of parallel reflectors with a high amplitude and good continuity, followed by medium to low amplitude reflectors, which are parallel to subparallel with a fair continuity. At the top the unit tends to be reflection free.

Unit 6 lies between reflectors RN (16) and Q (5) with the most prominent reflector band at its base with high amplitudes and good continuity. Above this band there is

a ca. 30–50 ms thick interval with low reflectivity, only some low amplitude, high frequency reflectors with moderate continuity are visible. The thick top interval consists of low to medium, sometimes high amplitude reflectors. Apart from the high amplitude reflectors, the continuity is fair to discontinuous. The cycle breadth is varying.

Unit 7 lies between reflector Q (5) and the seafloor (0). Apart from the high amplitude reflection at the base, the reflectors have a low to medium amplitude, but a medium to good continuity. The cycle breadth is narrow and very constant.

Comparison between reflectors found at DSDP Site 397 (Wissmann, 1979; von Rad, Ryan et al., 1979) or ODP Sites 955 and 956 (Schmincke, Weaver, Firth et al., 1995) south of Gran Canaria is hampered by the different reflection patterns due to influence by the continental slope. Furthermore, no direct correlation from south to north is possible across the channels between Gran Canaria and Fuertventura/Tenerife because the reflectors onlap the volcanic basement or reflection patterns become chaotic in the proximity of the islands. This is the reason why reflector names introduced at DSDP Site 397 for the southern basin cannot be used in the north. Considering only the ages and not the lithologies, reflector R7 at DSDP Site 397 approximately corresponds to reflector M in the north, whereas reflector R3 roughly fits with the northern reflector RN, indicating that the material was deposited during the same phases of volcanic activity on Gran Canaria.

Site 954

Correlation between Site 954 and the seismic data was hampered by the proximity of the site to the island slope and the low core recovery in combination with the lack of logging data. The latter fact means that the synthetic seismogram had to be computed by discrete velocity and density measurements from the recovered core (only about one half of the hole). Thus, many reflectors may have been lost in the synthetic seismogram. The location of Site 954 is 214 m upslope of profile P210 which is roughly situated tangential to the island flank. A distance of 214 m corresponds to 68 CMP which, as Fig. 31 shows, can make a noticeable difference since the individual reflectors are divergent and have different dips. Nevertheless, some reflectors could be correlated with some reliability and are listed in Table 5.

The prominent reflection band at around 4850 ms TWT in Fig. 31 corresponds to lithologic Unit II and to the reflector band around reflector RN at Site 953. The thickness of the reflection band contradicts the only 2 m thick lithologic Unit II. Since the core recovery at that depth interval was low, the thickness of the Unit II seems in reality to be larger.

The deepest reflector in the synthetic seismogram at around 5.1 s TWT, defining the top of lithologic Unit IV, does not represent the volcanic shield of Gran Canaria, which can be correlated at a depth of roughly 5.25 s TWT. Furthermore, a number of reflections can be seen between the top of Unit IV and the volcanic basement. These reflectors may represent material deposited during the Mogan and Fataga phase of volcanism on Gran

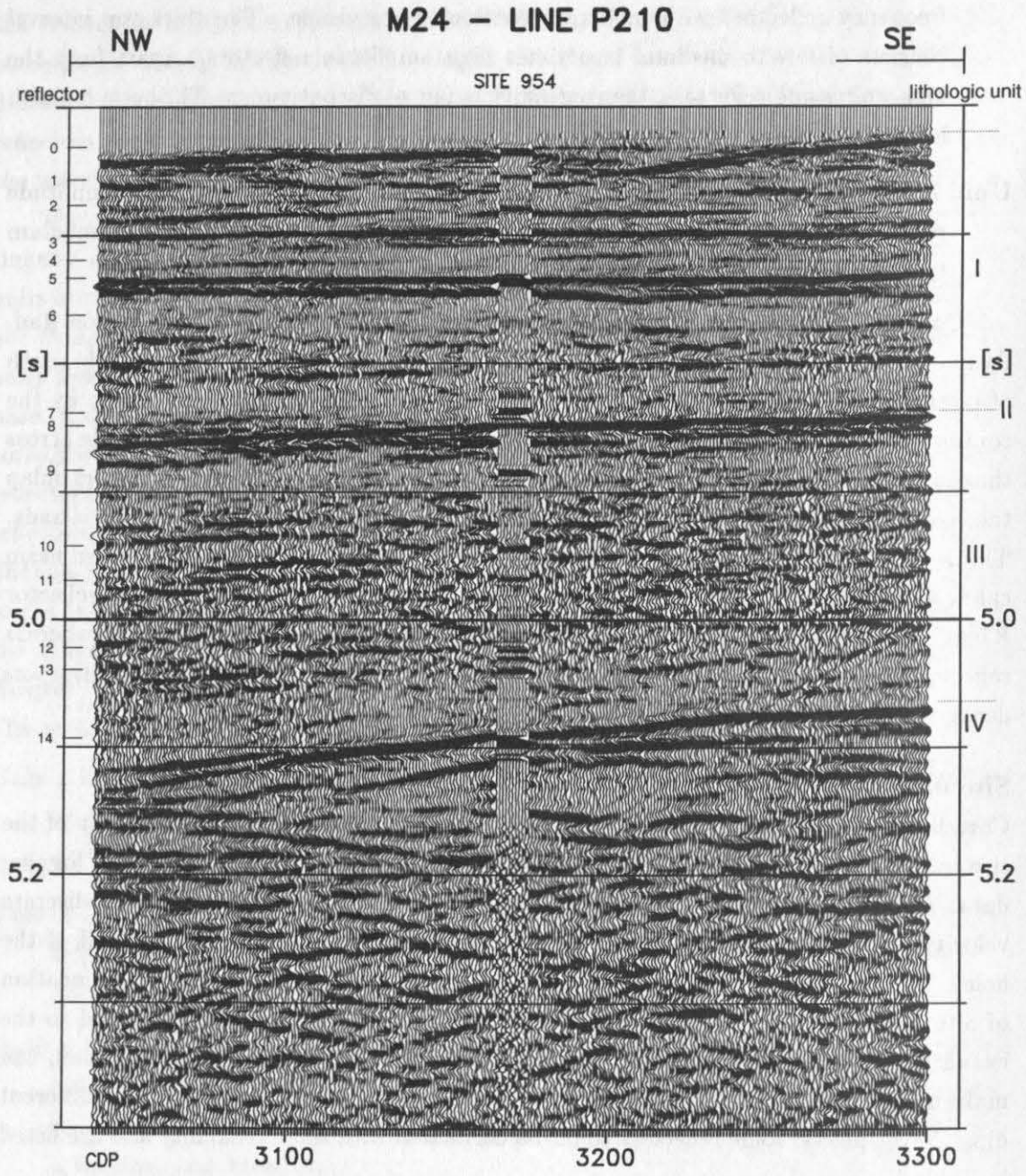

Figure 31: Part of seismic line P210 plotted together with the synthetic seismogram at ODP Site 954. The seismic data are stacked, scaled with an AGC (50–200 ms) and band-pass filtered (30–230/160 Hz). Random noise was added to the 10 synthetic traces. The labels and numbers at the left side refer to reflectors which could be correlated at Site 954 and are listed in Table 5. Lithologic Unit I is located between reflectors 0 and 7; reflector 7 corresponds to Unit II, Unit III is between reflectors 7 and 14 and Unit IV is below reflector 14.

Reflector	Depth [mbsf]	TWT [ms]	Age [Ma]	Reflection causing lithologies (and comments)
0	0.00	4632	0.00	seafloor
1	18.82	4657	0.00–0.46	clayey nannofossil ooze interbedded in sand
2	36.24	4677	0.46–0.78	calcareous sandstone
3	56.77	4706	0.78–0.83	calcareous sand with lithics
4	68.03	4720	0.83–1.06	density variation in nannofossil ooze (weak reflection)
5	80.53	4734	1.60	lapillistone (below this unit 28 m with no recovery)
6	111.92	4763	ca. 2.40	density variation in nannofossil ooze ? (samples from a 54 cm thick ash-layer just above the given depth were not taken)
7	177.81	4839	(3.15)–3.79	lapillistone (low recovery in this zone)
8	189.65	4849	3.77–3.79	density reduction in nannofossil ooze
9	217.73	4884	4.01–4.39	sandstone ?
10	266.43	4943	5.88–6.50	density variation in nannofossil chalk with clay
11	288.94	4970	6.50	density variation in nannofossil chalk with clay
12	334.53	5023	7.30–7.62	slump unit (chaotic nannofossil mixed ooze and chalk)
13	351.35	5040	7.62–8.03	silty claystone with lithic crystal sandstone
14	406.66	5094	>10.7	basaltic breccia (lithologic Unit IV)

Table 5: Correlation of reflectors at ODP Site 954. Reflector numbers are shown in Fig. 31. The reflections are caused by the impedance contrasts between the given lithologies and the (hemipelagic) background sediments. Lithologies and ages are from Schmincke, Weaver, Firth et al. (1995).

Canaria. These were subsequently overridden by a slide deposit formed by the basaltic breccia found in Unit IV which consisted of 14 my old rocks and slid at ca. 12 Ma.

5.3 The submarine volcanic flanks

The submarine flanks of Gran Canaria, Tenerife and Fuerteventura are represented in the northern apron of Gran Canaria. The top of the massive island flanks is the most remarkable feature in the reflection seismic lines due to the strong reflection amplitude and the unconformable contact with the overlying units, with numerous baselaps. ODP Leg 157 (Schmincke, Weaver, Firth et al., 1995) showed that the volcanic flanks consist of hyaloclastite tuffs, breccias, lapillistones and sandstones. In general, the volcanic flanks comprise material with high density and P-wave velocity compared to the overlying sediments. A high impedance increase at the top boundary, and therefore high amplitude reflections, results. Furthermore, the steep slopes of the islands are characterized by numerous diffraction hyperbolas in the unmigrated sections. The diffractions are caused by the rough morphology of the volcanic products and many of them are side echos. The dip of the slope of Gran Canaria is up to 25–30° (e.g. on profile P134, Fig. 34). Further off the islands the dip of the flanks decreases and the occurrence of diffraction hyperbolas at the top of the flanks becomes rare. The seismic facies of the flank here is characterized by a high amplitude reflection with a discountinous mounded structure. Close to the feather edge the flank is gentle, almost horizontal, and sometimes short branches of underlying

reflectors become visible. They are mostly horizontal and discontinuous (Funck et al., 1996).

Prior to the ODP drilling, some information was available about the submarine shield-building phases of the islands of Fuerteventura, Gran Canaria, and Tenerife: The DSDP Site 397 drilled four thick volcaniclastic debris flows from which three are believed to come from the submarine shield of Fuerteventura (Schmincke and von Rad, 1979). The subaerial parts of the three islands are well investigated (McDougall and Schmincke, 1976; Schmincke, 1982; Ancochea et al., 1990; Coello et al., 1992) but do not allow conclusions about the submarine portions apart from the emerged basal complex on Fuerteventura (Le Bas et al., 1986) which, however, does not represent the shield-building phase of the island.

The lithologic Unit VI at ODP Site 953 is believed to represent the thin outermost flank of the shield volcano of Gran Canaria (Schmincke, Weaver, Firth et al., 1995). The age of the unit is middle Miocene, around 15 Ma, indicating a rapid growth of the submarine shield (duration around 1 my). The feather edge of the flank of Fuerteventura (Amanay Bank) lies stratigraphically just below the penetration depth at Site 953 (Fig. 35). The biostratigraphy gives a minimum age of 15.8 Ma for the bottom of the drill-hole, the maximum age is 17.4 Ma. Therefore, the age of the submarine part of southern Fuerteventura can be estimated between 16 and 18 Ma. Coello et al. (1992) have obtained K-Ar ages between 15.8 to 14.9 Ma for the subaerial southern edifice of Fuerteventura. Assuming roughly the same age for the Amanay Bank, the geomorphological guyot connected with Fuerteventura whose flank was actually investigated on seismic line P135, a submarine shield building stage of less than 2 my duration is realistic.

The submarine flank of Northeast Tenerife is interbedded in the sedimentary basin northwest of Gran Canaria (Figs. 44, 45, 51) at a stratigraphic position where the age data at Site 953 are much more exact and reliable than for the flanks of Gran Canaria and Fuerteventura. The outermost flank of Tenerife corresponds stratigraphically to a depth of ca. 350 mbsf at ODP Site 953. Using the magnetostratigraphy, the age is between 5.87 and 6.12 Ma, while the biostratigraphy would allow ages of up to 6.50 Ma. The combined fitted curve tends to favor an age of about 6 Ma (Schmincke, Weaver, Firth et al., 1995). The samples of Ancochea et al. (1990) from the Anaga massif at the northeastern tip of Tenerife yielded maximum ages of 6.5 Ma at the western side of the massif, which is situated on the opposite side of the island. The maximum age at the eastern side is given as 5.7 Ma. Therefore, the duration of the submarine shield stage of the Anaga massif is estimated to be less than 0.8 Ma, possibly as low as 0.3 Ma.

The temporal succession of the submarine shield stages of the islands – Fuerteventura as the oldest, followed by Gran Canaria and Tenerife – has influenced the shape of the individual island shields. The building of Fuerteventura to the west was into the open ocean; no preexisting islands could influence the deposition of the volcanic material. Gran Canaria, however, had to its east the shield of Fuerteventura, hampering the growth of the shield towards that direction. This effect can be seen well in Fig. 32 which shows the

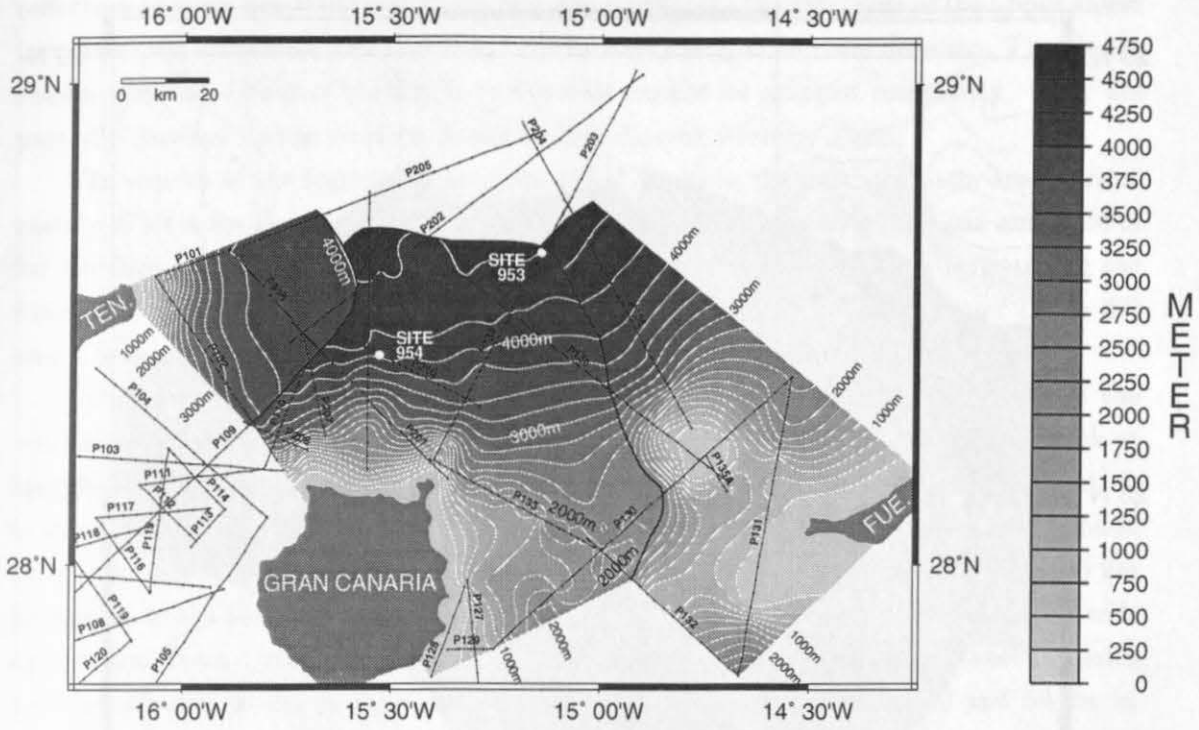

Figure 32: Depth of the volcanic island flanks in the northern apron of Gran Canaria. The contour interval is 250 m. A water velocity of 1500 m/s was used for depth conversion and the sediment thickness of the overlying sediments was taken into account by the formula given in the *Processing* chapter, page 37. For the gridding procedure, the points along the mapped profiles were supplied with zero values along the coast lines. The bold lines mark the outermost extension of the submarine flanks. Where the flanks overlap, no statement can be made about the underlying shield.

depth of the top of the submarine island flanks. On profile P135 the outermost flank of Fuerteventura extends some 85 km from the shoreline or around 50 km from the Amanay Bank, both resulting in a position of the outer limits of the Fuerteventura flank close to the eastern coastline of Gran Canaria, assuming radial symmetry. The growth of Gran Canaria began approximately at the end of the shield building phase of the southern edifice of Fuerteventura. Volcanic material deposited to the east of Gran Canaria had to be transported uphill at the southwestern flank of Fuerteventura, causing a ponding of the Gran Canaria shield against the submarine flank of Fuerteventura. This ponding can be seen on seismic line P130 (Fig. 36) located between the two islands and in the gentle dip of the Gran Canaria flank towards the east compared to the uninfluenced north (Fig. 32). The limited eastern depositional room was filled up until the material reached the steep flanks of Fuerteventura and of the Amanay Bank. These depositional barriers diverted the volcanic deposits to the north and the south. The northward diversion can be seen in Fig. 32 where the isolines north of Gran Canaria are not radially symmetric but extend northward when moving to the east.

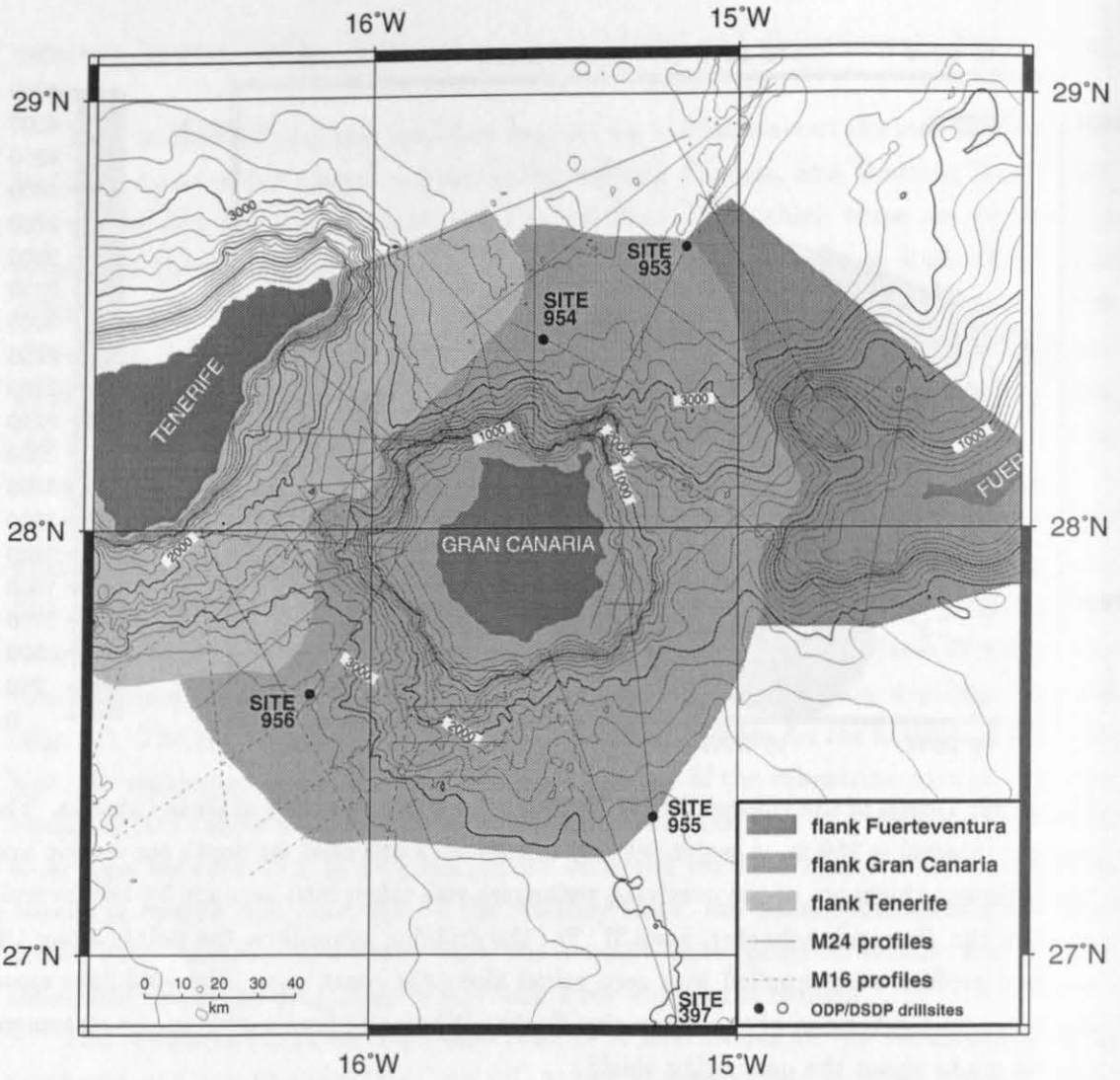

Figure 33: Extension of the submarine flanks of Fuerteventura, Gran Canaria and Tenerife, shown together with the bathymetry, contour interval 200 m (from Funck et al., 1996).

The western part of the Gran Canaria shield grew into the open ocean, limiting the depositional room for the later emerging island of Tenerife. This resembled the phenomena between Fuerteventura and Gran Canaria, namely a ponding of the Tenerife deposits against the flank of Gran Canaria. The main difference is that the area of the (younger) channel between Gran Canaria and Tenerife was filled some 8 my ago with pelagic sediments and volcaniclastics from Gran Canaria prior to the growth of Tenerife, whereas there was almost no gap between the shield-building stages of Fuerteventura and Gran Canaria. The sedimentary infill into the channel prior to the evolution of Tenerife can be seen on seismic line P102 (Fig. 48), covered by the flank of Tenerife which onlaps the flank deposits of Gran Canaria.

In general, volcanic flanks overlain by younger volcanic shields cannot be detected on the seismic lines because the upper volcanic edifice forms the acoustic basement. Nevertheless, on some lines parts of the underlying flanks can be recognized as weak and dipping

reflectors (e.g. on line P102 and P130, Fig. 48 and 36). As the thickness of the upper shield increases, the amplitude and continuity of the underlying reflections decrease. That is the reason why the extent of the flanks to the west cannot be mapped completely – they are partially masked by the younger flanks of the adjacent western island.

The depths of the feather edges of the island flanks in the northern basin are approximately 4750 m for Fuerteventura, between 4500 and 4600 m for Gran Canaria and 4000 m for Tenerife (Fig. 32). The two-way travel times were converted to depth by applying the fitted velocity function for the sediments described in the *Processing* chapter (page 37) and a water velocity of 1500 m/s.

Using all the seismic lines from METEOR cruises No. 16 and 24, the extent of the volcanic flanks was also mapped in the basin south of Gran Canaria (Fig. 33, Funck et al., 1996). The massive island flank of Gran Canaria extends 44 to 72 km off the coast. It is closest to the island in the east, where its growth was limited by the preexisting shield of Fuerteventura as discussed above. In the northern basin the flank extends some 60 km seawards, in the southern basin between 54 and 72 km. To the west, the flank of Tenerife approaches Gran Canaria as close as 22 km. The extent of the flank of Tenerife varies between 30 and 40 km in the channel towards Gran Canaria, between 40 and 50 km in the southern region and around 50 km in the northeast.

5.4 Description of the seismic lines

In order to gain a detailed insight into the structure of the apron north of Gran Canaria the seismic lines in this area are described in detail below. The location of the profiles is shown in Figure 26.

Line P134

Line 134 (Fig. 34) is located radial to Gran Canaria in a SSW–NNE direction. Its southern end is 3.5 km away from the La Isleta peninsula which is characterized by Quaternary volcanism (Schmincke, 1994). ODP Site 953 is located at CMP 17780. The flank facies comprising the volcanic edifice is characterized by steep flanks up to a dip of 32° close to the island. Towards the basin, the dip decreases from 1.4° (CMP 4500-12000) to 0.6° (CMP 12000-18000). The flat flank is defined by a high amplitude, long period reflector with a discontinuous mounded structure. Several small-scale faults are visible. Internal reflectors show a shingled northward dipping pattern. The southernmost volcanic edifice on line 134 is formed by two volcanic cones which seem to represent the offshore continuation of the volcanism on La Isleta. The flank of the cone at CMP 1000 has a dip of 18°. In Fig. 22, the position of a small volcano and three radial ridges starting from there are shown. The northwest and north running ridges are crossing line 134 and are interpreted as lava flows. Fissure eruptions as an alternative interpretation can be excluded at least for the northern feature since there are no fissures visible in the underlying sediments. The NW ridge represents a broad almost reflection-free structure between CMP 1700 and 3700 with downlap onto the former seafloor at its toe. The second lava flow is visible around CMP 4500. The flow is some 1500 m broad and 40 m thick and contains some low amplitude discontinuous reflectors. This flow also shows a downlap onto the seafloor. Therefore, both lava flows are very recent features indicating ongoing volcanism at the La Isleta submarine complex.

On a large scale, the entire sedimentary sequence shows infill characteristics with onlap onto the flank of Gran Canaria. The slope facies, with chaotic patterns above the volcanic shield, roughly represents the lower third of the sequence, succeeded by relatively regular stacks of mounded structures in the upper part. Mounded onlapping fill facies like at CMP 5500 (4.5 s TWT) suggests deposition by gravity-controlled flows along the seafloor (i.e. a high energy depositional system). Outside the slope facies, which extends some 45 km from Gran Canaria, the seismic facies changes to a more regular basin-fill facies with parallel or basinward diverging reflectors. Individual reflectors can be correlated within the slope facies where the correlation gradually decreases by a transition into more complex patterns. The basin facies adjacent to the slope facies is characterized by a series of wedges and mounded sheets which extend up to ca. CMP 20000. The mound at the top of seismic unit 4 (i.e. between reflector H and T) between CMP 13500 and 17000 is compensated by thinning of the overlying unit.

Further seaward the reflections become almost horizontal above reflector M. Below there is a small islandward dip (less than 0.5°). Reflections below the island flank are discontinuous and the amplitude decreases with the thickening of the volcanic pedestal.

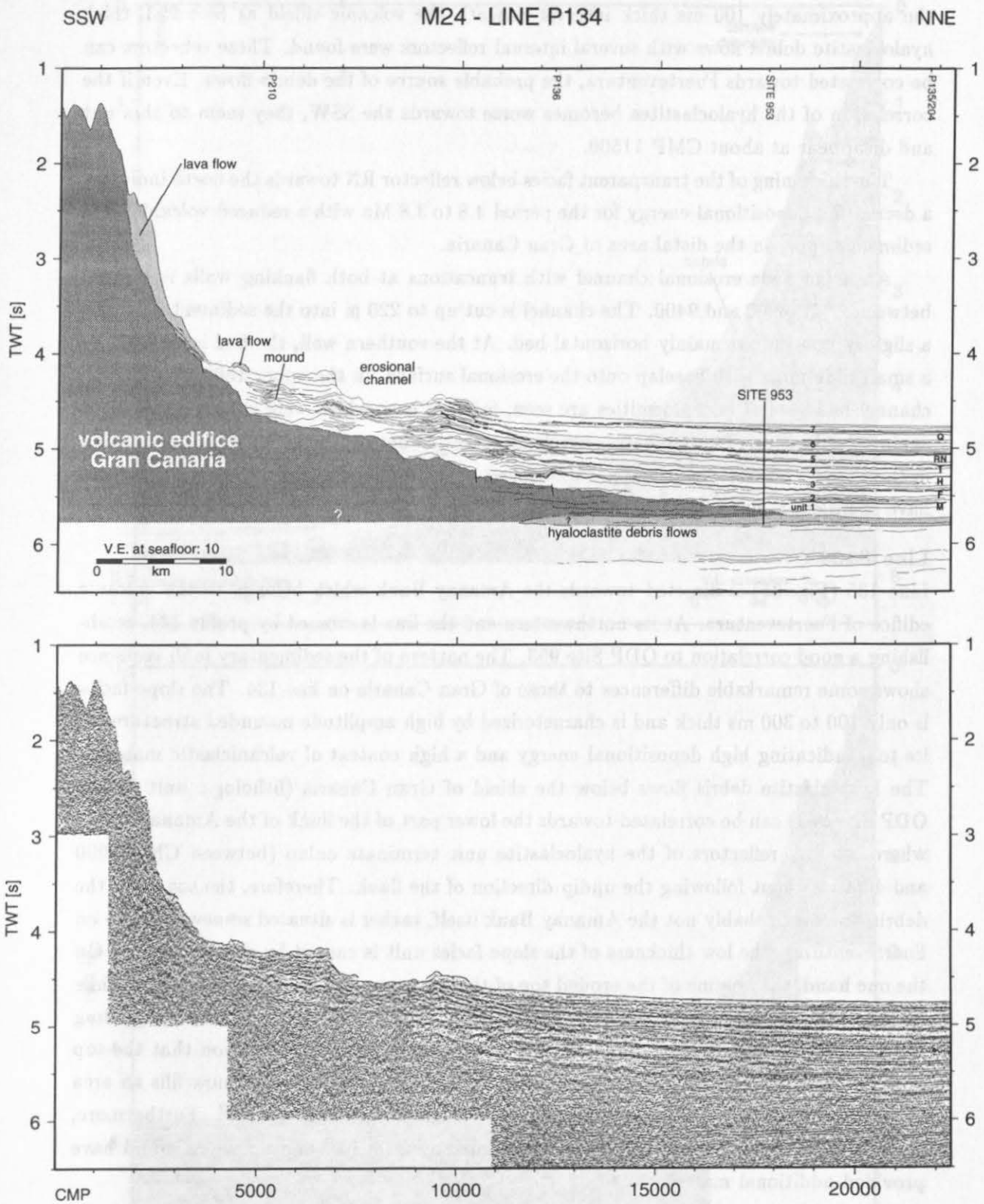

Figure 34: Seismic line P134 with linedrawing.

The dip of these reflectors again becomes more or less horizontal but this is probably due to the pull up by a thickening of the high velocity shield on the time section. In the approximately 100 ms thick interval beneath the volcanic shield at Site 953, thick hyaloclastite debris flows with several internal reflectors were found. These reflectors can be correlated towards Fuerteventura, the probable source of the debris flows. Even if the correlation of the hyaloclastites becomes worse towards the SSW, they seem to thin out and disappear at about CMP 11500.

The thickening of the transparent facies below reflector RN towards the north indicates a decreasing depositional energy for the period 4.8 to 3.8 Ma with a reduced volcaniclastic sediment supply in the distal area of Gran Canaria.

An 8 km wide erosional channel with truncations at both flanking walls is located between CMP 6900 and 9400. The channel is cut up to 220 m into the sediments and has a slightly uneven but mainly horizontal bed. At the southern wall, the bed is covered by a small slide mass with baselap onto the erosional surface. In the upper 150 ms below the channel bed several unconformities are seen, forming lows which were subsequently filled again by sediments. This indicates complex interaction between erosion and sedimentation in the channel. Analysis of these patterns results in the estimation that erosional processes have been active since at least 4.8 m.y.

Line P135

Line 135 (Fig. 35) is directed towards the Amanay Bank which belongs to the volcanic edifice of Fuerteventura. At its northwestern end the line is crossed by profile 134, establishing a good correlation to ODP Site 953. The pattern of the sedimentary infill sequence shows some remarkable differences to those of Gran Canaria on line 134. The slope facies is only 100 to 300 ms thick and is characterized by high amplitude mounded structures at its top, indicating high depositional energy and a high content of volcaniclastic material. The hyaloclastite debris flows below the shield of Gran Canaria (lithologic unit VII at ODP Site 953) can be correlated towards the lower part of the flank of the Amanay Bank, where internal reflectors of the hyaloclastite unit terminate onlap (between CMP 2000 and 4000) without following the updip direction of the flank. Therefore, the source of the debris flows is probably not the Amanay Bank itself, rather is situated somewhere else on Fuerteventura. The low thickness of the slope facies unit is caused by several factors. On the one hand, the volume of the eroded top of the Amanay volcano is not very large, while on the other hand, the bank prevents volcaniclastic input from Fuerteventura. Regarding the shape of the isobaths of the bank, one can estimate from extrapolation that the top of the former volcano was 500 to 600 m above the present plateau which now fills an area of roughly 100 km^2. This leads to an eroded volume of less than 20 km^3. Furthermore, there is no evidence for volcanic activity at Amanay after its build-up which could have provided additional material.

Most reflectors of the sedimentary infill of the basin facies terminate onlap onto the slope facies, in contrast to line 134 at Gran Canaria where the reflectors can be correlated within the slope facies. This is another sign for the low volcaniclastic input from the

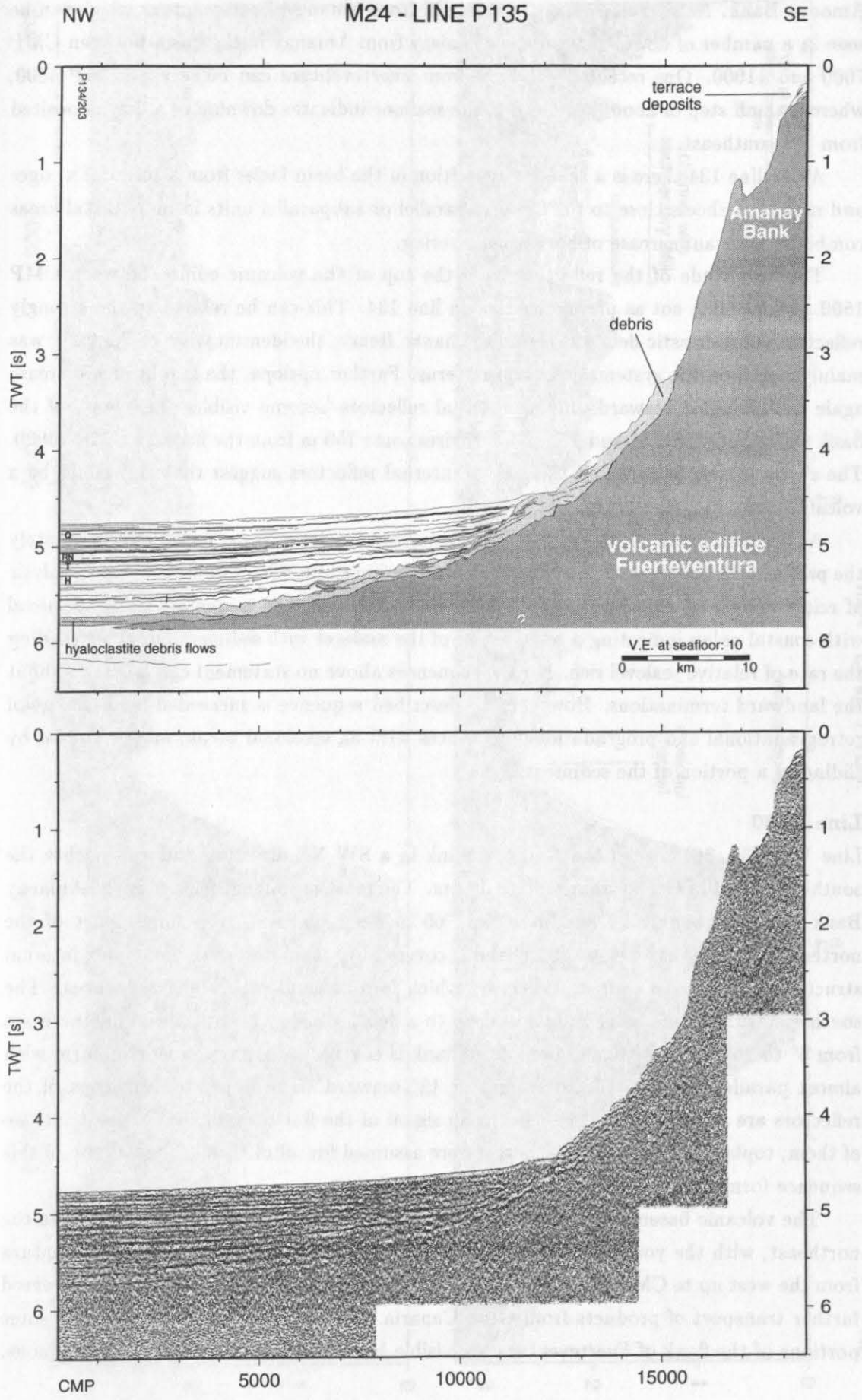

Figure 35: Seismic line P135 with linedrawing.

Amanay Bank. Nevertheless, there is also infill from Amanay/Fuerteventura which can be seen in a number of downlap terminations away from Amanay in the basin between CMP 7000 and 11000. One recent debris flow from Fuerteventura can be seen at CMP 4400, where a small step of about 7 meters at the seafloor indicates downlap of a flow deposited from the southeast.

As on line 134 there is a seaward transition in the basin facies from a series of wedges and mounded sheets close to the flank to parallel or subparallel units in more distal areas combined with an increase of horizontal layering.

The amplitude of the reflection from the top of the volcanic edifice between CMP 1500 and 10000 is not as pronounced as on line 134. This can be related to the strongly reflective volcaniclastic debris covering the flank. Hence, the identification of the flank was mainly based on the systematic onlap patterns. Further upslope, the amplitudes increase again and shingled seaward dipping internal reflectors become visible. The slope of the flank varies between 0.5° and 15°. A body rises some 150 m from the flank at CMP 16800. The shape of this feature and the lack of internal reflectors suggest that this could be a volcanic cone.

At the shelf break of the Amanay Bank some terrace deposits are found. Unfortunately the profile does not cover all landward reflector terminations which would allow an analysis of relative sealevel changes. Nevertheless, the lower sequence is sigmoid progradational with coastal onlap indicating a relative rise of the sealevel with sediment supply exceeding the rate of relative sealevel rise. For the sequences above no statement can be made about the landward terminations. However, the described sequence is succeeded by a change of retrogradational and progradational sequences with an erosional break, maybe caused by sliding of a portion of the sediments.

Line P130

Line 130 (Fig. 36) crosses the Amanay Bank in a SW-NE direction and approaches the southwest coast of Gran Canaria up to 12 km. The most prominent feature is the Amanay Bank with its roughly 12 km broad and 60 m deep plateau. The upper part of the northeastern flank has a slope of 12° and is covered by a thin unit with a complex internal structure of northeast dipping reflectors which form several prograding sequences. The southwestern volcanic flank is flattened up to a depth of 300 m where the slope increases from 6° to 24°. This flattened part of the flank is covered by a prograding clinoform with almost parallel internal reflectors, dipping 12° seaward. The upper terminations of the reflectors are usually masked by the strong signal of the flat seafloor, but at least for two of them, toplap is discernible and is therefore assumed for all of them. The flat top of this sequence forms the continuation of the volcanic plateau.

The volcanic basement on line 130 is formed by Fuerteventura (Amanay Bank) in the northeast, with the younger shield of Gran Canaria onlapping the flank of Fuerteventura from the west up to CMP 17000, where the increased slope of the Amanay Bank prevented further transport of products from Gran Canaria. Between CMP 14500 and 17000 some portions of the flank of Fuerteventura are visible beneath Gran Canaria as discontinuous,

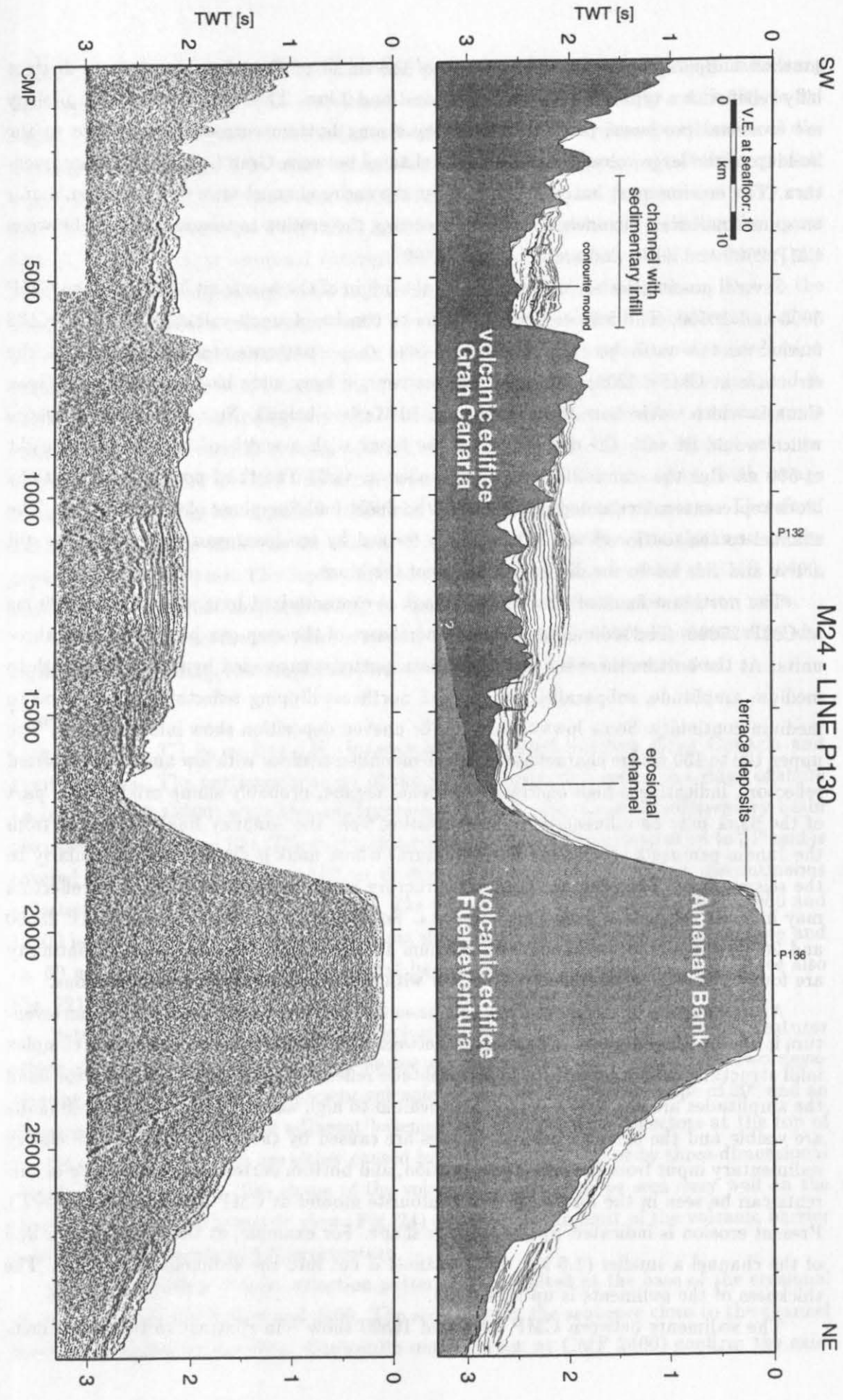

Figure 36: Seismic line P130 with linedrawing.

southwest dipping reflectors. The surface of the shield of Gran Canaria shows a distinct hilly relief with a typical wavelength between 1 and 3 km. The reason for this morphology are erosional processes, probably caused by strong bottom currents as response to the buildup of the large volcanic barrier in the channel between Gran Canaria and Fuerteventura. The erosion must have affected almost the entire channel after its formation. Later on some small scale channels developed, focussing the erosion to these areas (e.g. between CMP 2500 and 6000, and around CMP 16600).

Several possibilities are conceivable for the origin of the basement block between CMP 5000 and 10500. The feature does not seem to consist of small volcanoes as on line 133 further to the north because the typical cone shape patterns are missing (except the structure at CMP 10200). The next alternative is a large slide block coming from Gran Canaria which would have to be older than 10 Ma (see below). No scar is known onshore which would fit with the dimensions of the block with a width of 14 km and a height of 500 m. But the scar could have been eroded as well. The third possibility is that the block represents material deposited during the shield building phase of Gran Canaria. The channel to the southwest was subsequently formed by erosional processes which are still active and this led to the distinctive shape of the block.

The northeast flank of the Amanay Bank is characterized by a step of some 300 ms at CMP 27000. The sedimentary column northeast of the step can be divided into three units. At the bottom there is a cover of chaotic patterns succeeded by a number of high to medium amplitude, subparallel, uneven and northeast-dipping reflectors, with a good to medium continuity. Some lows caused by the uneven deposition show infill patterns. The upper 100 to 150 ms are characterized by the mounded seafloor with low amplitude internal reflectors, indicating a high energy depositional regime, probably slump origin. This part of the flank may be influenced by mass wasting from the Amanay Bank as well as from the Jandia peninsula (southwest Fuerteventura) whose flank is dipping perpendicularly to the seismic line. The observed complex structure at the seafloor with crossing reflectors may indicate deposition from Fuerteventura. Southwest of the step between CMP 25500 and 26700 three reflector bands with medium to high amplitudes and a good continuity are found. Elsewhere the reflectivity is low with only some discontinuous reflections.

A large portion of the uneven volcanic basement between Gran Canaria and Fuerteventura is filled with sediments. The channel between CMP 2500 and 6000 shows very complex infill structures with a prominent high amplitude reflector band. Below this reflector band the amplitudes are low, whereas they are medium to high above. Several small scale faults are visible and the complex infill structures are caused by the interaction of high energy sedimentary input from Gran Canaria, erosion, and bottom currents. The influence of currents can be seen in the formation of a contourite mound at CMP 5250 (2250 ms TWT). Present erosion is indicated by the seafloor shape. For example, at the northeastern wall of the channel a smaller (1.5 km wide) channel is cut into the sedimentary column. The thickness of the sediments is up to 450 ms.

The sediments between CMP 8000 and 16500 show – in contrast to the above men-

tioned channel – much better stratified infill patterns, with parallel to divergent or wavy reflection configurations. The amplitudes are in general high and the continuity is excellent. In the lower part of the sequence some faults have developed with vertical displacements of less than 5 m, while erosion has influenced the upper part of the sequence, especially between CMP 14000 and 16500 with chaotic reflection patterns and wavy cuts into the seafloor. Between CMP 8000 and 14000 the erosion is noticeable in the upper 100 ms, showing slight erosional cuttings which were subsequently filled. However, the erosion was not strong enough here to interrupt the stratified sedimentation. Due to the isolated location of this sedimentary infill structure, it is impossible to correlate any reflector directly into the apron north or south of Gran Canaria. A comparison of the reflection patterns is difficult as well, because the distinct vertical change of amplitudes as found in the apron is missing, including the reflection-free intervals. Nevertheless, there are some consistencies in the vertical spacing of reflectors which suggest that the deepest reflector band found in the low at CMP 12600 corresponds to reflector H in the apron, with an age of some 9.3 Ma. The low at CMP 10600 still contains some older sediments. Therefore, the beginning of the infill can be estimated to be around 10 Ma. The thickness of the sequence is up to 670 ms. The depth of reflector H is 530 ms below seafloor at CMP 10600, similar to Site 953 (526 ms), indicating no significant variation of sedimentation rates.

The sediments northeast of the erosional channel at CMP 16600 represent slope detritus with prograding, low amplitude reflectors which are eroded at their toe.

Line P133

Line 133 (Fig. 37) is, as line 130, located in the channel between Gran Canaria and Fuerteventura. The northwestern end of the profile crosses the submarine ridge offshore La Isleta (CMP 13000) while the southeastern end lies in the stratified sedimentary basin discussed above for line 130. The submarine ridge of La Isleta has a slope of up to 24° and is covered with a sequence of some 100 ms thick detritus with low amplitudes, discontinuous reflectors and a contorted configuration. The erosional channel between CMP 10000 and 12000 is filled with some detritus and three slide blocks which are some 700 m wide and ca. 60 m high. The channel can be traced basinwards where it crosses line 134 (see also Fig. 22).

Between CMP 10000 and 4000 the volcanic basement shows three elevated features which are interpreted as part of a submarine volcanic complex. The top of the two elevations at CMP 7000 and 4800 represent volcanic cones, the latter with a slope of 30° and an elevation of 840 m above the adjacent basement. Several internal reflectors at the top of the two northwestern rises are either caused by deposited detritus or by three-dimensional effects, i.e. side echoes. The shape of the volcanic complex can be seen very well on the three-dimensional bathymetric view (Fig. 24) at the northern limit of the volcanic barrier between Gran Canaria and Fuerteventura.

Sediments with a chaotic reflection pattern are deposited at the base of the erosional channel between CMP 3600 and 4400. The sediments in the sequence close to the channel have been eroded by currents. Contourite mounds (e.g. at CMP 2400) confirm the exis-

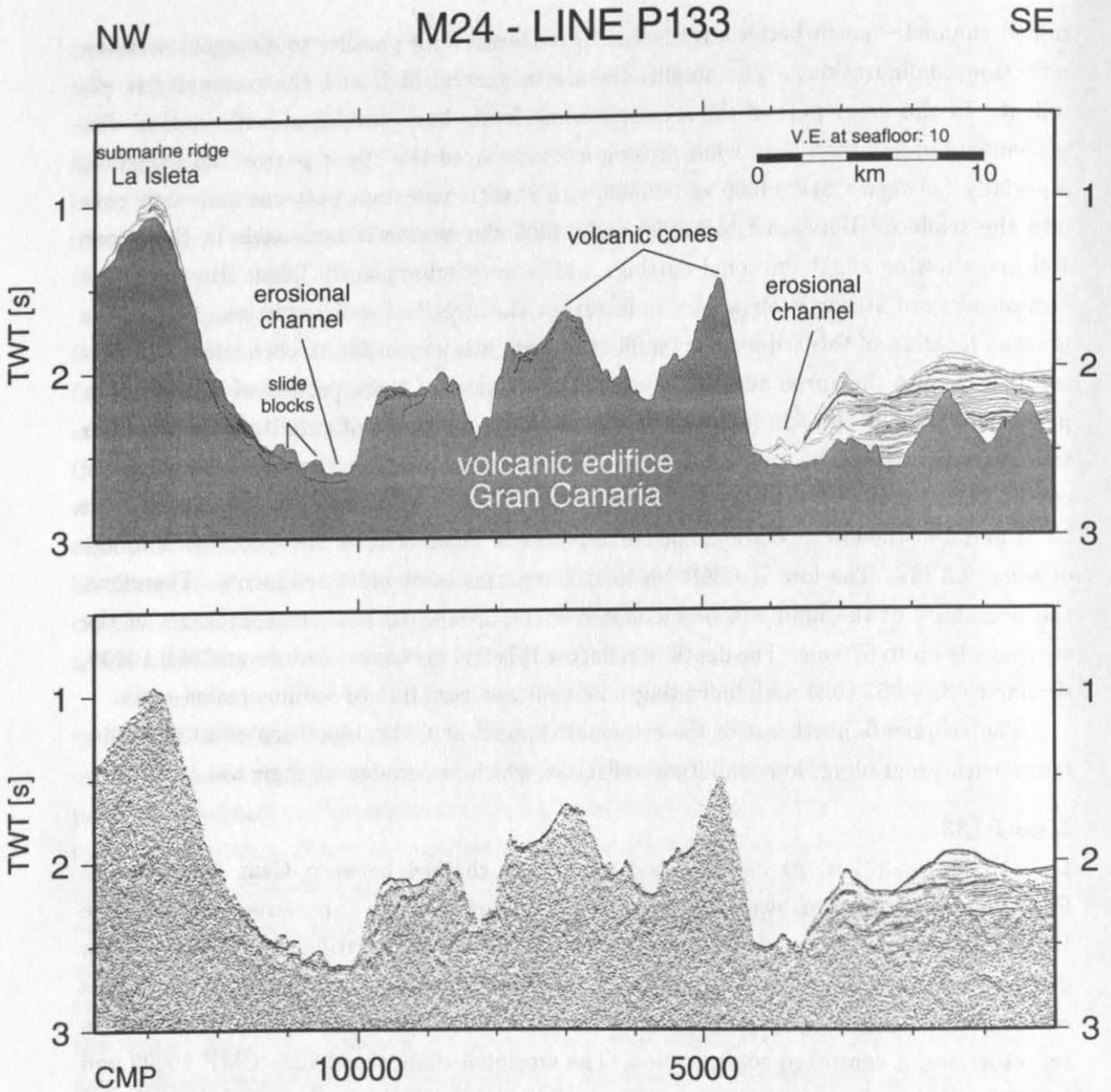

Figure 37: Seismic line P133 with linedrawing.

tance of currents which must have originated, or at least noticeably strengthened, after the build-up of the volcanic complex. Exact age correlation of the sediments on this line is not possible since this profile has no crosslines and reflection patterns are different from the apron and from line 130. Taking the thickness of the sediments into account and assuming sedimentation rates similar to those in the apron, currents must have been active since at least 5 my. The two cuts into the upper part of the sedimentary sequence around CMP 2400 and 400 represent erosional truncations.

The sediment unit covers two basement elevations at CMP 1500 and 400. Several reflectors of the surrounding sediments cross these basement structures. This three-dimensional effect indicates that the features are completely surrounded by sediments suggesting a cone shape, probably volcanic cones.

Line P136

The last profile crossing the Amanay Bank is line 136 (Fig. 38) with a SE-NW orientation into the basin north of Gran Canaria. The southeastern half of the volcanic top of the bank is almost horizontal and no sediments are deposited, whereas the northwestern half is gently dipping seaward (2.5°) and is covered with sediments. Between CMP 3600 and 5000 the sedimentary sequence shows a sigmoid progradational configuration with several toplap terminations at its upper boundary (seafloor) indicating erosional activity. The surface of the bank dipping towards the northwest is also seen on line 135. This suggests that erosion was stronger in the northern than in the southern part of the bank. This is quite reasonable as the Canary Islands are located in the northeast tradewind belt with a long term wave direction from the north.

At CMP 900 there is a 150 m high scarp in the basement. Below this scarp the flank is covered with a thin prograding sequence at the bottom, succeeded by an onlap fill unit. This fill unit is only partly seen at the margin of the line but probably represents the fill of the channel between the Amanay Bank and the Jandia peninsula. To the northwest the slope of the bank is up to 17°.

The top of the volcanic shield of Gran Canaria can be correlated along the profile from the crosspoint with line 134. Between CMP 23200 and 18000 the top is represented by a high amplitude and long period reflector, sometimes disrupted where small mounds have formed, but usually with a good continuity. The slope is around 1° as between CMP 25500 and 23200, but there the amplitudes and continuity are only moderate. Further upslope the amplitude becomes quite variable with low to medium values and a discontinuous mounded structure. At CMP 12200 the reflector terminates onlap onto the flank of the Amanay Bank. Between CMP 12200 and 19000 short discontinuous branches with low to medium amplitudes are visible beneath Gran Canaria. Northwest of CMP 19000 internal medium to high amplitude, discontinuous, subparallel to hummocky reflectors become visible below the flank of Gran Canaria.

Due to the tangential orientation of the profile relative to Gran Canaria, the reflection patterns of the sedimentary fill are quite different than the radial lines, such as e.g. P134. The reflectors are in general less continuous and noticeably uneven and many of them terminate onlap or downlap onto the underlying dipping reflectors. Furthermore, a number of small scale infill structures are observed, in general < 1 km wide. From CMP 19500 upslope the sediments are quite mounded and wavy. The structure between CMP 16800 and 15600 at around 4.8 s TWT represents a contourite and a migrating wave, deposited between 9.5 and 5.5 Ma. The northwest dipping parts of these wavy reflectors often form unconformities with onlap onto them whereas the lows formed by the wavy reflectors show onlap fill. The mounded structures with the observed contourites suggest a major sediment supply from the channel between Gran Canaria and Fuerteventura rather than from the Amanay Bank. Input from the bank seems to be limited mainly to the area upslope of CMP 12500 with a composition of prograded fill and chaotic reflection patterns. The continuing influence of the channel on the sedimentation is visible in a recently formed

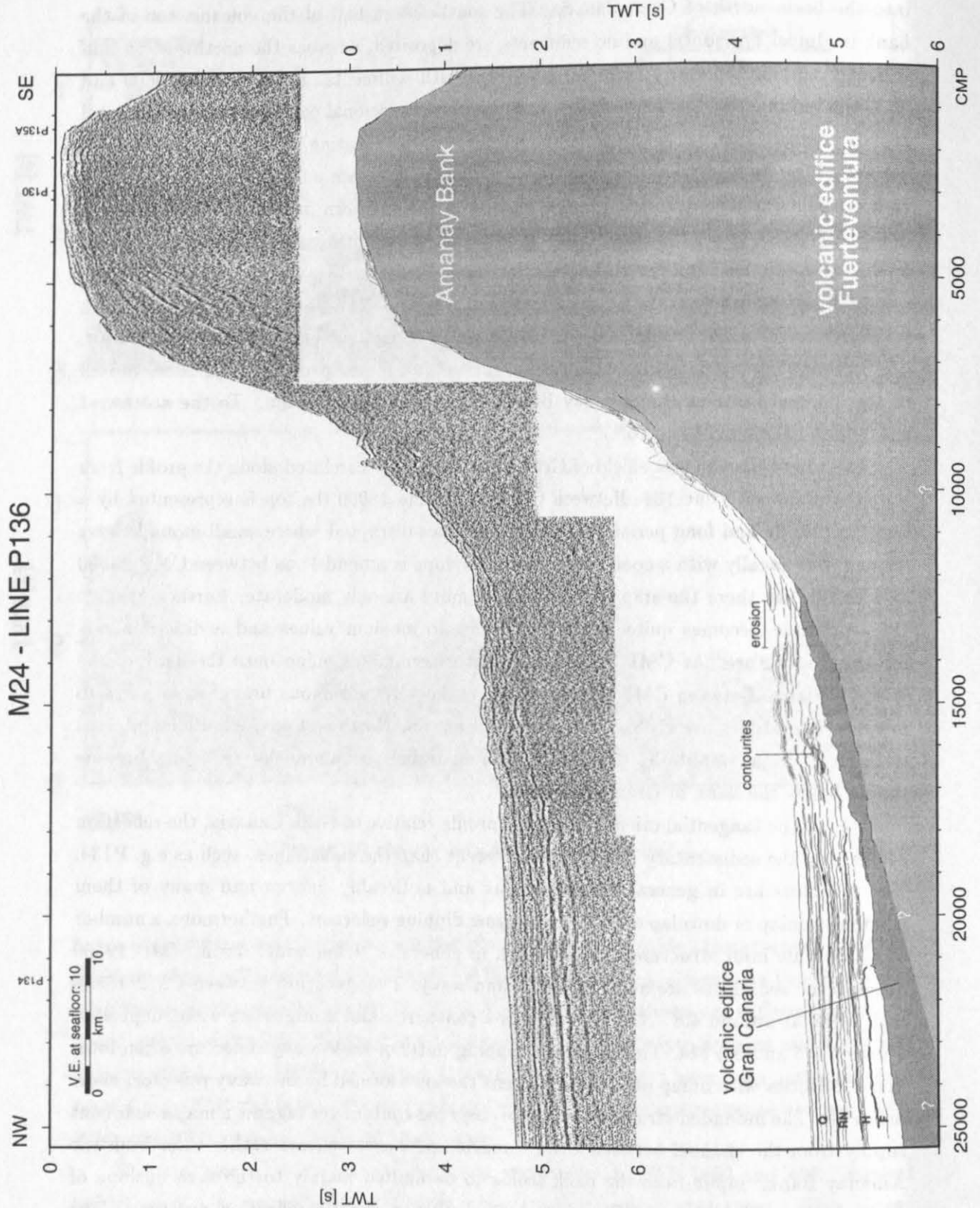

Figure 38: Seismic line P136 with linedrawing.

erosional truncation between CMP 12600 and 13600, probably induced by bottom currents from the channel.

The correlation of reflectors is often hampered by the discontinuous patterns and ends in general in the wavy area southeast of ca. CMP 17000. Between reflector F and the shield of Gran Canaria the reflectors are extremely discontinuous, hummocky and with low to medium amplitudes, indicating a high depositional energy of this sequence (> 12 Ma) with probably a high amount of slumped material.

Line P301

Line 301 (Fig. 39) is orientated north-south and approaches the shore line of Gran Canaria up to 6 km. In contrast to line 134, the flank of Gran Canaria has only a moderate slope of 6° averaged between CMP 34 and 8600. At CMP 8600 the average slope decreases almost immediately to 0.7° up to CMP 17300. Here the feather edge of the flank is located 61 km north of Gran Canaria at 5780 ms TWT. The amplitude of the flank is medium to high south of CMP 11000; further north it is only low to moderate. The shape of the flank shows several steplike variations: steeper parts are alternating with flatter intervals. Between CMP 3000 and 6200 these flat parts have a seaward dip of ca. 4° and are covered with up to 275 ms thick sediments, in contrast to the steeper, almost sediment free parts in between. Internal reflectors of the volcanic shield show northward dipping patterns: they are discontinuous and have low amplitudes.

Between CMP 2000 and 3600 the flank is characterized by a rise of some 375 m (500 ms TWT) of height, showing many chaotic internal reflectors in contrast to the surrounding volcanic basement. This feature corresponds to a part of the northeast striking submarine ridge of Galdar on the bathymetric map (Fig. 26, 22), and is interpreted as a slide deposit.

The patterns of the sediment fill on line 301 differ significantly from the profiles discussed so far. First, the slope facies is less conspicuous due to its limited extent. It extends no further basinward than up to CMP 11000 and the thickness is < 275 ms, and seaward of CMP 7000 is in general < 100 ms. The chaotic patterns are rarely distinct, e.g. the reflector RN can be correlated up to the flank where it onlaps. The structure and size of the slope facies indicate a low sedimentary input from Gran Canaria on this profile, and also the depositional energy is low.

Secondly, the reflectivity of the basin facies is reduced compared to line 134. This comprises the amplitude as well as the continuity of the reflectors. Except for the reflector bands around reflectors RN and Q and some deeper reflectors (below 5.5 s TWT at the northern end of the profile), almost no medium to high amplitude reflections are visible which could be correlated over large distances. The intervals between the seafloor and reflector band Q and between reflectors Q and RN, respectively, tend to be reflection free, the narrow cycle breadth as found on line 134 is missing. Seaward of CMP 11000 the reflection patterns of reflector bands Q and RN change from continuous and almost parallel to subparallel and disrupted. At CMP 15700 some small faults can be seen around reflector Q. The reflectivity in the sedimentary sequence is reduced for the entire line 301, whereas the two crossing lines 205 (Fig. 44) and 202 (Fig. 45) show a gradual decrease of

reflectivity from east to west.

Therefore, the transport of volcaniclastic material from Gran Canaria was directed preferably to the northeast. The reason can be seen in the Galdar Ridge (Fig. 22), whose seaward extension coincides well with the amplitude decrease of the tangential profiles in the north. This would also imply that the paths of the volcaniclastic transport onshore Gran Canaria avoided the Galdar Ridge and is indicated by the lack of large canyons in this area as well as the indistinct slope facies on line 301. The deposition of the Roque Nublo volcaniclastics on profile 301 suggests different paths of transportation compared to the older volcanic deposits, probably combined with a higher depositional energy. For some of the sediments in the Quaternary interval (sandlayers above reflector Q), Tenerife is conceivable as source, bypassing the ridge of Galdar.

The influence of the Galdar Ridge on almost the entire sedimentary column suggests that the process which has formed the ridge has taken place only shortly after the shield-building phase of Gran Canaria. It is not clear whether the lowermost reflectors (below ca. 5.5s TWT at CMP 19500) were already affected by the ridge, because they still show a westward decrease of amplitude, even though not as clear as the overlying reflectors. In case they were not influenced, the age of the origin of the ridge/slide can be estimated as 12 Ma, otherwise between 15 and 12.5 Ma.

Between CMP 8800 and 11200 a thick debris flow, whose top was drilled at Site 954 can be correlated as corresponding to lithologic unit IV (Schmincke, Weaver, Firth et al., 1995). Further upslope the correlation is hampered by a small fracture with chaotic patterns to the south. Around CMP 11200 the amplitudes decrease, which prevents a reliable correlation basinward, but the debris flow probably continues in the medium to high amplitude band indicated by a question mark in Fig. 39. This gives an age of 12.1-12.3 Ma for the mass wasting event (between reflector 39 and 40 at Site 953, see Table 4).

The last point to discuss on line 301 is the well-stratified sedimentary body between CMP 5300 and 6200, with a thickness of some 200 ms. It is interpreted as a slide block because it downlaps onto the older seafloor. The reflection patterns between CMP 7500 in the basin and the slide are very similar with regard to the spacing of reflectors and their amplitude relations. This allows an estimate of the age of the displaced sediments. The base of the slide is represented by reflector RN (3.8 Ma), i.e. that the glide plane is possibly formed by lapillistone. If this is the case, perhaps high pore pressure in the porous lapillistone drilled at Site 954 may have facilitated the displacement. The sediments at the top are recent and the slide movement must have taken place quite recently. The well preserved internal structure suggests a very slow motion which possibly still continues because the block is located on an inclined surface (3.5°).

The low deformation of the slide allows some assumptions with regard to the original deposition area. First of all this area must be located north of CMP 3300 because the Galdar Ridge represents a morphological barrier for downslope movements. This restricts the search on the two dipping plateaus between CMP 3300 and 4300, and between CMP

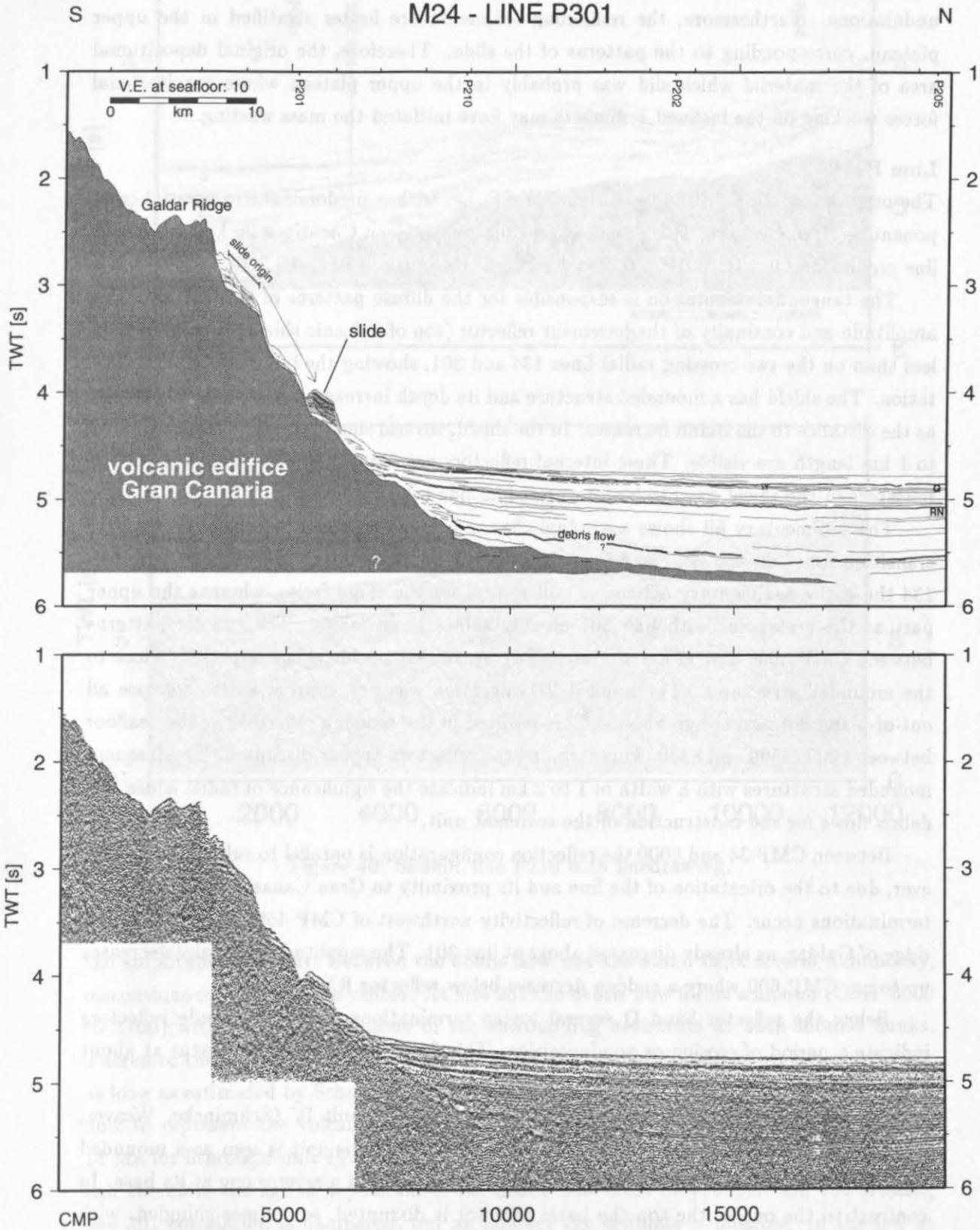

Figure 39: Seismic line P301 with linedrawing.

4500 and 5300, respectively. Both places fit well with the dimensions of the slide, but the first one has a very flat surface in contrast to the lower plateau, with some small-scale undulations. Furthermore, the remaining sediments are better stratified in the upper plateau, corresponding to the patterns of the slide. Therefore, the original depositional area of the material which slid was probably in the upper plateau where gravitational forces working on the inclined sediments may have initiated the mass wasting.

Line P210

The orientation of line 210 (Fig. 40) is NW-SE, i.e. with a predominant tangential component to Gran Canaria. The closest approximation to Gran Canaria is 20 km, where the line crosses profile 134. ODP Site 954 is located 214 m south of CMP 3264.

The tangential orientation is responsible for the diffuse patterns of this section. The amplitude and continuity of the basement reflector (top of volcanic shield) is considerably less than on the two crossing radial lines 134 and 301, showing the influence of the orientation. The shield has a mounded structure and its depth increases towards the northwest as the distance to the island increases. In the shield, several short reflection branches of up to 1 km length are visible. These internal reflectors are dipping to the northwest. Other reflectors in the shield have to be interpreted as side echos.

The sedimentary fill shows a gradual change from slope facies in the southeast to a transition zone between slope and basin facies in the northwest. At the crosspoint with line 134 the entire sedimentary column is still typical for the slope facies, whereas the upper part at the crosspoint with line 301 already shows basin facies. The chaotic patterns between CMP 6000 and 12000 are intensified by numerous side echos, especially close to the mounded structures. The applied 2D-migration was not appropriate to collapse all out-of-plane diffraction hyperbolas. This resulted in the crossing reflectors at the seafloor between CMP 6500 and 8300. Furthermore, the reflectors appear disrupted. The frequent mounded structures with a width of 1 to 2 km indicate the significance of radial slides and debris flows for the construction of the sediment unit.

Between CMP 34 and 6000 the reflection configuration is parallel to subparallel. However, due to the orientation of the line and its proximity to Gran Canaria, many downlap terminations occur. The decrease of reflectivity northwest of CMP 4500 is caused by the ridge of Galdar, as already discussed above at line 301. The amplitude gradually decreases up to ca. CMP 600 where a sudden decrease below reflector RN occurs.

Below the reflector band Q several toplap terminations of low amplitude reflectors indicate a period of erosion or nondeposition. This fits with the observed hiatus at about 80 mbsf at Site 954 (Schmincke, Weaver, Firth et al., 1995).

The most interesting feature on line 210 is lithologic unit IV (Schmincke, Weaver, Firth et al., 1995) drilled at Site 954. In the seismic data this unit is seen as a mounded reflector band with a normal polarity reflection at its top and a reverse one at its base. In contrast to the one at the top the basal reflector is disrupted, sometimes shingled, with varying amplitudes, and therefore more difficult to correlate. The unit is interpreted as a debris flow and terminates onlap on the island flank at CMP 5200; west of CMP 450

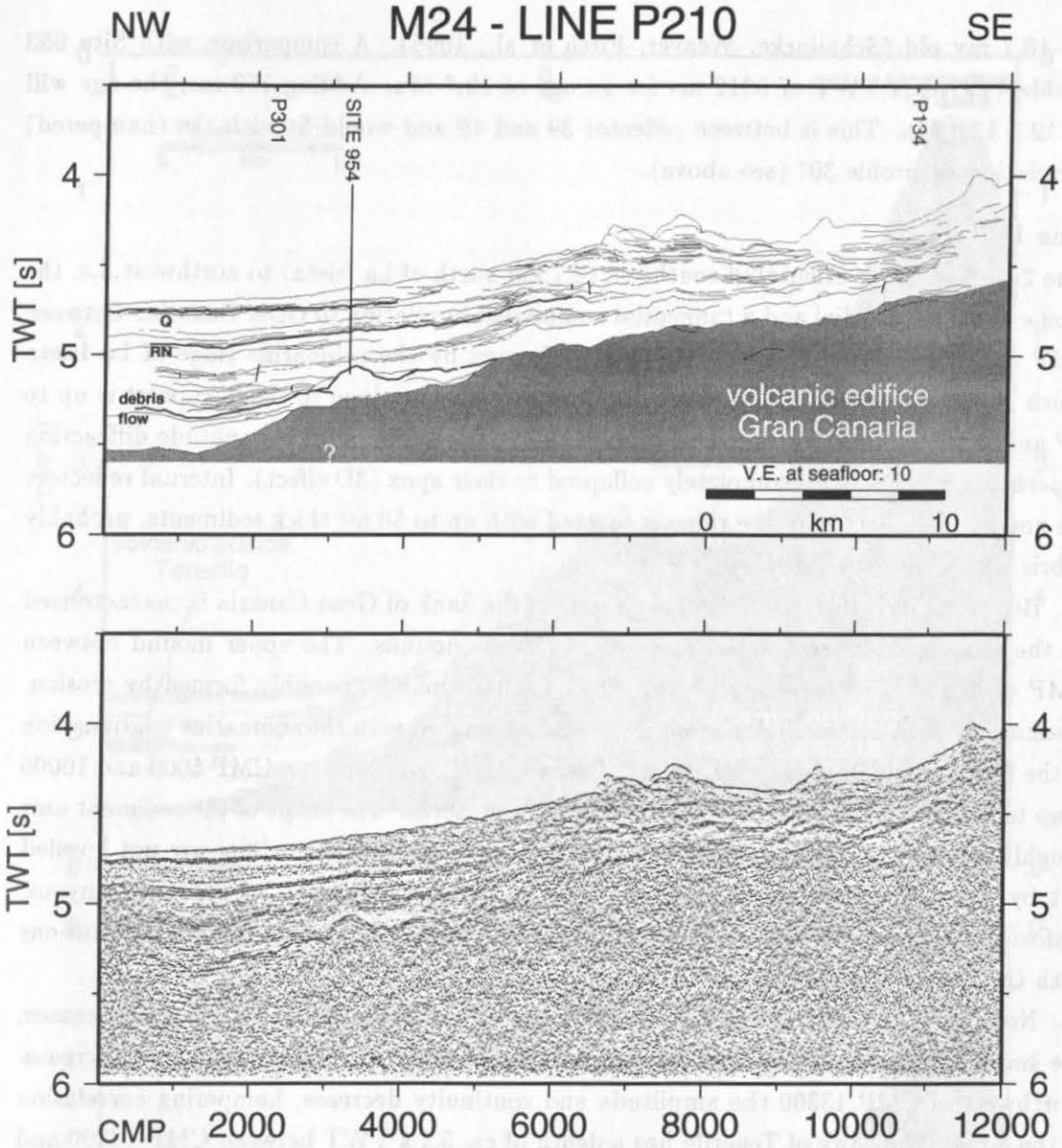

Figure 40: Seismic line P210 with linedrawing.

the amplitude fades out. Between the debris flow and the island flank several hummocky, discontinuous reflectors are visible. At Site 954 the debris flow forms a mound (CMP 3000 to 3700) with onlap terminations of the surrounding sediments at both mound flanks. Therefore the top of the mound is characterized by a depositional hiatus, but not lasting as long as estimated by Schmincke, Weaver, Firth et al. (1995). They interpret the debris flow to represent the volcanic shield of Gran Canaria and therefore assumed an age of 14 Ma for lithologic unit IV. But the seismic data show the volcanic shield below unit IV and therefore the age of deposition of the debris flow must be younger. On the crossing line 301 correlation is hampered, but an indirect age estimate is possible. In the low at CMP 1250 some 150 ms thick sediments were deposited which show onlap terminations onto the mound at Site 954. The oldest sediments above the debris flow at Site 954 are

ca. 10.7 my old (Schmincke, Weaver, Firth et al., 1995). A comparison with Site 953 (Table 4) gives a TWT of 5312 ms for an age of 10.7 Ma. Adding 150 ms, the age will be 12.1-12.3 Ma. This is between reflector 39 and 40 and would fit with the (hampered) correlation on profile 301 (see above).

Line P201

Line 201 (Fig. 41) is orientated southeast (2.7 km north of La Isleta) to northwest, i.e. the profile has both a radial and a tangential component in relation to Gran Canaria. Between CMP 34 and 4500 the volcanic basement is formed by the submarine ridge of La Isleta which is obliquely crossed at a water depth of 320 m. The slope to the northwest is up to 16° and the steep flank is composed of remnants of a number of high amplitude diffraction hyperbolas which are not completely collapsed to their apex (3D effect). Internal reflectors are not visible. The top of the ridge is covered with up to 50 ms thick sediments, probably debris with chaotic reflection patterns.

Between CMP 4500 and 10500 the shape of the flank of Gran Canaria is characterized by the crossing ridge of Galdar, showing two large mounds. The upper mound between CMP 4500 and 8800 is composed of several smaller mounds, possibly formed by erosion. The cut around CMP 5200, for example, can be correlated with the submarine continuation of the Barranco de Azuaje (see Fig. 22). The sediment cover between CMP 5000 and 10000 is up to 250 ms thick and shows chaotic reflection patterns. The shape of the sediment unit roughly follows the basement morphology, i.e. lows in the volcanic edifice are not levelled out by the subsequent sedimentation. This is another indication of crossing canyons. Unfortunately the coverage with swath bathymetry does not allow further correlations with the canyon system onshore.

Northwest of CMP 10500 the apparent dip of the flank of Gran Canaria decreases, the mounds become flatter and wider, and the number of internal reflectors increase. Northwest of CMP 13300 the amplitude and continuity decrease, hampering correlation of the flank. The flank of Tenerife has a depth of ca. 5.1 s TWT between CMP 13700 and 16000 and overlies the flank of Gran Canaria. The amplitude of Tenerifes shield is low and therefore difficult to identify in Fig. 41. The pedestal is relatively thin and therefore some energy is reflected from the underlying sediments, although their amplitudes are only low to moderate. These low amplitudes may be related to the generally low reflectivity west of the Galdar Ridge.

The sedimentary fill is characterized by more or less chaotic patterns with mounds such as that at CMP 14000 (5.2 s): discontinuous and disrupted reflectors with many baselap terminations onlap as well as downlap.

Line P206

The northwestern continuation of profile 201 is line 206 (Fig. 42) which is located tangential to the northeastern tip of Tenerife and approaches the island as close as 25 km. The profile crosses the channel between Gran Canaria and Tenerife at its northern entrance.

The volcanic pedestal of Tenerife with a depth between 4950 and 5050 ms divides the

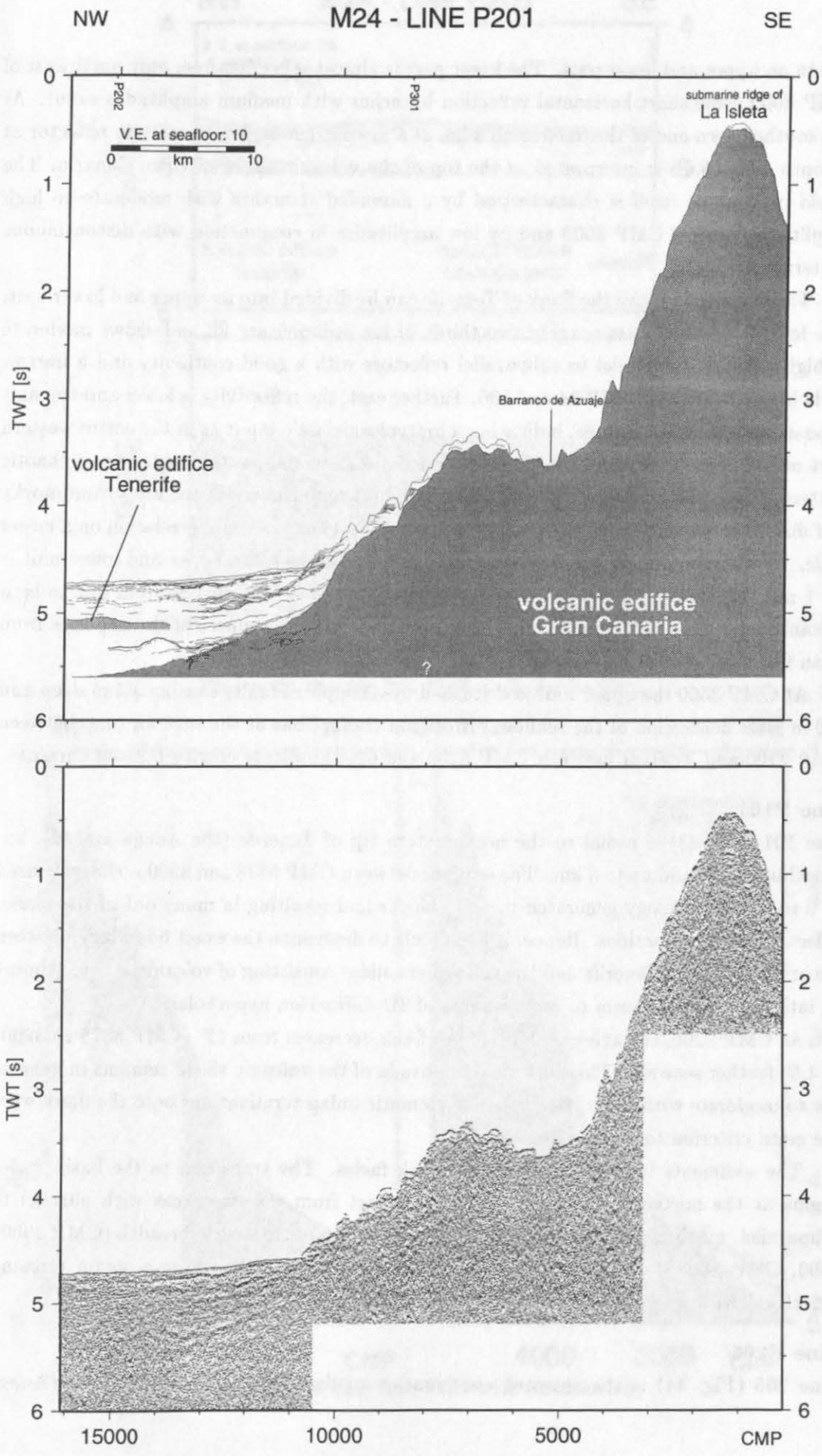

Figure 41: Seismic line P201 with linedrawing.

line in an upper and lower part. The lower part is almost reflection-free; only northwest of CMP 4000 some short horizontal reflection branches with medium amplitudes occur. At the southeastern end of the line, some 3 km of a discontinuous, low amplitude reflector at a depth of ca. 5.6 s is interpreted as the top of the volcanic shield of Gran Canaria. The shield of Tenerife itself is characterized by a mounded structure with moderate to high amplitudes west of CMP 3000 and by low amplitudes in conjunction with discontinuous patterns elsewhere.

The sediments above the flank of Tenerife can be divided into an upper and lower unit. The lower part comprises roughly two thirds of the sedimentary fill and shows moderate to high amplitude, parallel to subparallel reflectors with a good continuity and a narrow cycle breadth between CMP 34 and 600. Further east, the reflectivity is lower and the unit appears almost reflection free, indicating a low volcaniclastic input as in the entire western part of the apron (see line 205). The upper unit is some 100 ms thick and shows chaotic patterns. Individual reflectors have a medium to high amplitude, but the wavy/hummocky and disrupted patterns with numerous baselaps and toplaps prevent correlation on a larger scale. At the crosspoint with line 202, the boundary between the upper and lower unit is ca. 1 my old. Hence, the lower unit is some 6 to 1 my old. The change from low to high volcaniclastic input at around 1 Ma indicates a change of the source of the deposits from Gran Canaria to Tenerife.

At CMP 3500 the upper unit is disturbed by a couple of faults causing a 4 m deep and 120 m wide depression of the seafloor. Erosional truncations at the seafloor (e.g. between CMP 2100 and 3300, or between CMP 5200 and 6200) indicate erosive bottom currents.

Line P101

Line 101 (Fig. 43) is radial to the northeastern tip of Tenerife (the Anaga massif), approaching the island up to 6 km. The seafloor between CMP 5878 and 3900 is characterized by a rough morphology generated by slide blocks and resulting in many out-of-the-plane-reflections and diffractions. Hence, it is difficult to determine the exact boundary between the original flank of Tenerife and the subsequent slides consisting of volcaniclastics. Almost all internal reflectors seem to be remnants of 3D-diffraction hyperbolas.

At CMP 3200, the average slope of the flank decreases from 12° (CMP 5878 to 3200) to 4.5° further seaward. The reflection amplitude of the volcanic shield remains in general low to moderate with a low continuity. Systematic onlap terminations onto the flank were the main criterion to detect the flank.

The sediments belong mainly to the flank facies. The transition to the basin facies begins at the northeastern end of the line. Apart from the two areas with parallel to subparallel, medium to high amplitude reflectors with a narrow cycle breadth (CMP 1900–1000, CMP 800–34), the general patterns are more or less chaotic (e.g. again crossing reflectors) with many mounds, best seen at the seafloor.

Line P205

Line 205 (Fig. 44) is the seaward continuation of line 101, radial to Tenerife (Anaga

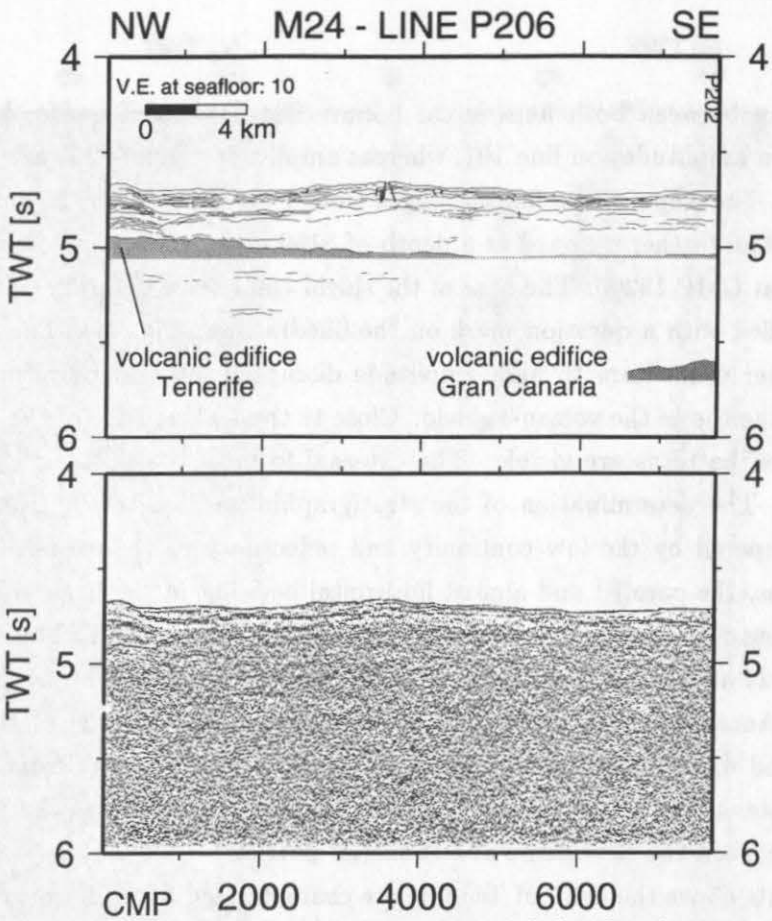

Figure 42: Seismic line P206 with linedrawing.

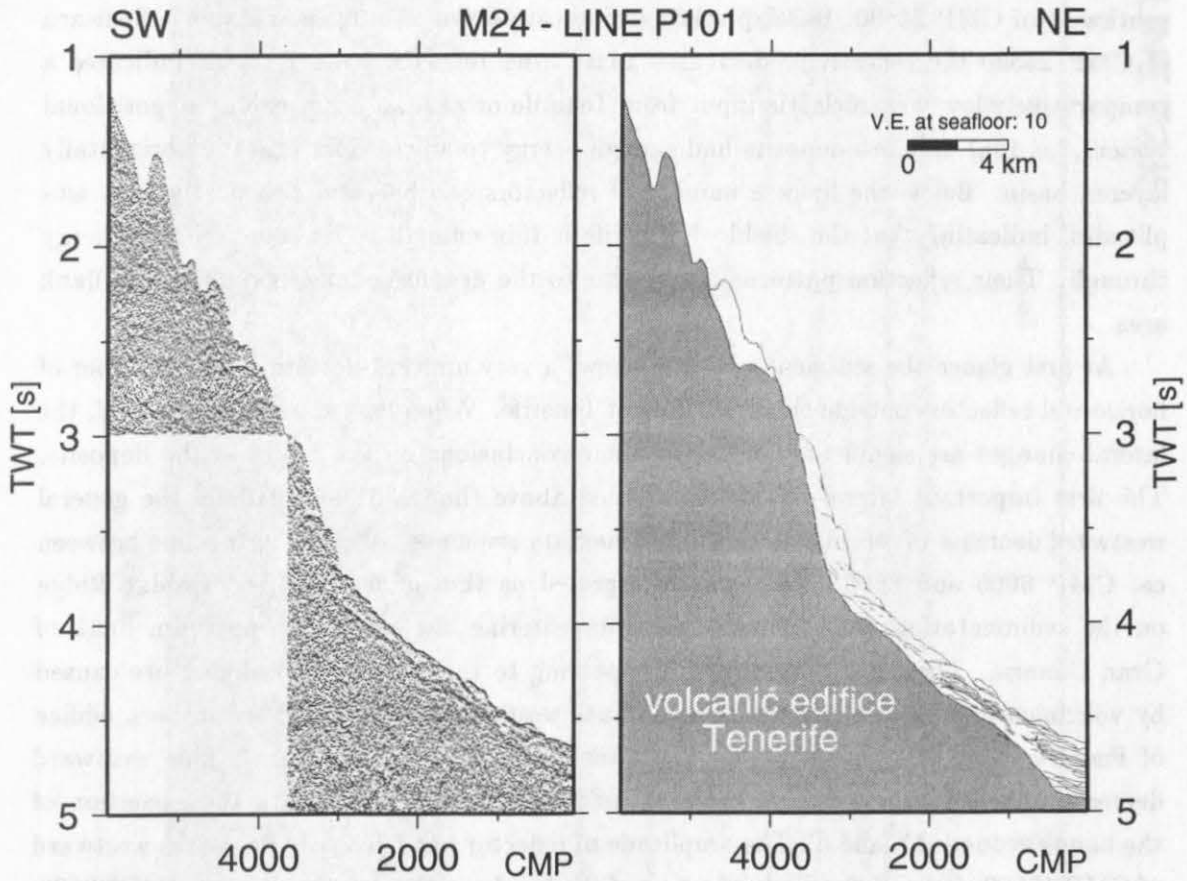

Figure 43: Seismic line P101 with linedrawing.

massif). The gap between both lines is ca. 1 km. The flank of Tenerife shows low to medium reflection amplitudes on line 101, whereas amplitudes on line 205 are high with a good continuity. The slope of the flank changes from 1° between CMP 25400 and 22300 to almost horizontal further seaward at a depth of 5190 ms where the reflection from the shield fades out at CMP 19200. The base of the shield can not be determined exactly and is therefore labelled with a question mark on the linedrawing (Fig. 44). The shield itself contains a number of medium to high amplitude disrupted internal reflectors, which in general parallel the top of the volcanic shield. Close to the feather edge of the shield some shingled reflection patterns are visible. The external form of the shield is characterized by flat mounds. The determination of the stratigraphic position of the feather edge in the basin is hampered by the low continuity and reflectivity in the western part of the line. Nevertheless, the parallel and almost horizontal bedding in the basin allows a good estimate of the age of the flank. It is some 30 ms deeper than reflector T. This corresponds to reflectors 23/24 at Site 953 (Table 4), with an age of ca. 6 Ma. The maximum K-Ar dates given by Ancochea et al. (1990) are 5.7 Ma for the eastern part of the subaerial Anaga massif and 6.5 Ma for the western part, which is further away from the seismic line. This indicates a rapid growth of the submarine shield of Anaga as there is no large age difference between the submarine and subaerial portion.

The sediments above the flank of Tenerife are characterized by medium to high amplitude, parallel to subparallel reflectors with a narrow cycle breadth and a wavy tendency southwest of CMP 24500. Baselap relations indicate downslope mass transport. Seaward of CMP 24500 the reflectivity decreases apart from reflector band Q. This indicates a comparatively low volcaniclastic input from Tenerife or at least a low energy depositional system, i.e. that only few deposits had enough energy to advance far into the horizontally layered basin. Below the flank a number of reflectors can be seen with partly high amplitudes, indicating that the shield of Tenerife is thin enough to let some seismic energy through. Their reflection patterns are similar to the deeper sediments outside the flank area.

At first glance the sedimentary basin shows a very uniform pattern with a number of horizontal reflectors outside the flank area of Tenerife. When looked at in more detail, the lateral changes are significant and allow some conclusions on the origin of the deposits. The first important lateral change mentioned above (lines 301 and 210) is the general westward decrease of reflectivity in the sedimentary sequence, starting on this line between ca. CMP 6000 and 8000. This was interpreted as the influence of the Galdar Ridge on the sedimentation paths of volcaniclastics entering the sea at the northern flank of Gran Canaria. Therefore, reflections disappearing to the west most probably are caused by volcaniclastics from Gran Canaria, because westward input from the southern edifice of Fuerteventura is expected to be low after its shield building phase. This westward decrease of reflectivity is visible between reflector bands Q and F with the exception of the bands around RN and T. The amplitude of reflector band RN first decreases westward of CMP 17500. Some individual reflectors of the band can be correlated up to CMP 23500.

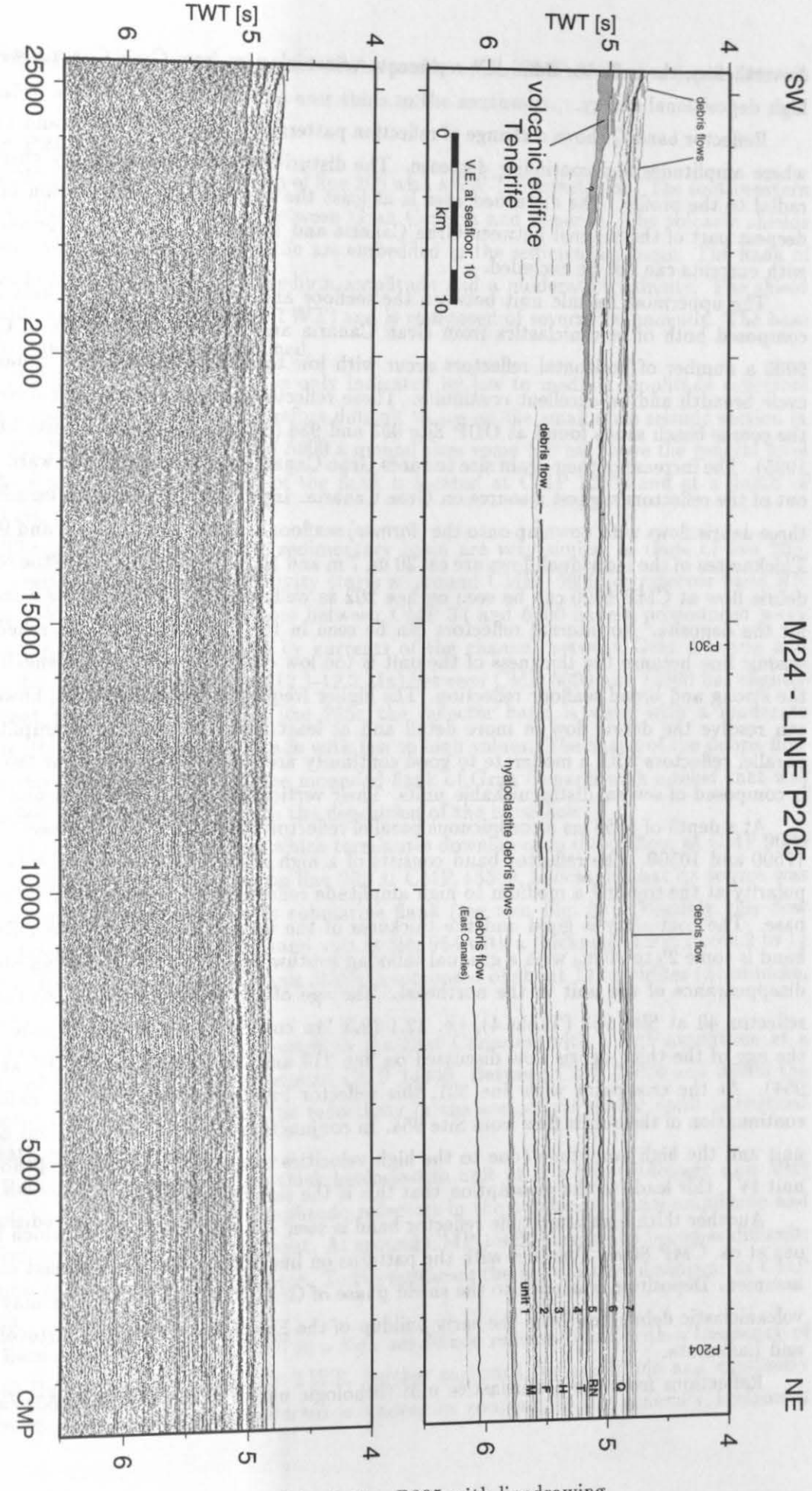

Figure 44: Seismic line P205 with linedrawing.

Nevertheless, the reflector band RN represents volcaniclastics from Gran Canaria with a high depositional energy.

Reflector band Q shows a change of reflection patterns between CMP 16000 and 11200 where amplitudes and continuity decrease. The disturbance may be caused by currents radial to the profile. The disturbed area is at least the approximate continuation of the deepest part of the channel between Gran Canaria and Tenerife. Therefore, a connection with currents can not be excluded.

The uppermost seismic unit between the seafloor and reflector Q (seismic unit 7) is composed both of volcaniclastics from Gran Canaria and Tenerife. Northeast of CMP 9000 a number of horizontal reflectors occur with low to medium amplitudes, a narrow cycle breadth and an excellent continuity. These reflectors are interpreted as caused by the coarse beach sands found at ODP Site 953 and 954 (Schmincke, Weaver, Firth et al., 1995). The increase of their grain size towards Gran Canaria and the lateral westward fade out of the reflectors suggest a source on Gran Canaria. Input from Tenerife can be seen in three debris flows with downlap onto the (former) seafloor at CMP 25000, 23500 and 9000. Thicknesses of the individual flows are ca. 20 m, 7 m and 10 m, respectively. The toe of the debris flow at CMP 9000 can be seen on line 202 as well, suggesting Tenerife as a source for the deposits. No internal reflectors can be seen in this debris flow on the reflection seismic line because the thickness of the unit is too low compared to the wavelength and the strong and broad seafloor reflection. The higher frequency Parasound data, however, can resolve the debris flow in more detail and at least four low to medium amplitude, parallel reflectors with a moderate to good continuity are visible, indicating that the flow is composed of several distinguishable units. Their vertical spacing is between 1 and 2 m.

At a depth of 5550 ms a conspicuous parallel reflector band can be seen between CMP 17500 and 10500. The reflector band consists of a high amplitude reflector with normal polarity at the top and a medium to high amplitude reflector with reverse polarity at the base. The continuity is good and the thickness of the unit represented by the reflector band is some 25 to 30 ms with a gradual thinning southwest of CMP 16000 and an abrupt disappearance of the unit in the northeast. The age of the unit corresponds to that of reflector 40 at Site 953 (Table 4), i.e. 12.1-12.3 Ma corresponding approximately with the age of the thick debris flow discussed on line 210 and 301 (lithologic unit IV at Site 954). At the crosspoint with line 301, this reflector band corresponds to the assumed continuation of the debris flow from Site 954. In conjunction with the lateral extent of the unit and the high amplitude (due to the high velocities of up to 5 km/s in the lithologic unit IV), this leads to the assumption that this is the same debris flow unit.

Another thick high amplitude reflector band is seen at a depth of 6050 ms which fades out at ca. CMP 8000. Together with the patterns on line 202, a source in the east can be assumed. Deposition was prior to the shield phase of Gran Canaria. Hence, this may be a volcaniclastic debris flow from the early buildup of the East Canary islands Fuerteventura and Lanzarote.

Reflections from the hyaloclastite unit (lithologic unit VII at ODP Site 953) can be

correlated on the northeastern part of the profile up to CMP 9500 at a depth between ca. 5740 and 5820 ms TWT. The unit thins to the southwest.

Line P202

Line 202 (Fig. 45) is located south of line 205 with a SW-NE orientation. The southwestern end is directed to the channel between Gran Canaria and Tenerife. The volcanic shields of both Gran Canaria and Tenerife are embedded in the sedimentary basin. The flank of Tenerife is characterized by a medium amplitude and a moderate continuity. The shield extends up to CMP 6500 (5.2 s TWT) and is composed of several flat mounds. The base of the shield can not be determined.

The flank of Gran Canaria is only indicated by low to medium amplitude reflectors with a low continuity and is therefore difficult to see on the small scale seismic section in Fig. 45. Between CMP 3700 and 5900 a mound rises some 100 ms above the general level of the flank. The feather edge of the flank is located at CMP 12700 and at a depth of 5640 ms.

The general features of the sedimentary basin are very similar to those of line 205. The westward decrease of reflectivity starts at around CMP 15000 for reflector band RN at ca. CMP 10000. The reflectors between CMP 34 and 6400 have a pronounced wavy character interpreted as caused by currents of the channel between Gran Canaria and Tenerife. The thick debris flow (12.1-12.3 Ma) between CMP 5000 and 14500 has slightly different patterns compared to line 205: the reflector band is wavy with a moderate continuity and a variable amplitude with low to high values. The shape of the debris flow is for the most part caused by the mounded flank of Gran Canaria with a relief that was not filled up horizontally prior to the deposition of the mass flow.

The Quaternary debris flow which terminates downlap onto the seafloor at CMP 9000 on line 205 has its termination on line 202 at CMP 15500, indicating that its source was somewhere on Tenerife or at its submarine flank (see also Fig. 58). Possibly this flow corresponds to the very shallow sand unit at Site 954 with a thickness of 9 m (from 2 to 11 mbsf). This sand unit with volcanic lithics is composed of about 12 turbidites (Schmincke, Weaver, Firth et al., 1995).

The debris flow, possibly sourced in the East Canaries, with a high amplitude at a depth of 6050 ms, thins out at around CMP 14000. Between CMP 30000 and 33000 the reflector is hardly visible since the reflectivity in the area of the domal uplift is reduced beneath reflector M.

Reflectors belonging to the thick hyaloclastite unit at Site 953 (lithologic unit VII) are visible as medium to high amplitude reflectors in the northeast, whose amplitude and continuity decrease to the southwest. At around CMP 15000 correlation becomes difficult; the unit is expected to thin out here. To the northeast the hyloclastites disappear at CMP 28800.

Between CMP 16100 and 20700 a high amplitude reflector band with a frequency of ca. 40 Hz can be seen below 7 s TWT. Further eastward the amplitude and continuity decrease. The shape of the reflector is uneven in contrast to the generally horizontal

bedding patterns in the basin. This reflector is interpreted to represent the oceanic crustal basement based on its shape and depth. Refraction seismic data (Ye et al., 1996) suggest a basement depth of roughly 7.5 s TWT; similar values were found in the basin south of Gran Canaria and Tenerife during the Charles Darwin cruise No. 82 (Watts et al., 1993).

The northeastern end of the profile is characterized by domal uplifts. The origin of these features is discussed below. Here, only a description of the structures is given. The area influenced by the uplift starts at around CMP 29500 with a dip of some 0.5° for the elsewhere nearly horizontal reflector M. Between CMP 31400 and 31900 reflector M and seismic unit 2 are pierced by the uplifted material. The reflectors in seismic units 3 to 5 and in the lower part of unit 6 can be correlated across the uplifted structure, but are domed up. Two faults in seismic units 3 and 4, and several small faults affecting reflector band M, reflect the tectonic stress that accompanied the uplift. Below reflector M reflection patterns in the uplifted area are chaotic, but the short visible reflection branches seem to form mounded structures up to a depth of 6 s TWT. Northeast of the large dome a further rise of reflectors occurs in seismic units 2 to 4, with some onlap fill in the syncline formed by reflector band M at CMP 32100. This indicates, together with the faults connected with reflector M, a first uplifting between ca. 14-13 Ma. Since sediments up to an age of ca. 2 Ma still show domed deformations, uplift may have continued up to this age.

Line P203

Line 203 (Fig. 46) orientated SSW–NNE is the seaward continuation of profile 134 on which ODP Site 953 is located. This line shows a well-stratified sedimentary basin with some interesting features.

At the crosspoint with line 202 two domal uplift structures are seen. The southwestern one is identical with the dome described on profile 202, whereas the northeastern dome pierces seismic unit 2 and most of unit 3. Faults occur in unit 3 and 4, and overlying strata are domed up to the lower half of unit 6. Between CMP 4500 and 1700, a ca. 30 ms deep rim syncline is seen, the base of which is formed by reflector band M where onlap terminations indicate infill during early deposition of seismic unit 2. This is another confirmation for an initial uplift at around 14–13 Ma. Chaotic patterns with generally mounded structures can be recognized under the uplifted strata up to a depth of at least 5.8 s TWT.

Reflector band M is also conspicuous with regard to subsidence in the basin because it represents an unconformity with almost horizontal strata above and SSW dipping reflectors below. Several onlap terminations onto the reflector band can be seen. The dip of the reflectors below reflector M is around 0.3°. On crossline 204 no dip is seen up to 6 s, so that the true dip is to the southwest, towards Gran Canaria. This island is thought to be responsible for the subsidence of the originally horizontally deposited sediments below reflector M. Subsequent to the rapid shield-building phase of Gran Canaria, the underlying lithosphere has responded to the volcanic load. Bodine et al. (1981) have shown that the response time of the lithosphere is some 0.5 to 1 my. This fits well with the age of reflector M (13.5–14 Ma) and the buildup of the volcanic shield at around 15–14 Ma (Schmincke,

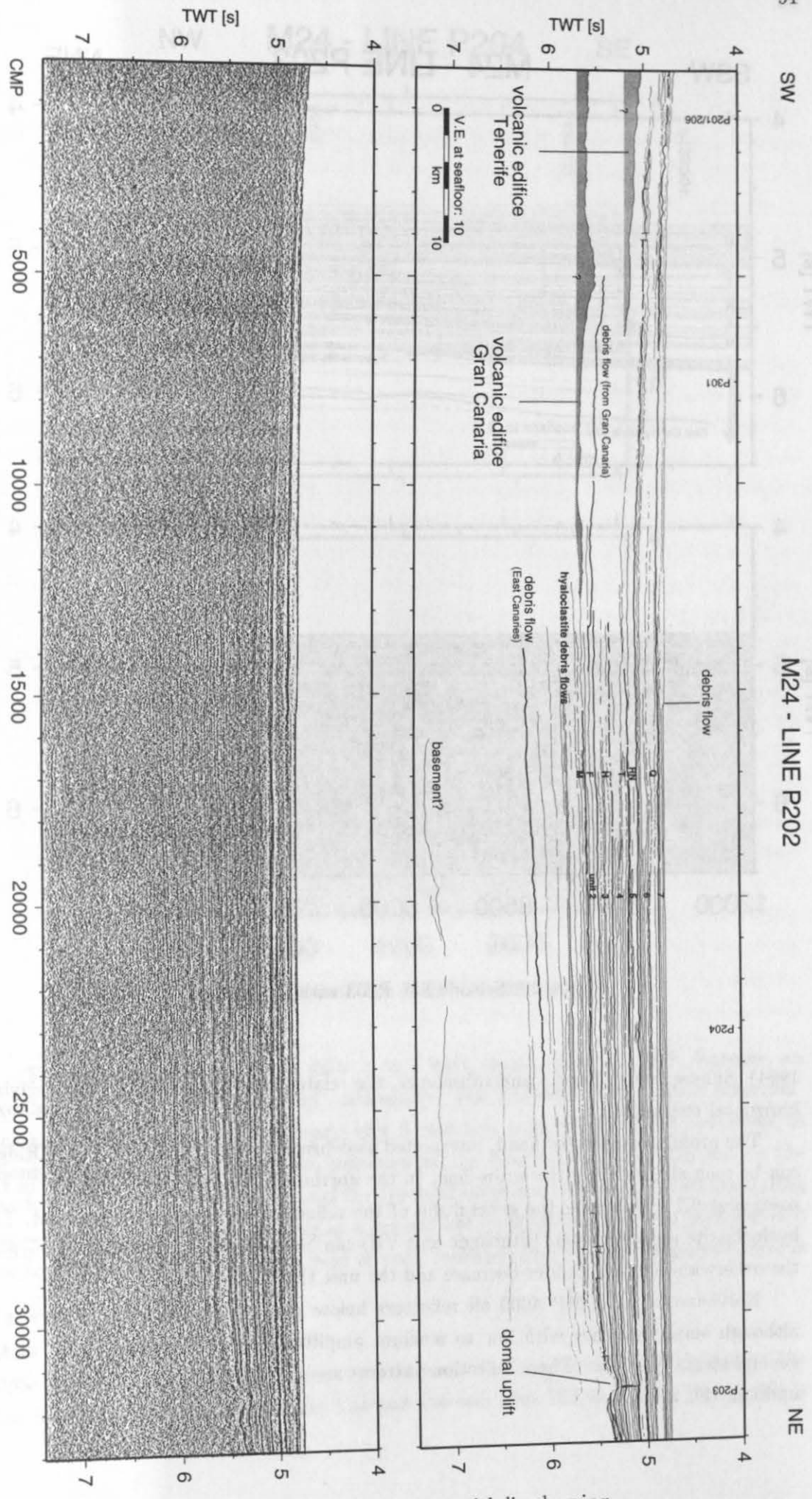

Figure 45: Seismic line P202 with linedrawing.

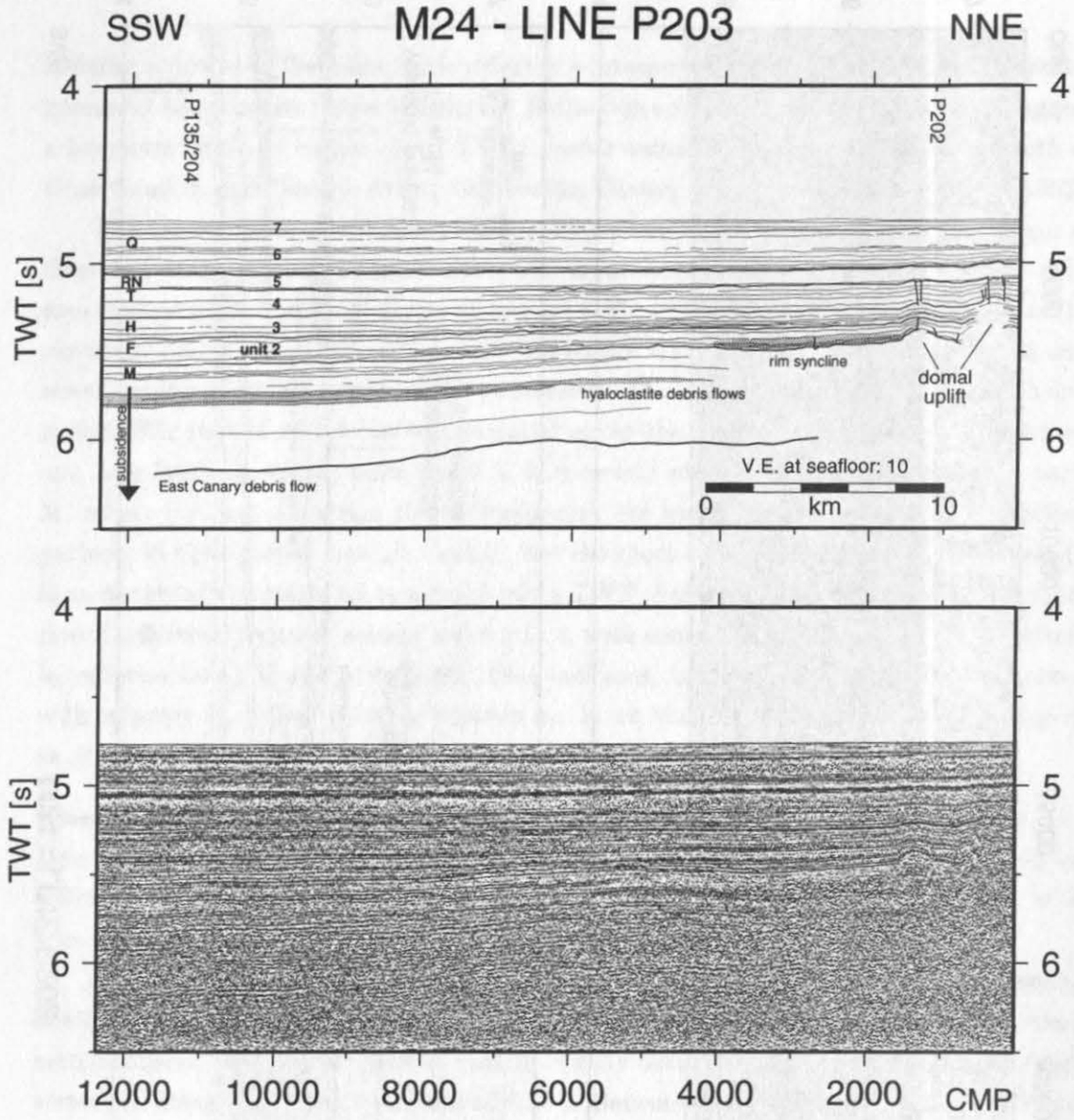

Figure 46: Seismic line P203 with linedrawing.

1994). Subsequent to flexure and subsidence, the related moat was filled by the overlying horizontal sediments.

The prominent reflector band, interpreted as debris flow from the East Canary Ridge, can be seen almost along the entire line. In the northeast, its depth is around 6 s, in the southwest 6.2 s, following the general dip of the reflectors below reflector band M. The hyaloclastite unit of Site 953 (lithologic unit VII) can be correlated up to CMP 4000 where the otherwise high amplitudes decrease and the unit thins out.

Northeast of ca. CMP 4000 all reflectors below reflector M are hard to correlate, although small branches with low to medium amplitudes still allow recognition of the general stratal patterns. These reflection patterns are probably connected with the domal uplift in this area.

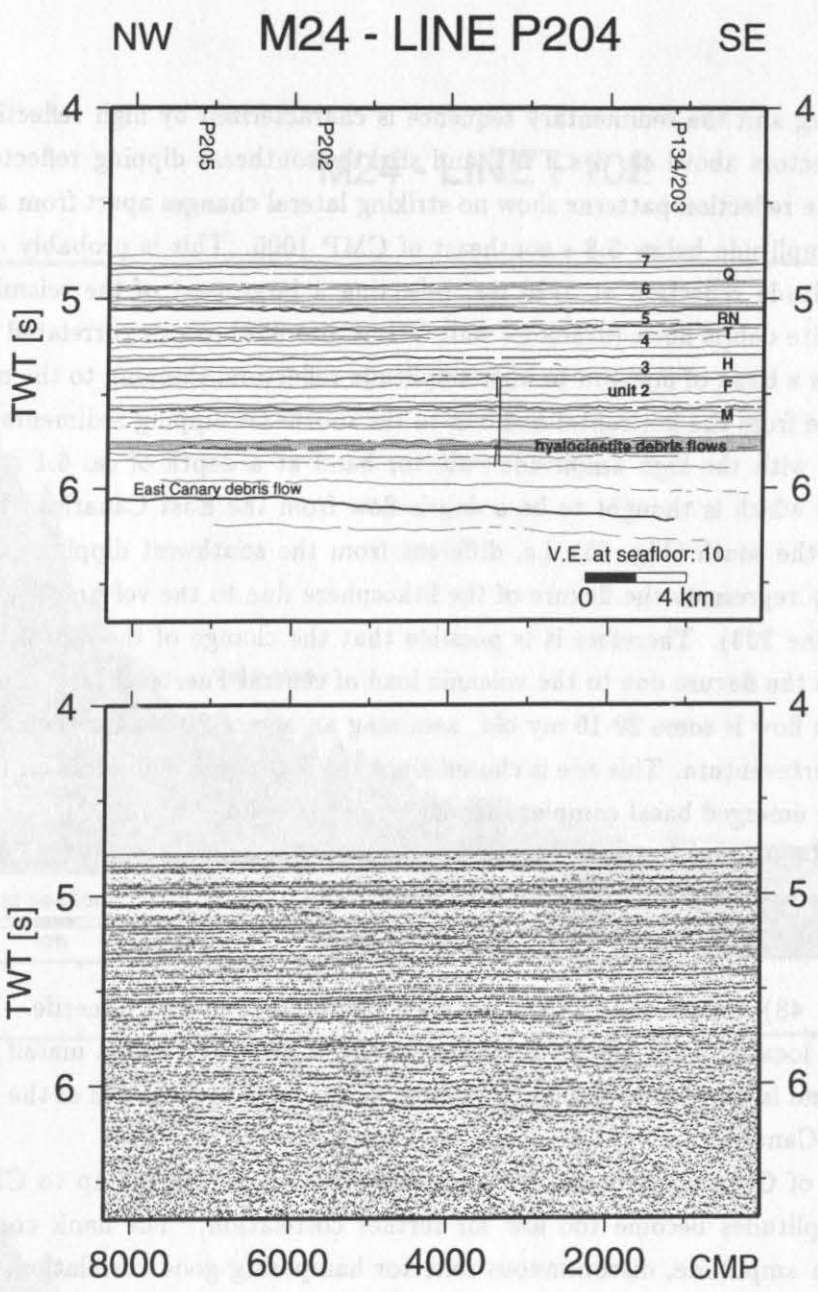

Figure 47: Seismic line P204 with linedrawing.

The reflectors in the seismic units 2 to 7 have, apart from the uplift features, an excellent continuity and are bedded horizontally. The thickness of the almost reflection-free zone in the upper half of seismic unit 6 increases from 40 ms in the southwest to about 80 ms at CMP 4000 as the reflectors at the base of this zone thin out to the northeast. This indicates a decrease of the depositional energy of the volcaniclastics during the sedimentation of unit 6, as well as a general low input of volcaniclastic material into the sedimentary sequence. The period of time corresponding to the transparent layer is 2–1 Ma.

Line P204

Line 204 (Fig. 47) is the northwestern continuation of profile 135 and represents the link between ODP Site 953 on line 134 and the two lines 202 and 205. The profile is

only 26 km long and the sedimentary sequence is characterized by high reflectivity with horizontal reflectors above ca. 6 s TWT and slightly southeast dipping reflectors below (ca. 0.15°). The reflection patterns show no striking lateral changes apart from a decrease of reflection amplitude below 5.8 s southeast of CMP 1000. This is probably caused by the high amplitude reflection at 5720 ms, reflecting a large part of the seismic energy. The hyaloclastite debris flows (lithologic unit VII at Site 953) can be correlated along the entire profile as a band of medium to high amplitude reflectors, thinning to the northwest.

The change from the horizontal bedding to the southeast dipping sediments coincides approximately with the high amplitude reflector band at a depth of ca. 6.1 s TWT (in the northwest) which is thought to be a debris flow from the East Canaries. The dip of the flow is to the south (Fig. 66), i.e. different from the southwest dipping reflector M which probably represents the flexure of the lithosphere due to the volcanic load of Gran Canaria (see line 203). Therefore it is possible that the change of the dip of the debris flow represents the flexure due to the volcanic load of central Fuerteventura. This implies that the debris flow is some 20-19 my old, assuming an age of 20 Ma for the rapid shield building of Fuerteventura. This age is chosen since the oldest volcanic rocks on the island, apart from the emerged basal complex, are 20 my old (Coello et al., 1992).

At CMP 3400 some fractures are visible between 5.4 and 5.9 s TWT. The vertical displacement is very small and hard to determine.

Line P102

Line 102 (Fig. 48) crosses the channel between Gran Canaria and Tenerife. Its northwestern end is located 6 km off the northeastern tip of Tenerife (Anaga massif) while its southeastern end is directed to the northern limit of the large indentation of the northwest coast of Gran Canaria.

The flank of Gran Canaria can be correlated from the southeast up to CMP 11600 where the amplitudes become too low for further correlation. The flank consists of a low to medium amplitude, discontinuous reflector hampering good correlation, especially southeast of CMP 15000 where the slope of the flank is between 8° and 16°. In this area the flank is covered with a sequence of some 300 to 400 ms thick sediments with chaotic patterns. This unit seems to be almost transparent since the amplitudes are very low. Northwest of CMP 15000 the amplitudes of the reflections from the flank are higher and several internal reflectors of the volcanic edifice become visible. The sediments above the shield still show chaotic patterns but they can be subdivided into two units. The upper unit is some 100 ms thick and the reflection branches have medium to high amplitudes and a narrow cycle breadth, whereas the lower unit contains only a few reflectors with low to medium amplitudes and appears therefore almost transparent, similar to the sediments southeast of CMP 15000. These transparent areas are probably composed of relatively homogeneous material (in terms of seismic impedance). The transparency of the unit is probably connected with the westward decrease of reflectivity (see lines 202 and 205), so that this area west of the Galdar Ridge is almost free from volcaniclastic input from Gran Canaria, i.e. the transparent unit represents the normal background sedimentation. The

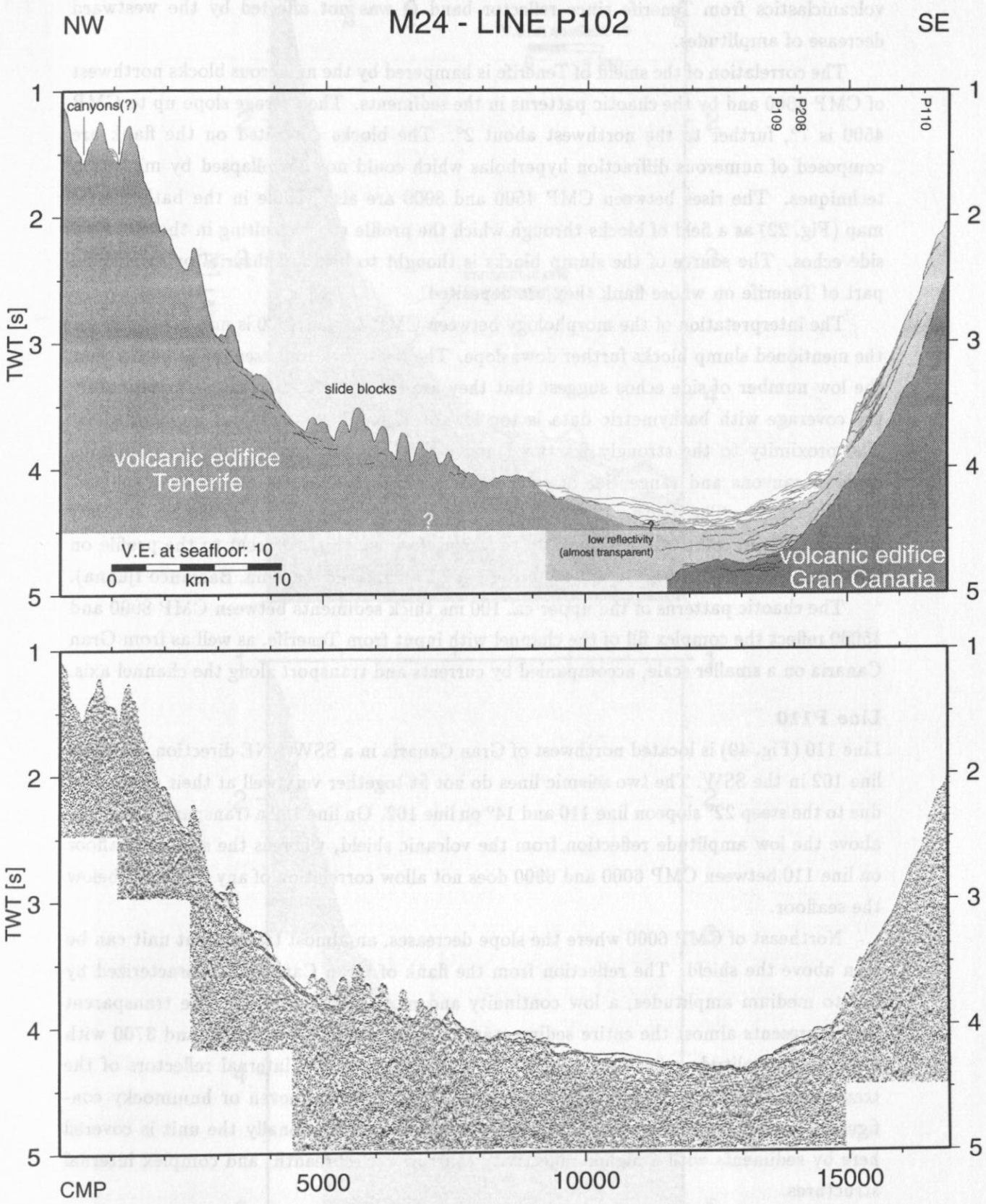

Figure 48: Seismic line P102 with linedrawing.

upper sediments, with medium to high amplitudes, are thought to be mainly Quaternary volcaniclastics from Tenerife since reflector band Q was not affected by the westward decrease of amplitudes.

The correlation of the shield of Tenerife is hampered by the numerous blocks northwest of CMP 8000 and by the chaotic patterns in the sediments. The average slope up to CMP 4500 is 7°, further to the northwest about 2°. The blocks deposited on the flank are composed of numerous diffraction hyperbolas which could not be collapsed by migration techniques. The rises between CMP 4500 and 8000 are also visible in the bathymetric map (Fig. 22) as a field of blocks through which the profile runs, resulting in the observed side echos. The source of the slump blocks is thought to be the subaerial or submarine part of Tenerife on whose flank they are deposited.

The interpretation of the morphology between CMP 34 and 1600 is not as easy as for the mentioned slump blocks further downslope. The rises could represent slide blocks, but the low number of side echos suggest that they are the walls of canyons. Unfortunately the coverage with bathymetric data is too low to allow an unambigious interpretation. The proximity to the strongly fractured and eroded Anaga massif, with its numerous onshore canyons and tangential orientation of profile towards Tenerife, would support this hypothesis. The depth of the assumed canyons at CMP 400 is ca. 250 m, at CMP 1100 ca. 200 m, comparable to the 200 to 300 m deep canyons adjacent to the profile on northeast Tenerife (Barranco de Roque Bermejo, Barranco de Anosma, Barranco Ijuana).

The chaotic patterns of the upper ca. 100 ms thick sediments between CMP 8000 and 15000 reflect the complex fill of the channel with input from Tenerife, as well as from Gran Canaria on a smaller scale, accompanied by currents and transport along the channel axis.

Line P110

Line 110 (Fig. 49) is located northwest of Gran Canaria in a SSW-NNE direction, crossing line 102 in the SSW. The two seismic lines do not fit together very well at their crosspoint due to the steep 22° slopeon line 110 and 14° on line 102. On line 102 a transparent unit lies above the low amplitude reflection from the volcanic shield, whereas the steeper seafloor on line 110 between CMP 6000 and 6900 does not allow correlation of any reflectors below the seafloor.

Northeast of CMP 6000 where the slope decreases, an almost transparent unit can be seen above the shield. The reflection from the flank of Gran Canaria is characterized by low to medium amplitudes, a low continuity and mounded structures. The transparent unit represents almost the entire sedimentary column between CMP 6000 and 3700 with a few low amplitude reflectors, whereas further northwestward internal reflectors of the transparent unit have slightly higher amplitudes, with more uneven or hummocky configuration, and show onlap terminations onto the flank. Additionally the unit is covered here by sediments with a higher reflectivity (narrow cycle breadth) and complex internal structures.

Again, the transparent unit probably corresponds to mainly nonvolcanic deposits. The upper unit with its higher reflectivity represents alternating volcaniclastic sediments

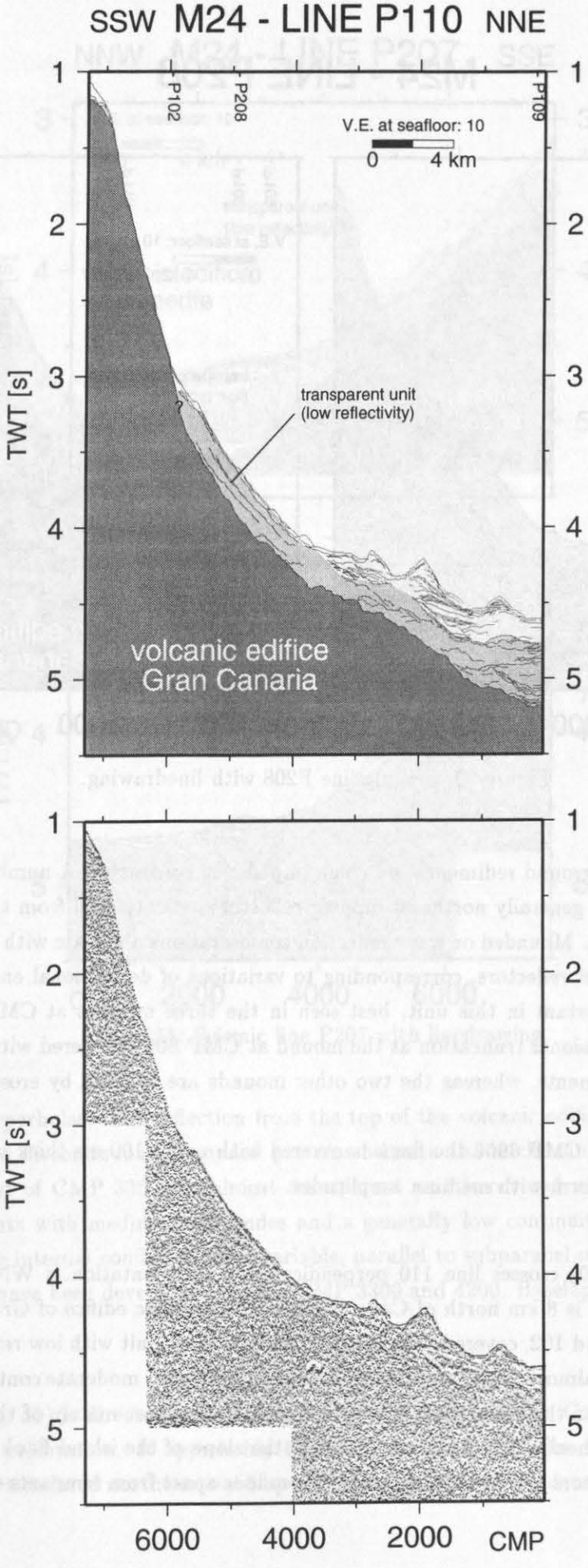

Figure 49: Seismic line P110 with linedrawing.

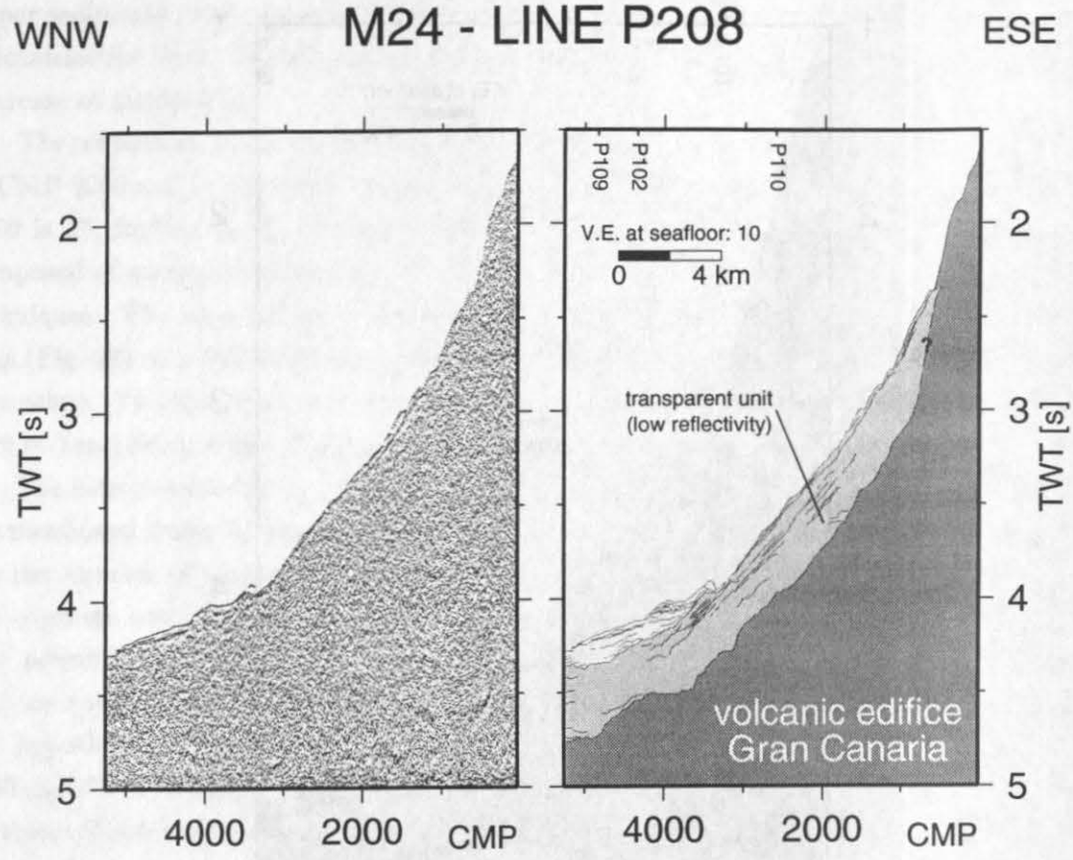

Figure 50: Seismic line P208 with linedrawing.

and normal background sedimentation (high impedance contrasts). A number of baselap terminations and generally northeast dipping reflectors indicate a fill from the southwest, i.e. Gran Canaria. Mounded or wavy reflection configurations alternate with bands of parallel or subparallel reflectors, corresponding to variations of depositional energy. Erosion is also very important in this unit, best seen in the three mounds at CMP 2700, 2000 and 800. The erosional truncation at the mound at CMP 800 is covered with some 25 ms of stratified sediments, whereas the two other mounds are affected by erosion up to the present.

Southwest of CMP 6900 the flank is covered with up to 100 ms thick sediments of a prograding clinoform with medium amplitudes.

Line P208

Line 208 (Fig. 50) crosses line 110 perpendicularly, its orientation is WNW-ESE. The southeastern end is 8 km north of Cape Galdar. The volcanic edifice of Gran Canaria is, as on lines 110 and 102, covered with an up to 450 ms thick unit with low reflectivity. The reflectors in this almost transparent unit have low amplitudes, moderate continuity and are roughly parallel to the flank. The unit is interpreted to consist mainly of the nonvolcanic background sediments. Southeast of CMP 800 the slope of the island flank increases and no internal reflectors can be seen beneath the seafloor apart from remnants of out of plane

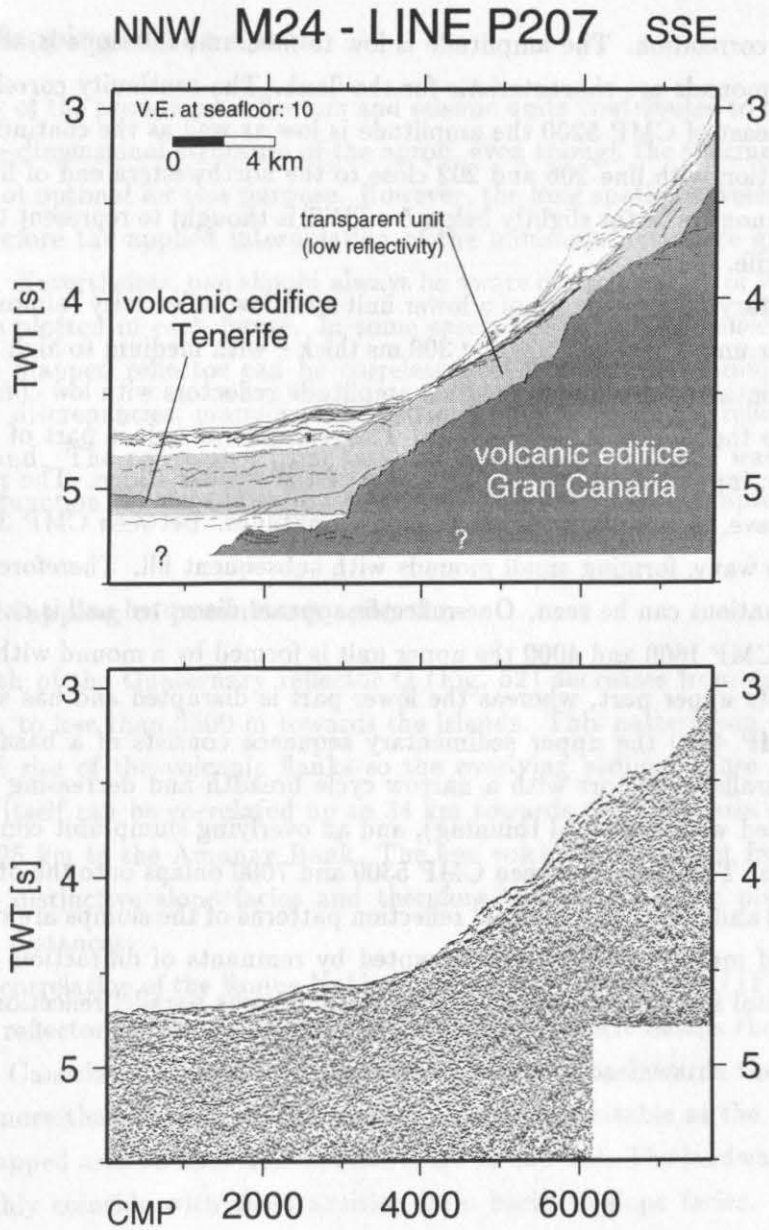

Figure 51: Seismic line P207 with linedrawing.

diffraction hyperbolas. The reflection from the top of the volcanic edifice has only a low amplitude and discontinuous, mounded patterns beneath the thick transparent unit.

Northwest of CMP 3300 the almost transparent unit is covered with up to 200 ms thick sediments with medium amplitudes and a generally low continuity with disrupted patterns. The internal configuration is variable, parallel to subparallel or hummocky, and two mounds have been developed between CMP 3300 and 4200. Baselap terminations are widespread.

Line P207

Line 207 (Fig. 51) is directed radial to the northwest coast of Gran Canaria (Galdar) in a NNW-SSE orientation. It approaches the coast up to 11 km. The flank of Gran Canaria can be correlated northwestward up to CMP 1300, where the decrease in amplitude

hampers further correlation. The amplitude is low to medium, the slope is about 8° and small faults and mounds are characteristic for the flank. The continuity correlates to the amplitude, southeast of CMP 5200 the amplitude is low as well as the continuity.

From correlation with line 206 and 202 close to the northwestern end of line 207, the low and discontinuous reflector slightly below 5 s TWT is thought to represent the volcanic pedestal of Tenerife.

The sedimentary fill is made up of a lower unit with low reflectivity (almost transparent) and an upper unit – between 100 and 300 ms thick – with medium to high reflectivity. The lower unit contains a few low to medium amplitude reflectors with low continuity and some onlaps onto the flank of Gran Canaria. The transparent unit is part of the zone of low volcaniclastic input from Gran Canaria west of the Galdar Ridge. The reflectors in the upper unit have, in general, medium to high amplitudes. Between CMP 34 and 1600 the reflectors are wavy, forming small mounds with subsequent fill. Therefore, a number of baselap terminations can be seen. One reflector appears disrupted and is cut by several faults. Between CMP 1600 and 4000 the upper unit is formed by a mound with contourite like patterns in its upper part, whereas the lower part is disrupted and has some faults. Southeast of CMP 4000 the upper sedimentary sequence consists of a basal unit with parallel to subparallel reflectors with a narrow cycle breadth and decreasing amplitudes upslope (connected with a general thinning), and an overlying slump unit containing two individual slumps. The slump between CMP 5300 and 7000 onlaps onto the other one between CMP 4000 and 5600. The internal reflection patterns of the slumps are chaotic with short branches of medium amplitudes, disrupted by remnants of diffraction hyperbolas. The original stratal features are still recognizable (numerous parallel reflections).

5.5 Mapping of the apron

Mapping of the prominent reflectors and seismic units contributes to the understanding of the three-dimensional structure of the apron, even though the spacing and location of the lines is not optimal for this purpose. However, the long spatial wavelength trend is correct and therefore the applied interpolation of the minimum curvature gridding algorithm is justified. Nevertheless, one should always be aware of the location of the profiles which are therefore plotted in each figure. In some cases, the prominent reflector band associated with the mapped reflector can be correlated further than the individual reflector itself. To avoid discrepancies, mapping was restricted to the individual reflectors and not to an entire band. The conversion from two-way travel time to depth was done by the fitted velocity function for the sediments described in the *Processing* chapter (page 37).

5.5.1 Mapping of prominent reflectors

The depth of the Quaternary reflector Q (Fig. 52) decreases from more than 3650 m in the basin to less than 3500 m towards the islands. This pattern can be explained by the landward rise of the volcanic flanks so the overlying sediments are rising as well. The reflector itself can be correlated up to 34 km towards Gran Canaria and Tenerife and as close as 25 km to the Amanay Bank. The low volcaniclastic input from the bank results in a less distinctive slope facies and therefore the correlation is possible even in more proximal distances.

The correlation of the Roque Nublo lapillistones of reflector RN (Fig. 53) is even better than for reflector Q. On profile 301 (Fig. 39), reflector RN onlaps the island flank 27 km off Gran Canaria at a depth of some 3600 m, further basinwards the depth increases to slightly more than 3850 m. Uplift structures are recognizable at the northeastern corner of the mapped area on lines 202 and 203 (Fig. 45 and 46). The landward limits of reflector RN roughly coincide with the transition from basin to slope facies. On profile 205 it is somewhat closer to Tenerife.

The correlation below reflector RN is limited to the northeastern region since the Galdar Ridge has influenced the deposition of volcaniclastics in such a way that debris from northern Gran Canaria was generally deviated to the eastern part of the apron. Reflector T (Fig. 54) has a depth of some 3950 m in the basin, decreasing islandward. The domal uplift in the northeast is of the same scale as for the reflector RN.

Reflector H (Fig. 55) has a maximum depth of ca. 4100 m, decreasing to 3875 m, at which depth it onlaps onto the debris on the flank of the Amanay Bank. In the southern area the reflector dips northward. The uplift in the northeast amounts to > 50 m.

Reflector F (Fig. 56) dips to the southwest in the northeast, in the south the layer rises towards Gran Canaria and Fuerteventura. On profile 135 the reflector onlaps the debris-covered flank of the Amanay Bank at a depth of ca. 3950 m, while the depth in more distal regions is up to 4300 m.

The patterns of reflector M (Fig. 57) are completely different from those discussed

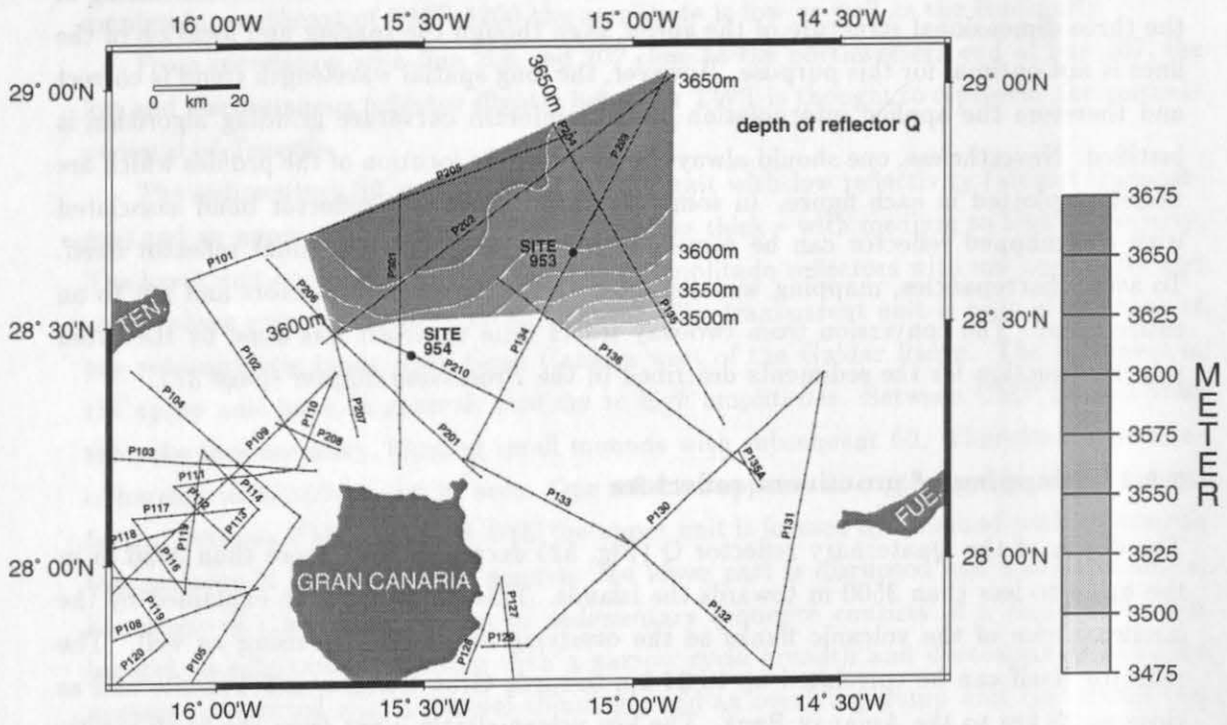

Figure 52: Depth of reflector Q in meters below sea level. Contour interval is 25 m.

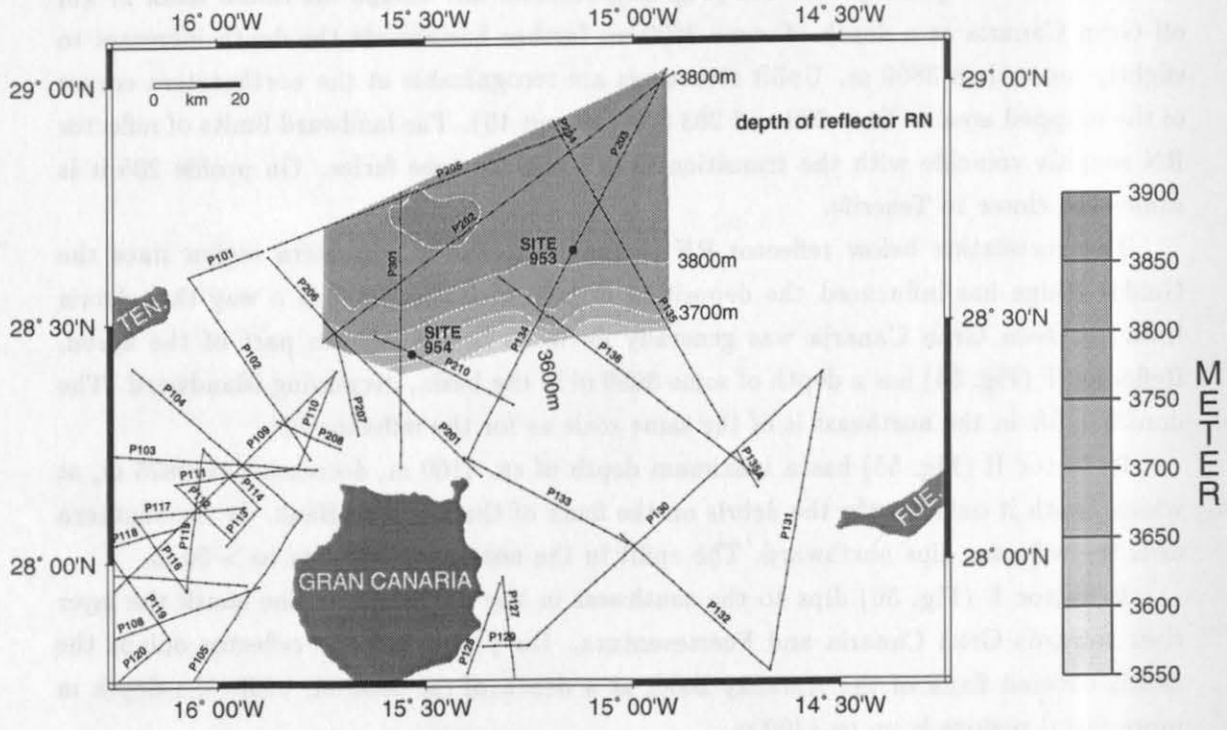

Figure 53: Depth of reflector RN in meters below sea level. Contour interval is 50 m.

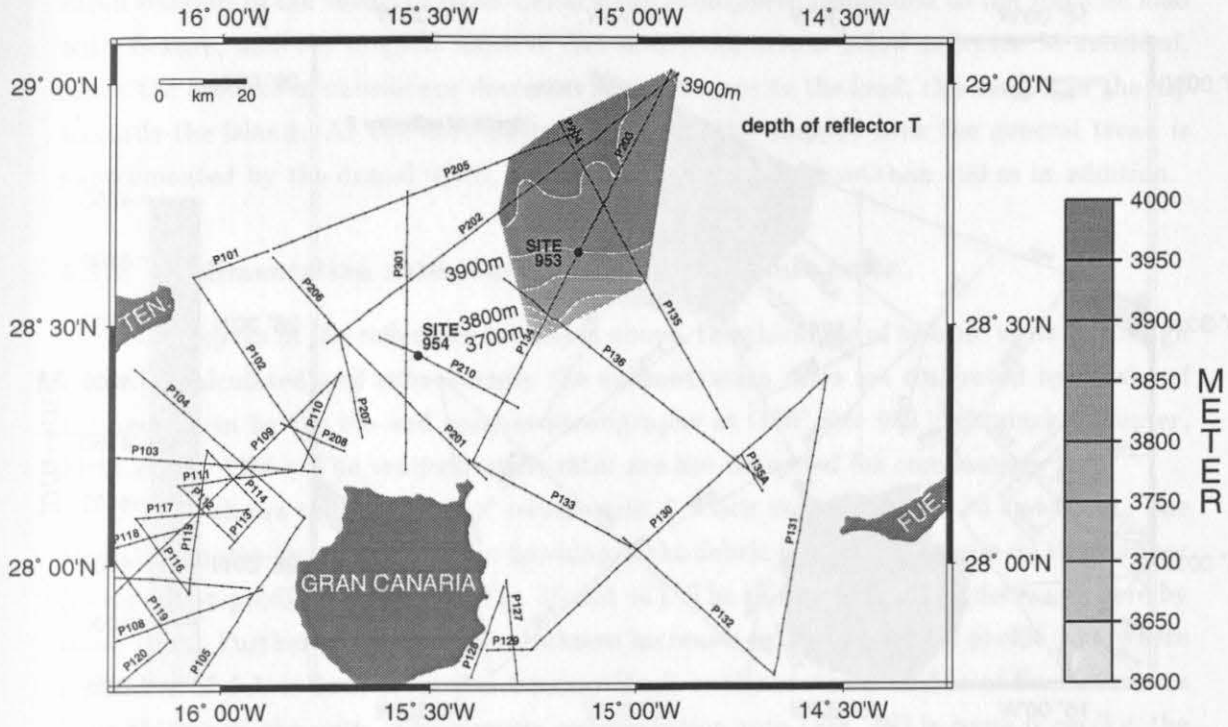

Figure 54: Depth of reflector T in meters below sea level. Contour interval is 50 m.

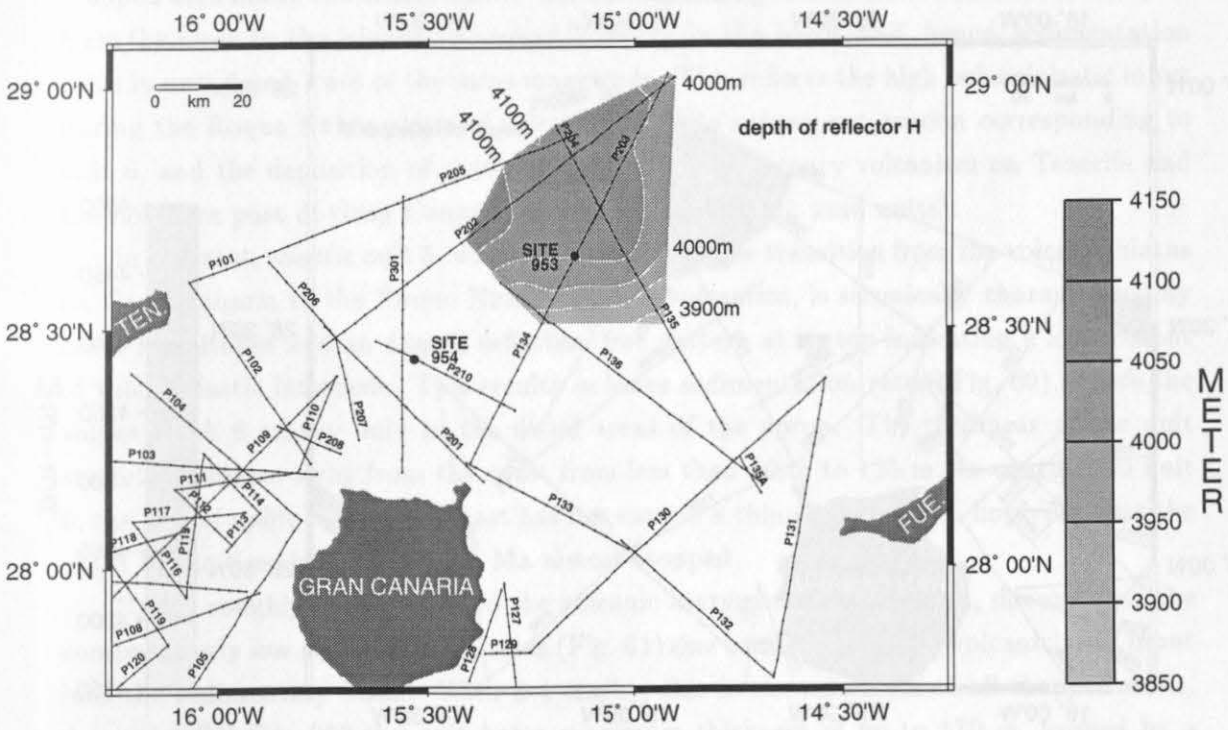

Figure 55: Depth of reflector H in meters below sea level. Contour interval is 50 m.

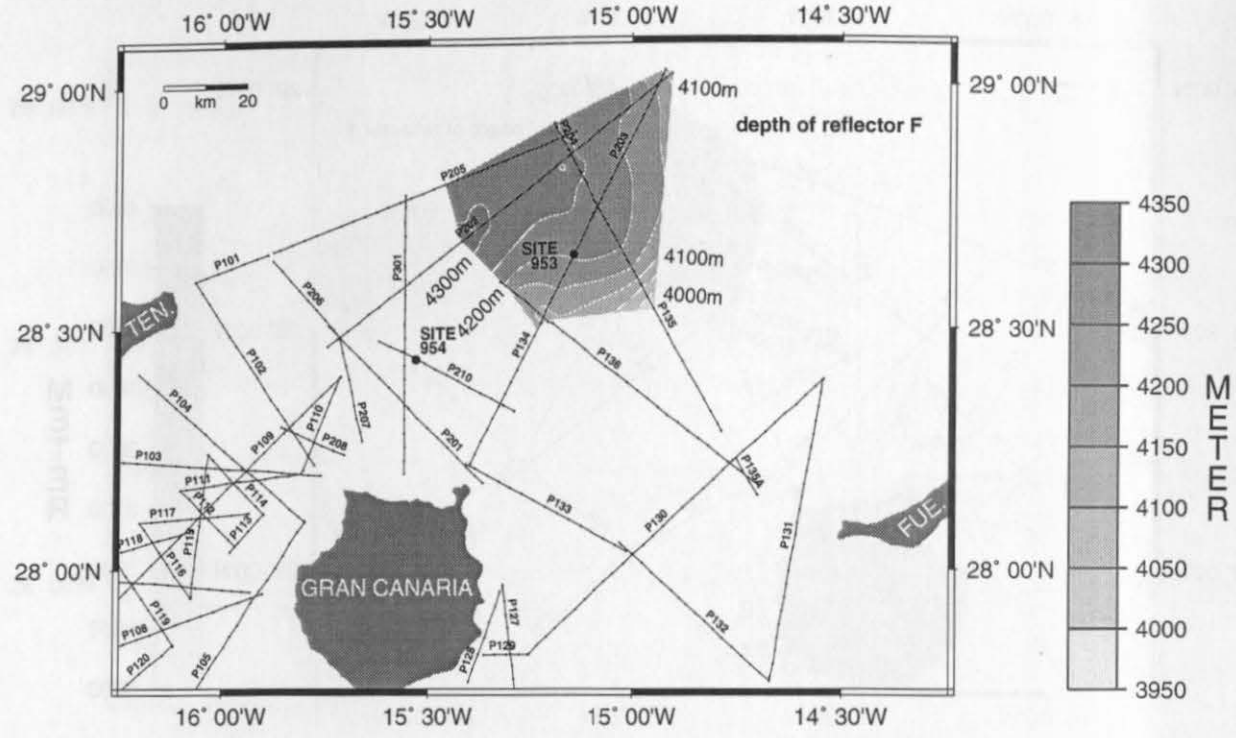

Figure 56: Depth of reflector F in meters below sea level. Contour interval is 50 m.

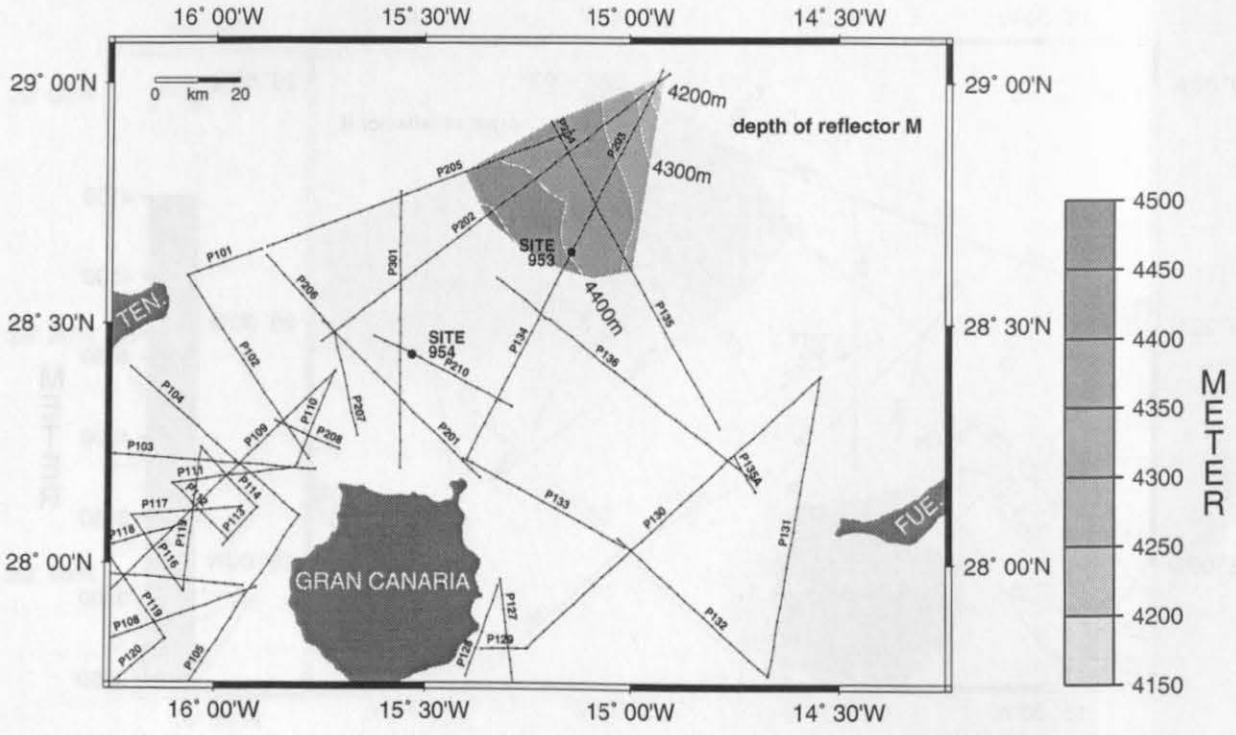

Figure 57: Depth of reflector M in meters below sea level. Contour interval is 50 m.

previously. Here, the reflector deepens to the southwest towards Gran Canaria. The suspected reason for this was mentioned in the description of seismic line 203: after the rapid buildup of the shield of Gran Canaria the lithosphere responded to the volcanic load with flexure, and the original more or less horizontal strata below reflector M subsided. Since the amount of subsidence decreases with distance to the load, this results in the dip towards the island. At the northeastern corner of the mapped area the general trend is supplemented by the domal uplift, raising the reflector by more than 100 m in addition.

5.5.2 Sedimentation rates and thickness of seismic units

With the depths of the reflectors presented above, the thickness of seismic units 2 through 7 can be calculated and subsequently the sedimentation rates are computed by means of the ages given by the bio-and magnetostratigraphy at ODP Site 953 (Schmincke, Weaver, Firth et al., 1995). The sedimentation rates are not corrected for compaction.

Fig. 58 shows the thickness of seismic unit 7 which varies between 30 and 65 m. The black line marks the position of the downlap of the debris flow from Tenerife on the seafloor (observed on profile 202 and 205, Fig. 45 and 44). The thickness of unit 7 decreases here by some 10 m. Further to the east the thickness increases again to 65 m on profile 135, where a number of debris flows from the Amanay Bank or the southern edifice of Fuerteventura have thickened the unit. The average sedimentation rate (Fig. 58) is some 6 cm/ky, the maximum values are about 8 cm/ky.

The average thickness of seismic unit 6 (Fig. 59) is slightly less than 200 m in the basin, towards the islands the sediments are thinning as in the northeastern corner of the mapped area above the domal uplift. The corresponding sedimentation rates increase from 5 cm/ky close to the islands to around 7 cm/ky in the basin, and, hence, sedimentation rates in unit 6 and 7 are of the same magnitude. This reflects the high volcaniclastic input during the Roque Nublo phase of volcanism and its subsequent erosion corresponding to unit 6, and the deposition of material during the Quaternary volcanism on Tenerife and the northern part of Gran Canaria in unit 7 (mainly thick sand units).

In contrast, seismic unit 5, which corresponds to the transition from the volcanic hiatus on Gran Canaria to the Roque Nublo phase of volcanism, is seismically characterized by lower amplitudes and an almost reflection free pattern at its top indicating a low content of volcaniclastic interbeds. This results in lower sedimentation rates (Fig. 60), where the values reach 6 cm/ky only in the distal areas of the apron. The thickness of the unit steadily increases away from the coast from less than 50 m to 125 m. In contrast to unit 6, the domal uplift in the northeast has not caused a thinning of unit 5, implying that the uplift in the time interval 5.5-3.5 Ma almost stopped.

Unit 4 roughly corresponds to the volcanic hiatus on Gran Canaria, documented the comparatively low sedimentation rates (Fig. 61) due to the decrease of volcaniclastic input into the sedimentary basin. With 3-4 cm/ky, this is the minimum of all mapped units. Around ODP Site 953 the unit has a maximum thickness of up to 170 m, formed by a mound in the upper part of the unit. To the south and the north the unit becomes thinner,

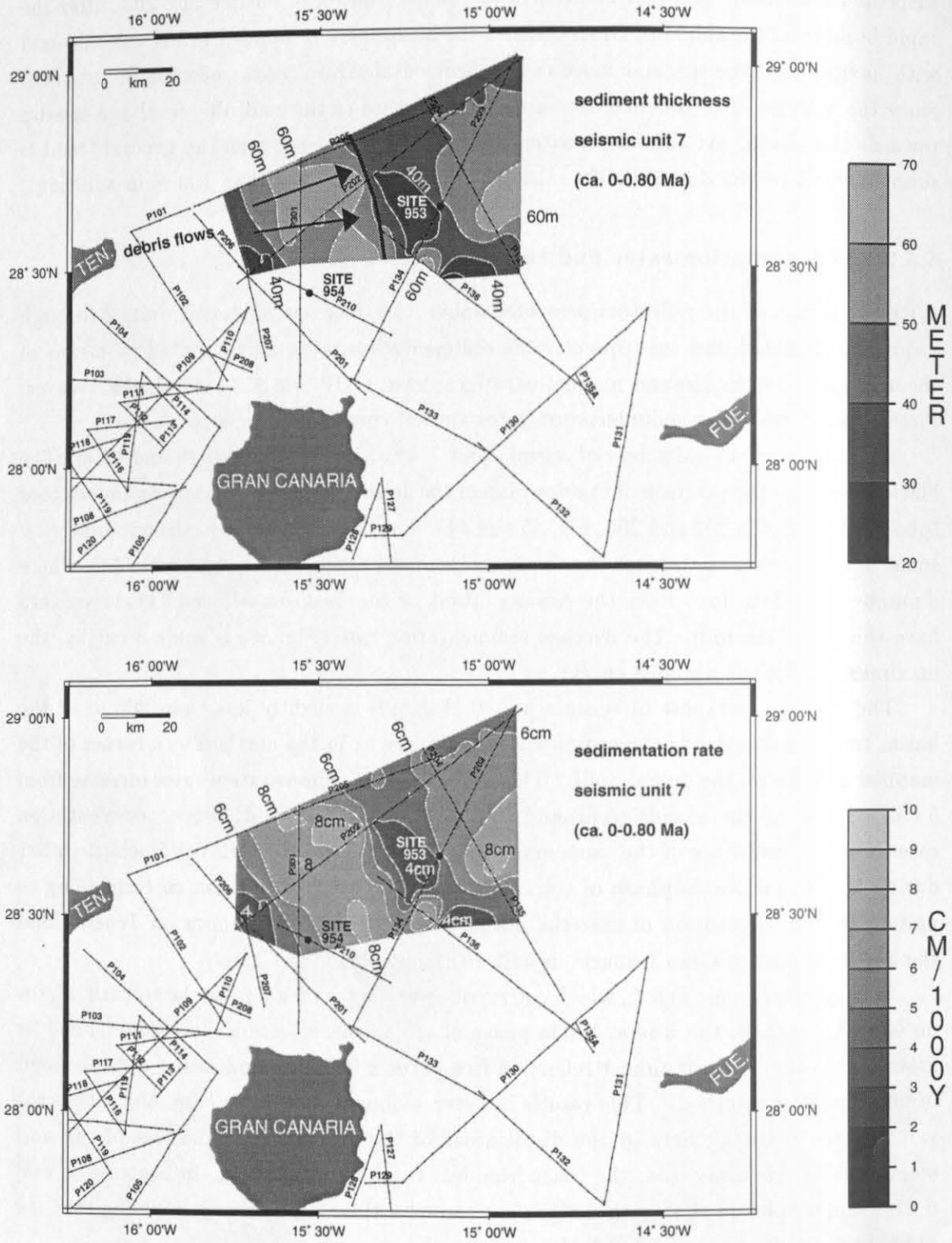

Figure 58: Iopach map of seismic unit 7 (0-0.8 Ma) and its sedimentation rate. The contour interval is 10 m for the thickness and 1 cm/ky for the sedimentation rate.

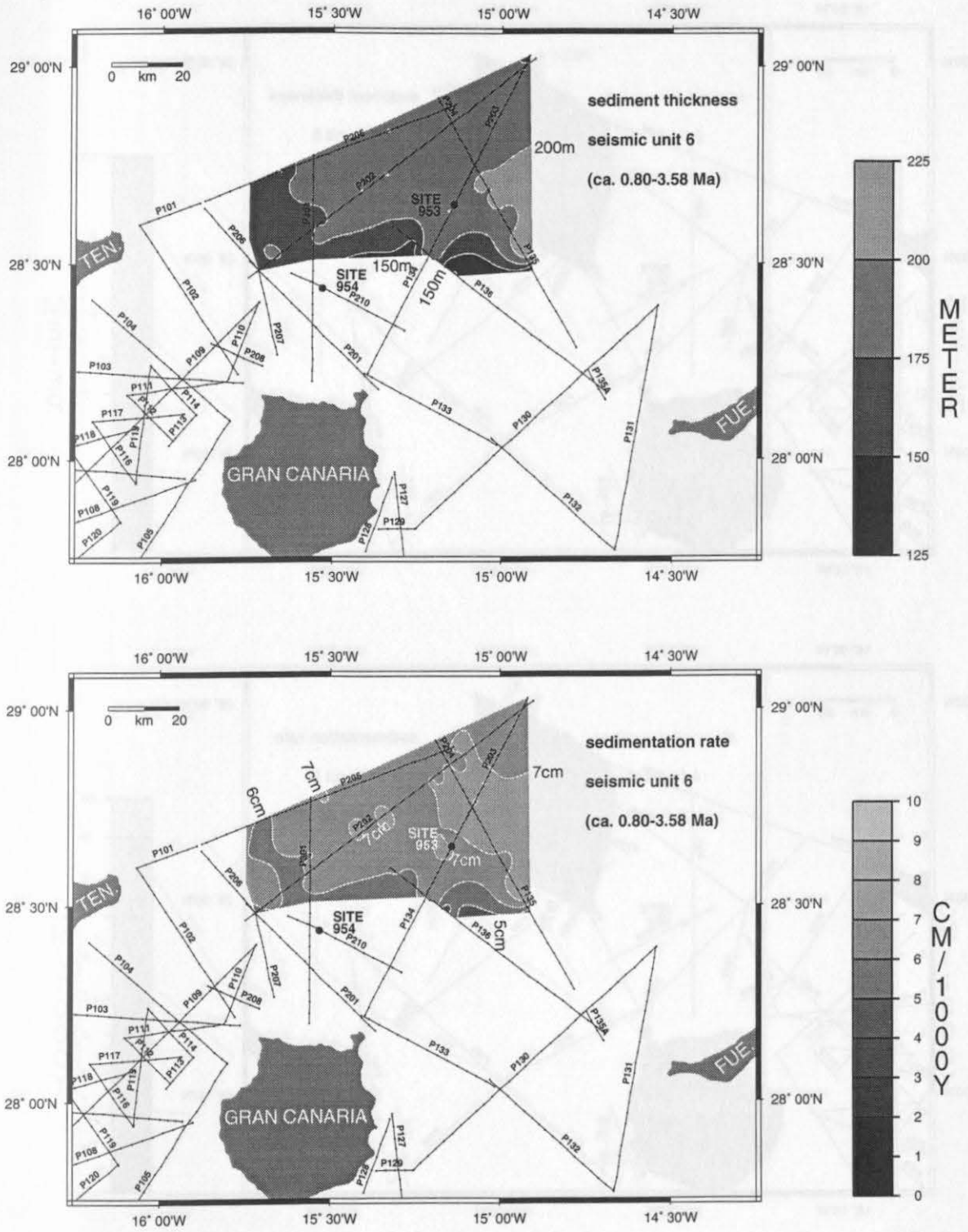

Figure 59: Iopach map of seismic unit 6 (ca. 0.8-3.58 Ma) and its sedimentation rate. The contour interval is 25 m for the thickness and 1 cm/ky for the sedimentation rate.

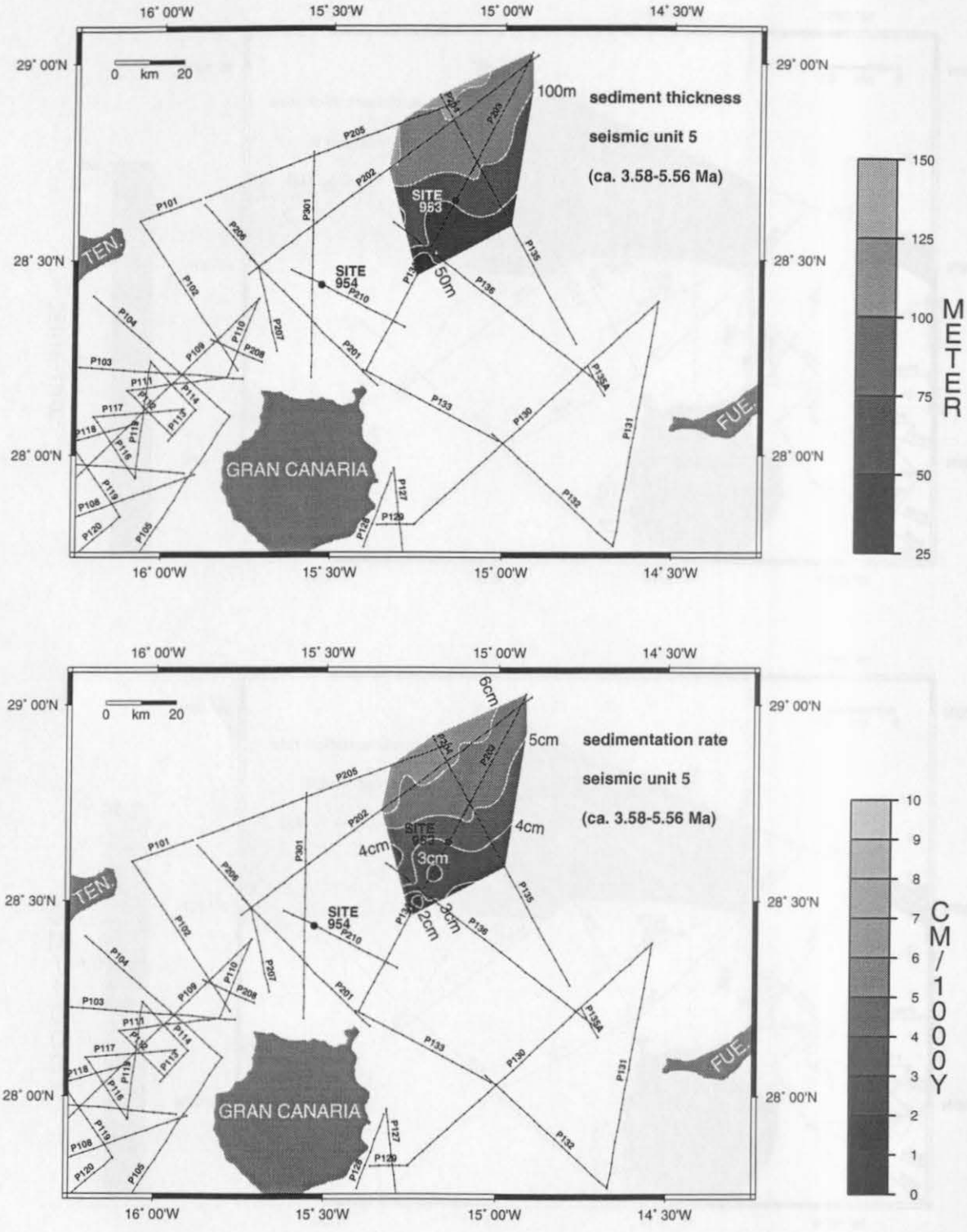

Figure 60: Iopach map of seismic unit 5 (ca. 3.58-5.56 Ma) and its sedimentation rate. The contour interval is 25 m for the thickness and 1 cm/ky for the sedimentation rate.

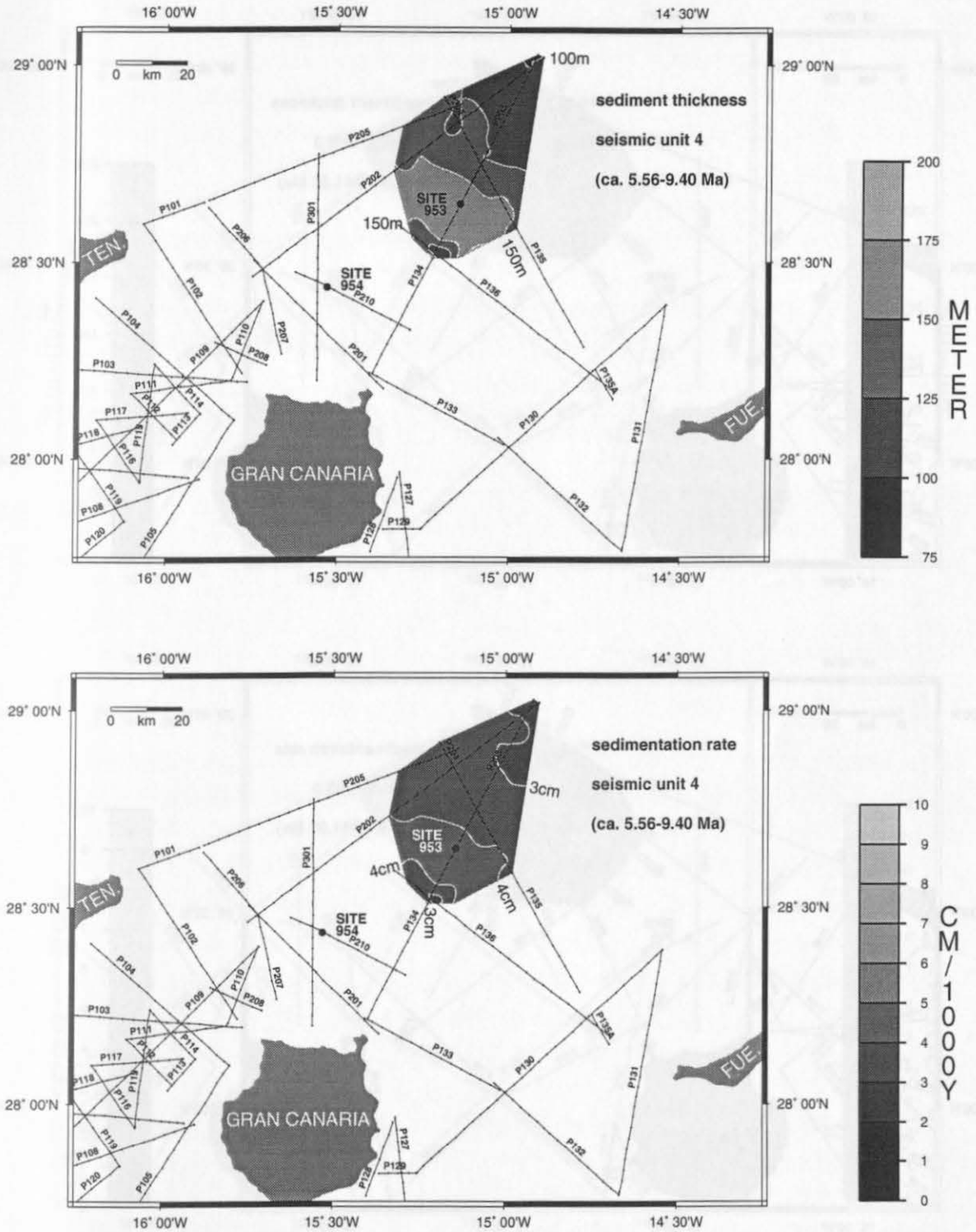

Figure 61: Iopach map of seismic unit 4 (ca. 5.56-9.4 Ma) and its sedimentation rate. The contour interval is 25 m for the thickness and 1 cm/ky for the sedimentation rate.

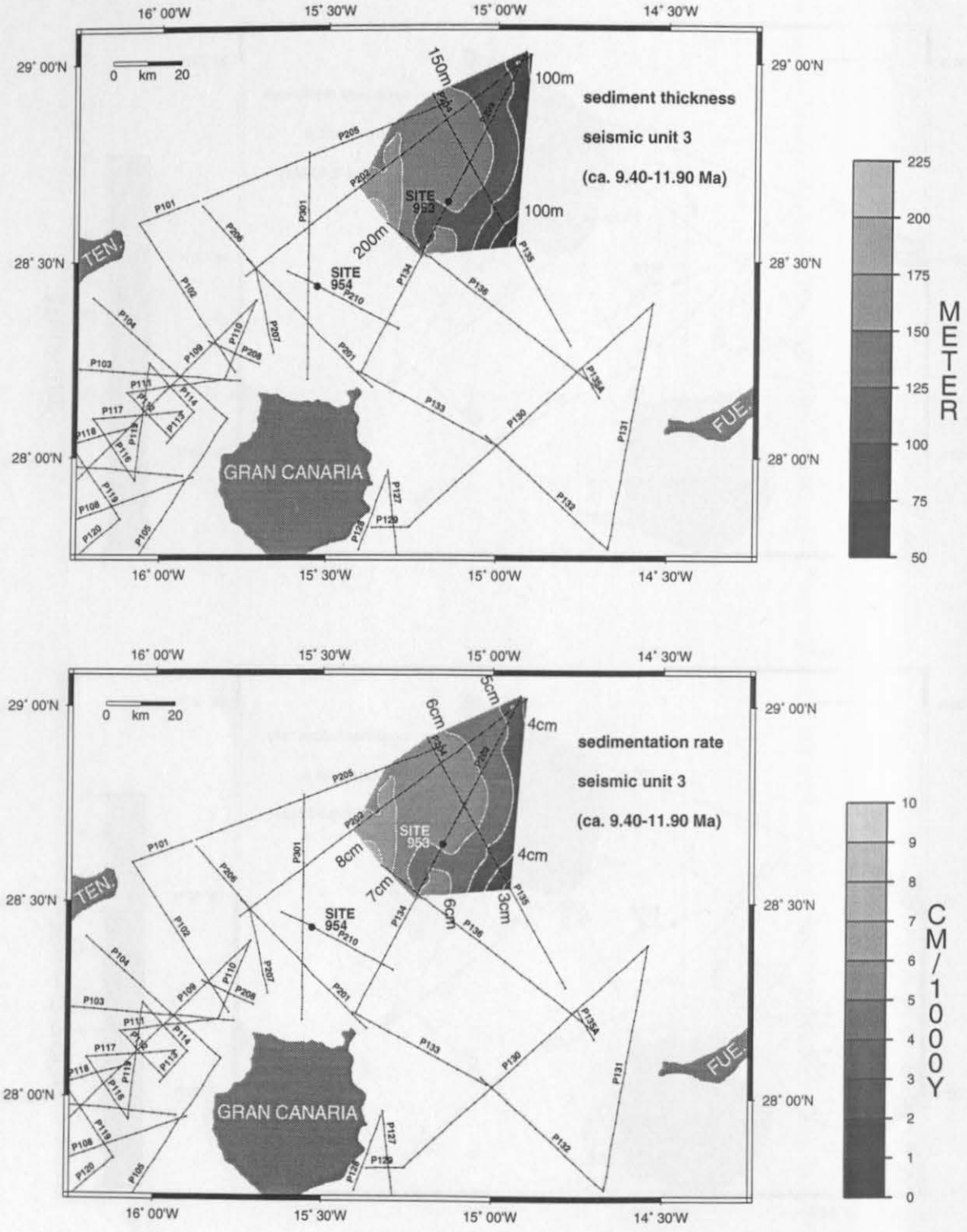

Figure 62: Iopach map of seismic unit 3 (ca. 9.4-11.9 Ma) and its sedimentation rate. The contour interval is 25 m for the thickness and 1 cm/ky for the sedimentation rate.

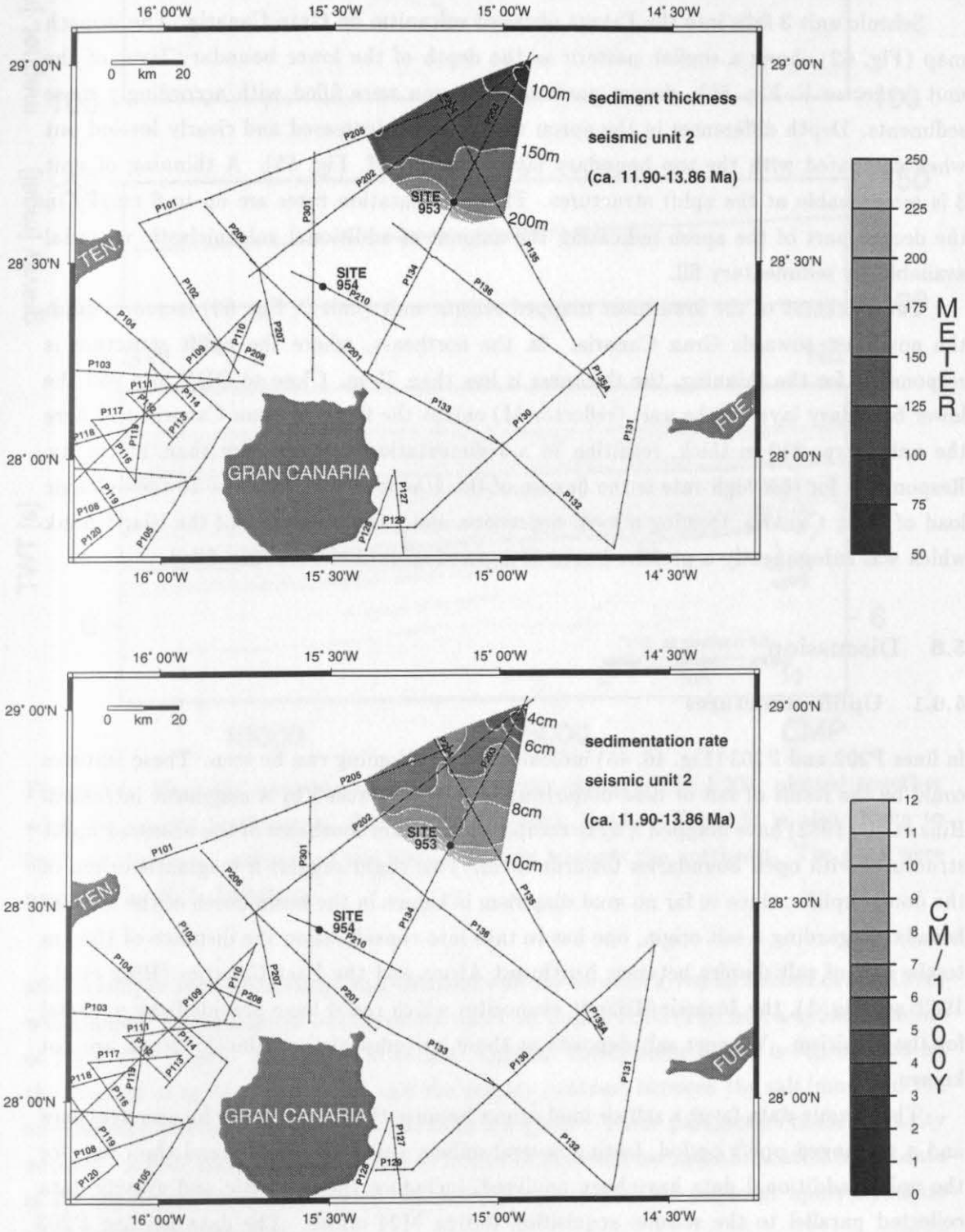

Figure 63: Iopach map of seismic unit 2 (ca. 11.9-13.86 Ma) and its sedimentation rate. The contour interval is 25 m for the thickness and 1 cm/ky for the sedimentation rate.

and at the uplift structure in the northeast the unit is only about 100 m thick, indicating uplift during the volcanic hiatus.

Seismic unit 3 falls into the Fataga phase of volcanism on Gran Canaria. The isopach map (Fig. 62) shows a similar pattern as the depth of the lower boundary layer of the unit (reflector F, Fig. 56): deeper parts of the apron were filled with accordingly more sediments. Depth differences in the apron were thereby decreased and clearly leveled out when compared with the top boundary layer (reflector H, Fig. 55). A thinning of unit 3 is recognizable at the uplift structures. The sedimentation rates are up to 8 cm/ky in the deeper part of the apron indicating the amount of additional volcaniclastic material available for sedimentary fill.

The thickness of the lowermost mapped seismic unit (unit 2, Fig. 63) increases from the northeast towards Gran Canaria. In the northeast, where the uplift structure is responsible for the thinning, the thickness is less than 75 m. Close to ODP Site 953 the lower boundary layer of the unit (reflector M) onlaps the flank of Gran Canaria and here the unit is ca. 230 m thick, resulting in a sedimentation rate of more than 11 cm/ky. Responsible for this high rate is the flexure of the lithosphere as response to the volcanic load of Gran Canaria, forming a local depression along the outer rim of the island flank which was subsequently a preferred area of deposition until the low was filled.

5.6 Discussion

5.6.1 Uplift structures

In lines P202 and P203 (Fig. 46, 45) indications for updoming can be seen. These features could be the result of salt or mud diapirism, or could be caused by a magmatic intrusion. Hinz et al. (1982) have mapped a dyke complex just 15 km southeast of the observed uplift structures with open boundaries towards them. This could suggest a magmatic origin of the domal uplifts, since so far no mud diapirism is known in the basin north of the Canary Islands. Regarding a salt origin, one has to take into consideration the distance of 150 km to the belt of salt diapirs between Northwest Africa and the East Canaries (Hinz et al., 1982; see Fig. 1), the Jurassic/Triassic evaporites which could have provided the material for the diapirism. Younger salt deposits at these latitudes of the Atlantic Ocean are not known.

The seismic data favor a salt or mud origin because there is evidence for rim synclines and a prolonged uplift period, lasting several million years. To understand the cause for the uplift, additional data have been analysed, including the magnetic and gravity data collected parallel to the seismic acquisition during M24 cruise. The data for line P203 were kindly provided by G.A. Dehghani and are shown in Fig. 64. The magnetic anomaly varies between some 110 and 140 nT, its minimum is at the northeastern end of the profile where the uplifts are located. The gravity is plotted together with the best linear fit, showing an almost linear increase of the values towards the northeast.

To compute the gravity effect of a salt/mud dome, or alternatively a magmatic intru-

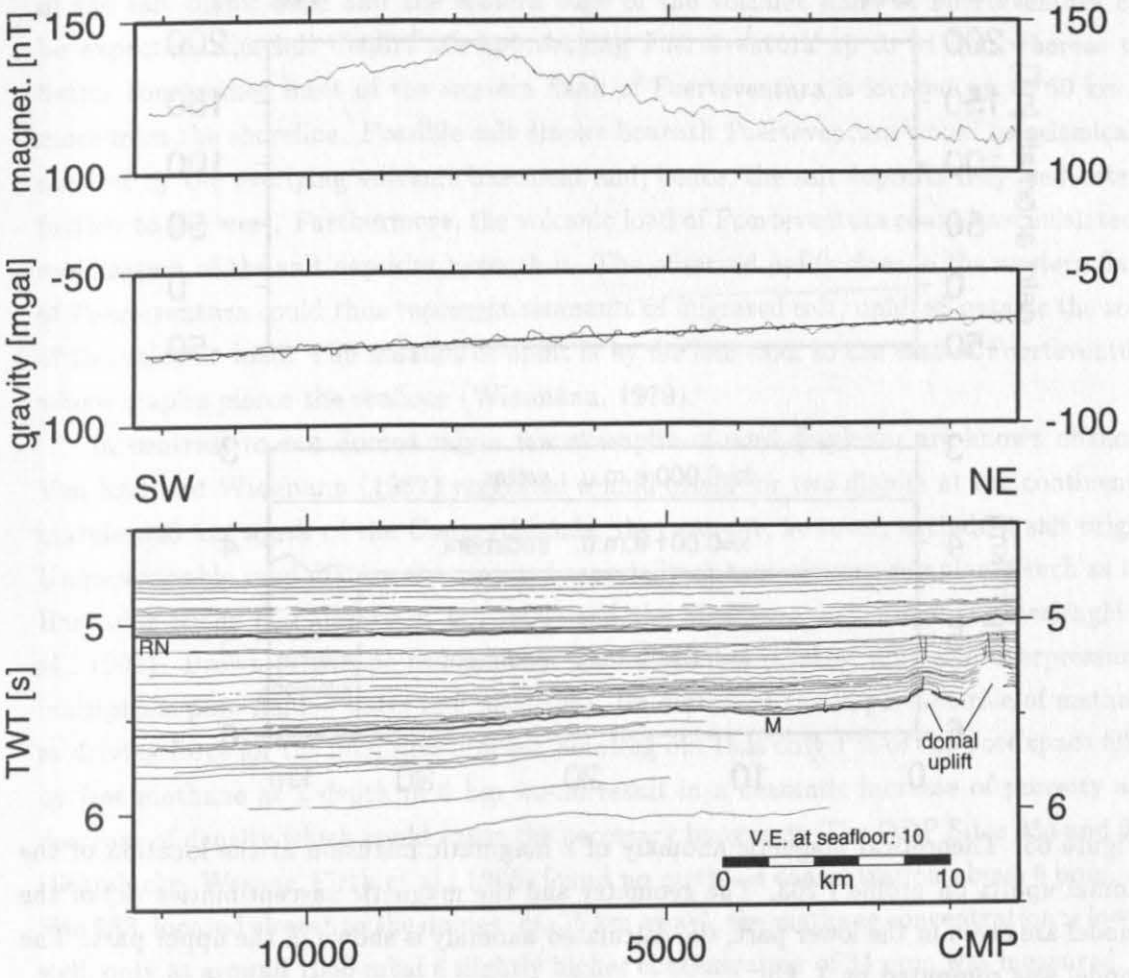

Figure 64: Magnetic anomaly and free-air gravity along profile P203, plotted together with the seismic linedrawing. For the gravity data, the best linear fit is also shown to indicate the linear increase of the free-air gravity towards the northeast. The data were provided by G.A. Dehghani.

sion, a simple cylindrical shape was assumed and the formula given in Telford et al. (1990) was applied. Regarding the southwestern uplift on profile P203 (Fig. 64), a cylinder radius of 1 km was chosen. The depth is at least 4200 m, the cylinder height is represented by the amount of uplift (some 60 m) and the density contrast between the salt/mud and the surrounding sediments is assumed less than 0.2 g/cm^3. These parameters cause a gravity anomaly of 0.01 mgal which is by far too low to be detected because the scatter of the data is already around 2–3 mgal. Even the combined effect with the adjacent uplift structure would not be recognizable.

In case of a magmatic intrusion, the cylinder height would be 3 km or more, because the material had to penetrate the whole sedimentary column up to the top of the intrusion. The sediment thickness above the the crust is ca. 4 km in this area (Ye et al., 1996). The depth and radius of the cylinder remain the same but the density contrast is larger, probably as high as 0.7 g/cm^3. The gravity effect would be 1.4 mgal. Larger dimensions

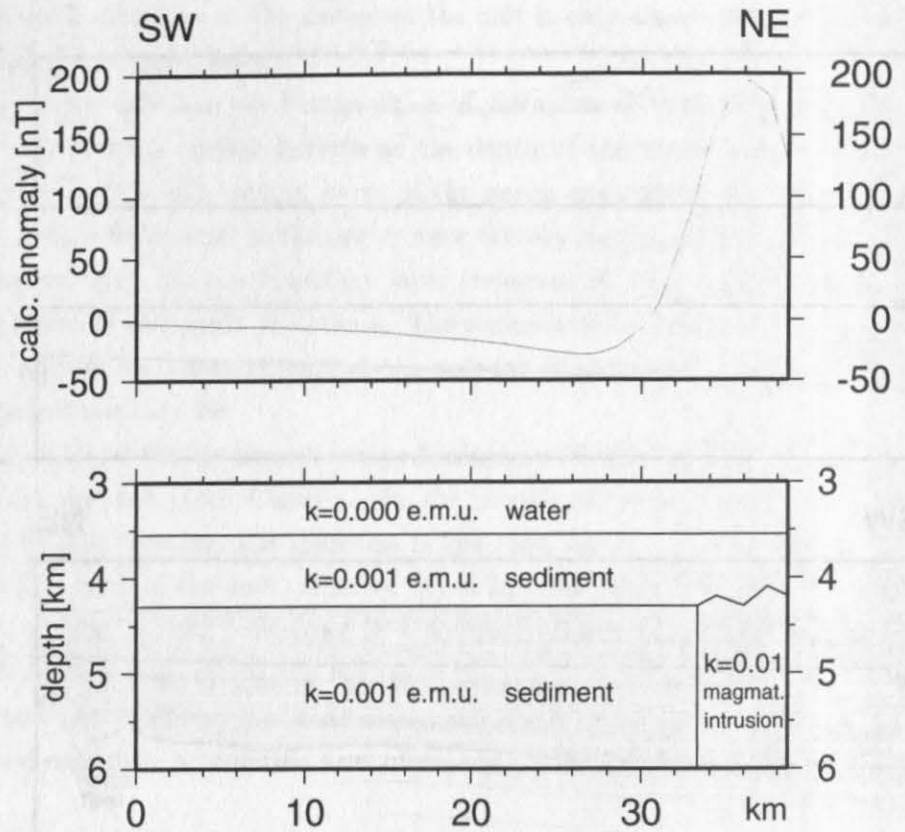

Figure 65: Theoretical magnetic anomaly of a magmatic intrusion at the location of the domal uplifts on profile P203. The geometry and the magnetic susceptibilities (k) of the model are given in the lower part, the calculated anomaly is shown in the upper part. The model was computed by J. Liu.

of the intrusion are suggested by the neighboring uplift and a radius of 2 km would result in an anomaly of 5.3 mgal. This value should be visible in the data set, but there is no evidence for a broad gravity increase above the uplift.

To estimate the magnetic effect of a magmatic intrusion a simple model was constructed (Fig. 65), assuming a magnetic susceptibility (k) of 0 emu for the water, 0.001 emu for the surrounding sediments and 0.01 emu for the intrusion. The result is a strong magnetic anomaly of 200 nT, which does not fit the measured data (Fig. 64).

A non-magmatic origin of the observed uplift structures is thus indicated using three different lines of evidence. The question of salt versus mud diapirism remains. In the case of a salt structure, one has to explain the origin of the salt. A NNW–SSE trending zone of salt diapirs (Fig. 1) which runs northward from east of the island of Fuerteventura has been mapped by Hinz et al. (1982). They assume a single evaporite basin in that area, which existed before the separation of the African and North American plate, providing the salt deposits for the diapirism. Even though the seaward extent of the submarine shield of Fuerteventura is poorly constrained – Hinz et al. (1982) have not mapped the area between Fuerteventura and the salt diapirs, and the seismic data presented in Wissmann (1979) do not have sufficient penetration – a rough coincidence between the western limit

of the salt diapir zone and the eastern edge of the volcanic flank of Fuerteventura can be expected: the salt diapirs are approaching Fuerteventura up to 34 km, whereas the better constrained limit of the western flank of Fuerteventura is located up to 60 km or more from the shoreline. Possible salt diapirs beneath Fuerteventura would be seismically masked by the overlying volcanic basement and, hence, the salt deposits may well extend further to the west. Furthermore, the volcanic load of Fuerteventura could have initiated a moblisation of the salt deposits beneath it. The observed uplift close to the western flank of Fuerteventura could thus represent remnants of migrated salt, uplifted outside the zone of the volcanic load. The amount of uplift is by far less than to the east of Fuerteventura where diapirs pierce the seafloor (Wissmann, 1979).

In contrast to salt domes only a few examples of mud diapirism are known offshore. Von Rad and Wissmann (1982) suggested a mud origin for two diapirs at the continental margin 300 km south of the Canary Islands; they cannot, however, exclude a salt origin. Unquestionable mud diapirs are reported especially at accretionary complexes such as the Barbados Ridge (e.g. Henry et al., 1990) and the Mediterranean Ridge (Camerlenghi et al., 1992). Brown (1990) points out that mud diapirism involves mud and overpressured multiphase pore fluids (water and methane). He described the important role of methane as driving force for the intrusion process, pointing out that only 1 % of the pore space filled by free methane at a depth of 6 km would result in a dramatic increase of porosity and decrease of density which could cause the necessary buoyancy. The ODP Sites 954 and 956 (Schmincke, Weaver, Firth et al., 1995) found no methane concentration above 6 ppm. At Site 953, located closest to the domes (ca. 35 km away), the methane concentration is low as well, only at around 1050 mbsf a slightly higher concentration of 34 ppm was measured. In contrast, the two sites closest to the continental margin show a higher methane content. At Site 955 values of up to 54965 ppm were recorded. The methane content in gas pockets found at DSDP Site 397 varied between 1 and 83 % (Whelan, 1979), with, in general, high values for the Miocene and the drilled Cretaceous interval. In summary, the methane content can change over short distances and considerable concentrations can occur locally. Sediments close to the continental margin have an especially high methane content, suggesting a relation to the sediment supply from the continent. Therefore, a high methane content in the deep northern basin below the drilling penetration is conceivable, as there are sediments which were deposited prior to the buildup of the topographic barrier of the Eastern Canary Islands which are protected from further sediment supply from Africa. Because of that, mud diapirism on profile 203 and 202 is not impossible, but the presence of evaporites appears to be more likely.

5.6.2 Mass wasting

So far only little is known about mass wasting and slides at the Canary Islands, in contrast to e.g. the Hawaiian Islands, where Moore et al. (1989) detected large submarine landslides by means of the side-scan sonar system GLORIA. For Hawaii this is a very powerful tool since background sedimentation rates are low, and, hence, slide deposits remain visible at

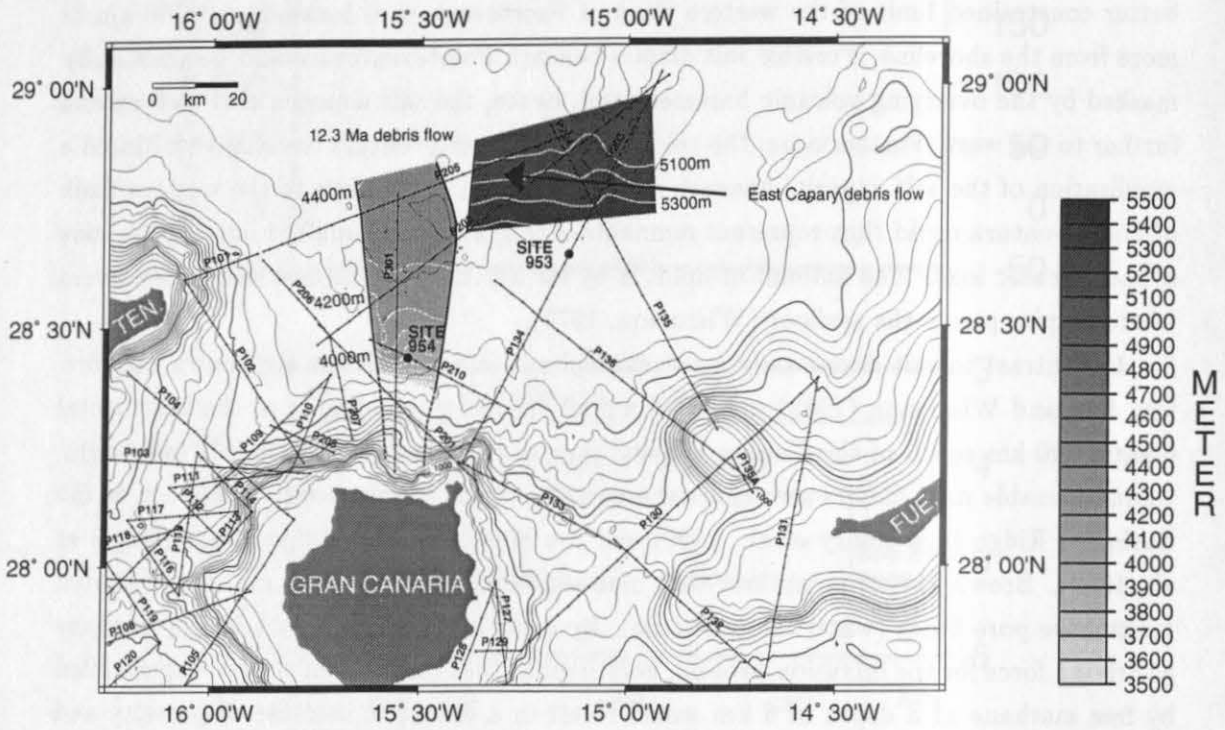

Figure 66: Depth of the ca. 12.3 Ma debris flow from northern Gran Canaria and the East Canary debris flow (given in meters below sea level). The contour interval is 100 m for the derbis flow and 200 m for the bathymetry.

the seafloor for a longer time than at the Canary Islands, where such deposits would be masked more rapidly by sediments. In the case of the young (younger than 1.2 Ma) giant landslide of Orotava on Tenerife, Watts and Masson (1995) could still see its submarine extension and shape with the GLORIA system. Older slides in the more than 20 Ma old history of the Canary Islands cannot be detected so easily, even if the islands morphology and studies onshore can provide evidence for large mass wasting events. By means of an adequate set of seismic lines, these sediment covered slides can be recognized. This was done in the apron north of Gran Canaria.

Lithologic unit IV at Site 954 was interpreted by Schmincke, Weaver, Firth et al. (1995) as a basaltic breccia emplaced by one or more debris flows at ca. 14 Ma after completion of the shield of Gran Canaria. However, the seismic data suggest an emplacement at ca. 12 Ma. Mapping of the corresponding reflectorband (Fig. 66 and 67) gives a very consistent image of the unit, even if the correlation was sometimes interrupted on line 301. The lateral east-west extension on the lines 210, 202, and 205 (Fig. 66) fits remarkably well and suggests an origin of the debris flow at northern Gran Canaria.

The seismic results do not contradict the assumed basaltic composition of lithologic unit IV and its age of some 14 Ma derived from matrix foraminifera. The data in its entirety support the assumption that unit IV represents a displacement of a 14 my old

primary debris flow as consequence of a collapse at the northern flank of Gran Canaria at ca. 12 Ma. The observed hiatus between unit IV and the ca. 10.7 my old overlying sediments is caused by the drill position of Site 954 into the top of a mound formed by the basaltic unit IV. Hence, the hiatus represents a local interval of non-deposition. Nevertheless, at the flanks of the mound, older sediments are recognizable, deposited between ca. 10.7 and 12 Ma.

This mound can be seen in Fig. 66, showing the depth of the top of the debris flow. The shape of the unit becomes increasingly smoother to the north. At line 205 (Fig. 44) the reflectors are almost horizontally layered. Furthermore an isopach map of the debris unit was computed by measuring the two-way travel time between the top and base reflector and applying a velocity of 5.0 km/s, found to be the average velocity of the unit at Site 954 (see Fig. 16). To the east and west the deposits thin rapidly. To the north, the thickness increases to > 80 m on line 205. The northward limit of the deposits is out of the seismic net and to the south the basaltic debris flow cannot be seismically distinguished from the similar basaltic island flank. The volume of the deposits was calculated for the mapped area in Fig. 67 (909 km^2), resuting in 58.5 km^3 of material. This yields an average thickness of 64 m. Regarding the fact that the thickest portions of the debris flow are located in the north where the seismic lines stop, one can expect several tens of km^3 more of material associated with the mass wasting event.

This brings up the question of the origin of the debris flow. Fig. 66 shows the eastern and western boundary of the flow running towards the indentation at the northern coast/shelf of Gran Canaria. This indentation is thought to be a slide scar, forming the amphitheatre from which the basaltic material advanced more than 70 km into the volcanic apron. The exact shape of the amphitheatre is difficult to determine since the Quaternary volcanism on the La Isleta peninsula in the east probably has changed its original shape. The detailed bathymetric map of Fig. 22 suggests an indentation of some 10 to 12 km width, cut ca. 3 km into the island. Estimating the thickness of the slump block to be somewhere between 2 and 4 km yields a volume between (10x3x2=) 60 km^3 and (12x3x4=) 144 km^3, which is in good accordance with the measured debris flow volume. The amphitheatre and the advance of the debris into distal areas of the apron suggest a rapid emplacement of the deposits, possibly by a debris avalanche which turned into debris flows further basinwards before passing ODP Site 954.

Fig. 66 shows the depth of a debris flow unit mapped in the northeastern part of the apron. The thinning and termination of the flow to the west suggest an origin on the East Canaries. The present dip of the debris flow is to the south, in contrast to the more southwesterly dips of the overlying sediments up to reflector M. This change in dip may be caused by the flexure of the lithosphere due to the volcanic load of Fuerteventura. In other words, flow was emplaced some 0.5 to 1 my after the rapid shield building of the island which has been dated around 20 Ma for the central edifice (Coello et al., 1992). This would imply high sedimentation rates between the shieldbuilding of Fuerteventura and Gran Canaria. The debris flow is ca. 300 ms TWT below the hyaloclastite debris

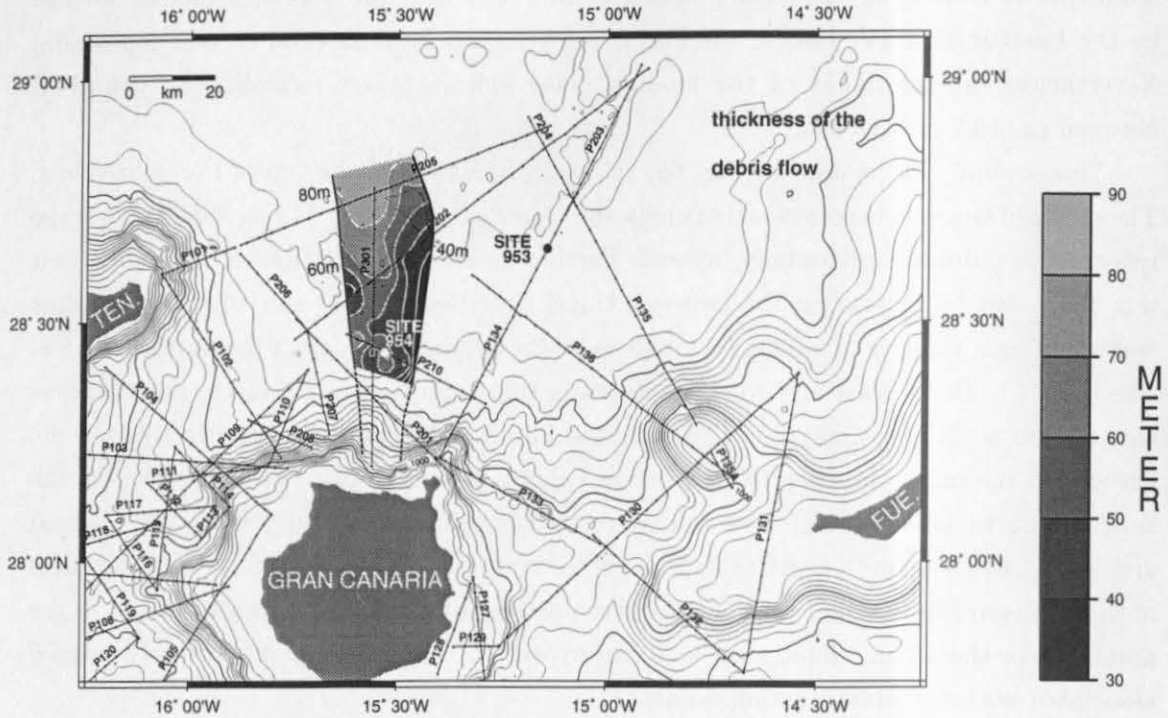

Figure 67: Thickness in meters of the ca. 12.3 Ma debris flow from northern Gran Canaria. The contour interval is 10 m. The two-way travel time was converted to depth by applying a velocity of 5.0 km/s. The contour interval of the bathymetry is 200 m.

flows found in the lowermost lithologic unit of Site 953. The age of the hyaloclastites is somewhere between 15.8 and 17.4 Ma, but could not be determined more precisely due to the lack of nannofossils and foraminifera (Schmincke, Weaver, Firth et al., 1995). The 300 ms of intercalated sediments correspond to ca. 400 m thickness, resulting in a minimum sedimentation rate of about 10 cm/ky when assuming 20 Ma for the debris flow and 16 Ma for the hyaloclastites. This rate is comparable with values of up to 12 cm/ky in seismic unit 2 subsequent to the shield building of Gran Canaria. On the other hand, taking 17.4 Ma for the hyaloclastites and 19 Ma for the East Canary debris flow would result in 25 cm/ky which appears unrealistically high. Alternatively, the debris flow unit may consist of shallow submarine volcaniclastics from the basal complex of Fuerteventura of Oligocene age.

The most spectacular mass wasting event was the emplacement of lithologic unit 7 at ODP Site 953 which consists of hyaloclastite debris flow and turbidite deposits (Schmincke, Weaver, Firth et al., 1995). They were probably formed by shallow submarine eruptions of basaltic magma and were deposited by debris flows and high concentration turbidity currents. The thickness at Site 953 is at least 190 m, where drilling terminated. Seismically, the unit is composed of a number of internal reflectors with medium to high amplitudes. The identification of the bottom reflection is not unambigous, as other medium to high

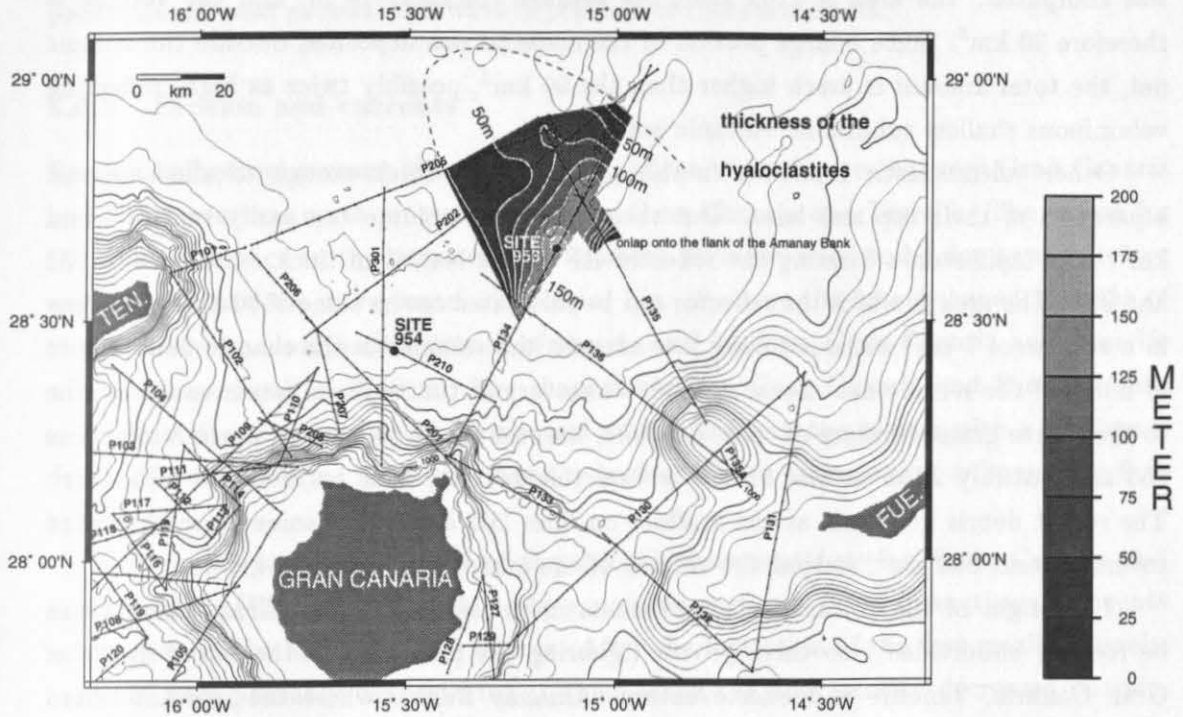

Figure 68: Isopach map of the hyaloclastite unit (lithologic unit 7 at ODP Site 953). The contour interval is 25 m (200 m for the bathymetry). The dashed line is the estimated extent of the unit outside the seismic net.

amplitude reflectors are visible below, but their continuity is less and the cycle breadth changes. These reflectors are also thought to represent volcaniclastic debris flow deposits.

To map the thickness of the hyaloclastite unit (Fig. 68) the two-way travel times were converted to depth by assuming a velocity of 3.3 km/s. This velocity results from the computation of synthetic seismograms at Site 953 after applying a correction of -306 m/s to the measurements done with the Hamilton frame (see *Synthetic seismograms* chapter, page 33). The thickness reaches a maximum with slightly less than 200 m in the vicinity of Site 953. At line 135 the unit thins out when it onlaps onto the flank of the Amanay Bank. The northeastern extent was mapped on lines 202 and 203, the southwestern one on lines 202 and 205. The correlation of the unit on line 134 southwest of Site 953 was hampered by the thickening of the overlying shield of Gran Canaria. Nevertheless, the suspected limit on line 134 fits well with the limits on lines 202 and 205.

The patterns of the isopach map suggest the source of the mass flows somewhere on the (submarine) southern edifice of Fuerteventura. The flat onlap of the unit onto the flank of the Amanay Bank favors a source outside the bank because otherwise remnants of the material would be expected further upslope and the reflection patterns would possibly be more chaotic. Schmincke (personal communication) concludes from comparison of the petrographic-geologic succession at Site 953 and 956 that the main source of the

hyaloclastite unit was Gran Canaria, only the lower part is interpreted to be possibly from Fuerteventura. From the area mapped in Fig. 68 the volume of the hyaloclastites was computed: the area is 1162 km^2, the average thickness 78 m, and the volume is therefore 90 km^3. Since a large portion of the material was deposited outside the seismic net, the total amount is much higher than the 90 km^3, possibly twice as high, reflecting voluminous shallow submarine volcanic activity.

Other volcaniclastic interbeds in the apron are not thick enough to allow seismic separation of their top and base. But their individual volume can easily reach several km^3. The lapillistones forming the reflector RN are at least 2 m thick, both at Site 953 and 954. The area in which the reflector can be correlated covers some 3500 km^2, resulting in a volume of 7 km^3 without taking into account the volumes in the chaotic flank region or north of the seismic net. Because the low recovery at that interval was most likely due to the coarse grained nature of these deposits, the real thickness may be up to 8 m at Site 953 and possibly 20 m at Site 954. The real volumes may thus be in excess of 50 km^3. The recent debris flow seen at the seafloor on lines 202 and 205 is some 10 m thick and covers at least 800 km^2, so that the volume of the mass flow is about 8 km^3.

The origin of the volcaniclastic sediments in the basin north of Gran Canaria can be roughly subdivided into three groups (ignoring the proximity to the island flanks of Gran Canaria, Tenerife and Fuerteventura (Amanay Bank), where the relevant island contribution increases):

1. Prior to the shield building of Gran Canaria the input was most probably from the East Canaries, such as the discussed *East Canary debris flow* and the hyaloclastite unit (following the seismic intepretation).

2. The volcaniclastic interbeds of the seismic units 1 to 6 (i.e. after the basaltic shield building of Gran Canaria until ca. 1 Ma) were predominantly derived from Gran Canaria. Apart from the reflector band around RN, the deposition was mainly to the northeastern part of the apron because the Galdar Ridge deflected the sediments entering the sea in the north to that direction. The distribution of the Roque Nublo deposits further to the northwest is thought to be caused by the character of volcanism with different paths of sedimentation. Subsequent to the shield building of Tenerife, minor supply was from this island, but much less than from Gran Canaria.

3. Since ca. 1 Ma (seismic unit 7 and transition to unit 6), volcaniclastic sediment input has come from both Gran Canaria and Tenerife.

With repsect to the Galdar Ridge, another point to discuss is, namely the role of sediments entering the sea west of the ridge. These sediments come e.g. from the Barranco de Agaete and the large erosional platform in the northwest. The westward decrease of reflectivity in the northern apron suggests that these volcaniclastic sediments were deposited rather to the west or the northwest than to the north. Deposits older than the the shield of Tenerife (ca. 6 Ma) are therefore probably masked by the overlying flank of

the island. Younger volcaniclastic sediments are abundant in the channel between Gran Canaria and Tenerife compared to the western part of the northern apron, confirming the predominant west or northwestward deposition of these sediments.

5.6.3 Erosion and currents

Erosion by bottom currents has had a strong influence on the area between Gran Canaria and Fuerteventura, much more than between Gran Canaria and Tenerife. The reason for the smaller impact on the latter channel is above all interpreted to be due to the greater water depth and the more funnel-like shape. Fig. 19 shows the funnel-shaped isobaths of the northern and southern entrance of the channel between Gran Canaria and Tenerife with a water depth of 2250 m. The channel between Gran Canaria and Fuerteventura in contrast forms a more or less horizontal barrier between the islands with a maximum depth of only 1550 m. This enormous reduction of the cross-section enlarges the flow velocity.

The (small scale) hilly relief of the volcanic basement between Gran Canaria and Fuerteventura (Fig. 36) is thought to be generated partly by these strengthened currents subsequent to the buildup of the barrier. After the formation of the first small channels, currents were probably concentrated to them while the flow velocity decreased outside. Bathymetric lows of the volcanic basement were filled with stratified sediments. On profile 133 (Fig. 37) these sediments tower above the surrounding volcanic basement and their top sequence is therefore affected by erosional currents (around CMP 500 and 2500).

This shows that the erosional activity is not a stationary process, new channels are formed and the flow velocity in existing channels can change. The emergence of the volcanic cones on profile 133 has certainly caused a strengthening of the bottom currents and enforced the formation of the southeastern erosional channel on that line.

The conspicuous channel on line 130 (Fig. 36), where the shield of Gran Canaria onlaps the steep flank of the Amanay Bank, is probably also the cause of the erosional feature on line 136 (Fig. 38) at CMP 13500, at a similar distance to the flank of the bank. The contourites (9.5 to 5.5 Ma) further downslope could represent the paleo-extent of this channel. Material eroded by the currents in the channel was subsequently deposited at these contourite mounds, whereas the current today has an erosive effect at the crossing with line 136.

The Barranco de Guiniguada, a canyon on northeast Gran Canaria (Fig. 22), extends underwater and crosses lines 133 (Fig. 37) and 134 (Fig. 34). In contrast to other onshore canyons in the south or the east (e.g. Baranco de Arguineguin, Barranco de Tirajana), the Barranco de Guiniguada did not form a sedimentary apron when entering the sea. The bottom current system between Gran Canaria and Fuerteventura has transported the material further into the basin north of Gran Canaria. Hence, the present shape of the submarine channel probably represents a complex interaction between subaerial erosion of the canyon, erosion by the transport of debris down the submarine slope and erosion by bottom currents, resulting in a wide and long channel, which has advanced some 40 km

into the basin. The cross section of line 133 (Fig. 37) shows that the channel is flanked by the submarine extent of the La Isleta peninsula to the west and by the volcanic cones to the east. This constriction of the channel may have caused and directed the strong bottom currents which prevent sedimentation on line 133 apart from some detritus and slide blocks.

Several authors conclude from the association of submarine canyons with land canyons, that the offshore portions were carved as subaerial canyons, and subsequently drowned during subsidence. This was suggested for the Hawaiian islands Oahu and Molokai (Andrews and Bainbridge, 1972; Coulbourn et al., 1974; Moore et al., 1989), and most recently for Tenerife (Watts and Masson, 1995).

In the case of Gran Canaria several land canyons can be correlated with submarine extensions (see Fig. 22), e.g. the Barranco de Moja, Azuaje, and Guiniguada in the northern half of Gran Canaria, but their submarine parts have probably not been carved subaerially. The Barrancos de Moya and Azuaje can easily be traced on the volcanic flank down to a depth of 1300 m. This would suggest a relative rise of the sea level of the same order which cannot be explained with eustatic changes of the sea level, but would require a corresponding subsidence of the island itself. The sedimentary basin north of Gran Canaria shows only evidence for major subsidence at ca. 13.5 to 14 Ma (associated with reflector M, see description of seismic line 203 and Fig. 46). This would yield an age of more than 13.5 Ma for the canyons. This is certainly wrong since the amphitheatre in which they are carved was generated by a slide some 12 Ma ago, as discussed above. In consequence, the submarine canyons were most probably eroded by the transport of mass flows down the submarine slopes, in some cases partly supported by bottom currents (Barranco de Guiniguada).

6 Conclusions

Reflection seismic profiling, bathymetric mapping, and drilling results of ODP Leg 157 allowed a detailed analysis of the structure of the apron north of Gran Canaria. Not all features could be precisely dated since the correlation of reflectors was difficult or impossible proximal to the islands, and below the maximum penetration depth of ODP Site 953 no reliable stratigraphy is available. The temporal development and fill of the apron can be summarized as follows:

- Prior to the Canary volcanism, hemipelagic and terrigeneous sediments were deposited on the Jurassic oceanic crust close to the West African continental margin.
- The volcanic flank of the central edifice of Fuerteventura was not covered by the seismic net, but a debris flow at a depth of about 5.2 km is thought to be derived from there, advancing more than 100 km to the west. The change of the dip of the reflectors above and below the debris flow suggests deposition during the crustal deformation due to the volcanic load of Fuerteventura, which is estimated to have taken place some time after the beginning of the subaerial volcanism, i.e. ca. 20-19 Ma, or with the formation of the basal complex in the Oligocene. With the build-up of the East Canary ridge the region to the west was more or less shielded from sediment supply from Africa.
- The southern edifice of Fuerteventura emerged later than the central one. The present Amanay Bank is an eroded part of the southern shield of Fuerteventura and its flank extends ca. 50 km from the plateau into the apron down to a depth of ca. 4750 m.
- A thick hyaloclastite unit onlaps the feather edge of the flank of the Amanay Bank. The emplacement of the hyaloclastite debris flows and turbidites was somewhere between 15.8 and 17.4 Ma and they were probably formed by shallow submarine eruptions of basaltic magma (Schmincke, Weaver, Firth et al., 1995). The mapping of the thickness of the unit results in a total volume of more than 90 km^3 and suggests a source on the southern edifice of Fuerteventura even though Schmincke (personal communication) expects from the petrographic-geologic succession at Site 953 an origin on Gran Canaria. The maximum thickness is about 200 m.
- Subsequent to the hyaloclastites, the volcanic shield of Gran Canaria was formed (ca. 15–16 Ma). To the east the shield was ponded against the preexisting flank of Fuerteventura forming a presently 1550 m deep topographic barrier with a reduction of the cross-section, resulting in strong bottom currents with the formation of erosional channels. To the north the flank extends ca. 60 km seaward. Its depth at the outer rim is between 4500 and 4600 m.
- The subsequent sedimentation is characterized by intercalation of volcaniclastic interbeds into the hemipelagic background sediments. Most of the volcaniclastic mate-

rial came from Gran Canaria in the form of mass flows or ash layers. The transition from the slope to the basin facies occurs ca. 30-40 km off the present coast of Gran Canaria. The Galdar Ridge has deflected volcaniclastic material from Gran Canaria to the northeastern part of the apron (low reflectivity in the western region), with the exception of the Roque Nublo deposits.

- Reflector band M (ca. 13.8 Ma) represents an unconformity, dipping towards Gran Canaria, with almost horizontal layering of the overlying sediments. This unconformity is interpreted to have been caused by the lithospheric flexure due to the load of Gran Canaria.

- Domal uplifts (salt or mud diapirism) were initiated in the northeastern area at the time of the unconformity represented by reflector M (ca. 13.8 Ma). Uplifting continued until 3–2 Ma.

- At about 12 Ma the northern flank of Gran Canaria collapsed and more than 60 km^3 (possibly more than 100 km^3) of volcaniclastic material formed basaltic debris flows, advancing more than 70 km northward into the apron where they are up to 80 m thick.

- The shield of the Anaga massif on northeast Tenerife was rapidly formed at ca. 6 Ma and onlaps onto the older flank of Gran Canaria in the east. The depth of the Anaga shield is 4000 m and it extends some 50 km to the northeast, covering older sediments and masking them seismically.

- Additional volcaniclastic input into the basin north of Gran Canaria occured with the emergence of Tenerife. During the last 1 Ma widespread reflectors from Tenerife are visible, reflecting intense volcanic activity on Tenerife during this period. The Quaternary activity on northern Gran Canaria is reflected as well during this period.

- The Pliocene reflector band RN is the most conspicuous reflector in the northern apron. It can be correlated across the entire northern survey area, representing probably more than 10 km^3 of lapillistones deposited to the north.

- At the northern part of the barrier between Gran Canaria and Fuerteventura a volcanic complex with two volcanic cones is located, which seems to be older than 5 Ma and has caused a re-orientation of the channel currents.

- The Quaternary volcanism on La Isleta extends to the northeast, where a submarine volcano with several young lava flows has formed.

The processing and interpretation of the seismic data in a volcaniclastic apron show a number of peculiarities. The principal processing problem are the steep island flanks with their rough morphology, resulting in a number of side echos (diffractions) which cannot be treated by means of a 2D-migration. Additionally, one has to take care of spatial aliasing

which occurred despite a trace spacing of only 3.125 m. For a successful migration removing this aliased energy is essential. Furthermore one has to apply a migration algorithm which is effective for steeply dipping events without introducing much dispersive noise.

The interpretation of the seismic data in terms of the classical sequence stratigraphy was hampered due to the large amount of reflection terminations which are not systematic and not confined to specific horizons. As the volcaniclastic interbeds represent the majority of the observed reflectors, additional problems occur when they thin out, e.g. related to the observed westward decrease of reflectivity in the apron.

The thickness of the volcaniclastic interbeds in the apron is generally less than half of the seismic wavelength, and, therefore, below the vertical resolution where the top and base reflector can be distinguished. This prevents a seismic determination of their thickness and requires special care when computing synthetic seismograms. A filtering of the logs can, for instance, easily destroy the characteristics of thin interbeds, whereas omission of filtering can introduce erroneous values.

The alternating hemipelagic layers and volcaniclastic deposits produce sufficient impedance contrasts to generate reflections. Their narrow spacing in conjunction with the drilling allows a high temporal resolution of the apron. On the other hand, one has to take care in assigning all stratified reflectors to a change from hemipelagic to volcaniclastic deposits. The up to 200 m thick hyaloclastite unit is, for example, free from pelagic material, but the internal composition of individual debris flows and the transition from breccia to tuff produce similar reflection patterns such as pelagic intercalations. Another point to pay attention to are volcaniclastic layers whose top and bottom can be resolved by two individual reflectors. Since the majority of volcaniclastic interbeds can only be seen as a single reflection, the top and bottom reflector could be interpreted at first glance as two different volcaniclastic interbeds. Sometimes impedance contrasts are quite low, making the interpretation more difficult. An example for this is basaltic debris deposited on basaltic island flanks.

The seismic investigation of the apron, in conjunction with the additional bathymetric and drilling data, was an effective method to reconstruct the volcanic islands' development by its deposits found in the apron, as well as enabling the geometry of the large submarine portions of the volcanic shield to be determined precisely. Slides and debris flows were detected seismically, whereas a study based only on bathymetry, as applied by Moore et al. (1989) at the Hawaiian Islands, would fail for the Canaries since the high sedimentation rates cover these features in a much shorter time period. Furthermore, the nonvolcanic background sediments represent an ideal contrast medium for seismic detection of thin volcaniclastic layers. A seismic investigation in aprons hence benefits from high background sedimentation rates and is therefore more useful in a case such as the Canary Islands than as Hawaii.

For further investigations in the apron north of Gran Canaria one should decrease the spacing of the seismic profiles in order to get a better spatial resolution. Furthermore, an extension of the lines to the north and the east would be desirable, allowing a

better assessment of the extent of the volcaniclastic deposits to the north. Particularly, the geometry of the large debris flow from the northern flank of Gran Canaria could be determined more precisely. The eastern extent would allow a better control of the input from Fuerteventura. Gaps in the coverage with bathymetric data exists above all in the proximal areas of Gran Canaria, namely the shelf. These gaps should be filled because they present the link between the subaerial and submarine canyons, and possibly slide scars in the flanks could be detected easier. A more complete coverage in the channel between Gran Canaria and Fuerteventura would allow a more detailed mapping of the current system there. The measurement of flow velocities, especially in the recognized erosional channels, would also be of some interest.

References

Ancochea, E., Fúster, J.M., Ibarrola, E., Cendrero, A., Coello, J., Hernán, F., Cantagrel, J.M., Jamond, C., 1990. Volcanic evolution of the island of Tenerife (Canary Islands) in the light of new K–Ar data. J. Volcanol. Geotherm. Res., 44, 231–249.

Ancochea, E., Hernán, F., Cendrero, A., Cantagrel, J.M., Fúster, J.M., Ibarrola, E., Coello, J., 1994. Constructive and destructive episodes in the building of a young oceanic island, La Palma, Canary Islands, and genesis of the Caldera de Taburiente. J. Volcanol. Geotherm. Res., 60, 243–262.

Anderson, D.L., Tanimoto, T., Zhang, Y.-S., 1992. Plate tectonics and hotspots: The third dimension. Science, 256, 1645–1651.

Andrews, J.E., Bainbridge, C., 1972. Submarine canyons off eastern Oahu. Pac. Sci., 26, 108–113.

Anguita, F., García Cacho, L., Colombo, F., González Camacho, A., Vieira, R., 1991. Roque Nublo Caldera: a new stratocone caldera in Gran Canaria, Canary Islands. J. Volcanol. Geotherm. Res., 47, 45–63.

Badley, M.E., 1985. Practical seismic interpretation. Prentice Hall, Englewood Cliffs, 266 pp.

Banda, E., Dañobeitia, J.J., Suriñach, E., Ansorge, J., 1981. Features of crustal structure under the Canary Islands. Earth Planet. Sci. Lett., 55, 11–24.

Bodine, J.M., Steckler, M.S., Watts, A.B., 1981. Observations of flexure and the rheology of the oceanic lithosphere. J. Geophys. Res., 86 (B5), 3695–3707.

Bosshard, E. , Macfarlane, D.J., 1970. Crustal structure of the Western Canary Islands from seismic refraction and gravity data. J. Geophys. Res., 75, 4901–4918.

Boyce, R.E., 1976. Definitions and laboratory determination of compressional sound velocity parameters and wet-water content, wet-bulk density and porosity parameters by gravimetric and gamma-ray attenuation techniques. In: Schlanger, S.O., Jackson, E.D., et al.: Init. Rep. Deep Sea Drill. Proj., 33, 931–958.

British Oceanographic Data Center, 1994. General bathymetric chart of the oceans (GEBCO), 5th edition. Bidstone Observatory, Birkenhead, Merseyside.

Brown, K.M., 1990. The nature and hydrogeologic significance of mud diapirs and diatremes for accretionary systems. J. Geophys. Res., 95 (B6), 8969–8982.

Bugge, T., Belderson, R.H., Kenyon, N.H., 1988. The Storegga Slide. Philos. trans. R. Soc. London, 325, 357–388.

Bundesamt für Seeschiffahrt und Hydrographie, 1991. Navigational chart No. 831: Nordatlantischer Ozean, marokkanische Küste: Agadir bis Cabo Bojador und Kanarische Inseln. Bundesamt für Seeschiffahrt und Hydrographie, Hamburg.

Camerlenghi, A., Cita, M.B., Hieke, W., Ricchiuto, T., 1992. Geological evidence for mud diapirism on the Mediterranean Ridge accretionary complex. Earth Planet. Sci. Lett., 109, 493–504.

Cantagrel, J.M., Cendrero, A., Fúster, J.M., Ibarrola, E., Jamond, C., 1984. K-Ar chronology of the volcanic eruptions in the Canarian Archipelago. Island of La Gomera. Bull. Vulcanol., 47-3, 597–609.

Coello, J., Cantagrel, J.-M., Hernán, F., Fúster, J.-M., Ibarrola, E., Ancochea, E., Casquet, C., Jamond, C., Díaz de Téran, J.-R., Cendrero, A., 1992. Evolution of the eastern volcanic ridge of the Canary Island based on new K-Ar data. J. Volcanol. Geotherm. Res., 53, 251–274.

Coulbourn, W.T., Campbell, J.F., Moberly, R., 1974. Hawaiian submarine terraces, canyons, and Quaternary history evaluated by seismic-reflection profiling. Mar. Geology, 17, 215–234.

Dañobeitia, J.J., Canales, J.P., Dehghani, G.A., 1994. An estimation of the elastic thickness of the lithosphere in the Canary Archipelago using admittance function. Geophys. Res. Lett., 21 (24), 2649–2652.

Dañobeitia, J.J., Collette, B.J., 1989. Estudio mediante sísmica de reflexión de un grupo de estructuras submarinas situadas al Norte y Sur del archipelago Canario. Acta Geològica Hispànica, 24, 147–163.

Duncan, R.A., 1981. Hotspots in the southern oceans – an absolute frame of reference for the motion of the Gondwana continents. Tectonophysics, 74, 29–42.

Embley, R.W., 1976. New evidence for the occurence of debris flow deposits in the deep sea. Geology, 4, 371–374.

Filmer, P.E., McNutt, M.K., 1989. Geoid anomalies over the Canary Islands Group. Mar. Geophys. Res., 11, 77–87.

Filmer, P.E., McNutt, M.K., Webb, H.F., Dixon, D.J., 1994. Volcanism and archipelagic aprons in the Marquesas and Hawaiian Islands. Mar. Geophys. Res., 16, 385–406.

Filmer, P.E., McNutt, M.K., Wolfe, C.J., 1993. Elastic thickness of the lithosphere in the Marquesas and Society Islands. J. Geophys. Res., 98 (B11), 19565–19577.

Freundt, A., Schmincke, H.-U., 1995a. Petrogenesis of rhyolite-trachyte-basalt composite ignimbrite P1, Gran Canaria, Canary Islands. J. Geophys. Res., 100 (B1), 455–474.

Freundt, A., Schmincke, H.-U., 1995b. Eruption and emplacement of a basaltic welded ignimbrite during caldera formation on Gran Canaria. Bull. Vulcanol., 56, 640–659.

Funck, T., Dickmann, T., Rihm, R., Krastel, S., Lykke-Andersen, H., Schmincke, H.-U., 1996. Reflection seismic investigations in the volcaniclastic apron of Gran Canaria and implications for its volcanic evolution. Geophys. J. Int., 125, 519–536.

Fúster, J.M., Hernán, F., Cendrero, A., Coello, J., Cantagrel, J.M., Ancochea, E., Ibarrola, E., 1993. Geocronología de la Isla de El Hierro (Islas Canarias). Bol. R. Soc. Hist. Nat. (Sec. Geol.), 88 (1–4), 85–97.

García Cacho, L., Díez-Gil, J.L., Araña, V., 1994. A large volcanic debris avalanche in the Pliocene Roque Nublo Stratovolcano, Gran Canaria, Canary Islands. J. Volcanol. Geotherm. Res., 63, 217–229.

Geisslinger, A., 1993. Prozessing und Interpretation reflexionsseismischer Profile aus dem Bereich der Kanarischen Inseln. M.S. thesis, Institut für Geophysik, Universität Hamburg, 104 pp.

Hausen, H., 1962. New contributions to the geology of Gran Canary (Gran Canaria, Canary Islands). Soc. Sci. Fennica, Comm. Phys.-Math, 43(1), 418 pp.

Henry, P., Le Pichon, X., Lallemant, S., Foucher, J.-P., Westbrook, G., Hobart, M., 1990. Mud volcano field seaward of the Barbados accretionary complex: a deep-towed side scan sonar survey. J. Geophys. Res., 95 (B6), 8917–8929.

Hess, H.H., 1946. Drowned ancient islands of the Pacific Basin. Am. J. Sci., 244, 772–791.

Hinz, K., 1979. Seismic sequences of Cape Bojador, Northwest Africa. In: von Rad, U., Ryan, W.B.F., et al.: Init. Rep. Deep Sea Drill. Proj., 47 (1), 485–489.

Hinz, K., Dostmann, H., Fritsch, J., 1982. The continental margin off Morocco: seismic sequences, structural elements and geological development. In: von Rad, U., Hinz, K., Sarnthein, M., Seibold, E. (eds.): Geology of the Northwest African continental margin, Springer-Verlag, Berlin, Heidelberg, New York, 34–60.

Hinz, K., Seibold, E., Wissmann, G., 1974. Continental slope anticline and unconformities off West Africa. "Meteor" Forsch.–Ergebnisse, Reihe C, 17, 67–73.

Hirschleber, H.B., Dañobeitia, J.J., Dehghani, G.A., Gallart, J., von Haugwitz, W., Herber, R., Radomski, S., Schnaubelt, M., 1992. Geophysical investigations southwest of Gran Canaria (Canary Islands). Ocean-Continent Boundary Newsletter, 1, 33–39.

Hoernle, K.A., Schmincke, H.-U., 1993a. The role of partial melting in the 15-Ma geochemical evolution of Gran Canaria: A blob model for the Canary Hotspot. J. Petrol., 34, 599–626.

Hoernle, K.A., Schmincke, H.-U., 1993b. The petrology of the tholeiites through melilite nephelinites on Gran Canaria, Canary Islands: crystal fractionation, accumulation, and depths of melting. J. Petrol., 34, 573–597.

Hoernle, K.A., Zhang, Y.-S., Graham, D., 1995. Seismic and geochemical evidence for large-scale mantle upwelling beneath the eastern Atlantic and western and central Europe. Nature, 374, 34–39.

Holcomb, R.T., Searle, R.C., 1991. Large landslides from oceanic volcanoes. Mar. Geotechnol., 10, 19–32.

Holik, J.S., Rabinowitz, P.D., 1991. Effects of Canary hotspot volcanism on structure of oceanic crust off Morocco. J. Geophys. Res., 96 (B7), 12039–12067.

Instituto Tecnológico Geo Minero de España, 1990. Mapa geologico de España, Isla de Gran Canaria, map No. 21-21, 21-22.

Kearey, P., 1993. The encyclopedia of the solid earth sciences. Blackwell Scientific Publications, Oxford, 713 pp.

Klitgord, K.D. and Schouten, H., 1986. Plate kinematics of the Central Atlantic. In: Vogt, P.R. and Tucholke, B.E. (eds.), The Geology of North America, Vol. M, The Western North Atlantic Region. Geological Society of America, 351–378.

Krastel, S., 1995. Hochauflösende reflexionsseismische Messungen im vulkaniklastischen Schuttfächer südwestlich Gran Canarias. M.S. thesis, Institut für Geophysik, Universität Kiel, 133 pp.

Larsen, H.C., Saunders, A.D., Clift, P.D. and Shipboard Scientific Party, 1994. Proceedings of the Ocean Drilling Program, Initial Reports, Vol. 152.

Le Bas, M.J., Rex, D.C., Stillman, C.J., 1986. The early magmatic chronology of Fuerteventura, Canary Islands. Geol. Mag., 123, 287–298.

Lénat, J.-F., Vincent, P., Bachèlery, P., 1989. The off-shore continuation of an active basaltic volcano: Piton de la Fournaise (Reunion Island, Indian Ocean); structural and geomorphological interpretation from sea beam mapping. J. Volcanol. Geotherm. Res., 36, 1–36.

Lietz, J., Schmincke, H.-U., 1975. Miocene-Pliocene sea-level changes and volcanic phases on Gran Canaria (Canary Islands) in the light of new K-Ar ages. Palaeogeogr., Palaeoclimatol., Palaeoecol., 18, 213–239.

Martí, J., Mitjavila, J., Araña, V., 1994. Stratigraphy, structure and geochronology of the Las Cañadas caldera (Tenerife, Canary Islands). Geol. Mag., 131 (6), 715–727.

Masson, D.G., Kidd, R.B., Gardner, J.V., Huggett, Q.J., Weaver, P.P.E., 1992. Saharan continental rise: facies distribution and sediment slides. In: Poag, C.W., de Graciansky, P.C. (eds.): Geologic evolution of Atlantic continental rises, Van Nostrand Reinhold, New York, 326–343.

McDougall, I., Schmincke, H.-U., 1976. Geochronology of Gran Canaria, Canary Islands: Age of shield building volcanism and other magmatic phases. Bull. Volcanol., 40 (1), 57–77.

McNutt, M.K., 1984. Lithospheric flexure and thermal anomalies. J. Geophys. Res., 89 (B13), 11180–11194.

Mehl, K.W., 1993. Structure and emplacement of the Pliocene Roque Nublo debris avalanche deposit, Gran Canaria, Spain. PhD thesis, Fakultät für Geowissenschaften der Ruhr-Universität Bochum, 186 pp.

Menard, H.W., 1956. Archipelagic aprons. Bull. Amer. Assoc. Petrol. Geol., 40, 2195–2210.

Menard, H.W., 1964. Marine geology of the Pacific. McGraw-Hill, New York, 271 pp.

Menard, H.W., 1983. Insular erosion, isostasy, and subsidence. Science, 220, 913–918.

Minster, J.B. and Jordan, T.H., 1978. Present-day plate motions. J. Geophys. Res., 83 (B11), 5331–5354.

Mitchum, R.M., Vail, P.E., Thompson, S., 1977. The depositional sequence as a basic unit for stratigraphic analysis. In: Payton, C.E. (ed.): Seismic stratigraphy – applications to hydrocarbon exploration. Am. Assoc. Petrol. Geol. Mem. 26, 53–62.

Monnerau, M., Cazenave, A., 1990. Depth and geoid anomalies over oceanic hotspot swells: a global survey. J. Geophys. Res., 95 (B10), 15429–15438.

Moore, J.G., Bryan, W.B., Beeson, M.H., Normark, W.R., 1995. Giant blocks in the South Kona landslide, Hawaii. Geology, 23 (2), 125–128.

Moore, J.G., Clague, D.A., Holcomb, R.T., Lipman, P.W., Normark, W.R., Torresan, M.E., 1989. Prodigious submarine landslides on the Hawaiian Ridge. J. Geophys. Res., 94 (B12), 17465–17484.

Moore, J.G., Normark, W.R., 1994. Giant Hawaiian landslides. Annu. Rev. Earth Planet. Sci., 22, 119-144.

Morgan, W.J., 1983. Hotspot tracks and the early rifting of the Atlantic. Tectonophysics, 94, 123–139.

National Geophysical Data Center, 1993. Database for marine geophysical data. NOAA E/GC4, Dept. 940, Boulder.

Northwood, E.J., Weisinger, R.C., Bradley, J.J., 1967. Recommended standards for digital tape formats. Geophysics, 32 (6), 1073–1084.

Rees, B.A., Detrick, R.S., Coakley, B.J., 1993. Seismic stratigraphy of the Hawaiian flexural moat. Geol. Soc. Am. Bull., 105, 189–205.

Rijks Geologische Dienst, 1994. Steam '94. Cruise report. Rijks Geologische Dienst, Haarlem, 18 pp.

Roeser, H.A., 1982. Magnetic anomalies in the magnetic quiet zone off Morocco. In: von Rad, U., Hinz, K., Sarnthein, M., Seibold, E. (eds.): Geology of the Northwest African continental margin, Springer-Verlag, Berlin, Heidelberg, New York, 60–68.

Roest, W.R., Dañobeitia, J.J., Verhoef, J., Collette, B.J., 1992. Magnetic anomalies in the Canary Basin and the Mesozoic evolution of the Central North Atlantic. Mar. Geophys. Res., 14, 1–24.

Rothe, P., Schmincke, H.–U., 1968. Contrasting Origins of the eastern and western islands of the Canarian Archipelago. Nature, 218, 1152–1154.

Schmincke, H.-U., 1967. Cone sheet swarm, resurgence of Tejeda Caldera, and the early geologic history of Gran Canaria. Bull. Volcanol., 31, 153–162.

Schmincke, H.-U., 1968. Faulting versus erosion and the reconstruction of the Mid-Miocene shield volcano of Gran Canaria. Geol. Mitt., 8, 23–50.

Schmincke, H.-U., 1973. Magmatic evolution and tectonic regime in the Canary, Madeira, and Azores Island Groups. Geol. Soc. Am. Bull., 84, 633–648.

Schmincke, H.-U., 1976. Geology of the Canary Islands. In: Kunkel, G. (ed.), Biogeography and ecology in the Canary Islands. W. Junk, The Hague, 67–184.

Schmincke, H.-U., 1982. Volcanic and chemical evolution of the Canary Islands. In: von Rad, U., Hinz, K., Sarnthein, M., Seibold, E. (eds.): Geology of the Northwest African continental margin, Springer-Verlag, Berlin, Heidelberg, New York, 273–306.

Schmincke, H.-U., 1994. Geological field guide Gran Canaria, Part I and II. Pluto Press Kiel, 149 pp.

Schmincke, H.-U., Rihm, R., 1994. Ozeanvulkan 1993, Cruise No. 24, 15 April – 9 May 1993. Meteor–Berichte, Universität Hamburg, 94–2, 88 pp.

Schmincke, H.-U., von Rad, U., 1979. Neogene evolution of Canary Island volcanism inferred from ash layers and volcaniclastic sandstones of DSDP Site 397 (Leg 47A). In: von Rad, U., Ryan, W.B.F., et al.: Init. Rep. Deep Sea Drill. Proj., 47 (1), 703–716.

Schmincke, H.-U., Weaver, P.P.E., et al., 1992. Drilling into the clastic apron of Gran Canaria and the Madeira Abyssal Plain: Volcanic island evolution, continental margin sediment instability, global sealevel history and basin analysis. Proposal for ODP drilling, combined proposals 380 and 59A, 95 pp.

Schmincke, H.-U., Weaver, P.P.E., Firth, J., 1994. Leg 157 scientific prospectus: Drilling into the clastic apron of Gran Canaria and into the Madeira Abyssal Plain. Ocean Drilling Program, Scientific Prospectus No. 57, 95 pp.

Schmincke, H.-U., Weaver, P.P.E., Firth, J. and Shipboard Scientific Party, 1995. Proceedings of the Ocean Drilling Program, Initial Reports, Vol. 157, in press.

Segall, P., Delaney, P., Arnadottir, T., Freymueller, J., Owen, S., 1992. Deformation of the south flank of Kilauea Volcano. Eos Trans. AGU (Abstr.), 73, 505–506.

Seibold, E., 1972. Cruise 25/1971 of R.V. "Meteor": continental margin of West Africa. General report and preliminary results. "Meteor" Forsch.–Ergebnisse, Reihe C, 10, 17–38.

Seibold, E., Hinz, K., 1976. German cruises to the continental margin of North West Africa in 1975: general reports and preliminary results from "Valdivia" 10 and "Meteor" 39. "Meteor" Forsch.–Ergebnisse, Reihe C, 25, 47–80.

Servicio Geográfico del Ejército, 1981–1992. Mapa militar de España, scale 1:100000, maps No. 19-20 (1982), 19/20-21 (1982), 20-20 (1982), 21-21 (1992), 21-22 (1990), 22/23-21 (1981), 23/24-20/21 (1981).

Simkin, T., Siebert, L., 1994. Volcanoes of the world, 2nd edition. Geoscience Press Inc., Tucson, 349 pp.

Sleep, N.H., 1990. Hotspots and mantle plumes: some phenomenology. J. Geophys. Res., 95 (B5), 6715–6736.

Smoot, N.C., 1980. Interpretation of deep sea sounding data. Paper presented at the Fall Technical Meeting, Am. Congr. of Surv. and Mapp., Niagara Falls, New York.

Spieß, V., 1992. Paradigma. Handbuch zum Programmsystem Digitalisierung von Parasound-Seismogrammen, Universität Bremen, 39 pp.

Staudigel, H., Feraud, G., Giannerini, G., 1986. The history of intrusive activity on the island of La Palma (Canary Islands). J. Volcanol. Geotherm. Res., 27, 299–322.

Staudigel, H., Schmincke, H.-U., 1984. The pliocene seamount series of La Palma/Canary Islands. J. Geophys. Res., 89 (B13), 11195–11215.

Stolt, R.H., 1987. Migration by Fourier transform. Geophysics, 43, 23–48.

Telford, W.M., Geldart, L.P., Sheriff, R.E., 1990. Applied geophysics, 2nd ed. Cambridge University Press, 770 pp.

ten Brink, U.S., Brocher, T.M., 1987. Multichannel seismic evidence for a subcrustal intrusive complex under Oahu and a model for Hawaiian volcanism. J. Geophys. Res., 92 (B13), 13687–13707.

ten Brink, U.S., Watts, A.B., 1985. Seismic stratigraphy of the flexural moat flanking the Hawaiian Islands. Nature, 317, 421–424.

Thywissen, K., Wong, H.K., 1993. Teilabschlußbericht zum Projekt reflexionsseismische Untersuchungen im Bereich der Kanaren – METEOR-Fahrt 16/4 – Presite-Survey im Rahmen von VICAP im Schwerpunkt "Auswertung der METEOR-Expeditionen". Deutsche Forschungsgemeinschaft, 90 pp.

Uchupi, E., Emery, K.O., Bowin, C.O., Phillips, J.D., 1976. Continental margin off Western Africa: Senegal to Portugal. Am. Assoc. Petrol. Geol. Bull., 60, 809–878.

van den Boogard, P., Schmincke, H.-U., Freundt, A., Hall, C.M., York, D., 1988. Eruption ages and magma supply rates during the Miocene evolution of Gran Canaria. Single-crystal $^{40}Ar/^{39}Ar$ laser ages. Naturwissenschaften, 75, 616–617.

Verhoef, J., Collette, B.J., Dañobeitia, J.J, Roeser, H.A., Roest, W.R., 1991. Magnetic anomalies off West-Africa (20-38° N). Mar. Geophys. Res., 13, 81–103.

von Rad, U., Ryan, W.B.F., et al., 1979. Init. Rep. Deep Sea Drill. Proj., 47 (1), 835 pp.

von Rad, U., Wissmann, G., 1982. Cretaceous-Cenozoic history of the Western Saharan Continental Margin (NW Africa): development, destruction and gravitational sedimentation. In: von Rad, U., Hinz, K., Sarnthein, M., Seibold, E. (eds.): Geology of the Northwest African continental margin, Springer-Verlag, Berlin, Heidelberg, New York, 106–131.

Watts, A.B., 1978. An analysis of isostasy in the world's oceans, 1. Hawaiian–Emperor seamount chain. J. Geophys. Res., 83, 5989–6004.

Watts, A.B., 1994. Crustal structure, gravity anomalies and flexure of the lithosphere in the vicinity of the Canary Islands. Geophys. J. Int., 119, 648–666.

Watts, A.B., Masson, D.G., 1995. A giant landslide on the north flank of Tenerife, Canary Islands. J. Geophys. Res., 100 (B12), 24487–24498.

Watts, A.B., Peirce, C., Collier, J., Henstock, T., 1993. R.R.S. Charles Darwin CD82 cruise report, 33 pp.

Watts, A.B., ten Brink, U.S., Buhl, P., Brocher, T.M., 1985. A multichannel seismic study of lithospheric flexure across the Hawaiian-Emperor seamount chain. Nature, 315, 105–111.

Weddeling, P., 1996. Influence of the flexure of the lithosphere due to the load of the Canary Islands on the Neogen stratigraphy of the adjacent Northwest African passive continental margin. PhD thesis, Mathematisch-Naturwissenschaftliche Fakultät der Christian-Albrechts-Universität zu Kiel, in preparation.

Wefer, G., Schulz, H.D., Schott, F., Hirschleber, H.B., 1992. Atlantik 91 – Expedition, Reise Nr. 16, 27. März – 8. Juli 1991. Meteor–Berichte, Universität Hamburg, 92–2, 288 pp.

Wessel, P., 1993. A re-examination of the flexural deformation beneath the Hawaiian Islands. J. Geophys. Res., 98 (B7), 12177–12190.

Wessel, P., Smith, W.H.F., 1991. Free software helps map and display data. EOS, Trans. Am. Geophys. Un., 72, 441–446.

Whelan, K., 1979. C_1 to C_7 hydrocarbons from IPOD Holes 397 and 397A. In: von Rad, U., Ryan, W.B.F., et al.: Init. Rep. Deep Sea Drill. Proj., 47 (1), 531–539.

Wilson, J.T., 1963. A possible origin of the Hawaiian Islands. Can. J. Phys., 41, 863–870.

Wissmann, G., 1979. Cape Bojador Slope, an example for potential pitfalls in seismic interpretation without the information of outer margin drilling. In: von Rad, U., Ryan, W.B.F., et al.: Init. Rep. Deep Sea Drill. Proj., 47 (1), 491–499.

Wolfe, C.J., McNutt, M.K., Detrick, R.S., 1994. The Marquesas archipelagic apron: Seismic stratigraphy and implications for volcano growth, mass wasting, and crustal underplating. J. Geophys. Res., 99 (B7), 13591–13608.

Ye, S., Rihm, R., Dañobeitia, J.J., Canales, J.P., Gallart, J., 1996. A crustal transect through the northern and northeastern part of the volcanic edifice of Gran Canaria. J. Geodynam., submitted.

Zhang, Y.-S., Tanimoto, T., 1992. Ridges, hotspots and their interaction as observed in seismic velocity maps. Nature, 355, 45–49.

Acknowledgement

I wish to thank my advisors: Prof. Hans-Ulrich Schmincke for the idea of this work, the encouraged geologic supervision with numerous stimulating discussions, and his help making my participation on ODP Leg 157 possible; Prof. Dietrich Ristow for the geophysical supervision, his helpful hints concerning the processing of the seismic data, and his open mind; Prof. Holger Lykke-Andersen for the warm reception at the University of Århus, Denmark, where I benefited from his strong background in seismic stratigraphy during several visits.

I gratefully acknowledge Dr. Roland Rihm for his detailed review of this manuscript, valuable discussions and making available his scientific contacts. Dr. Thomas Dickmann kindly introduced me to the processing software at Geomar, and I want to thank him for doing the main part of the bathymetric data processing. I am grateful to Dr. Rüdiger Kunze, Dr. Wilhelm Weinrebe and Gerhard Mach for keeping the necessary hardware and software running. Sebastian Krastel has worked on the M24 data between Gran Canaria and Tenerife and, hence, I thank him for sharing problems and the administrative work, as well as his constant helpfulness.

Scientists and crewmembers of the Meteor cruise M24 have collected the data in a professional manner, even during bad weather conditions. Likewise, during ODP Leg 157, where I made a number of contacts inspiring this work. On this occasion I want to thank Prof. Julie A. Hood for hosting my work at her laboratory at the Rosenstiel School of Marine and Atmospheric Science, University of Miami, USA, as well as for proofreading of the English in this manuscript.

From the Institute of Geophysics at the University of Hamburg, Germany, I wish to thank Dr. Jianxia Liu and Dr. Gholam Ali Dehghani for their support concerning the gravity and magnetic compilations. Prof. Anthony B. Watts from the University of Oxford, England put the seismic lines of the Charles Darwin cruise CD82 at my disposal and gave me useful advice for the computation of the bathymetric map.

Most of the figures were generated with GMT software; thanks to Paul Wessel and Walter F.H. Smith. Special thanks go to all the anonymous students and colleagues in Kiel, Århus, Miami and elsewhere, who have contributed to this work by discussions, technical support, and by establishing the necessary stimulating and human atmosphere.

This work was funded by a grant of the Deutsche Forschungsgemeinschaft (DFG), who finances the Graduiertenkolleg "Dynamik globaler Kreisläufe im System Erde". Further support and travel grants were provided by the DFG (Schm 250–54), the Bundesministerium für Forschung und Technologie, and the European Union (EPOCH, EVSV-CT93-0283).

Appendix - Processing sequences

profile No.	**101**		
beginning	15.89182°W, 28.65480°N (CMP 34)		
end	16.06783°W, 28.59983°N (CMP 3653)		
length	18.26 km		
course	250°		
wind			
shot rate	CMP 34–3653:	10 s	(3 fold)
processing sequence:			
reverse polarity	SEG normal polarity		
CMP sorting			
NMO correction	water:	v_{NMO} =1500 m/s	
	0-400 ms below seafloor	v_{NMO} =1600 m/s	
	end of data	v_{NMO} =2500 m/s	
offset-dependant scaling	time invariant equalizing of the 24 channels		
stack	fold is given with the shot rate		
resampling	sampling rate 2 ms		
scaling	AGC windowlength 200 ms		
migration	finite-difference migration in the fx-domain		
	water:	v_{INT} =1450 m/s	
	sediments:	v_{INT} =1700-2000 m/s	
	below flank:	v_{INT} =2500 m/s	
band-pass filter	seafloor:	30-210 Hz	
	end of data:	30-160 Hz	
tracemix	5 traces (weight 1 2 4 2 1)		
scaling	AGC windowlength:	50 ms at seafloor	
		200 ms at end of data	

profile No.	**102**		
beginning	16.06583°W, 28.59850°N (CMP 34)		
end	15.81162°W, 28.26500°N (CMP 16903)		
length	44.57 km		
course	146°		
wind			
shot rate	CMP 34–2447:	5 s	(6 fold)
	CMP 2448–4297:	7.5 s	(4 fold)
	CMP 4298–15127:	10 s	(3 fold)
	CMP 15128–16903:	7.5 s	(4 fold)
processing sequence:			
reverse polarity	SEG normal polarity		
CMP sorting			
NMO correction	water:	v_{NMO} =1500 m/s	
	0-400 ms below seafloor	v_{NMO} =1600 m/s	
	end of data	v_{NMO} =2500 m/s	
offset-dependant scaling	time invariant equalizing of the 24 channels		
stack	fold is given with the shot rate		
resampling	sampling rate 2 ms		
scaling	AGC windowlength 200 ms		
migration	finite-difference migration in the fx-domain		
	v_{RMS} =1500 m/s		
band-pass filter	seafloor:	30-235 Hz	
	400 ms below seafloor:	30-160 Hz	
	end of data:	30-160 Hz	
tracemix	5 traces (weight 1 2 4 2 1)		
scaling	AGC windowlength:	50 ms at seafloor	
		200 ms at end of data	

profile No.	**110**		
beginning	15.71717°W, 28.39950°N (CMP 34)		
end	15.80867°W, 28.19917°N (CMP 7309)		
length	23.95 km		
course	202°		
wind	NE 5–11 m/s		
shot rate	CMP 34–4287:	10 s	(3 fold)
	CMP 4288–6793:	7.5 s	(4 fold)
	CMP 6794–7309:	5 s	(6 fold)
processing sequence:			
reverse polarity	SEG normal polarity		
CMP sorting			
NMO correction	water:	v_{NMO} =1500 m/s	
	0-400 ms below seafloor	v_{NMO} =1600 m/s	
	end of data	v_{NMO} =2500 m/s	
offset-dependant scaling	time invariant equalizing of the 24 channels		
stack	fold is given with the shot rate		
resampling	sampling rate 2 ms		
scaling	AGC windowlength 200 ms		
migration	finite-difference migration in the fx-domain		
	v_{RMS} =1475 m/s		
band-pass filter	seafloor:	30-220 Hz	
	500 ms below seafloor:	30-200 Hz	
	800 ms below seafloor:	30-160 Hz	
	end of data:	20-160 Hz	
tracemix	5 traces (weight 1 2 4 2 1)		
scaling	AGC windowlength:	50 ms at seafloor	
		200 ms at end of data	

profile No.	**130**		
beginning	15.25250°W, 27.82383°N (CMP 34)		
end	14.54133°W, 28.39317°N (CMP 29841)		
length	94.15 km		
course	048°		
wind	N 9–13 m/s		
shot rate	CMP 34–5059:	5 s	(6 fold)
	CMP 5060–18335:	7.5 s	(4 fold)
	CMP 18336–25305:	5 s	(6 fold)
	CMP 25306–29841:	7.5 s	(4 fold)
processing sequence:			
reverse polarity	SEG normal polarity		
CMP sorting			
NMO correction	water:	v_{NMO} =1500 m/s	
	0-400 ms below seafloor	v_{NMO} =1600 m/s	
	end of data	v_{NMO} =2500 m/s	
offset-dependant scaling	time invariant equalizing of the 24 channels		
stack	fold is given with the shot rate		
resampling	sampling rate 2 ms		
predictive deconvolution	CMP 18400-25280, operator length: 256 ms		
scaling	AGC windowlength 200 ms		
migration	finite-difference migration in the fx-domain		
	water:	v_{INT} =1450 m/s	
	sediments:	v_{INT} =1500 m/s	
	below flank:	v_{INT} =1550 m/s	
band-pass filter	seafloor:	30-235 Hz	
	300 ms below seafloor:	30-160 Hz	
	end of data:	30-160 Hz	
tracemix	5 traces (weight 1 2 4 2 1)		
scaling	AGC windowlength:	50 ms at seafloor	
		200 ms at end of data	

profile No.	**133**		
beginning	15.01627°W, 28.03733°N (CMP 34)		
end	15.40850°W, 28.21850°N (CMP 13767)		
length	43.77 km		
course	298°		
wind	N 7–11 m/s		
shot rate	CMP 34–12451:	7.5 s	(4 fold)
	CMP 12452–13767:	5 s	(6 fold)
processing sequence:			
reverse polarity	SEG normal polarity		
CMP sorting			
NMO correction	water:	v_{NMO} =1500 m/s	
	0-400 ms below seafloor	v_{NMO} =1600 m/s	
	end of data	v_{NMO} =2500 m/s	
offset-dependant scaling	time invariant equalizing of the 24 channels		
stack	fold is given with the shot rate		
resampling	sampling rate 2 ms		
fk-filter	dip -2 to 2 ms/trace		
scaling	AGC windowlength 200 ms		
migration	finite-difference migration in the tx-domain		
	water:	v_{INT} =1450 m/s	
	sediments:	v_{INT} =2000 m/s	
	below flank:	v_{INT} =2500 m/s	
band-pass filter	above 2.5 s TWT:	30-235 Hz	
	below 3.2 s TWT:	30-200 Hz	
tracemix	5 traces (weight 1 2 4 2 1)		
scaling	AGC windowlength:	50 ms at seafloor	
		200 ms at end of data	

profile No.	**134**		
beginning	15.38483°W, 28.22117°N (CMP 34)		
end	15.07300°W, 28.76500°N (CMP 22379)		
length	67.57 km		
course	028°		
wind	N/NW 5–9 m/s		
shot rate	CMP 34–731:	5 s	(6 fold)
	CMP 732–951:	7.5 s	(4 fold)
	CMP 952–1337:	5 s	(6 fold)
	CMP 1338–3931:	7.5 s	(4 fold)
	CMP 3932–22379:	10 s	(3 fold)
processing sequence:			
reverse polarity	SEG normal polarity		
CMP sorting			
NMO correction	water:	v_{NMO} =1500 m/s	
	0-400 ms below seafloor	v_{NMO} =1600 m/s	
	end of data	v_{NMO} =2500 m/s	
offset-dependant scaling	time invariant equalizing of the 24 channels		
stack	fold is given with the shot rate		
resampling	sampling rate 2 ms		
fk-filter	dip -3 to 3 ms/trace		
scaling	AGC windowlength 200 ms		
migration	finite-difference migration in the fx-domain		
	water:	v_{INT} =1450 m/s	
	sediments:	v_{INT} =1900 m/s	
	below flank:	v_{INT} =2100 m/s	
band-pass filter	seafloor:	30-230 Hz	
	200 ms below seafloor:	30-230 Hz	
	400 ms below seafloor:	20-160 Hz	
	end of data:	20-160 Hz	
scaling	AGC windowlength:	50 ms at seafloor	
		200 ms at end of data	
composed data stack	stack of 16 adjacent traces in Fig. 34		

profile No.	**135**		
beginning	15.09233°W, 28.76183°N (CMP 34)		
end	14.78133°W, 28.28550°N (CMP 18537)		
length	60.94 km		
course	150°		
wind	NW 5–6 m/s		
shot rate	CMP 34–14527:	10 s	(3 fold)
	CMP 14528–16661:	7.5 s	(4 fold)
	CMP 16662–18537:	5 s	(6 fold)
processing sequence:			
reverse polarity	SEG normal polarity		
CMP sorting			
NMO correction	water:	v_{NMO} =1500 m/s	
	0-400 ms below seafloor	v_{NMO} =1600 m/s	
	end of data	v_{NMO} =2500 m/s	
offset-dependant scaling	time invariant equalizing of the 24 channels		
stack	fold is given with the shot rate		
band-pass filter	20-240 Hz		
composed data stack	stack of 2 adjacent traces		
resampling	sampling rate 2 ms		
scaling	AGC windowlength 200 ms		
migration	finite-difference migration in the tx-domain		
	water:	v_{INT} =1450 m/s	
	sediments:	v_{INT} =1900 m/s	
	below flank:	v_{INT} =2100 m/s	
band-pass filter	40-240 Hz		
tracemix	3 traces (weight 1 2 1)		
scaling	AGC windowlength:	50 ms at seafloor	
		200 ms at end of data	

profile No.	**136**		
beginning	14.69367°W, 28.17267°N (CMP 34)		
end	15.32483°W, 28.59583°N (CMP 25477)		
length	77.63 km		
course	307°		
wind	N 9–13 m/s		
shot rate	CMP 34–7427:	5 s	(6 fold)
	CMP 7428–10597:	7.5 s	(4 fold)
	CMP 10598–25477:	10 s	(3 fold)
processing sequence:			
reverse polarity	SEG normal polarity		
CMP sorting			
NMO correction	water:	v_{NMO} =1500 m/s	
	0-400 ms below seafloor	v_{NMO} =1600 m/s	
	end of data	v_{NMO} =2500 m/s	
offset-dependant scaling	time invariant equalizing of the 24 channels		
stack	fold is given with the shot rate		
resampling	sampling rate 2 ms		
predictive deconvolution	CMP 34–7000, operator length: 128 ms		
scaling	AGC windowlength 200 ms		
migration	finite-difference migration in the fx-domain		
	water:	v_{INT} =1450 m/s	
	sediments:	v_{INT} =1500–1650 m/s	
	below flank:	v_{INT} =1800 m/s	
band-pass filter	seafloor:	30-235 Hz	
	200 ms below seafloor:	30-235 Hz	
	800 ms below seafloor:	30-160 Hz	
	end of data:	30-160 Hz	
tracemix	5 traces (weight 1 2 4 2 1)		
scaling	AGC windowlength:	50 ms at seafloor	
		200 ms at end of data	

profile No.	**201**		
beginning	15.19950°W, 28.18017°N (CMP 34)		
end	15.74483°W, 28.50750°N (CMP 16081)		
length	64.62 km		
course	315°		
wind	NE 6–11 m/s		
shot rate	CMP 34–3043:	5 s	(6 fold)
	CMP 3044–10329:	7.5 s	(4 fold)
	CMP 10330–16081:	10 s	(3 fold)
processing sequence:			
reverse polarity	SEG normal polarity		
CMP sorting			
NMO correction	water:	v_{NMO} =1500 m/s	
	0-400 ms below seafloor	v_{NMO} =1600 m/s	
	end of data	v_{NMO} =2500 m/s	
offset-dependant scaling	time invariant equalizing of the 24 channels		
stack	fold is given with the shot rate		
resampling	sampling rate 2 ms		
predictive deconvolution	CMP 34–2850, operator length: 32 ms		
fk-filter	dip -3 to 3 ms/trace		
scaling	AGC windowlength 200 ms		
migration	finite-difference migration in the fx-domain		
	water:	v_{INT} =1450 m/s	
	sediments:	v_{INT} =1700 m/s	
	below flank:	v_{INT} =1900 m/s	
band-pass filter	seafloor:	30-235 Hz	
	500 ms below seafloor:	30-200 Hz	
	end of data:	30-160 Hz	
scaling	AGC windowlength:	50 ms at seafloor	
		200 ms at end of data	
composed data stack	stack of 16 adjacent traces in Fig. 41		

profile No.	**202**		
beginning	15.74550°W, 28.46467°N (CMP 34)		
end	14.90150°W, 29.02067°N (CMP 33041)		
length	102.93 km		
course	053°		
wind	NNE/NNW 3–8 m/s		
shot rate	CMP 34–33041:	10 s	(3 fold)
processing sequence:			
reverse polarity	SEG normal polarity		
CMP sorting			
NMO correction	water:	v_{NMO} =1500 m/s	
	0-400 ms below seafloor	v_{NMO} =1600 m/s	
	end of data	v_{NMO} =2500 m/s	
offset-dependant scaling	time invariant equalizing of the 24 channels		
stack	fold is given with the shot rate		
resampling	sampling rate 2 ms		
composed data stack	stack of 4 adjacent traces		
scaling	AGC windowlength 200 ms		
migration	finite-difference migration in the tx-domain		
	water:	v_{INT} =1450 m/s	
	seafloor–5350 ms TWT:	v_{INT} =1550 m/s	
	5350–6200 ms TWT:	v_{INT} =1650 m/s	
	below 6200 ms:	v_{INT} =1750 m/s	
band-pass filter	seafloor:	30-235 Hz	
	5.4 s TWT:	30-235 Hz	
	5.7 s TWT:	20-160 Hz	
	end of data:	20-160 Hz	
scaling	AGC windowlength:	50 ms at seafloor	
		200 ms at end of data	

profile No.	**203**		
beginning	14.91917°W, 29.02617°N (CMP 34)		
end	15.10117°W, 28.72033°N (CMP 12385)		
length	38.27 km		
course	208°		
wind	N 3–6 m/s		
shot rate	CMP 34–12385:	10 s	(3 fold)
processing sequence:			
reverse polarity	SEG normal polarity		
CMP sorting			
NMO correction	water:	v_{NMO} =1500 m/s	
	0-400 ms below seafloor	v_{NMO} =1600 m/s	
	end of data	v_{NMO} =2500 m/s	
offset-dependant scaling	time invariant equalizing of the 24 channels		
stack	fold is given with the shot rate		
resampling	sampling rate 2 ms		
composed data stack	stack of 4 adjacent traces		
band-pass filter	30-230 Hz		
scaling	AGC windowlength 200 ms		
migration	finite-difference migration in the tx-domain		
	water:	v_{INT} =1450 m/s	
	seafloor–5200 ms TWT:	v_{INT} =1550 m/s	
	5200–6000 ms TWT:	v_{INT} =1650 m/s	
	below 6000 ms:	v_{INT} =1750 m/s	
band-pass filter	30-220 Hz		
scaling	AGC windowlength:	50 ms at seafloor	
		200 ms at end of data	

profile No.	**204**		
beginning	15.06567°W, 28.27200°N (CMP 34)		
end	15.19467°W, 28.29133°N (CMP 8363)		
length	25.43 km		
course	330°		
wind	NNE 3–5 m/s		
shot rate	CMP 34–8363:	10 s	(3 fold)
processing sequence:			
reverse polarity	SEG normal polarity		
CMP sorting			
NMO correction	water:	v_{NMO} =1500 m/s	
	0-400 ms below seafloor	v_{NMO} =1600 m/s	
	end of data	v_{NMO} =2500 m/s	
offset-dependant scaling	time invariant equalizing of the 24 channels		
stack	fold is given with the shot rate		
resampling	sampling rate 2 ms		
band-pass filter	seafloor:	30-160 Hz	
	5500 ms TWT:	30-160 Hz	
	7000 ms TWT:	20-70 Hz	
coherency filter	dip-analysis along 7 traces		
	weight filtered : unfiltered data = 7 : 3		
migration	finite-difference migration in the tx-domain		
	v_{INT} =1500 m/s		
scaling	AGC windowlength:	50 ms at seafloor	
		200 ms at end of data	

profile No.	**205**		
beginning	15.14067°W, 28.90333°N (CMP 34)		
end	15.87800°W, 28.65933°N (CMP 25441)		
length	76.91 km		
course	249°		
wind	NNE/NNW 3–6 m/s		
shot rate	CMP 34–25441:	10 s	(3 fold)
processing sequence:			
reverse polarity	SEG normal polarity		
CMP sorting			
NMO correction	water:	v_{NMO} =1500 m/s	
	0-400 ms below seafloor	v_{NMO} =1600 m/s	
	end of data	v_{NMO} =2500 m/s	
offset-dependant scaling	time invariant equalizing of the 24 channels		
stack	fold is given with the shot rate		
resampling	sampling rate 2 ms		
composed data stack	stack of 4 adjacent traces		
band-pass filter	20-235 Hz		
scaling	AGC windowlength 200 ms		
migration	finite-difference migration in the tx-domain		
	water:	v_{INT} =1450 m/s	
	seafloor–5500 ms TWT:	v_{INT} =2000 m/s	
	below 5500 ms TWT:	v_{INT} =2500 m/s	
band-pass filter	seafloor:	30-235 Hz	
	5.0 s TWT:	30-235 Hz	
	6.5 s TWT:	30-160 Hz	
tracemix	3 traces (weight 1 2 1)		
scaling	AGC windowlength:	50 ms at seafloor	
		200 ms at end of data	

profile No.	**206**		
beginning	15.87750°W, 28.64083°N (CMP 34)		
end	15.71733°W, 28.48333°N (CMP 7729)		
length	23.46 km		
course	138°		
wind	NW 4–6 m/s		
shot rate	CMP 34–7729:	10 s	(3 fold)
processing sequence:			
reverse polarity	SEG normal polarity		
CMP sorting			
NMO correction	water:	v_{NMO} =1500 m/s	
	0-400 ms below seafloor	v_{NMO} =1600 m/s	
	end of data	v_{NMO} =2500 m/s	
offset-dependant scaling	time invariant equalizing of the 24 channels		
stack	fold is given with the shot rate		
resampling	sampling rate 2 ms		
band-pass filter	20-235 Hz		
scaling	AGC windowlength 200 ms		
migration	finite-difference migration in the tx-domain		
	v_{INT} =1500 m/s		
band-pass filter	seafloor:	30-235 Hz	
	below 5.15 s TWT:	20-160 Hz	
tracemix	5 traces (weight 1 2 4 2 1)		
scaling	AGC windowlength:	50 ms at seafloor	
		200 ms at end of data	

profile No.	**207**		
beginning	15.71533°W, 28.47767°N (CMP 34)		
end	15.62833°W, 28.26767°N (CMP 7681)		
length	24.79 km		
course	168°		
wind	NNW 5 m/s		
shot rate	CMP 34–6175:	10 s	(3 fold)
	CMP 6176–7681:	7.5 s	(4 fold)
processing sequence:			
reverse polarity	SEG normal polarity		
CMP sorting			
NMO correction	water:	v_{NMO} =1500 m/s	
	0-400 ms below seafloor	v_{NMO} =1600 m/s	
	end of data	v_{NMO} =2500 m/s	
offset-dependant scaling	time invariant equalizing of the 24 channels		
stack	fold is given with the shot rate		
resampling	sampling rate 2 ms		
band-pass filter	20-235 Hz		
composed data stack	stack of 2 adjacent traces		
scaling	AGC windowlength 200 ms		
migration	finite-difference migration in the tx-domain		
	water:	v_{INT} =1450 m/s	
	sediments:	v_{INT} =2000 m/s	
	below flank:	v_{INT} =2500 m/s	
band-pass filter	seafloor:	30-235 Hz	
	0.4 s below seafloor:	30-235 Hz	
	0.9 s below seafloor:	30-160 Hz	
	end of data:	30-160 Hz	
tracemix	3 traces (weight 1 2 1)		
scaling	AGC windowlength:	50 ms at seafloor	
		200 ms at end of data	

profile No.	**208**		
beginning	15.70500°W, 28.23950°N (CMP 34)		
end	15.85600°W, 28.29667°N (CMP 5271)		
length	16.10 km		
course	294°		
wind	N/NE 3–7 m/s		
shot rate	CMP 34–3191:	7.5 s	(4 fold)
	CMP 3192–5271:	10 s	(3 fold)
processing sequence:			
reverse polarity	SEG normal polarity		
CMP sorting			
NMO correction	water:	v_{NMO} =1500 m/s	
	0-400 ms below seafloor	v_{NMO} =1600 m/s	
	end of data	v_{NMO} =2500 m/s	
offset-dependant scaling	time invariant equalizing of the 24 channels		
stack	fold is given with the shot rate		
resampling	sampling rate 2 ms		
scaling	AGC windowlength 200 ms		
migration	finite-difference migration in the fx-domain		
	v_{INT} =1475 m/s		
band-pass filter	seafloor:	30-230 Hz	
	0.2 s below seafloor:	30-230 Hz	
	0.5 s below seafloor:	20-160 Hz	
	end of data:	20-160 Hz	
tracemix	5 traces (weight 1 2 4 2 1)		
scaling	AGC windowlength:	50 ms at seafloor	
		200 ms at end of data	

profile No.	**210**		
beginning	15.62050°W, 28.47450°N (CMP 34)		
end	15.30133°W, 28.33450°N (CMP 12009)		
length	34.91 km		
course	117°		
wind	NW/NNW 6–9 m/s		
shot rate	CMP 34–12009:	10 s	(3 fold)
processing sequence:			
reverse polarity	SEG normal polarity		
CMP sorting			
NMO correction	water:	v_{NMO} =1500 m/s	
	0-400 ms below seafloor	v_{NMO} =1600 m/s	
	end of data	v_{NMO} =2500 m/s	
offset-dependant scaling	time invariant equalizing of the 24 channels		
stack	fold is given with the shot rate		
resampling	sampling rate 2 ms		
scaling	AGC windowlength 200 ms		
migration	finite-difference migration in the fx-domain		
	water:	v_{INT} =1450 m/s	
	sediments:	v_{INT} =1520–1600 m/s	
	below flank:	v_{INT} =1650 m/s	
band-pass filter	seafloor:	30-235 Hz	
	end of data:	20-160 Hz	
tracemix	5 traces (weight 1 2 4 2 1)		
scaling	AGC windowlength:	50 ms at seafloor	
		200 ms at end of data	

profile No.	**301**		
beginning	15.55881°W, 28.19983°N (CMP 34)		
end	15.55817°W, 28.77500°N (CMP 19743)		
length	63.75 km		
course	360°		
wind	N 3–6 m/s		
shot rate	CMP 34–6335:	7.5 s	(4 fold)
	CMP 6336–19743:	10 s	(3 fold)
processing sequence:			
reverse polarity	SEG normal polarity		
CMP sorting			
NMO correction	water:	v_{NMO} =1500 m/s	
	0-400 ms below seafloor	v_{NMO} =1600 m/s	
	end of data	v_{NMO} =2500 m/s	
offset-dependant scaling	time invariant equalizing of the 24 channels		
stack	fold is given with the shot rate		
resampling	sampling rate 2 ms		
scaling	AGC windowlength 200 ms		
migration	finite-difference migration in the fx-domain		
	water:	v_{INT} =1450 m/s	
	sediments:	v_{INT} =1700–1900 m/s	
	below flank:	v_{INT} =2200 m/s	
band-pass filter	seafloor:	30-230 Hz	
	0.2 s below seafloor:	30-230 Hz	
	0.4 s below seafloor:	20-160 Hz	
	end of data:	20-160 Hz	
scaling	AGC windowlength:	50 ms at seafloor	
		200 ms at end of data	
composed data stack	stack of 16 adjacent traces in Fig. 39		

GEOMAR REPORTS

1 GEOMAR FORSCHUNGSZENTRUM FÜR MARINE GEOWISSENSCHAFTEN DER CHRISTIAN-ALBRECHTS-UNIVERSITÄT ZU KIEL
BERICHT FÜR DIE JAHRE 1987 UND 1988. 1989. 71 + 6 pp.
In German

2 GEOMAR FORSCHUNGSZENTRUM FÜR MARINE GEOWISSENSCHAFTEN DER CHRISTIAN-ALBRECHTS-UNIVERSITÄT ZU KIEL
JAHRESBERICHT / ANNUAL REPORT 1989. 1990. 96 pp.
In German and English

3 GEOMAR FORSCHUNGSZENTRUM FÜR MARINE GEOWISSENSCHAFTEN DER CHRISTIAN-ALBRECHTS-UNIVERSITÄT ZU KIEL
JAHRESBERICHT / ANNUAL REPORT 1990. 1991. 212 pp.
In German and English

4 ROBERT F. SPIELHAGEN
DIE EISDRIFT IN DER FRAMSTRASSE WÄHREND DER LETZTEN 200.000 JAHRE. 1991. 133 pp.
In German with English summary

5 THOMAS C. W. WOLF
PALÄO-OZEANOGRAPHISCH-KLIMATISCHE ENTWICKLUNG DES NÖRDLICHEN NORDATLANTIKS SEIT DEM SPÄTEN NEOGEN
(ODP LEGS 105 UND 104, DSDP LEG 81). 1991. 92 pp.
In German with English summary

6 SEISMIC STUDIES OF LATERALLY HETEROGENOUS STRUCTURES - INTERPRETATION AND MODELLING OF SEISMIC DATA.
Edited by ERNST R. FLUEH
Commission on Controlled Source Seismology (CCSS), Proceedings of the 8th Workshop Meeting, held at
Kiel - Fellhorst (Germany), August 27-31, 1990. 1991. 359 pp.
In English

7 JENS MATTHIESSEN
DINOFLAGELLATEN-ZYSTEN IM SPÄTQUARTÄR DES EUROPÄISCHEN NORDMEERES: PALÖKOLOGIE UND PALÄO-OZEANOGRAPHIE. 1991. 104 pp.
In German with English summary

8 DIRK NÜRNBERG
HAUPT- UND SPURENELEMENTE IN FORAMINIFERENGEHÄUSEN - HINWEISE AUF KLIMATISCHE UND OZEANOGRAPHISCHE ÄNDERUNGEN
IM NÖRDLICHEN NORDATLANTIK WÄHREND DES SPÄTQUARTÄRS. 1991. 117 pp.
In German with English summary

9 KLAS S. LACKSCHEWITZ
SEDIMENTATIONSPROZESSE AM AKTIVEN MITTELOZEANISCHEN KOLBEINSEY RÜCKEN (NÖRDLICH VON ISLAND). 1991. 133 pp.
In German with English summary

10 UWE PAGELS
SEDIMENTOLOGISCHE UNTERSUCHUNGEN UND BESTIMMUNG DER KARBONATLÖSUNG IN SPÄTQUARTÄREN SEDIMENTEN DES ÖSTLICHEN
ARKTISCHEN OZEANS. 1991. 106 pp.
In German with English summary

11 FS POSEIDON - EXPEDITION 175 (9.10.-1.11.1990)
175/1: OSTGRÖNLÄNDISCHER KONTINENTALRAND (65° N)
175/2: SEDIMENTATION AM KOLBEINSEYRÜCKEN (NÖRDLICH VON ISLAND)
Hrsg. von J. MIENERT und H.-J. WALLRABE-ADAMS. 1992. 56 pp. + app.
In German with some English chapters

12 GEOMAR FORSCHUNGSZENTRUM FÜR MARINE GEOWISSENSCHAFTEN DER CHRISTIAN-ALBRECHTS-UNIVERSITÄT ZU KIEL
JAHRESBERICHT / ANNUAL REPORT 1991. 1992. 152 pp.
In German and English

13 SABINE E. I. KÖHLER
SPÄTQUARTÄRE PALÄO-OZEANOGRAPHISCHE ENTWICKLUNG DES NORDPOLARMEERES UND EUROPÄISCHEN NORDMEERES ANHAND VON
SAUERSTOFF- UND KOHLENSTOFF- ISOTOTPENVERHÄLTNISSEN DER PLANKTISCHEN FORAMINIFERE
Neogloboquadrina pachyderma (sin.). 1992. 104 pp.
In German with English summary

14 FS SONNE - FAHRTBERICHT SO 78 PERUVENT: BALBOA, PANAMA - BALBOA, PANAMA, 28.2.1992-16.4.1992
Hrsg. von ERWIN SUESS. 1992. 120 pp.
In German with some English chapters

15 FOURTH INTERNATIONAL CONFERENCE ON PALEOCEANOGRAPHY (ICP IV): SHORT- AND LONG-TERM GLOBAL CHANGE:
RECORDS AND MODELLING 21-25 SEPTEMBER 1992, KIEL/GERMANY
PROGRAM & ABSTRACTS. 1992. 351 pp.
In English

16 MICHAELA KUBISCH
DIE EISDRIFT IM ARKTISCHEN OZEAN WÄHREND DER LETZTEN 250.000 JAHRE. 1992. 100 pp.
In German with English summary

17 PERSISCHER GOLF: UMWELTGEFÄHRDUNG, SCHADENSERKENNUNG, SCHADENSBEWERTUNG AM BEISPIEL DES MEERESBODENS; ERKENNEN
EINER ÖKOSYSTEMVERÄNDERUNG NACH ÖLEINTRÄGEN. Schlußbericht zu den beiden BMFT-Forschungsvorhaben 03F0055 A+B. 1993. 108 pp.
In German with English summary

18 TEKTONISCHE ENTWÄSSERUNG AN KONVERGENTEN PLATTENRÄNDERN / DEWATERING AT CONTINENTAL MARGINS.
Hrsg. von / ed. by ERWIN SUESS. 1993. 106 + 32 + 68 + 16 + 22 + 38 + 4 + 19 pp.
Some chapters in English, some in German

19 THOMAS DICKMANN
DAS KONZEPT DER POLARISATIONSMETHODE UND SEINE ANWENDUNGEN AUF DAS SEIMISCHE VEKTORWELLENFELD IM WEITWINKELBEREICH. 1993. 121 pp.
In German with English summary

20 GEOMAR FORSCHUNGSZENTRUM FÜR MARINE GEOWISSENSCHAFTEN DER CHRISTIAN-ALBRECHTS-UNIVERSITÄT ZU KIEL
JAHRESBERICHT / ANNUAL REPORT 1992. 1993. 139 pp.
In German and English

21 KAI UWE SCHMIDT
PALYNOMORPHE IM NEOGENEN NORDATLANTIK - HINWEISE ZUR PALÄO-OZEANOGRAPHIE UND PALÄOKLIMATOLOGIE. 1993. 104 + 7 + 41 pp.
In German with English summary

22 UWE JÜRGEN GRÜTZMACHER
DIE VERÄNDERUNGEN DER PALÄOGEOGRAPHISCHEN VERBREITUNG VON *BOLBOFORMA* - EIN BEITRAG ZUR REKONSTRUKTION UND DEFINITION VON WASSERMASSEN IM TERTIÄR.1993. 104 pp.
In German with English summary

23 RV PROFESSOR LOGACHEV - Research Cruise 09 (August 30 - September 17, 1993): SEDIMENT DISTRIBUTION ON THE REYKJANES RIDGE NEAR 59°N
Edited by H.-J. WALLRABE-ADAMS & K.S. LACKSCHEWITZ. 1993. 66 + 30 pp.
In English

24 ANDREAS DETTMER
DIATOMEEN-TAPHOZÖNOSEN ALS ANZEIGER PALÄO-OZEANOGRAPHISCHER ENTWICKLUNGEN IM PLIOZÄNEN UND QUARTÄREN NORDATLANTIK. 1993. 113 + 10 + 25 pp.
In German with English summary

25 GEOMAR FORSCHUNGSZENTRUM FÜR MARINE GEOWISSENSCHAFTEN DER CHRISTIAN-ALBRECHTS-UNIVERSITÄT ZU KIEL
JAHRESBERICHT / ANNUAL REPORT 1993. 1994. 69 pp.
In German and English

26 JÖRG BIALAS
SEISMISCHE MESSUNGEN UND WEITERE GEOPHYSIKALISCHE UNTERSUCHUNGEN AM SÜD-SHETLAND TRENCH UND IN DER BRANSFIELD STRASSE - ANTARKTISCHE HALBINSEL. 1994. 113 pp.
In German with English summary

27 JANET MARGARET SUMNER
THE TRANSPORT AND DEPOSITIONAL MECHANISM OF HIGH GRADE MIXED-MAGMA IGNIMBRITE TL, GRAN CANARIA: THE MORPHOLOGY OF A LAVA-LIKE FLOW. 1994. 224 pp.
In English with German summary

28 GEOMAR LITHOTHEK. Edited by JÜRGEN MIENERT. 1994. 12 pp + app.
In English

29 FS SONNE - FAHRTBERICHT SO 97 KODIAK-VENT: KODIAK - DUTCH HARBOR - TOKYO - SINGAPUR, 27.7. - 19.9.1994
Hrsg. von ERWIN SUESS. 1994.
Some chapters in German, some in English

30 CRUISE REPORTS:
RV LIVONIA CRUISE 92, KIEL-KIEL, 21.8.-17.9.1992: GLORIA STUDIES OF THE EAST GREENLAND CONTINENTAL MARGIN BETWEEN 70° AND 80°N
RV POSEIDON PO200/10, LISBON-BREST-BREMERHAVEN, 7.-23.8.1993: EUROPEAN NORTH ATLANTIC MARGIN: SEDIMENT PATHWAYS, PROCESSES AND FLUXES
RV AKADEMIK ALEKSANDR KARPINSKIY, KIEL-TROMSØ, 5.-25.7.1994: GAS HYDRATES ON THE NORTHERN EUROPEAN CONTINENTAL MARGIN
Edited by JÜRGEN MIENERT. 1994.
In English; report of RV AKADEMIK ALEKSANDR KARPINSKIY cruise in English and Russian

31 MARTIN WEINELT
BECKENENTWICKLUNG DES NÖRDLICHEN WIKING-GRABENS IM KÄNOZOIKUM - VERSENKUNGSGESCHICHTE, SEQUENZSTRATIGRAPHIE, SEDIMENTZUSAMMENSETZUNG. 1994. 85 pp.
In German with English summary

32 GEORG A. HEISS
CORAL REEFS IN THE RED SEA: GROWTH, PRODUCTION AND STABLE ISOTOPES. 1994. 141 pp.
In English with German summary

33 JENS A.HÖLEMANN
AKKUMULATION VON AUTOCHTHONEM UND ALLOCHTHONEM ORGANISCHEM MATERIAL IN DEN KÄNOZOISCHEN SEDIMENTEN DER NORWEGISCHEN SEE (ODP LEG 104). 1994. 78 pp.
In German with English summary

34 CHRISTIAN HASS
SEDIMENTOLOGISCHE UND MIKROPALÄONTOLOGISCHE UNTERSUCHUNGEN ZUR ENTWICKLUNG DES SKAGERRAKS (NE NORDSEE) IM SPÄTHOLOZÄN. 1994.
In German with English summary

35 BRITTA JÜNGER
TIEFENWASSERERNEUERUNG IN DER GRÖNLANDSEE WÄHREND DER LETZTEN 340.000 JAHRE.
DEEP WATER RENEWAL IN THE GREENLAND SEA DURING THE PAST 340,000 YEARS.1994. 6 + 109 pp.
In German with English summary

36 JÖRG KUNERT
UNTERSUCHUNGEN ZU MASSEN- UND FLUIDTRANSPORT ANHAND DER BEARBEITUNG REFLEXIONSSEISMISCHER DATEN AUS DER KODIAK-SUBDUKTIONSZONE, ALASKA. 1995. 129 pp.
In German with English summary

37 CHARLOTTE M. KRAWCZYK
DETACHMENT TECTONICS DURING CONTINENTAL RIFTING OFF THE WEST IBERIA MARGIN: SEISMIC REFLECTION AND DRILLING CONSTRAINTS. 1995. 133 pp.
In English with German summary

38 CHRISTINE CAROLINE NÜRNBERG
BARIUMFLUSS UND SEDIMENTATION IM SÜDLICHEN SÜDATLANTIK - HINWEISE AUF PRODUKTIVITÄTSÄNDERUNGEN IM QUARTÄR. 1995. 6 + 108pp.
In German with English summary

39 JÜRGEN FRÜHN
TEKTONIK UND ENTWÄSSERUNG DES AKTIVEN KONTINENTALRANDES SÜDÖSTLICH DER KENAI-HALBINSEL, ALASKA. 1995. 93 pp.
In German with English summary

40 GEOMAR FORSCHUNGSZENTRUM FÜR MARINE GEOWISSENSCHAFTEN DER CHRISTIAN-ALBRECHTS-UNIVERSITÄT ZU KIEL
JAHRESBERICHT / ANNUAL REPORT 1994. 1995.
In German and English

41 FS SONNE - FAHRTBERICHT / CRUISE REPORT SO 103 CONDOR 1 B: VALPARAISO-VALPARAISO, 2.-21.7.1995.
Hrsg. von ERNST R. FLUEH. 1995. 140 pp.
Some chapters in German, some in English

42 R/V PROFESSOR BOGOROV CRUISE 37: CRUISE REPORT "POSETIV": Vladivostok - Vladivostok, September 23 - October 22, 1994.
Edited by CHRISTOPH GAEDICKE, BORIS BARANOV and EVGENIY LELIKOV. 1995. 48 + 33 pp.
In English

43 CHRISTOPH GAEDICKE
DEFORMATION VON SEDIMENTEN IM NANKAI-AKKRETIONSKEIL, JAPAN. BILANZIERUNG TEKTONISCHER VORGÄNGE ANHAND VON SEISMISCHEN PROFILEN UND ERGEBNISSEN DER ODP-BOHRUNG 808. II + 89 pp.
In German with English summary

44 MARTIN ANTONOW
SEDIMENTATIONSMUSTER UM DEN VESTERIS SEAMOUNT (ZENTRALE GRÖNLANDSEE) IN DEN LETZTEN 250.000 JAHREN. 1995.
In German with English summary

45 INTERNATIONAL CONGRESS: CORING FOR GLOBAL CHANGE - ICGC '95. KIEL, 28 - 30 June, 1995.
Edited by JÜRGEN MIENERT and GEROLD WEFER. 1996.
In English

46 JENS GRÜTZNER
ZUR PHYSIKALISCHEN ENTWICKLUNG VON DIAGENETISCHEN HORIZONTEN IN DEN SEDIMENTBECKEN DES ATLANTIKS. 1995. 96 pp.
In German with English summary

47 INGO A. PECHER
SEISMIC STUDIES OF BOTTOM SIMULATING REFLECTORS AT THE CONVERGENT MARGINS OFFSHORE PERU AND COSTA RICA. 1996. 159 pp.
In English with German summary

48 XIN SU
DEVELOPMENT OF LATE TERTIARY AND QUATERNARY COCCOLITH ASSEMBLAGES IN THE NORTHEAST ATLANTIC. 1996. 120 pp. + 7 pl.
In English with German summary

49 FS SONNE - FAHRTBERICHT / CRUISE REPORT SO 108 ORWELL: SAN FRANCISCO - ASTORIA, 14.4. - 23.5.1996
Edited by ERNST R. FLUEH and MICHAEL A. FISHER. 1996.

50 GEOMAR FORSCHUNGSZENTRUM FÜR MARINE GEOWISSENSCHAFTEN DER CHRISTIAN-ALBRECHTS-UNIVERSITÄT ZU KIEL
JAHRESBERICHT / ANNUAL REPORT 1995. 1996. 93 pp.
In German and English

51 THOMAS FUNCK
STRUCTURE OF THE VOLCANIC APRON NORTH OF GRAN CANARIA DEDUCED FROM REFLECTION SEISMIC, BATHYMETRIC AND BOREHOLE DATA. 1996. VI, 144 pp.
In English with German summary

52 PETER BRUNS
GEOCHEMISCHE UND SEDIMENTOLOGISCHE UNTERSUCHUNGEN ÜBER DAS SEDIMENTATIONSVERHALTEN IM BEREICH BIOSTRATIGRAPHISCHER DISKONTINUITÄTEN IM NEOGEN DES NORDATLANTIK, ODP LEG 104, SITES 642B UND 643A. 1993. V, 73 pp.
n German with English summary